UNIVERSITY OF TECHNOLOGY SYDNEY

Gold nanoparticles to ameliorate obesity related glucose intolerance

Jane Phui Mun NG

Submitted in total fulfilment of the requirements of the degree of Doctor of Philosophy (PhD)

4th January 2016

School of Life Sciences

Faculty of Science

University of Technology Sydney

Abstract

Obesity is associated with a number of metabolic disorders such as insulin resistance, glucose intolerance, and dyslipidaemia. The main objective of this research work focused on potential therapeutic applications of "naked" gold nanoparticles (AuNPs) in the treatment of obesity-related metabolic diseases. In this thesis, 21 nm spherical citrate-coated, unmodified also known as "naked" AuNPs were studied and assessed using both *in vitro* cell and *in vivo* animal studies. We observed an increased rate of "naked" AuNPs cellular uptake non-selectively and non-specific accumulation in all cell types studied compared to surface modified AuNPs. Macrophages in adipose tissue played a crucial role contributing to the low-grade chronic inflammation present in obesity and pathogenesis of obesity-related metabolic disorders. Our *in vitro* studies also showed that AuNPs can act on the complex adipocyte-macrophage interaction altering the adipocytes lipid and fatty acid metabolic markers in a macrophage-dependent manner.

Based on this unique finding, we further investigated the long-term safety of AuNP treatment and their effect on adipose tissue macrophages using *in vivo* mice model with dietary obesity. In this study, 7 week old male C57Bl/6 mice were fed a high fat diet (HFD) and received daily intraperitoneal injection of AuNPs (0.785 μg or 7.85 μg/g/day) for 9 weeks. Our results showed that the AuNP-treated mice with dietary obesity showed significantly improved body morphometry measurement with significantly reduced blood lipid levels and prevented the development of glucose intolerance. We proposed that the alterations in the local pro-inflammatory cytokine environment due to modification of macrophage activity by AuNPs may be the key underlying mechanism for the weight loss observed in the HFD-fed mice. In addition, there was no indication of liver toxicity after 9 weeks of daily AuNPs exposure.

Following that, male C57Bl/6 mice (7 week old) feeding a 10 week HFD were used as an *in vivo* obese model with chronic obesity and metabolic disorder to study the effect of short-term AuNP treatment. At week 10, the obese mice were continued on a HFD and AuNP treatment (0.0785 μg, 0.785 μg, or 7.85 μg/g/day) administered daily via intraperitoneal injection for an additional 5 weeks. Our findings showed that the 5

weeks AuNP-treated obese mice had little to no impact on body morphometric measurements of mice with existing obesity. However, all obese mice treated with 5 weeks of AuNPs showed amelioration of glucose intolerance. Our results also showed altered the inflammatory cytokines, lipid, and glucose marker expression in the liver. Our findings suggest that obese mice treated with AuNPs could have a lower the risk of developing obesity-related complications such as glucose intolerance and liver steatosis.

This research work demonstrated the anti-obesity and anti-diabetic properties of AuNPs which has led to our proposal that AuNPs can serve as a novel therapeutic treatment strategy in the prevention of obesity and obesity-related metabolic disorders.

Certificate of Original Authorship

I certify that the work in this thesis has not previously been submitted for a degree nor has it been submitted as part of requirements for a degree except as part of the collaborative doctoral degree and/or fully acknowledged within the text.

I also certify that the thesis has been written by me. Any help that I have received in my research work and the preparation of the thesis itself has been acknowledged. In addition, I certify that all information sources and literature used are indicated in the thesis.

Signature of Student:

(Jane Phui Mun Ng)

Date:

This research is supported by the University of Technology Sydney (UTS) International Research Scholarship and Australian Technology Network and International Strategic Technology Alliance (ATN ISTA) Nano Network Scholarship through Institute of Nanoscale Technology.

Acknowledgements

My sincere gratitude to the school,

This research work is a collaborative and interdisciplinary study under the expert supervision from some of the greatest intellects in the field biology, medicine, chemistry, and biomedical engineering. My ideas would still be an idea without your acceptance and support. Thank you.

To the greatest minds of the science world,

It has been such a great honour to have met and learned from you all. First and foremost, I would like to thank my principal supervisor, A/Prof. Stella M. Valenzuela and co-supervisors, Dr. Hui Chen, Prof. Bruce K. Milthorpe, and A/Prof. Andrew D. McDonagh. Thank you for your guidance and taking the time to mentor me. Without your help, I would be lost. No words will ever describe the enormous role the both of you had played in my life and to making this thesis happen. Thank you.

I would like to express my sincere appreciation to A/Prof. Michael B. Cortie and Dr. Michael Coutts for their expertise in gold nanoparticles synthesis and characterization; Dr. Yi Tan who supported me in the first animal work along with animal house manager, Ms. Fiona Reed, and Dr. David P Bishop who assisted with the ICP-MS analysis. Special thanks to Dr. Kristine McGrath, Dr. Cathy Gorrie, Dr. Michael Johnson, Dr. Richard Wuhrer, Ms. Katie McBean, Dr. Freddrick Luk, Mr. Yik Lung Chan, and my peers at UTS. Each of you played a crucial part supporting me in this research. Thank you. Special thanks to my best friend Ms. Kit Yee Ng for writing macros to support my data and image analyses. To my mentors, Ms. Christine Gan, Mr. John & Mrs. Kerrie Wiersma for their encouragement through this impossible journey. Thank you.

To my beloved family, Esther, Thomas, Paul and John. Thank you for your unconditional love and support. I would not be here without you. I love you.

To my many friends that I may had missed, thank you for your kind support. I want to thank Australia and its people, for the hospitality and generosity this great country has provided me. Last but not least, I want to thank our Lord Jesus Christ for being there every step of the way.

Table of contents

List of Figures

List of Tables

Abbreviations

AC	adipocytes control
AF594	Alexa Fluor 594 cadevarine
AF594	Alexa Fluor 594 cadaverine
AH	adipocytes treated with high dose of AuNPs
AHH	adipocytes treated with extremely high dose of AuNPs
AL	adipocytes treated with low dose of AuNPs
ALT	alanine aminotransferase
ANOVA	analysis of variance
ARMΦC	adipocyte-macrophage co-culture control
ARMΦH	adipocyte-macrophage co-culture treated with high dose of AuNPs
ARMΦHH	adipocyte-macrophage co-culture treated with extremely high dose of AuNPs
ARMΦL	adipocyte-macrophage co-culture treated with low dose of AuNPs
AST	aspartate aminotransaminase
ATGL	adipose triglyceride lipase
ATM	adipose tissue macrophage
AUC	area under the curve
$AuCl_4$	chloroaurate
AuNP	gold nanoparticle
BAEC	bovine aortic endothelial
BMI	body mass index
BSA	bovine serum albumin

BSA-AuNP	BSA-conjugated AuNPs
CD	cluster of differentiation
cDNA	complementary DNA
Chow-C	chow-fed mice control
CLS	crown-like structure
CPT	carnitine palmitoyl transferace
DCF	2’,7’-dicholorofluorescein
DEPC	diethylpyrocarbonate
DL	detection limit
DMEM	dulbecco's modified eagle's medium
DNA	deoxyribonucleic acid
DNase	deoxyribonuclease
dNTP	deoxyucleotide
DPBS	dulbecco's PBS
EDTA	ethylenediaminetetraacetic acid
EDC	1-ethyl-3-(3-dimethylaminopropyl) carbodiimide
F4/80	expressing ATMs
FASN	fatty acid synthase
FBS	fetal bovine serum
FOX	forkhead box
GLUT	glucose transporter
GM-CSF	granulocyte-macrophage colony-stimulating factor
H&E	harris haematoxylin and eosin

H_2-DCFDA	2',7'-dicholorofluorescein diacetate
$HAuCl_4$	tetrachlorouauric acid
HCAEC	human coronary artery endothelial cell
HFD	high fat diet
HFD-C	HFD-fed mice control
HFD-HAu	HFD-fed mice treated with high doses AuNPs
HFD-LAu	HFD-fed mice treated with low dose of AuNPs
HRP	horseradish peroxidase
HR-SEM	high resolution scanning electron microscopy
ICP-MS	inductively–coupled plasma mass spectroscopy
IFN	interferon
IKK	inhibitory kappa kinase
IL	interleukin
IP	intraperitoneal
IPGTT	intraperitonoteal glucose tolerance test
IκB	inhibitory kappaB
LPS	lipopolysaccharide
M1	pro-inflammatory macrophage
M2	anti-inflammtory macrophage
MES	2-(*N*-morpholino)ethanesulfonic acid
MΦ	macrophage
MPC	monolayer protected cluster
mRNA	messenger RNA

MTT	3-(4,5-dimethylthiazol-2-yl)-2,5-diphenyltetrazolium bromide
NCS	new calf serum
NEFA	non-esterified fatty acid
NF-κB	nuclear factor-kappa B
NHS	N-hydroxysuccinimide
OB-C	obese mice control
OB-EAu	obese mice treated with extremely low dose of AuNPs
OB-HAu	obese mice treated with high dose of AuNPs
OB-LAu	obese mice treated with low dose of AuNPs
P/S	penicillin and streptomycin
PBS	phosphate buffered saline
PC	pre-adipocyte or 3T3-L1 fibroblast control
PCR	polymerase chain reaction
PEG	polyethelyne glycol
PEPCK	phosphoenolpyruvate carboxykinase
pf-DMEM	phenol-red free Dulbecco's Modified Eagle Medium
PMA	phorbol 12-myristate 13-acetate
PPAR	peroxisome proliferator-activated receptor
RMΦ	RAW 264.7 macrophages
RMΦC	RAW 264.7 macrophages control
RMΦH	RAW 264.7 macrophages treated with high dose of AuNPs
RMΦHH	RAW 264.7 macrophages treated with extremely high dose of AuNPs

RMΦL	RAW 264.7 macrophages treated with low dose of AuNPs
RMΦLPSH	high dose LPS stimulated RAW 264.7 macrophage
RMΦLPSL	low dose LPS stimulated RAW 264.7 macrophages
RNA	ribonucleic acid
ROS	reaction oxygen speacies
RPMI	roswell park memorial institute
RT-PCR	real-time PCR
S.E.M	standard mean of error
SAA	serum amyloid A
SPR	surface plasmon resonance
SREBP	sterol regulatory element binding protein
TEM	transmission electron microscopy
TLR-4	toll-like receptor-4
TNF	tumor necrosis factor
UMΦ	U937 monocytes
UMΦC	PMA-differentiated U937 control
UMΦC_LPS	PMA-differentiated U937 with LPS stimulation control
UMΦH	PMA-differentiated U937 treated with high dose AuNP
UMΦH_LPS	PMA-differentiated U937 treated with high dose AuNPs and LPS
UMΦ_HH	PMA-differentiated U937 treated-with extremely high dose AuNPs
UMΦ_HH_LPS	PMA-differentiated U937 treated with extremely high dose AuNPs and LPS
UMΦL	PMA-differentiated U937 treated with low dose AuNPs

CHAPTER 1

Literature Review

1. Literature review

1.1 Nanomedicine

Nanotechnology is a relatively new and rapidly expanding field that has generated a tremendous interest in the past two decades. The research in nanotechnology focused on the understanding, manipulation, and exploitation of matter in the nano-scale for creation of functional materials, devices, and systems. It has tremendously impacted other fields such as material science, electronics, and medicine through downsizing and miniaturization of electronic components, bio-molecular device, and delivery systems (De Franceschi & Kouwenhoven 2002; Mnyusiwalla, Daar & Singer 2003). The word "nano" is derived from the Greek "nanos" which means dwarf, describing any material or system with a size range between 1 to 100 nm. One nanometer is roughly about the length of ten aligned atoms. At the nanoscale, the properties and phenomenal were different from bulk (Dreaden et al. 2012a; Dreaden et al. 2012b).

In general, nanomaterials are great diagnostic probe and delivery system due to their large surface-to-volume ratio at small size, tailorable physical and optical properties corresponding to particle size/composition/shape, modifiable surfaces, and overall structural robustness (Rosi & Mirkin 2005). At the nano-size range, nanoparticles can be rationally designed and tailored for application in biological system due to the unique interactions between these nanoscale materials with majority of proteins and antibodies which are approximately 10 nm in size (Eustis & El-Sayed 2006; Rosi & Mirkin 2005).

Following the clinical approval of Sandimmune®, a micellar drug to be administered in human by U.S. Food and Drug Administration (FDA) in 1983, many other protein-drug nanoconjugates with a size between 1–100 nm have been systematically accepted for their application in medicine (Ramanathan & Helderman 2001). There has been an enormous worldwide effort in the research of nanoscale diagnostic and therapeutic agents giving rise to the field of nanomedicine (Alkilany & Murphy 2010). To date, more than two dozen of bio-diagnostic or therapeutic nanotechnologies such as micelles, liposomes, dendrimers, inorganic nanoparticles, and other polymer–drug

nanoconjugates have been approved for clinical use with 250 others in clinical development (Dreaden et al. 2012a).

1.2 Gold nanoparticles (AuNPs)

Amongst the engineered inorganic nanomaterials, gold nanoparticles (AuNPs) hold great potential for biomedical application as drug and gene delivery vehicle, photothermal therapeutics, bio-sensor, diagnostic tracer, and biological contrast agents for photoacoustic, computed tomography, Raman, differential interference contrast, and dark field imaging platforms (Boisselier & Astruc 2009; Cai et al. 2007; Chandra, Das & Abdelwahab 2010; Hermann, Walther & Müller 1996; Pissuwan et al. 2007). Bulk gold is an inert metal. The nobility of gold stems from its properties of density, softness, low toxicity compared to other metals, and very good thermal/electrical conductivity. Unlike bulk gold or ionic gold, nanoscale gold exhibits unique electrical, chemical, mechanical, thermal and optical properties at nano-sized that different from bulk gold. AuNPs possess high chemical stability compared to other metallic NPs, narrow control of size or shape distribution during synthesis, easy surface functionalization with amines or thiols, and high biocompatibility (Eustis & El-Sayed 2006; Yah 2013).

The first synthesis of colloidal gold, which is AuNPs within suspension appeared well before the existence of peer-reviewed literature in 1857 by Michael Faraday (Faraday 1857; Thompson 2007). He was the first to describe “ruby gold” which is a brilliance ruby suspension containing very fine gold particles formed through the aqueous reduction of gold chloride by phosphorous, stabilized by the addition of carbon disulphide. Since then, advances in chemistry, physics, and microscopy have led to synthesis of AuNPs with narrow control of particle size and shape distribution for various applications (Dreaden et al. 2012a).

1.2.1 Synthesis of AuNPs

Bottom up synthesis technique which employs a capping agent to stop growth of particles has been commonly used for the preparation of nano-sized AuNPs. The capping materials, such as a surfactant or polymer are used in this technique also acts to

prevent aggregation and precipitation of the metal nanoparticles out of solution. The choice of the reduction technique, time, and capping material allow the synthesis of AuNPs in various size and shape. Generation of spherical AuNPs is commonly carried out by the citrate reduction method reported by Turkevich et al. in 1951 and then developed by Frens in 1973. Gold salt and citrate are stirred in water, while the temperature, the ratio of gold to citrate, and the order of addition of the reagents control the size distribution of spherical AuNPs (size range 16–147 nm) generated (Frens 1973; Turkevich, Stevenson & Hillier 1951). The seeding technique is another popular method for generation of large spherical and nonspherical AuNPs (Murphy et al. 2005). The method for preparation of gold nanorods is a seed-mediated process whereby a small spherical nanoparticle seeds were first generated. This is followed by the addition of growth solution and surfactant such as cetyl trimethyl ammonium bromide (CTAB) with more metal ions to induce anisotropic growth. The directional growth of nanorods was attributed to the steric interaction of the stabilizer forms bilayer structures along the longitudinal axis of the nanorod to allow growth only along the transverse axis.

1.2.2 Surface modification and ligand conjugation of AuNPs

The surfaces of AuNPs can be tailored to achieve compatibility and specificity to suit various biomedical applications. Ideally, an engineered nanoparticle system should remain in their nano-size after assembly, stealth coating to prevent spontaneous protein opsonisation in the blood, avoid clearance through reticuloendothelial system, hydrophilic, long circulation time to allow passive or active sequester in and around tissue of interest, and modification of specific ligands on the surface of these nanoparticle vectors (Paciotti, Kingston & Tamarkin 2006).

Faulk and Taylor (1971) were the first to describe a method that used antibody-functionalized AuNPs for visualizing the surface antigens of salmonellae by transmission electron microscopy. Those antibody-conjugated AuNPs are also known as “immunogold” (Faulk & Taylor 1971).Since then, many studies have been devoted to the application of gold nanoparticles conjugated with biomolecules including antibodies, lectins, and enzymes in broad range of biological and medical applications. To date, commercially available antibody-conjugated gold nanoparticles have been

widely used due to their small size and electron density which can be easily identified microscopically and distinguished from biological debris (Hyatt & Eaton 1992). The antibody-conjugated AuNPs were prepared via direct physisorption (passive adsorption) of antibodies to the surface through electrostatic and hydrophobic interactions (Eck et al. 2008a). However, this resulted in a system wherein at equilibrium, both nanoparticle-bound and free (non-bound) antibody exists. They tend to agglomerate overtime as antibody dissociate from the surface of AuNPs, exhibits poor biocompatibility or protein repellency result (Eck et al. 2008b; Herrwerth et al. 2003). The fact that PBS, an electrolyte/ionic solution, commonly used as solvent for antibodies has also rendered the preparation of antibody-conjugated nanoparticles stable against aggregation difficult.

In order to overcome this problem and minimizing the loss of antibody via equilibrium or nonspecific protein adsorption on the surface, AuNPs can be chemically modified with thiolated-ligands including polyethylene glycol (PEG), polyethylene oxide, poly-L-lysine, and polyN-vinyl-2-pyrrolidone (Pillay et al. 2010; Wuelfing et al. 1998). In particular, PEG has been the polymer of choice as surface modifying agent due to its amphiphilicity, non-toxic and non-ionic nature as well as approved by FDA for internal ingestion (Pissuwan, Niidome & Cortie 2009; Yah 2013). The PEGylated nanoparticles with diameters below 100 nm have shown to be “stealth” with increased circulating time in the bloodstream, evade recognition by T cells and macrophages in vivo and avoid rapid clearance by the immune system (Moghimi, Hunter & Murray 2001). Therefore, AuNPs surface modified with PEG are resistant against protein adsorption, enhances their biocompatibility, and stabilizes them against agglomeration in biological environments.

In addition, the surfaces of AuNPs can also be specifically modified with hetero-bifunctional PEG that have two different functional ends; a thiol group at one end that binds to the surface of AuNPs and a functional group such as carboxyl or hydroxyl on the other (Maus, Spatz & Fiammengo 2009; Simpson et al. 2011). The thiol end readily displaces the citrate adsorbed on the surfaces of AuNPs through hydrogen bonding during synthesis to form a strong thiol bond. The functional carboxyl ends on the outer layer of PEGylated AuNPs allow attachment of antibodies with –NH3 ends via amide

bond formations. Antibody immobilized MPCs with increased stability and biocompatibility can be used for a specific targeting and labelling of cells (Simpson et al. 2011; Templeton, Wuelfing & Murray 2000).

1.2.3 Physical and optical properties of AuNPs

1.2.3.1 Surface plasmon resonance

The optical properties of colloidal gold arose from the absorption and scattering of light by the AuNPs in suspension (Mie 1908). When nanoparticles between 5−200 nm are irradiated by electromagnetic field at certain frequencies, this result in a collective oscillation of electrons on the surfaces of the particles, termed surface plasmon resonance (SPR). The SPR peak of AuNPs is highly influenced by their bulk dielectric constant which lies in the visible region of the electromagnectic spectrum, thus strongly absorbing light at their resonance frequency (El-Sayed 2001). A gradual increase in size can shift the SPR peak, altering the absorption and scattering of light, resulting in change of color of the spherical gold colloids (Figure 1.1 and Figure 1.2) (El-Sayed 2001; Murphy et al. 2008). However, the SPR peak of spherical AuNPs is extremely dependent on dielectric constant of environment where difference in solvent or surface modifications may result in a shift in position. In addition, aggregation of spherical AuNPs will lead to a prominent colorimetric transition from burgundy to purple (El-Sayed 2001; Hu et al. 2006).

Interestingly, anisotropic shaped gold nanorods displayed two SPR bands (one in the visible and another in either visible or near-infrared spectrum); correspond to the transverse (short-axis) and longitudinal (long-axis) plasmon modes. The transverse plasmon resonance is effectively of the same nature as the plasmon resonance observed for spherical AuNPs. The additional longitudinal plasmon resonance is due to the oscillation of electron along the nanorod which provides a greater extinction coefficient. Therefore, the plasmon resonances are tunable depending on the aspect ratio which is the value of the length divided by the width of the rod-shaped AuNPs (Kelly et al. 2003; Papavassiliou 1979). The shift in longitudinal band absorption of nanorods with increasing aspect ratio contribute the varied colorimetric of the nanorod solutions as

illustrated in Figure 1.2. Similarly, gold nanorods are sensitive to the dielectric properties of their environment where dispersion in different solvents with varying refractive indices also alters their color. Therefore, changes in the surface plasmon resonance absorbance can be used to determine the adsorbed species in the field of chemical, biochemical, biosensing, and medical.

1.2.3.2 Scattering

Following the absorption of light, the electrons in the metallic nanoparticles oscillate at the same frequency of the electromagnetic field of the incident wave causing scattering of the same electromagnetic radiation in all directions (Aslan, Lakowicz & Geddes 2005). AuNPs have been shown to absorb and scatter light with efficiencies greater than expected from their physical cross-section when they are illuminated by light which matches with the principal maximum plasmon absorption. Under the illumination of white light, spherical AuNPs with a diameter of 58 nm and 78 nm showed scattering green and yellow light, respectively; while rod-shaped AuNPs scatters red light (Hu et al. 2006). The enhanced scattering cross section due to surface field effects can be used as a powerful technique to image biological systems. In addition, this scattering signal can be observed from a simple optical microscope.

1.2.3.3 Photothermal

AuNPs have been shown as an effective photothermal coupling agent due to their strong absorption of a broad spectrum of electromagnetic waves and advantage over the existing photoabsorbing dyes which photobleach after repeated irradiation. Photoexcitation of AuNPs leads to thermal conduction of electrons and subsequent thermal equilibration with the lattice and dissipation of heat within a few picosecond (Link & El-Sayed 1999). However, repeated excitation of laser in nanosecond on AuNPs result in the built up of lattice internal energy which allows direct heating of the local environment. Therefore, the use of AuNPs as coupling agent for photothermal cancer therapy through the creation of localized heating effect that induce irreversible thermal cell damage through denaturation and coagulation of protein as well as membrane destruction.

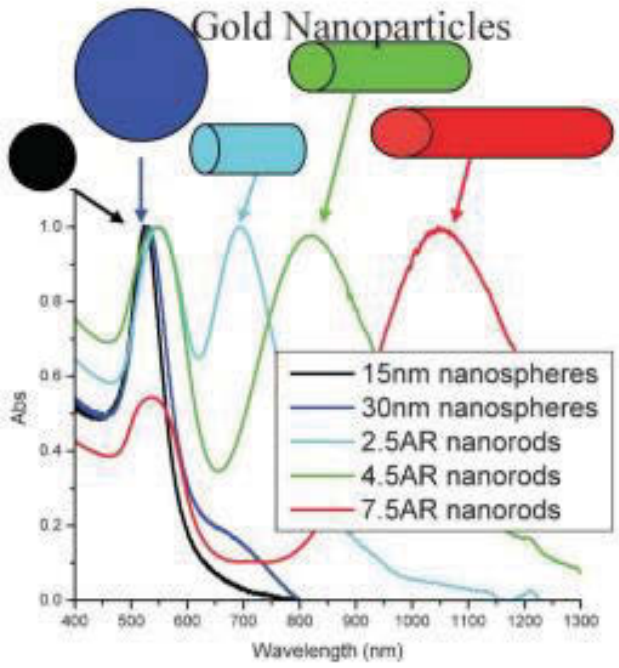

Figure 1.1 UV-VIS absorption spectra showing SPR bands and peaks for various sizes and shapes of AuNPs. Adapted from (Eustis & El-Sayed 2006).

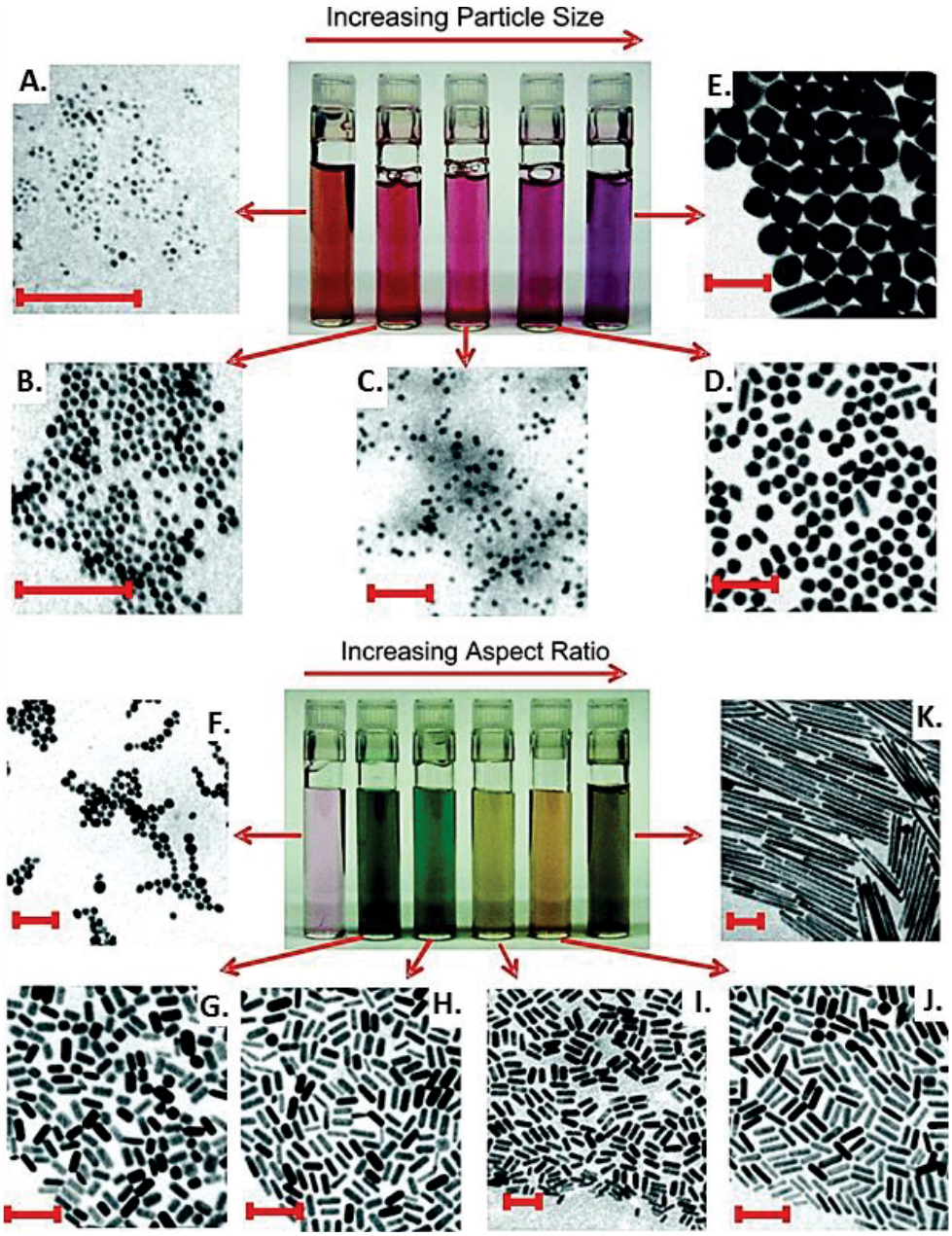

Figure 1.2 Transmission electron microscopy (TEM) images and colour intensity of various size and shaped colloidal gold

Photographs showing colorimetric difference of colloidal gold as a function of increasing size spherical-shaped AuNPs (upper panels) and increasing dimensions for rod-shaped AuNPs (lower panels). (A–E) corresponding TEM images of spherical-shaped AuNPs with increasing size 4 – 40 nm (F – K) corresponding TEM images of rod-shaped AuNPs with increasing aspect ratio from 1.3–20 and. Scale bars = 100 nm. Adapted from (Murphy et al. 2008).

1.2.4 Cellular uptake and toxicity of AuNPs

The interactions of nanoparticles at the cellular level with vital components including the membrane, mitochondria, nucleus, and proteins could induce adverse effects on biological system. These adverse outcomes such as damage to organelle or deoxyribonucleic acid (DNA), oxidative stress, cellular apoptosis, mutagenesis, and up/down-regulation of intracellular proteins characterized the *in vitro* and *in vivo* cytotoxicity of nanomaterials (Aillon et al. 2009; Alkilany & Murphy 2010; Unfried et al. 2007).

The size, shape, and surface charge of AuNPs all played a role in their facilitated cellular uptake and internalization which ultimately led to cellular toxicity (Connor et al. 2005; Mironava et al. 2010; Pernodet et al. 2006; Yen, Hsu & Tsai 2009; Zhang et al. 2011). Spherical AuNPs were more easily internalized and uptake by cells compared to rod shaped particles (Chithrani, Ghazani & Chan 2006b). Studies have shown that at a small size of < 5 nm, AuNPs can penetrate the cells and irreversibly bind to DNA; whereas larger diameter 15nm gold particles do not show cytotoxicity (Pan et al. 2007; Schmid 2008). AuNPs with charged surface of either positive or negative renders them highly reactive and cytotoxic to cell inducing mitochondria oxidative stress (Schaeublin et al. 2011).

Studies with the as synthesized citrate-coated AuNPs have shown cellular uptake without significant cytotoxicity (Chithrani, Ghazani & Chan 2006b; Connor et al. 2005; Khan et al. 2007) . However, nanoparticle size and shape as well as modification with antibodies or proteins change their cellular fate, uptake, metabolism and clearance (Chithrani, Ghazani & Chan 2006b; De Jong et al. 2008). Spherical “naked” AuNPs with a protective electrostatically-adsorbed layer of citrate ions have been shown to have a higher rate of cellular uptake compared to certain biomolecule-conjugated AuNPs (Chithrani, Ghazani & Chan 2006a; Chithrani, Ghazani & Chan 2006b).

Suspension of “naked” AuNPs in plasma or growth media supplemented with serum, results in the spontaneous adherence of protein from the growth media/plasma onto the surfaces of AuNPs. This corona of protein can in turn prevent the AuNPs from

aggregating in the biological media due to the presence of electrolytes with high ionic concentration, and it can also facilitate the process of cellular uptake (Lynch & Dawson 2008; Ojea-Jimenez & Puntes 2009; Vesaratchanon, Nikolov & Wasan 2007). Studies also showed that cellular uptake of AuNPs occurs via a receptor-mediated or non-receptor-mediated endocytosis or pinocytosis (Chithrani et al. 2009; Steirtman, Brodie & Cohn 1976). According to Cho et al. (2009 and 2011), cellular uptake of the AuNPs occurs in two steps: adsorption onto the membrane of the cell, followed by internalization by the cell (Cho et al. 2009; Cho, Zhang & Xia 2011). However, the rate of AuNPs internalization is dependent on their particle sedimentation rate and availability of AuNPs on cell surfaces.

Although there have been an extensive literature on the *in vitro* cytotoxicity, it is crucial to carefully examine the underlying methodology behind these studies to ensure that the results across laboratories are comparable. Most of the studies were performed *in vitro* due to its simplicity to provide a basis for understanding the underlying mechanism to which uptake of nanoparticles induces cellular toxicity using single cell line on culture plate. Therefore, the result from the two dimension *in vitro* cytotoxicity may not accurately predict the *in vivo* interactions in a complex physiological environment (Alkilany & Murphy 2010; Griffith & Swartz 2006).

1.2.5 Biological interactions of AuNPs *in vivo*

Toxicological studies in a whole organism is much more complex than a single cell due, therefore, assessments of nanoparticle safety should include general health indicators such as behavioural abnormality, weight loss, percent of mortality, change in fur conditions and average life span. It has been suggested that nanoparticle toxicological studies should be carried out at a tissue specific manner by characterization of hepatotoxicity (liver), nephrotoxicity (kidney), immunogenicity, haematological toxicity (blood), inflammatory, or oxidative stress markers (Alkilany & Murphy 2010). It is noteworthy that bio-distribution kinetics of AuNPs is dependent on the size, shape and route of nanoparticle administration. All organs of reticuloendothelial system are the basic primary target for accumulation of GNPs within the size range of 10 to 100 nm, and the uniformity of distribution increases with a decrease in particle size (Khlebtsov

& Dykman 2011). Rapid clearance of AuNPs in the blood into the liver and spleen which can remain there for long period of time before excretion may possibly led to tissue inflammation. For example, 40 nm AuNPs administered intravenously were eliminated via the reticuloendothelial systems through the liver with localization of AuNPs in lysosomes or endosomes of Kupffer cells which can persist there for as long as 6 months (Sadauskas et al. 2009; Sadauskas et al. 2007).

AuNPs has been presumed to not elicit any cytotoxic effects at concentrations relevant for the envisaged applications based upon their known low toxicity of bulk gold. Despite that, there has been discrepancy in the potential toxicity of AuNPs *in vitro* and *in vivo* depending on their size, surface modification, administration route or length of exposure. The biodistribution and toxicity of engineered gold nanoparticles *in vitro* and *in vivo* has been extensively reviewed (Khlebtsov & Dykman 2011). In the past 2 decades, the short-term and long-term toxicity and biocompatibility of spherical unmodified or "naked"AuNPs at a different size, surface modification, concentration and route of administration have been extensively investigated *in vivo* using small animals (Table 1.1). AuNPs can be tailored for different route of administration including injection via intravenous, intraperitoneal, subcutaneous, intramuscular, and tail vein (small animal) as well as orally ingested (Khlebtsov & Dykman 2011; Zhang et al. 2010).

Table 1.1 A summary of *in vivo* toxicity and biocompatibility studies using unmodified or modified AuNPs. Modified from (Zhang et al. 2010).

Routh of administration, animal model	Synthesis, surface coating, solvent	Size	Study period	Dose	Reference
Single dose injection					
Oral,BALB/c mice	Citrate sol, unmodified, water (2.5% maltodextrin)	4, 10, 28, and 58 nm	7 d	20 μg/g	(Hillyer & Albrecht 2001)
Tail vein, WU Winstar-rats	SPI Supplies, unconjugated, PBS	10, 50, 100, and 250 nm	24 h	0.077–0.12 μg/g	(De Jong et al. 2008)
Tail vein	Naked	15, 50, 100, and 200 nm	24 h	1 μg/g	Sonavane33
Tail vein, C57Bl/6 mice	PBS buffered	20 and 100 nm	24 h	1 μg/g	(Kim et al. 2009)
Intraperitoneal, C56Bl/6 mice	Citrate sol, unmodified, water	21 nm	1, 24, 72 h	7.85 μg/g	(Chen et al. 2013)
Intratracheal and intravenous, Wistar-Kyoto rats	Citrate sol, unmodified,	1.4 and 18 nm	24 h	0.054–0.53 μg/g	(Semmler‐Behnke et al. 2008)
Intravenous	Citrate sol, unmodified, water	20 nm	1 d, 1 wk, 1 and 2 mths	0.010 μg/g	(Balasubramanian et al. 2010)
Intravenous, C57BL/6 mice	Naked	2, 40 nm	1, 4, 24 h	0.6–3.2 μg/g	(Sadauskas et al. 2007)
Intravenous, C57BL/6 mice	Naked	2, 40 nm	1 d, 1, 3, and 6 mths	1.4–1.6 μg/g	(Sadauskas et al. 2009)
Continuous daily injection					
Intraperitoneal, BALB/C mice	Citrate sol, unmodified, PBS, pH 7.4	8, 12, 17, 37 nm	21 d	8 μg/g/week	(Chen et al. 2009)
Intraperitoneal, C57BL/6 mice	Citrate sol, unmodified, sodium citrate (1.2 mM)	12.5 nm	8 d	0.04,0.2,0.4 μg/kg/day	(Lasagna-Reeves et al. 2010)
Tail vein, oral, intraperitoneal, ICR mice	Citrate sol, unmodified, water, pH 7.2	13.5 nm	14, 28 d	0.1375-2.2 μg/kg/day	(Zhang et al. 2010)
Intraperitoneal, Albino mice (Diabetic)	Biologically synthesized, unmodified, water	50 nm	15 d	2.5 μg/g/day	(BarathManiKanth et al. 2010)
Intraperitoneal, Wistar rat	Citrate sol, unmodified, water	10 or 30nm	28 d	0.070 μg/g	(Ferreira et al. 2017)
Intraperitoneal, C56Bl/6 mice (Dietary obesity)	Citrate sol, unmodified, water	21 nm	8 weeks	0.785 and 7.85 μg/g	This work
Intraperitoneal, C56Bl/6 mice (Dietary obesity)	Citrate sol, unmodified, water	21 nm	5 weeks	0.0785, 0.785 and 7.85 μg/g	This work

1.3 Obesity

Obesity is defined as a disease in which the abnormal or excessive of lipid accumulation in fat tissue, to the extent that health is impaired. The body mass index (BMI) is commonly used as a graded classification for obesity, as it provides valuable insight on the extent of abnormal or excessive fat accumulation and monitor of increasing body fatness. In normal individuals with a sedentary lifestyle, BMI also serves as a good indicator of the variability in nutritional state and energy reserves, but not in athletes (WHO 1995). BMI is calculated by a person's body weight in kilograms divided by the square of his height in meters.

The measurements of waist circumference and waist-hip ratio are useful complementary method to BMI for the assessment of abdominal or central obesity. Table 1.33 showed the gender-specific the waist circumference and waist-to-hip continuum in adults recognized by the WHO (WHO 2008). However, the International Diabetes Federation suggested that it is important to account for the amount of body fat due to ethnic difference, proposing the ethnic specific waist circumference cut-off points of > 94 cm (men) for Europids; while > 90 cm (men) for South Asian, Chinese and Japanese (IDF 2006). Study by Han et al. (1995) suggested that clinicians should be alert of the potentially "increased" risk in metabolic complications such as cardiovascular disease for patients presenting a waist circumference greater than 94 cm (men) and 80 cm (women); while therapeutic action should be initiated for patients with waist circumference greater than 102 cm (men) and 88 cm (women) associated with "substantially increased" risk (Han et al. 1995).

Table 1.2Table 1.2 showed the international cut-off points of BMI for underweight, overweight, and obesity in adults determined by expert panels of the World Health Organization (WHO). Individuals with a BMI greater than or equal to 25 kg/m^2 is classified as overweight and at risk of obesity; while a BMI greater than or equal to 30 kg/m^2 is classified as obesity Although the body fatness in different populations may differ with different body proportions, the BMI continuum applies to both men and women at all adult age groups (NHLBI 1998; WHO 1995).

The measurements of waist circumference and waist-hip ratio are useful complementary method to BMI for the assessment of abdominal or central obesity. Table 1.33 showed the gender-specific the waist circumference and waist-to-hip continuum in adults recognized by the WHO (WHO 2008). However, the International Diabetes Federation suggested that it is important to account for the amount of body fat due to ethnic difference, proposing the ethnic specific waist circumference cut-off points of > 94 cm (men) for Europids; while > 90 cm (men) for South Asian, Chinese and Japanese (IDF 2006). Study by Han et al. (1995) suggested that clinicians should be alert of the potentially "increased" risk in metabolic complications such as cardiovascular disease for patients presenting a waist circumference greater than 94 cm (men) and 80 cm (women); while therapeutic action should be initiated for patients with waist circumference greater than 102 cm (men) and 88 cm (women) associated with "substantially increased" risk (Han et al. 1995).

Table 1.2 International BMI classification of underweight, overweight, and obesity for adults. Adapted from (NHLBI 1998; WHO 2015a).

	Graded classification	**BMI**
Underweight	Grade 1 (severe thinness)	<16.0
	Grade 2 (moderate thinness)	16.0–16.99
	Grade 1 (mild thinness)	17.0–18.49
Normal		18.5–24.99
Overweight (mild obesity)		25–29.99
Obesity	Grade 1 (moderate obesity)	30–34.99
	Grade 2 (severe obesity)	35–39.99
	Grade 3 (morbid obesity)	>40

Table 1.3 Waist circumferences and waist-hip ratio for adults predicts risk of metabolic complications. Adapted from (WHO 2008).

	Cut-off points	Risk in metabolic complications
Waist circumference	Men: > 94 cm Women: > 80 cm	Increased
Waist circumference*	Men: >102 cm Women: > 88 cm	Substantially increased
Waist-hip ratio	Men: ≥ 0.90 Women: ≥ 0.85	Substantially increased

In 2014, it is estimated that 39% which is more than 1.9 billion adults over 18 years and older globally were overweight (38% of men and 40% of women). Over 600 million of the adult population were obese which is more than doubled since 1980 (WHO 2014a, 2015b). The worldwide prevalence of overweight and obesity is increasing at an alarming rate in both developed and developing countries according to WHO in their recent global status report for non-communicable diseases (WHO 2014a). According to the Australian Bureau of Statistics, 63.4% of Australians aged 18 years and over were overweight or obese, comprised of 35.0% overweight and 28.3% obese in the Australian health survey 2011-12 (ABS 2012). In addition, the survey also noted that 60.3% of men and 66.6% in women aged 18 years and over had a waist circumference that put them at risk of developing chronic diseases including cardiovascular disease, type 2 diabetes and high blood pressure (ABS 2012). Therefore, the increase in overweight and obesity rates in recent decades is a major public health concern. Moreover, metabolic syndrome has also emerged as one of the major public health challenge worldwide associated with abdominal (central) obesity, dyslipidaemia, cardiovascular diseases, hypotension, and insulin resistance with/without glucose intolerance (Alberti et al. 2005; Grundy et al. 2004).

1.3.1 Role of adipose tissue

The abdominal fat is composed by two primary depots, subcutaneous and visceral (intra-abdominal) adipose tissue. Subcutaneous adipose tissues are located beneath the skin around the abdomen and in the periphery, accounts for 80% of total body fat in a healthy adult. Visceral fat are located in intra- and retroperitoneal region, represent about 10–20% and 5–10% of total body fat in men and women, respectively (Lafontan & Girard 2008). Adipose tissue is generally comprised of lipid-laden mature adipocytes and the stromal-vascular fraction including pre-adipocytes, fibroblasts, endothelial cells, and macrophages (Cawthorn & Sethi 2008; Heilbronn & Campbell 2008).

The adipose tissue has the ability to regulate energy and lipid homeostasis for maintenance of a relatively constant body weight (Yu & Ginsberg 2005). The main function of adipose tissue is lipid storage in our body providing long-term fuel reserve that can be mobilized when needed elsewhere. Excess energy was stored in the form of triglycerides, where energy is needed elsewhere in the body, was released in the form of fatty acid. Neutral lipids are stored in adipocytes in the form of lipid droplets, with a core of sterol esters and triacylglycerols (Goossens 2008; Yu & Ginsberg 2005). Lipid or triglyceride in the form of triacylglycerol cannot move across the cell membranes freely, they have to be breakdown by lipoprotein lipases into free fatty acids and glycerol. Long-term excessive dietary fat intake result in adipose tissue is overloaded with triglycerides to the extend where the adipocyte lipid storage has reached capacity not able to effectively store even more lipids.

1.3.1.1 Adipogenesis

Obesity if often characterized by the expansion of adipose tissue with an increased adipocyte size (hyperplasia) or increased number of adipocytes (hypertrophy) (Bays et al. 2008; Kershaw & Flier 2004). Adipocytes are the main cellular component making up to about 70% of adipose tissue and the mature adipocytes cannot divide (Cawthorn & Sethi 2008). Therefore, regeneration of adipocytes depends on the recruitment and terminal differentiation of pre-adipocytes or adipose-derived stem cells from

surrounding to form new fat cells. The process of new adipocyte formation through the differentiation of pre-adipocytes into mature adipocyte is known as adipogenesis.

Adipogenesis is a multi-step process involving a cascade of transcription factors such as peroxisome proliferator-activated receptor-γ (PPARγ), leading to formation of new adipocytes (Rosen et al. 1999; Rosen & Spiegelman 2000). In particular, PPARγ stimulation results in adipocyte differentiation to generate small adipocytes and insulin sensitivity. In obesity, the chronic excess dietary fatty acid and triglyceride leads to expansion of adipocytes to accommodate increased fat storage. Here in, further stimulation with PPARγ contribute to formation of hypertrophied adipocyte (Spiegelman 1998). Studies have shown that adipocyte hypertrophy during obesity have been associated with the development of systemic insulin resistance (Lönn et al. 2010). With the accumulation of fat, the adipocytes enlarge and undergo molecular and cellular alterations that affect systemic metabolism and trigger an inflammatory response (Stephens & Pekala 1991b).

1.3.1.2 Dysregulation of adipokines

Adipose tissue is a highly active endocrine tissue, and secretes a variety of bioactive factors through adipocytes (Kershaw & Flier 2004). The most studied are leptin and adiponectin for their role in appetite and energy homeostasis. It has been well established that adipose tissue is an endocrine organ where a variety of bioactive adipokine and hormones (e.g. leptin and adiponectin) are expressed and secreted by adipocytes (Kershaw & Flier 2004). In particular, leptin functions to regulate energy homeostasis via controlled food intake and energy expenditure (Shewan et al. 2000). Studies have shown strong association between the levels of circulating leptin and mRNA expression in adipose tissue with BMI and fat mass in the obese (Mironava et al. 2010). It is also noteworthy that both the expression and secretion of leptin are also regulated by other factors including insulin, TNFα, and free fatty acid. Adiponectin is a collagen-like protein produced and secreted exclusively by adipocytes. Plasma adiponectin concentration is reduced with increasing BMI in obesity, type 2 diabetes and coronary artery disease patients (Diez & Iglesias 2003; Matsuzawa, Funahashi & Nakamura 1999).

Long term HFD consumption leads to a chronic energy surplus and the expansion of adipocytes to handle excess lipid via the alteration in fatty acid metabolism (Gaidhu et al. 2010). This is evidenced by the defective carnitine palmitoyl transferase (CPT)-1α regulation of energy storage and fatty acids oxidative capacity (McGarry & Brown 1997). CPT-1α is a mitochondrial enzyme that mediates transport and uptake of FA through the binding to carnitine into mitochondria. In addition, CPT-1α is also essential for the β-oxidation of fatty acid mitochondria where dysregulation causes free fatty acid levels to elevate and fat accumulation in skeletal muscle and decreases the ability of muscles to oxidize fatty acid. The dysregulation of CPT-1a is commonly associated with the development of type II diabetes and insulin resistance (Dobbins et al. 2001).

Triglycerides are commonly stored in lipid droplets as the critical energy reservoir in the lipid storing adipocytes (Brown 2001). Triglycerides are commonly hydrolysed by intracellular lipases such as adipose triglyceride lipase (ATGL) into NEFA or free fatty acids, which are transported into the mitochondria by CPT-1α for fatty acid β-oxidation and energy production. Free fatty acid homeostasis in adipocytes is not only dependent on lipogenesis but also lipolysis (Bays et al. 2008). In chronic obesity, excess triglyceride storage in the fat tissue can up-regulate adipose ATGL to increase basal lipolysis (Gaidhu et al. 2010; Kosteli et al. 2010a). Consequently, the accumulation of adipose tissue macrophage (ATM) into the fat tissue is also increased, which promotes inflammatory responses in the adipose tissue by directly engaging toll-like receptors (TLR) to induce production of cytokines, such as TNFα and IL-6 (Kosteli et al. 2010a; Nguyen et al. 2007). As insulin resistance develops, there is a decreased insulin-mediated suppression of lipolysis where the impaired anti-lipolytic effect of insulin action led to increased activity of ATGL (Lönn et al. 2010).

During adipogenesis, insulin stimulates intracellular glucose transporter (GLUT)-4 protein translocation to the cell surface, thereby facilitating glucose uptake into adipocytes (Saltiel & Kahn 2001). In the absence of insulin stimulation, GLUT4 remains mainly in the cytoplasm but upon stimulation, GLUT-4 translocates from its intracellular location to the plasma membrane to facilitate glucose uptake into the adipocytes (Bryant, Govers & James 2002). The insulin responsiveness of GLUT-4 has

been shown to be significantly reduced in the adipose tissue of diabetic rats associated with the development of insulin resistance (Rosenbaum, Haber & Dunaif 1993).

1.3.2 Role of liver

The liver is a key metabolic organ that governs whole-body energy metabolism. Hepatocytes are the main cell type in the liver (~80%). They plays an important role in glycogen storage, plasma protein synthesis, and drug detoxification, it is a central organ for lipid metabolism. Liver acts as a hub connecting various metabolic tissues such as adipose tissue and the skeletal muscles (Rui 2014; van Herpen & Schrauwen-Hinderling 2008).

In the fed state, pancreatic β cells secret anabolic hormone insulin in response to an increase in blood glucose, which stimulates glycogen synthase thus increasing glycogen synthesis and suppressing breakdown of glycogen or glycogenolysis. Hepatocytes gluconeogenesis is the primary source of endogenous glucose production. In fasted state and during exercise, the catabolic hormone glucagon release of glucose from glycogen stored in the liver into the circulation and metabolized by muscle and adipose tissue. Phosphoenolpyruvate carboxykinase (PEPCK) is one of the essential gluconeogenic enzymes and forkhead box (FOX)-O1 a key transcription factor for hepatic glucose biogenesis and regulation of blood glucose (Chakravarty et al. 2001; Purushotham et al. 2009). During prolonged fasting, glycogen is depleted, and PEPCK in hepatocytes can stimulate glucose synthesis through de novo gluconeogenesis using lactate, pyruvate, glycerol, and amino acids. leading to de novo gluconeogenesis (Rui 2014).

1.3.2.1 Ectopic lipid deposition and insulin resistance

Ectopic lipid deposition is defined as excess storage of fat in peripheral non-adipose tissue that normally contain only small amounts of fat such as liver, skeletal muscles, heart, kidneys, and pancreas. This deposition of excess lipid in surrounding tissues is due to increase basal lipolysis in adipose tissue leading to elevated levels of intracellular and plasma free fatty acid in chronic obesity (Donnelly et al. 2005; Krawczyk, Bonfrate & Portincasa 2010). Lipid accumulation in non-adipose cells may ultimately impair

normal organ function leading to cell dysfunction or cell death, also known as lipotoxicity (Schaffer 2003).

During obesity, the liver is highly susceptible in ectopic fat and lipid deposition with the infiltration of fat into hepatocytes promoted by the influx of free fatty acid from the circulation and decreased fatty acid β-oxidation, ultimately increasing de novo lipogenesis leading to triglyceride accumulation (Browning & Horton 2004). The long-chain fatty acids are incorporated into triacylglycerol, phospholipids, and cholesterol esters in hepatocytes, and stored in the lipid droplets and membrane structures, or secreted into the circulation as very low density lipoproteins. Studies have shown that morbidly obese patients consuming a high fat diet leads to the ectopic lipid deposition in liver contributed to steatosis and liver insulin resistance, leading to the pathogenesis of type 2 diabetes, non-alcoholic fatty liver disease, and cardiovascular disease (Gaggini et al. 2013; Musso, Gambino & Cassader 2010; Perlemuter et al. 2007; Sanyal et al. 2001).

A major cause of liver steatosis, also known as fatty liver disease, is increased fatty acid flux to the liver, which is promoted by a high availability of plasma free fatty acids in relation to peripheral oxidative requirements(Roden 2006). Cellular lipogenesis is controlled by a family of membrane-bound transcription sterol regulatory element binding protein (SREBP)s localized in the endoplasmic reticulum as a precursor protein after synthesis (Reddy & Rao 2006; Roden 2006). SREBP-1c may be selectively involved in activation of genes in free fatty acid metabolism. SREBP-1c in liver and adipose tissues play a central role in the regulation of downstream lipogenic genes, while fatty acid synthase (FASN) is involved in de novo lipid synthesis and fat deposition in mammals (Wakil, Stoops & Joshi 1983). Studies have shown that pro-inflammatory cytokines released by macrophages can stimulate hepatic SREBP-1c overexpression and FASN activation leading to liver steatosis and impaired insulin sensing (Meek, Urieli-Shoval & Benditt 1994; Shimomura et al. 1999).

1.3.3 Adipose tissue macrophages (ATMs)

Macrophages can be classified based on their specific function covering host defence, wound healing, and immune regulation (Mosser & Edwards 2008). Pro-inflammatory (M1) macrophage cells are characterised as pro-inflammatory cells that are key players in host defence processes; while anti-inflammatory (M2) macrophage cells have an anti-inflammatory profile and are principally involved in wound healing and tissue repair processes (Lumeng et al. 2008; Nathan 1987). Macrophages are well-known as a source of pro-inflammatory cytokines, which are released upon engulfing a foreign particle (Nathan 1987).

In adipose tissue, the stromal-vascular fraction contains numerous metabolically relevant cell types including pre-adipocytes, fibroblasts, endothelial cells, smooth muscle cells, leukocytes, and macrophages (Cawthorn & Sethi 2008; Heilbronn & Campbell 2008). Apart from the adipose tissue resident macrophages (ATMs), a pro-inflammatory response can also be initiated by a variety of surrounding cells in the adipose tissue (e.g. adipocytes, fibroblasts or endothelial cells) which are also capable of producing pro-inflammatory cytokines (Coppack 2001; Watkins, Maier & Goehler 1995).

In most healthy non-obese humans, the ATMs exhibit an anti-inflammatory M2 phenotype that act to protect against adipocyte inflammation, as well as, involvement in the regulation of insulin sensitivity by the adipocytes (Lumeng et al. 2008; Mosser & Edwards 2008). During obesity, the phenotype of the ATMs progressively changes from an anti-inflammatory M2 phenotype to a pro-inflammatory M1 phenotype (Lumeng et al. 2008). Adipose tissue from lean individuals contains 5–10% of ATMs, while the ATMs located in the adipose tissue of the obese can make up as much as 50–60% of adipose stromal cells (Sárvári et al. 2015; Sorisky, Molgat & Gagnon 2013). There is growing evidence that these ATMs with an M1 phenotype contribute to significantly elevated local and systemic pro-inflammatory cytokine levels and to a chronic low-grade inflammation state within the expanded fat mass (Cinti et al. 2005; Mosser & Edwards 2008; Weisberg et al. 2003). This increase in pro-inflammatory cytokines, in particular, tumor necrosis factor (TNF)-α and (interleukin) IL-6 have been correlated

with increased adiposity especially visceral fat mass in obesity, contributing to the onset of obesity-related metabolic disorders such as insulin resistance and resulting hyperglycaemia (Heilbronn & Campbell 2008; Hotamisligil, Shargill & Spiegelman 1993a).

TNFα expression was found to be positively correlated with body mass index (Rosenson et al. 2004b). TNFα can stimulate lipolysis and increase circulating free fatty acid levels *in vivo* and *in vitro* (Hauner, Petruschke, Russ, Rohrig, et al. 1995; Kawakami et al. 1987; Souza et al. 1998). TNFα was shown to reduce free fatty acid transporter expression in the fat, and decrease the uptake of fatty acids to form fat cells via the inhibition of extracellular activity of lipoprotein lipase, thereby contributing to hyperlipidemia (Cornelius et al. 1988b; Hauner, Petruschke, Russ, Rohrig, et al. 1995; Semb et al. 1987a). TNFα plays a key role in insulin resistance by interfering with insulin receptor signalling. TNFα inhibits expression and translocation of GLUT-4 in adipocytes, reducing glucose uptake in fat tissue (Stephens & Pekala 1991a; Uysal et al. 1997). Pro-inflammatory, IL-1β cytokine release is incresed during obesity in response to increased fatty acid levels, which causes insulin resistance via TNFα dependent and independent mechanisms(Stephens, Lee & Pilch 1997). IL-6 levels are also positively correlated with fasting plasma glucose levels and insulin resistance (Bastard et al. 2000a). Plasma IL-6 concentration and adipose IL-6 protein levels are increased in obese subjects, while weight loss due to very low calorie diet can reverse them(Bastard et al. 2000a).

Additionally, ATMs produce platelet-derived growth factor, an angiogenesis promoter (Pang et al. 2008). As the growth of adipose tissue is dependent on angiogenesis, the increase in ATM derived platelet-derived growth factor during obesity may contribute to the increased number of adipocytes (Christiaens & Lijnen 2010), which can enhance the capacity of fat storage, resulting in increased fat mass.

1.4 Current treatment for obesity

In 2001, it has been reported that the medical care cost of obesity account for 5.5–7.0% of national health expenditures in the U.S. and this percentage is rising (Thompson &

Wolf 2001). In 2005, it has been estimated that a total of $21 billion has been spent on treatment and management of overweight and obesity at $6.5 billion and $14.5 billion, respectively in Australia (Colagiuri et al. 2010). There are many benefit of weight loss and early prevention for both overweight and obese patient, including the lowering blood glucose, blood lipid, blood pressure, prevent, and delay the onset of obesity-related metabolic diseases.

1.4.1.1 Pharmaceutical interventions

To date, there are five long term anti-obesity medications approved by the U.S. Food and Drug Administration, namely Orlistat (Xenical®, approved in May 1998 and Alli®, approved in February 2007), Lorcaserin (Belviq®, approved in June 2012), Phentermine-Topiramate (Qysmia®/Qnexa®/Qsiva®, approved in July 2012), Naltrexone-Bupropion (Contrave®, approved in September 2014), and Liraglutide (Saxenda®, approved in December 2014)(Bray & Ryan 2014). The Therapeutics Goods and Administration in Australia have approved only two of the five anti-obesity drug to assist with weight loss. As shown in Table 1.4, the approved use of anti-obesity drug Orlistat (Xenical® in 2000 and Alli® in 2007) is available over the counter and recently approved Liraglutide (Saxenda® in 2016) is available with medical prescription (Lee & Dixon 2017; Sweeting & Caterson 2017; TGA 2016). At present, several medications are yet to be approved by the Therapeutic Goods and Administration for weight loss have been used off-label in Australia to treat obese individuals with caution (Lee & Dixon 2017).

Table 1.4 Pharmacotherapy used in obesity management in Australia. Adapted from (Lee & Dixon 2017).

Drug	Starting dose	Available doses	Weight loss versus placebo (% or kg)	Side effects	Contraindications
Phentermine	15 mg	15, 30, 40 mg	3.6–4.5 kg at six months	Dry mouth, insomnia, agitation, constipation, and tachycardia	Severe hypertension, cardiovascular disease, glaucoma, history of drug or alcohol abuse, monoamine oxidase inhibitors, selective serotonin reuptake inhibitor use, pregnancy
Orlistat	120 mg TDS	120 mg	2.9–3.4% at one year	Steatorrhea, oily spotting, flatulence with discharge, faecal incontinence, fat-soluble vitamin malabsorption	Pregnancy
Liraglutide	0.6 mg	0.6–3.0 mg	5.4% at one year	Nausea, vomiting, diarrhea, constipation Rare: Pancreatitis, cholecystitis	Severe renal or hepatic insufficiency, pregnancy, past history of pancreatitis and major depression or psychiatric disorder
Off-label pharmacotherapy (not approved by Therapeutic Goods Administration for weight loss)					
Topiramate	12.5 mg	25, 50, 100 mg	3.4–5.0 kg	Paraesthesia, dry mouth, constipation, altered taste sensation, insomnia, dizziness, cognitive effects Rare: Closed angle glaucoma, depression or suicidal	Side effects of phentermine and topiramate
Phentermine - Topiramate	Phe: 15 mg; Top: 12.5 mg	Phe: 15 mg; Top: 12.5, 25, 50, 100 mg	5.0–6.6% at one year	Side effects of phentermineand topiramate	Contraindications to phentermine or topiramate

Monotherapy anti-obesity drug, Orlistat, is an inhibitor of pancreatic and gastrointestinal lipases, prevents the absorption of approximately 30% of dietary fat (Guerciolini 1997; Shi & Burn 2004). Orlistat can breakdown triglyceride, lowering the low-density lipoprotein and cholesterol levels independent of weight loss. This in turn reduce the progression to a diabetic state, and leads to better glycaemic control in overweight and obese patients with diabetes. Prolong use of Orlistat lead to side effects and impair absorption of fat-soluble vitamins or supplements with small amount of weight loss are negative aspect of this over the counter medication (Daneschvar, Aronson & Smetana 2016; Guerciolini 1997).

Liraglutide is a glucagon-like peptide-1 (GLP1) analogues, an injectable weight loss medication primary used to treat type 2 diabetes and demonstrated beneficial weight loss in obese patients (Guerciolini 1997; Ioannides-Demos, Piccenna & McNeil 2010). Liraglutide has a dual mechanism of action signal from the gastrointestinal tract to increase the secretion of leptin, result in the side effect of suppressed appetite, reduced energy intake and subsequent weight loss(Ioannides-Demos, Piccenna & McNeil 2010;

Vilsbøll et al. 2007). The common side effects of liraglutide are mostly gastrointestinal in nature, however, it has been shown that this medication has the strongest evidence base for cardiovascular safety (Lee & Dixon 2017).

Lorcaserin is a selective agonist of the serotonin activating (5-hydroxytryptamine) 2C receptor to control fat and caloric intake leading a suppressed appetite. Lorcaserin appears to be more effective with short-term treatment but slowly loses its ability to maintain long-term weight loss with risk of cancer, not recommended for women with known risk factors for breast cancer. Polytherapy anti-obesity drug, with phentermine as an anorectic agent and the antiepileptic drug Topiramate which acts on appetite regulation However, this combination therapy was rejected in Europe due to safety concerns and the clinical trials showed intolerable adverse effect in Australia (Lee & Dixon 2017). Another polytherapy anti-obesity drug, naltrexone-bupropion has an effect of reduced hunger, motivation of feeding, and the palatability of eating. This is a due to the naltrexone that as an opioid antagonist, whilst bupropion activates the dopamine and noradrenaline reducing cravings for nicotine(Daneschvar, Aronson & Smetana 2016). This treatment result in a larger degree of weight loss than orlistat, and its common effect profile is small.

In the past decade, the U.S. Food and Drug Administration have withdrawn several once promising weight-loss drugs due to various adverse side effects. For example, Aminorex has shown to cause pulmonary hypertension, fenfluramine and dexfenfluramine caused valvulopathy, phenylpropanolamine caused stroke, rimonabant consequence in suicidal ideation and behavior), and sibutramine lead to myocardial infarction and stroke (Colman et al. 2012; Ioannides-Demos, Piccenna & McNeil 2010). Many newly discovered and phase III clinical trial therapeutic agents were also hastily terminated due to unacceptable side effects (Colman et al. 2012). In addition, several anti-obesity drugs has also been discontinued if patients do not achieve a reduction of more than 4% of initial body weight after 12 weeks, due to potential side effects. At present, pharmaceutical companies have focused in many new and emerging classes of anti-obesity drugs in the hope of developing novel candidates for anti-obesity programs.

1.4.1.2 Surgical intervention

Obesity treatment through bariatric surgery such as gastrointestinal Roux-en-Y bypass, has been shown to be the only clinical and cost effective long-term weight loss strategy (Frandsen, Pedersen & Richelsen 1998; Picot et al. 2009). Roux-en-Y gastric bypass surgery restricts food intake by creating a small stomach pouch and surgically attaching a portion of the jejunum that allows food to bypass most of the gastrointestinal tract. Studies have shown alterations in secreted hormones, significantly improve glucose regulation and the perception of both hunger and satiety following such surgery (Buchwald et al. 2004; LeBlanc et al. 2011). This procedure however is often reserved for patients that are morbidly obese, as a last resort due to its complications which frequently require further follow up surgery (Buchwald et al. 2004; LeBlanc et al. 2011; Rubino et al. 2004; Tice et al. 2008; Whitson et al. 2007). After the surgery, the risk of obesity comorbidity and mortality are significantly reduced, particularly death from diabetes, cardiovascular disease, and cancer (Adams et al. 2007; Kral & Näslund 2007). Given these positive outcomes, alternative treatment strategies are urgently needed which facilitate an effective and sustained weight loss for patients with moderate or less severe obesity, which are not prioritized for such invasive surgical interventions.

1.5 Rationale of study

In a previous study from our group, we injected unmodified spherical citrate-stabilized AuNPs of 21 nm diameter into lean mice. (Chen et al. 2013). We found that the AuNPs accumulated rapidly in the abdominal fat tissue after a single intraperitoneal injection. C56Bl/C mice treated with AuNPs showed significant reduction in fat tissue compared to control mice, along with a reduced mRNA expression of the pro-inflammatory cytokines, TNF-α and IL-6, measured from the abdominal fat tissue (Chen et al. 2013) This is of great interest, as these two cytokines have been frequently linked to the comorbidities related to obesity. Several studies have also reported similar weight loss as a side effect from AuNPs exposure (BarathManiKanth et al. 2010; Zhang et al. 2010). However, our group was the first to envisage the potential application of

unmodified spherical 21 nm AuNPs in the treatment of obesity-related metabolic disorder (Chen et al. 2013).

1.5.1 Inhibition of ATMs reduces insulin resistance and fat mass

Interventions to reduce ATM recruitment were shown to partially protect mice from obesity-induced insulin resistance(Weisberg, Hunter, Huber, Lemieux, Slaymaker, Vaddi, Charo, Leibel & Ferrante 2006), while inhibition of ATM cytokine release was shown to increase lipolysis, thus reducing fat mass and improved insulin sensitivity in obese mice (Kosteli et al. 2010b; Schenk, Saberi & Olefsky 2008a). Neutralisation of circulating TNFα, can increase insulin sensitivity and glucose uptake in peripheral tissues (Hotamisligil 2006b; Hotamisligil, Shargill & Spiegelman 1993b), highlighting an important role of ATM inflammatory cytokine release in insulin resistance and glucose intolerance. Thus ATMs represent a promising target for reducing fat mass and improving insulin resistance and subsequent glucose metabolism in obesity.

1.5.2 Aims of thesis

The objective of this research work is to develop AuNPs as novel therapeutic agent for the treatment of obesity. *In vitro* and *in vivo* studies were employed to study the impact of AuNPs on high-fat diet induced obesity in mice and anti-inflammatory effects on adipose tissue macrophage. In particular, we investigated the potential role of AuNPs in the suppression of the pro-inflammatory cytokine secretion from the human macrophage-like cells *in vitro*. It remains unclear whether AuNPs can directly affect the cytokine release from the adipocytes (fat cells) or ATMs that contribute to a reduced cytokine expression in the fat tissue *in vivo*. It is also unknown whether AuNPs can cause changes in cytokine release by macrophages in the fat tissue *in vivo*. It is also unknown whether AuNPs can cause changes in cytokine release by macrophages in the peritoneal cavity surrounding the fat tissue, which may in turn affect cytokine production by the fat cells themselves. Therefore, both *in vitro* and future *in vivo* studies will be carried out to address these questions.

<u>The specific aims of this study are:</u>

Aim 1: To synthesize and characterize AuNPs and investigate their toxicity and uptake by cells, addressed in Chapter 2

Aim 2: investigate whether the *in vivo* effect of AuNPs to reduce inflammatory cytokine production in fat tissue is via a macrophage-dependent mechanism, addressed in Chapter 3

Aim 3: To investigate whether AuNP treatment on can cause fat loss and improve glucose tolerance in mice fed a high fat diet (HFD) to induce obesity, addressed in Chapter 4

Aim 4: To investigate whether AuNP treatment on can cause fat loss and ameliorate obesity-related metabolic disorders in obese mice with existing metabolic disorders, addressed in Chapter 5

CHAPTER 2

Gold Nanoparticle Synthesis, Surface Modification and Characterization for Use In Vitro *Cell and* In Vivo *Animal Studies*

2. Gold nanoparticle synthesis, surface modification and characterization for use in *in vitro* cell and *in vivo* animal studies.

2.1 Introduction

Neovascularization or the formation of new blood vessels is an important natural process occurring in biological systems as a result of vasculogenesis and angiogenesis (Bauer, Bauer & Velazquez 2005; Patan 2004; Stavrou 2008). The process of vasculogenesis is limited to the embryonic development stage where endothelial progenitor cells are recruited and differentiated into mature endothelial cells to form capillaries, arterioles and venules (Stavrou 2008; Tepper et al. 2005). Angiogenesis is the subsequent branching and remodeling of the vasculatures, forming the vascular network during development (Hirschi & D'Amore 1997). Overt angiogenesis is limited to the female ovulation cycle for the formation of the corpus luteum and during pregnancy for placenta development (Phillips et al. 1990; van Hinsbergh, Koolwijk & Hanemaaijer 1997). In healthy adults, angiogenesis generally occurs in a tightly-controlled manner in association with wound healing and restoring blood flow to tissues after injury (Folkman 1995; Folkman & Shing 1992; Hirschi & D'Amore 1997). Uncontrolled angiogenesis, in contrast, contribute to diverse pathological conditions such as obesity, diabetic retinopathy, asthma, solid tumor growth, and atherosclerosis; while the lack of angiogenesis underlies many medical issues including heart and brain ischemia, neurodegeneration, hypertension, and endometriosis (Aiello et al. 1994; Carmeliet 2003; Hirschi & D'Amore 1997; Patan 2004; Tahergorabi & Khazaei 2013).

Among all tissues, adipose tissues are highly vascularised with each adipocyte enclosed by one or more capillaries (Cao 2010; Lemoine, Ledoux & Larger 2013). Unlike other organs, adipose tissue displays higher level of plasticity and retains the potential to expand and regress throughout the entire lifetime under different nutritional conditions (Sun, Kusminski & Scherer 2011). A functional adipose vascular network is critical for the supply of nutrients, oxygen, growth factors, hormones, and cytokines to adipose tissue as well as waste product removal. These vasculatures is also crucial for the recruitment of circulating progenitor cells into the expanding adipose tissue to differentiate into adipocytes and endothelial cells as well as the means of inflammatory

cell infiltrate (Leinonen et al. 2003; Tahergorabi & Khazaei 2013). Neovascularisation through the processes of angiogenesis is critical and has been considered to be a rate-limiting step for adipose tissue expansion (Sun, Kusminski & Scherer 2011). Studies have shown that modulation of angiogenesis has the potential to impair the development of obesity. Therefore, alteration of the interaction between adipocytes and their blood vessels is an obvious target for the treatment of obesity.

In the present project, we proposed the use of unmodified (citrate-coated) AuNPs and preparation of a novel hetero-bifunctional PEGylated AuNPs, also termed monolayer-protected cluster (MPC) for targeted labelling of blood vessels. Anti-CD31 is an endothelial cell marker for which has been widely used for blood vessel detection and evaluation of angiogenesis, since they not only react with newly formed vessels but also with normal vessels (Sauer et al. 2005). We aim to conjugate anti-CD31 onto the surfaces of MPCs to study their cellular target labelling of endothelial cells in adipose tissue. Due to the limited in vitro models of endothelial cells, bovine aortic endothelial cells (BAEC) and human coronary artery endothelial cell (HCAEC) were used to study the effect of unmodified AuNPs and anti-CD31-conjugated MPCs target accumulation and toxicity.

2.2 Methods

All glassware and apparatus used in the preparation of gold nanoparticles were etched in aqua regia overnight in fume cupboard and then thoroughly rinsed three times with Milli-Q water (18.2 MΩ·cm) following by drying in an 80ºC oven overnight. Aqua regia solution consist of 3 parts of concentrated hydrochloric acid (37% HCl, ACS grade, BDH, Sturgeon Bay, WI, USA) and one part of concentrated nitric acid (69% HNO_3, ACS grade, BDH, Sturgeon Bay, WI, USA), is highly corrosive and handled using double gloves. Cleaning of surfaces using aqua regia removes any potentially interfering ionic residues and contamination that would disrupt or interfere with the Au colloids formation.

2.2.1 Preparation of tetrachloroauric acid ($HAuCl_4$) stock solution

Tetrachloroauric acid ($HAuCl_4$) starting solution was prepared for gold nanoparticles synthesis (Hiller & Erich 1999; Xu, Stevens & Cortie 2004). Briefly, 9.85 g of 99.99% pure Au pellets were dissolved in 80 mL of aqua regia ($HCl:HNO_3$ 3:1 v/v) and the solvent was heated under vacuum aspiration in water bath (Figure 2.1A). The dissolution of solid gold in aqua regia resulted in the formation of aqueous chloroaurate ($[AuCl_4]^-$) and NO_2 gas were removed under vacuum aspiration. Following that, the $HAuCl_4$ solution was further heat reduced twice with 80 mL of concentrated 37% HCl in the same manner under vacuum aspiration in order to remove residual HNO_3. Decomposition of HNO_3 in excess HCl resulted in formation of volatile nitrosyl chloride (NOCl) which can be further decompose into nitric oxide (NO) as shown in Figure 2.1B. Furthermore, NO reacts readily with atmospheric oxygen resulting in the formation of NO_2 gas. As the chlorine (Cl_2) and NO_2 gaseous formed was vacuum aspirated. The synthesis yields a concentrated viscous thick yellow solution (≈ 15 mL) which was cooled to room temperature, and then diluted to 500 mL in a volumetric flask to give 0.1 M $HAuCl_4$ stock solution (Figure 2.1C). It is accepted that some residual HCl content will have been present in the solution.

A.

C.

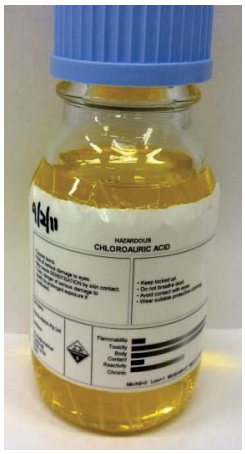

B.

Aqua regia decomposition of gold

$$Au\ (s) + 3\ HNO_3\ (aq) + 4\ HCl\ (aq) \rightarrow [AuCl_4]^-\ (aq) + 3\ NO_2\ (g) + [H_3O]^+\ (aq) + 2\ H_2O\ (l)$$

Decomposition of residual HNO_3

$$HNO_3\ (aq) + 3\ HCl\ (aq) \rightarrow NOCl\ (g) + Cl_2\ (g) + 2\ H_2O\ (l)$$

$$2\ NOCl\ (g) \rightarrow 2\ NO\ (g) + Cl_2\ (g)$$

$$2\ NO\ (g) + O_2\ (g) \rightarrow 2\ NO_2\ (g)$$

Figure 2.1 Preparation of $HAuCl_4$ stock solution

(A) laboratory set up for the dissolution of 99.99% pure solid gold in aqua regia under vacuum aspiration and heating in water bath; (B) as-prepared $HAuCl_4$ stock solution showing characteristic faint yellowish colour. (C) removal of NO_2 and Cl_2 gaseous formed under vacuum aspiration favours the dissolution of gold to chloroaurate.

2.2.2 Preparation of spherical citrate-coated AuNPs

Spherical AuNPs with a hydrodynamic diameter between 16–147 nm can be synthesized when the trisodium citrate-to-gold ratio was varied via the citrate sol method described by Turkevich, Stevenson, and Hillier (1951) and Fren (1973) (Frens 1973; Turkevich, Stevenson & Hillier 1951). In this study, spherical citrate-coated AuNPs with a size ranging between 20–30 nm were synthesized (Chen et al. 2013; Pissuwan et al. 2007). Briefly, 1 mM of $HAuCl_4$ starting solution (5 mL of a 0.1 M of $HAuCl_4 \cdot 3H_2O$ stock in 500 mL H_2O to give a faintly yellowish solution) was brought to roiling boil and thoroughly mixed on magnetic hotplate. Upon boiling, 50 mL of 38.8 mM tri-sodium citrate (Sigma Aldrich, St. Louis, MO, USA) dissolved in Milli-Q water was quickly added and vigorously stirred for 15 min. Upon the addition of tri-sodium citrate solution, the colour of the faith yellowish $HAuCl_4$ stock solution (0 sec) rapidly changed to clear blue (30 sec), then to grey followed by a dark purple appearance (60 sec), and finally lightened to the characteristic deep wine red or burgundy colour (120 sec).

Figure 2.2 showed the reduction of $HAuCl_4$ through oxidation of citrate to dicarboxyacetone, which forms intermediate bidentate complexes and atomic Au(0), changing the reaction mixture from faith yellow to clear blue. As the concentration of Au(0) increases until supersaturation, nucleation is initiated at which point gold atoms gather into clusters to form seeds or nuclei. Following that, aggregation occurs during the process of nucleation forming large particles demonstrated by the dark purple colour of the solution. Further disproportional reaction of Au(I) took place on the nuclei caused particle growth and re-dispersion into nanospheres until all Au(0) are removed from the solution. The formation of the Au colloids gives the suspension its characteristic burgundy colour. However, in the presence of metal or ionic contaminations the aggregation of atomic gold during nucleation will be permanent yielding thin sheets of gold in suspension.

This is a simple and robust methodology to produce modestly monodispersed spherical AuNPs dispersed in water. The citrate ions acts as a reducing agent at the beginning of the reaction but later adsorbed onto the surface of AuNPs to give an overall negatively–

charged protective capping, which stabilizes the suspension from aggregation. Milli-Q water was added to the cooled colloidal Au sol as necessary to bring the volume back up to 500 mL (to account for evaporation) using a volumetric flask and stored at 4°C. Various advance material techniques were employed to characterize the as synthesized size, surface charge, concentration, biochemical and optical properties of AuNPs. In this study, AuNPs spherical, 22 nm in size, SPR peak of 520 nm, with a nanoparticle concentration of ~2 nM (ICP-MS) were prepared.

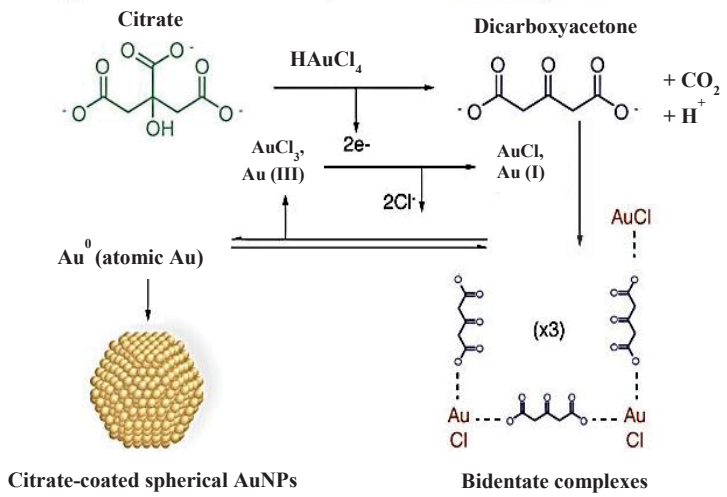

Figure 2.2 The Turkevich/Fren citrate sol method for preparation of spherical AuNPs

In the presence of $HAuCl_4$ and heating to boiling point, $[AuCl_4]^-$ was reduced to AuCl or Au(I) through oxidation of citrate to dicarboxyacetone. The Au(I) then forms a bidentate complex with dicarboxyacetone, which undergoes a disproportionation reaction to form $AuCl_3$ or Au(III) and atomic Au(0). Nucleation of Au(0) caused particle growth until all Au(0) are removed from the solution, followed by rapid re-dispersion into gold nanospheres. Adapted from (Dreaden, Austin, et al. 2012).

2.2.3 Direct conjugation of biomolecules onto AuNPs

Biomolecules such as bovine serum albumin (BSA) or antibodies can be conjugated to AuNPs through the physisorption or binding to the surfaces of AuNPs as previously published (Pissuwan et al. 2007). The direct conjugation of BSA or antibodies spontaneously forms protein corona as illustrated in Figure 2.3. The pH of the as-synthesized citrate-coated AuNPs was adjusted to 7.5 using 0.5 M of potassium hydroxide solution for all biomolecule conjugation studies. Briefly, 200 µL of BSA (1 mg/mL, Fraction V, A7888, Sigma Aldrich, St. Louis, MO, USA) was added to 1 mL of AuNPs (~2 nM) at pH 7.5 and incubated for 10–15 min at 37ºC. Then, the BSA-conjugated AuNPs can be purified via centrifugation at 13000 rpm for 30 mins to remove excess BSA and re-suspended in 10mM or 0.1 mM pf phosphate buffer saline (PBS). Similarly, antibody-conjugated AuNPs can be prepared by mixing excess of monoclonal mouse anti-human CD31 (0.5 mg/mL, M082329, DakoCytomation, Braeside, VIC, Australia) or monoclonal mouse anti-human CD11b (Mac1) (0.3 mg/mL, 555386, BD Biosciences to 1 mL of AuNPs. However, there are many limitations in the direct conjugation system due to the equilibrium and loss of antibody to the surrounding medium from the particle surfaces which lead to their instability in solvents with high ionic strength.

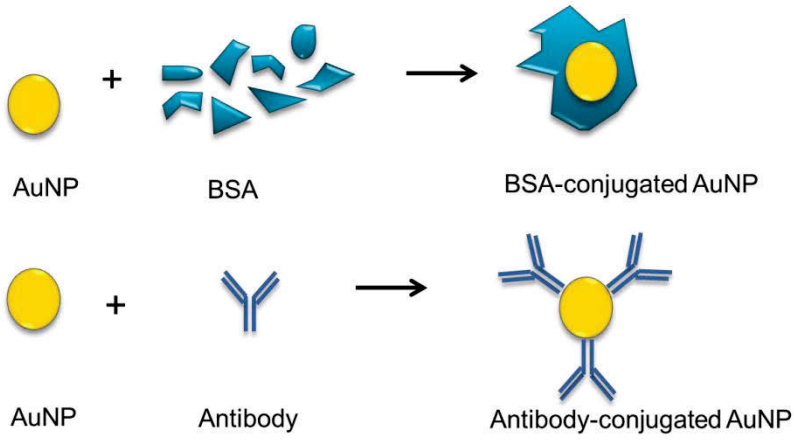

Figure 2.3 Schematic showing direct physisorption of BSA and antibodies, forming protein corona onto AuNP surfaces.

2.2.4 Preparation of MPCs

MPCs were prepared via monolayer self-assembly of mixed hetero-bifunctionalized PEGs with previously published method with modifications as illustrated in Figure 2.4A (Craig et al. 2010). Two length of PEG were chosen for this study, short-chained (MW=380–530) and long-chained (MW=5000). The MPCs in this study were specifically engineered with a mixture of functional end, as the highly reactive –COOH end can be easily activated for antibody conjugation but not the –OH or $–CH_3$ ends (Figure 2.4B). The short-chained PEGs, HS-PEG_{530}-COOH (TH003-m11.n6-1) and HS-PEG_{380}-COOH (TH001-m11.n4-1) were purchased from ProChimia Surfaces, Sopot, Poland. The long-chained PEGs, HS-PEG_{5000}-COOH (PEG3-004, MW5000) and HS-PEG_{5000}-CH_3 (PEG3-0021, MW5000) were purchased from Nanocs Inc., New York, NY, USA).

AuNPs were then mixed with an increasing PEG:nanoparticle mole ratio of 1000:1, 2500:1, 5000:1, 10000:1, 25000:1 and 50000:1 of to determine the optimal ratio of PEG molecules required to form a protective monolayer on the gold surfaces for both short-chain and long-chain PEGylation. In addition, an increasing percentage ratio of the mixed heterobifunctional PEGs were examined. Stock solutions, 19.49 mg/mL of HS-PEG_{530}-COOH, 14.07 mg/mL of HS-PEG_{380}-COOH, 185 mg/mL of HS-PEG_{5000}-COOH, and 185 mg/mL of HS-PEG_{5000}-CH_3 (PEG3-0021, MW5000) were prepared.

All MPCs prepared and studied in this chapter were listed in

Table 2.1. Briefly, 1 mL of the citrate-stabilized AuNPs was purified by centrifugation at 10500 rpm for 30 min, room temperature to remove excess citrate. The supernatant was discarded and the colloidal gold concentrate was redispersed in Milli-Q water. For short-chain PEGylation, MPC1 was prepared via an overnight strong agitation of 160 µL of HS-PEG_{380}-OH to 4 mL of AuNPs (~2 nM) on shaker. MPC2 was prepared by strong agitation of 160 µL of HS-PEG_{530}-COOH to 4 mL of AuNPs on shaker overnight. MPC3 was prepared by addition of 16 µL of HS-PEG_{530}-COOH and 144 µL of HS-PEG_{380}-OH (10%:90% v:v ratio) to 4 mL of AuNPs while MPC4 was prepared by addition of 80 µL of HS-PEG_{530}-COOH and 80 µL of HS-PEG_{380}-OH (50%:50% v:v ratio). Long-chain PEGylation of MPC5, MPC6, MPC7, and MPC8 were similarly prepared using the respective stock solutions. Then, the MPCs were purified via centrifugation at 13000 rpm for 30 min at room temperature twice and dispersed in water and stored at 4ºC.

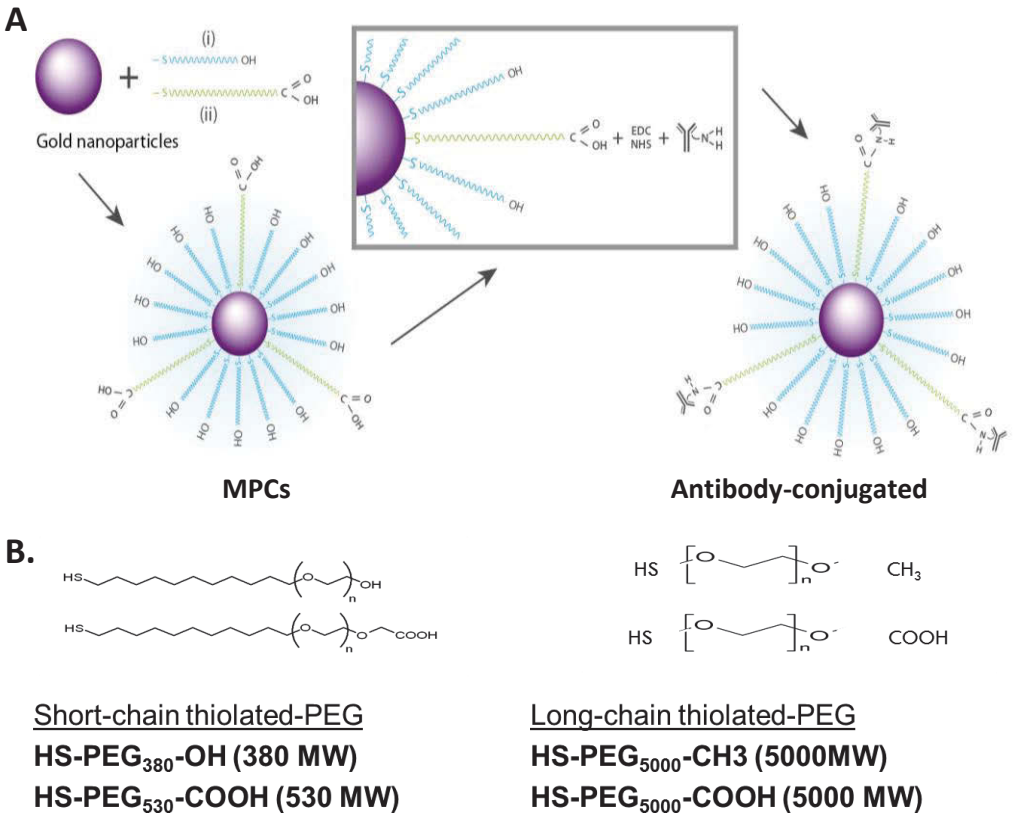

Figure 2.4 Schematic of MPCs prepared by mixed hetero-functionalized short-chain PEG or long-chain PEG

(A) short-chain thiolated PEG with reactive –COOH end or non-reactive –OH end (B) long-chain thiolated PEG with reactive –COOH end or non-reactive $–CH_3$ end. (C) The carboxyl ends of these MCPs were then activated using EDC/NHS for conjugation of antibody such as anti-CD31.

Table 2.1 List of summary for biomolecule and/or PEGylated AuNPs prepared and studied in this chapter

Prefix	Surface modification	Biomolecules conjugation
AuNPs	Citrate	-
BSA-AuNP	Citrate	BSA
anti-CD31-AuNP	Citrate	anti-CD31 antibody
anti-CD31/CD11b-AuNP	Citrate	anti-CD31 and anti-CD11b (Mac1) antibodies
Monolayer of hetero-bifunctionalized PEGylation		
MPC1	100% HS-PEG_{380}-OH	-
MPC2	100% HS-PEG_{530}-COOH	-
MPC3	100% HS-PEG_{5000}-CH_3	-
MPC4	100% HS-PEG_{5000}-COOH	-
Mixed monolayer of hetero-bifunctionalized PEGylation		
MPC5	10% HS-PEG_{530}-COOH and 90% HS-PEG_{380}-OH	-
MPC6	50% HS-PEG_{530}-COOH and 50% HS-PEG_{380}-OH	-
MPC7	10% HS-PEG_{5000}-COOH and 90% HS-PEG_{5000}-CH_3	-
MPC8	50% HS-PEG_{5000}-COOH and 50% HS-PEG_{5000}-CH_3	-
anti-CD31-MPC5	MPC 5	anti-CD31 antibody
anti-CD31-MPC6	MPC 6	anti-CD31 antibody
anti-CD31-MPC7	MPC 7	anti-CD31 antibody
anti-CD31-MPC8	MPC 8	anti-CD31 antibody
AF594-MPC5	MPC 5	Alexa Fluor 594 cadaverine
AF594-MPC7	MPC 7	Alexa Fluor 594 cadaverine
AF594/anti-CD31-MPC5	MPC 5	Alexa Fluor 594 cadaverine and anti-CD31 antibody
AF594/anti-CD31-MPC7	MPC 7	Alexa Fluor 594 cadaverine and anti-CD31 antibody

2.2.5 Biomolecule-conjugation of MPCs

Antibodies can be easily immobilized on MPCs due to the –COOH group on the heterobifunctional PEG through 1-ethyl-3-(3-dimethylaminopropyl) carbodiimide (EDC) and N-hydroxysuccinimide (NHS) coupling chemistry (Figure 2.4A). Stock solution of 0.2 M of EDC and 0.2 M NHS (Sigma Aldrich, St. Louis, MO, USA) were prepared fresh in 100mM of 2-(*N*-morpholino)ethanesulfonic acid (MES) buffer, pH 5. Eppendorf low protein binding tubes were used throughout the conjugation and centrifugation. Briefly, MPCs prepared in water were centrifuged and dispersed in MES buffer. Then 25 µL of EDC and 25 µL of NHS were added to 200 µL of MPCs (~1.7 nM) for 30 min, room temperature to activate the surface –COOH groups. The excess activating agents were removed via centrifugation in MES twice following the addition of concentrated activated MPCs to diluted antibodies in PBS at a concentration of 0.3 mM on ice. The mixture was then mixed by vortex and overnight inverted mixing on rotor at 4ºC. The covalently conjugated amine ($–NH_3$) groups on the antibodies form a stable amide bond with the –COOH group of MPCs. Finally, the antibody-conjugated MPCs were purified by centrifugation twice in PBS and finally re-suspended in 100 µL of PBS. The antibodies conjugated on MPCs were anti-CD31 and anti-CD11b (Mac1), while fluorophore conjugation to MPCs using Alexa Fluor 594 cadaverine (A-30678, Life Technologies, Carlsbad, CA, USA) were also studied (Table 2.1).

2.2.6 *In vitro* cell cultures

2.2.6.1 Bovine aortic endothelial cell (BAEC)

The cell line BAEC (ATCC, Rockville, MD, USA) was obtained from Dr. Megan Lord from the University of New South Wales. BAEC were cultured in Dulbecco's Modified Eagles' Medium (DMEM) (D5796, Sigma Aldrich, St. Louis, MO, USA) containing high glucose and L-glutamine with sodium bicarbonate, supplemented with 10% of Heat-inactivated Fetal Bovine Serum (FBS) (10099141, Life Technologies, Carlsbad, CA, USA) and 1% of penicillin and streptomycin (P/S) (15140122, Life Technologies, Carlsbad, CA, USA). BAEC were maintained in 37°C in a 5% CO_2 humidified tissue culture incubator (MCO-17AI, Sanyo, Osaka, Japan). The cells were routinely passaged

at ~80% confluence where the monolayer of adherent cells was detached from the bottom of the tissue culture flask using 0.05% trypsin-ethylene diamine tetraacetic acid (trypsin-ETDA) (15400-054, Life Technologies, Carlsbad, CA, USA). The detached cells were then re-suspended and seeded into 6-well or 96-well tissue culture plates at a desired concentration and allowed to adhere overnight before all cell experiments. At a density of 5000 cell/well, BAEC have stable growth up to 144 h before reaching confluency.

2.2.6.2 Human coronary artery endothelial cell (HCAEC)

The cell line HCAEC (ATCC, Rockville, MD, USA) was obtained from Dr. Kristine McGrath in the School of Life Sciences, University of Technology Sydney. HCAEC were cultured in MesoEndo cell growth medium (212-500, Cell applications, San Diego, CA, USA) supplemented with 10% FBS and 1% P/S. HCAEC were maintained in in 37°C in a 5% CO_2 humidified atmosphere and routinely passaged at ~80% confluence (not more than 1:4 dilution). The monolayer of adherent HCAEC was detached from the bottom of the tissue culture flask using 0.05% trypsin-ETDA. The detached cells were then suspended and seeded into 6-well or 96-well tissue culture plates at a density desired concentration and allowed to adhere overnight before all cell experiments. Due to the larger size of HCAEC, they have stable growth up to 72 h before reaching confluency at a seeding density of 1000 cell/well.

2.2.7 Characterization techniques

2.2.7.1 UV-VIS spectrophotometry

The UV-VIS spectra were acquired with a HP 8453 spectrophotometer (Agilent Technologies Deutschland GmbH, Waldbronn, Germany) using a quartz cells with 1 cm path length. The spectra were obtained over the range of 190–1100 nm. The characteristic SPR band and peaks of colloidal gold was found around 500–550 nm.

2.2.7.2 Dynamic light scattering (DLS) and zeta (ζ) potential

The hydrodynamic diameter of gold colloids was determined by Malvern NanosizerZS® instrument (Malvern, Worcestershire, UK) with permission from School of Engineering, University of Technology Sydney and Brookhaven ZetaPALS (Holtsville, NY, USA) with permission from ARC Centre of Excellence for Functional Nanomaterials, School of Chemical Engineering, University of New South Wales. Both of the instruments measure the hydrodynamic diameter of colloids through DLS using a quartz cells with 1 cm path length.. The value for the hydrodynamic diameter of the particles is obtained using the intensity scaling. The measurements were performed in triplicate at 20 cycles per run. Results were presented as mean ± standard error of the mean (S.E.M). Gold colloids were dispersed in water with exception of biomolecule-conjugated AuNPs suspended in PBS. ζ potential of gold colloids in water was measured using Malvern NanosizerZS® using a 2 mm, ~8–10 attenuators, clear disposal zeta cell. The measurements were performed in triplicate at 20 cycles per run. Results were presented as mean ± S.E.M. Due to the dispersion of antibody-conjugated MPCs in PBS which interferes with the ζ potential measurements, the changes in overall surface charge were determined using gel electrophoresis (see section 2.2.7.5).

2.2.7.3 Inductively–coupled plasma mass spectroscopy (ICP-MS)

The concentration of elemental Au of the as-synthesized and modified AuNPs was determined using ICP-MS (Agilent 7500 CX series, Agilent Technologies Inc., Forrest Hill, VIC, Australia). Samples were introduced via a MicroMist glass concentric nebulizer (Glass expansion, West Melbourne, VIC, Australia) and a Quartz Scot-type double pass spray chamber cooled to 2°C. The sample solution and the spray chamber waste were carried with the aid of a peristaltic pump. The ICP-MS operating parameters and the lens conditions were selected to maximize the sensitivity of a 1% HNO_3:HCl solution containing 1 ng/ml of Li, Co, Y, Ce and Tl. Helium was added into the octopole reaction cell to reduce interferences. Calibration curves were constructed and the result analyzed using Agilent Technologies Masshunter software. A certified Au calibration standard was obtained from Choice Analytical, Thornleigh, NSW, Australia. Calibration curves were constructed from seven known gold standards solution with

concentrations of 0, 1, 10, 50, 100, 500, and 1000 ng/ml. The high purity Basline® HNO_3 (67–69%) and Baseline® HCl (32–35%) used for ICP-MS were from Seastar Chemicals Inc., Sidney, BC, Canada.

2.2.7.4 High-resolution scanning electron microscopy (HR-SEM)

All HR-SEM images were obtained in either bright-field or backscatter mode using LEO Supra 55VP (Zeiss) scanning electron microscopy with electron backscatter diffraction. The HR-SEM was performed under system vacuum pressure greater than 3.4×10^6 Torr at high current of 20 kV.

Direct evaporation and drying of colloidal Au onto silicon (SiO_2) wafer commonly result in an uncontrollable coagulation of AuNPs and formation of AuNPs clusters which can be difficult for determination of size and morphology. In order to spread the AuNPs evenly onto the SiO2 wafer for HR-SEM, an amino-functional silane were used as an adhesion or anchoring agent for the AuNPs. The immobilization of monolayer AuNPs on silicon substrate using (3-aminopropyl)-triethoxysilane, APTS (Sato, Hasko & Ahmed 1997; Xu, Stevens & Cortie 2004). Briefly, the 1 cm by 1 cm silicon substrate (p-type 100, GASUF06, ProSciTech Pty Ltd, Kirwan, QLD, Australia) were cleaned with acetone and isopropanol with ultrasonic agitation, then etched in piranha solution for 30 mins. Piranha solution consisting 3 parts of sulfuric acid (H_2SO_4) (95-98%, ACS grade, 320501, Sigma Aldrich, St. Louis, MO, USA) and one part of hydrogen peroxide (H_2O_2) (30-31%, S021001-CHEF04, Baseline® Seastar Chemicals Inc., Sidney, BC, Canada), is extremely corrosive and highly evaporative which requires handling with extra precaution in the fume cupboard. Following that, the substrates with hydroxyl group terminated were thoroughly rinsed with Milli-Q water three times and dried with N_2 gas. Then, the substrates were immersed in freshly made 0.05% (v:v) APTS (99%, 440140, Sigma Aldrich, MO, USA) solution for 15 min. Then the surface-treated substrates were lifted off from solution, dried with nitrogen gas, and baked for 30 min at 120 °C in an oven. The surface-treated substrates were then immersed in the citrate Au sol for 3 h. After immersion, the samples were lifted off from the sol, dried by the nitrogen gun to eliminate the solution, and observed by HR-SEM.

2.2.7.5 Agarose gel electrophoresis

The PEGylated MPCs with/without antibody conjugations are highly stable against agglomeration in ionic solvents. Due to the different surface modification, the surfaces charges will be altered which can be observed through electrophoresis separation. During gel electrophoresis, the negatively charged MPCs migrate from the cathode (-) to anode (+); while positively charged MPCs migrates against the electrical current towards the cathode.

Agarose (0.1 g) was dissolved in 100 mL of Tris/Borate EDTA buffer (TBE, 1x) by microwave heating for 1 min, this solution was allowed to cool for 5 mins. The dissolved agarose were poured into gel casting tray to give a 1% agarose gel in a 20 x 30 cm gel tank. Bubbles were removed with a pipette tip and then 20 wells comb was added and allowed to set. Gel electrophoresis was carried out in a horizontal tank containing TBE buffer and running at 80 V/cm for approximately 1 h to allow separation of MPCs.

2.2.7.6 Critical flocculation concentrations

The critical flocculation concentration of AuNPs and MPCs were determined through a series of Eppendorf centrifuge tubes containing 100 µL of identical concentrations of gold nanoparticles (~1.2 nM). Increasing volumes of a 2 M NaCl stock solution were added to each sample with the final salt concentration ranging from 20 mM to 1 M. The tubes were vortexed and then allowed to incubate for 1, 18, and 72 h. Aggregation was assessed by monitoring changes in the characteristic gold nanoparticle SPR peak shift on UV-VIS spectra and colourimetric difference using naked eye. The threshold NaCl salt concentration in the gold sol, which caused the rapid aggregation of the particles, was determined as the critical flocculation concentrations.

2.2.7.7 Cytotoxicity assay

The potential cytotoxicity of an increasing dose treatment of AuNPs were studied in BAEC and HCAEC in a 96-well plate using 3-(4,5-dimethylthiazol-2-yl)-2,5-

diphenyltetrazolium bromide (MTT) (M2128, Sigma Aldrich, St. Louis, MO, USA) assay. This assay measured the catalytic cellular activity of mitochondrial dehydrogenases which convert the water soluble MTT into insoluble formazan. Briefly, 10 µL of MTT (1.2mM) was added to each well containing cells in 100 µL of fresh culture media. The 96-well plates were then incubated at 37˚C in a 5% CO_2 humidified atmosphere for 4 h after which time the supernatants were discarded. Then, 100 µL of dimethyl sulfoxide (D5879, Sigma Aldrich, St. Louis, MO, USA) was added to dissolve the purple coloured formazan precipitate formed in each well. The optical absorbance of the samples was then read at 570 nm using Synergy HT microplate spectrophotometer (Bio-Tek Instrument Inc., Winooski, VT, USA). Results were expressed as the mean percentage of viability ± S.E.M relative to the control.

2.2.7.8 Cellular imaging and microscopy

HR-SEM and fluorescence microscopy were employed to study the anti-CD31-MPCs cellular labelling of endothelial cells. Glass coverslips and silicon substrates were thoroughly cleaned in 90% ethanol and rinsed in culture in complete mediums, following an overnight coating in FBS to induce serum adsorption to surfaces. BAEC ($1x10^6$ cells/well) or HCAEC ($5x10^5$ cells/well) were seeded on the silicon wafer or glass coverslips placed on the bottom of 12 well-plate tissue culture dishes. The cells were incubation at 37°C with 5% CO_2 humidified atmosphere overnight for cells to adhere and attach to the bottom of the dishes and Si wafer.

For HR-SEM imaging, 500 µL of AuNPs, MPCs, or anti-CD31-MPCs was added to the cells for 24 h. Following that, the cells were fixed with cold 4% paraformaldehyde for 30 min, room temperature. The fixative was then aspirated and cells were washed gently with PBS three times. The cells fixed on silicon wafers were further step dehydration in a series of ethanol solution (10%, 20%, 50%, 70% and 95%) from Thermo Fisher Scientific Inc., Wilmington, MA, USA. Upon the final wash, silicon wafers with cells was mounted onto aluminum stud and left under vacuum for another 3–4 days to ensure cells are completely dried, after which they are carbon coated before for HR-SEM imaging (see section 2.2.7.4).

For confocal microscopy, the cells on coverslips were allowed to grown till overconfluence after 3 days and then fixed cold 4% paraformaldehyde, 30 min, room temperature. After that, the fixative was aspirated and cells were washed gently with PBS three times and blocked using BSA blocking buffer containing 1% (w/v) BSA in PBS for 1 h. Then the cells were thorough rinsed three times using PBS containing 0.05% (v:v) Tween-20 (PBST). Subsequently, mouse primary antibody anti-CD31 (1:50 dilution) or anti-CD31-MPCs in PBS + 1% BSA were incubated overnight at 4ºC. Following that, the cells were thoroughly washed. Quenching buffer containing 100 mM glycine in PBS was added to the cells along with 0.1% Triton X-100 in PBS for 20 min. Subsequently, a secondary antibody, Alexa Fluor 568 goat anti-mouse IgG (H+L) (A-11031, 1:1000 dilution in PBS + 1% BSA) were added to the all samples and incubated for 2 h in room temperature. The cells were thoroughly rinsed with PBST three times. Cells were also incubated with DAPI for 5 min in dark (under foil) at room temperature to enable visualization of cell nuclei (blue). Finally, the cells on coverslips were mounted in mounting media onto glass slides for cellular imaging using fluorescence microscope (BX51 Olympus Co., Tokyo, Japan) using a digital camera (Olympus) using cellSens software (version 1.7).

2.3 Results

2.3.1 Characterization of 21nm AuNPs

2.3.1.1 Size and morphology of unmodified AuNPs and MPCs

AuNPs prepared via the citrate-reduction method yielded a colloidal stable suspension and stored in 4˚C. The citrate-coated AuNPs were monodispersed in water and spherical shaped as observed using HR-SEM at high magnifications (Figure 2.5A). However, the citrate-coated AuNPs rapidly agglomerated in the presence of solvent with high ionic strength such as PBS as shown in Figure 2.5B. The particle core size of citrate-coated AuNPs was estimated to be 22.33 ± 1.45 nm using HR-SEM. DLS measurements of hydrodynamic diameter of AuNPs capped with citrate showed a narrow distribution of size between 20–30 nm in size (Table 2.2).

MPCs were prepared via the surface assembly of with short-chain or long-chain mixed hetero-bifunctionalized PEGs. Due to the stealth surface modification, MPCs do not form irreversible aggregation but clusters of evenly spaced AuNPs during agglomeration which is reversible (Figure 2.5C,D). The HR-SEM images of short-chain PEGylated MPCs showed closely packed and structurally aligned while the long-chain PEGylated MPCs were further apart from one another and irregularly distributed. DLS measurements showed approximately 1 nm increment of hydrodynamic diameter for short-chain PEGylated MPCs but greater than 25 nm increased in size for long-chain PEGylated MPCs. Conjugation of antibodies on short-chain PEGylated MPCs were indicated from an increased in the particle hydrodynamic diameter by 4–25 nm. However, the anti-CD31-MPCs of long-chain PEGs showed an increase of 9 nm but 3 nm reduced in the hydrodynamic diameter with the different DLS techniques.

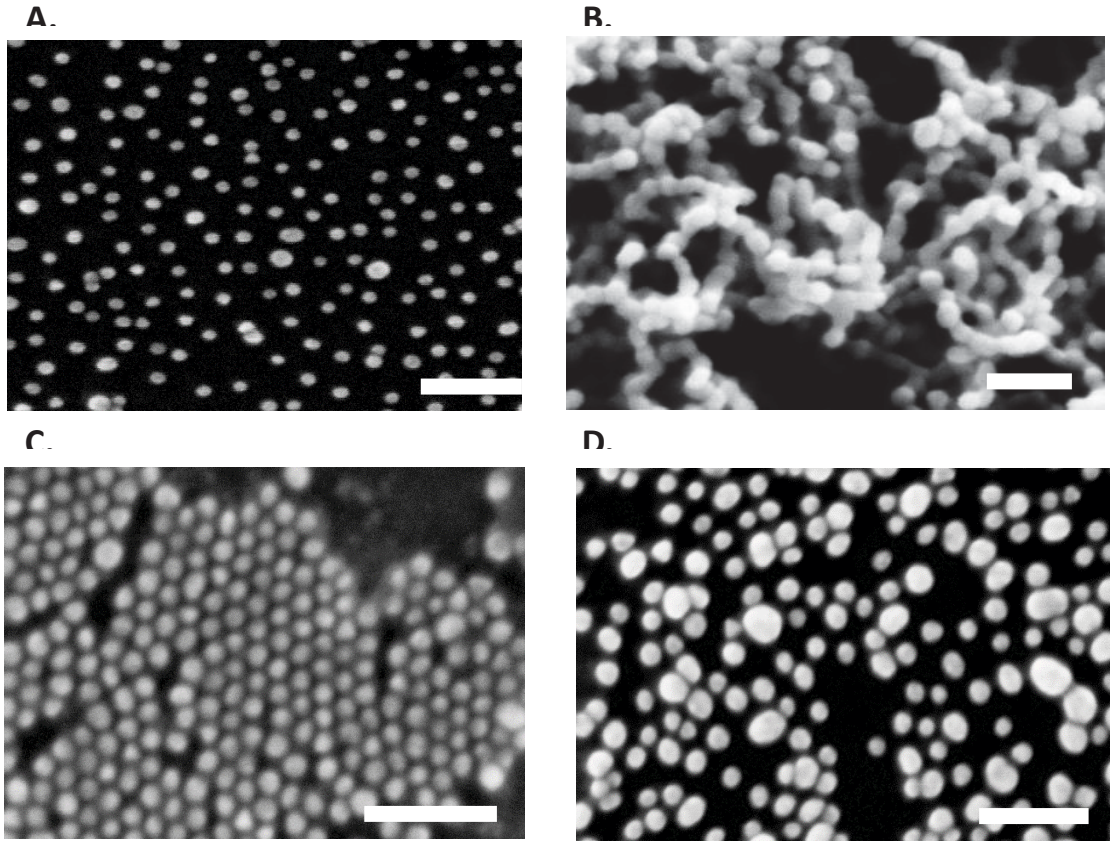

Figure 2.5 Representative HR-SEM images of AuNPs before and after PEGylation

(A) citrate-coated AuNPs dispersed in water, (B) citrate-coated AuNPs dispersed in 1x PBS, (C) short-chain PEGylated MPCs in 1x PBS, (D) long-chain PEGylated MPCs in 1x PBS. Scale bar = 100 nm.

Table 2.2 Particle size and hydrodynamic diameter using HR-SEM and DLS

Surface modification	Hydrodynamic diameter (nm)	
	Brookhaven Mastersizer	Malvern Zetasizer NanoZS
Citrate		
(HR-SEM core particle size = 22.33 ± 1.45 nm)		
AuNP	27.26 ± 0.50	24.41 ± 1.27
Short-chain PEGylation		
(HR-SEM core particle size = 20.45 ± 1.45 nm)		
MPC6	28.17 ± 0.28	28.36 ± 0.24
Anti-CD31-MPC6	32.60 ± 1.09	53.42 ± 7.27
Long-chain PEGylation		
(HR-SEM core particle size = 17.86 ± 0.62 nm)		
MPC8	55.28 ± 0.38	59.81 ± 0.95
Anti-CD31-MPC8	64.94 ± 1.97	56.56 ± 1.93

Data are expressed as mean ± S.E.M, n=3–5.

2.3.1.2 SPR band and peak of unmodified AuNPs and MPCs

Typically, gold nanospheres display a single absorption peak in the visible range between 510 nm and 550 nm. With increasing particle size, the absorption peak shifts to a longer wavelength and the width of the absorption spectra is related to the size distribution range. The as-synthesized citrate-coated AuNPs dispersed in water showed SPR peak of 520 nm determined from UV-VIS absorption spectrum. Figure 2.8 showed red shift in SPR peaks from 520 nm for all short-chain PEGylated MPCs. The magnitude of the red shift effect varied with the mole ratio between PEG:nanoparticles and the percentage of a slightly longer PEG_{530}–COOH ends. At a lower mole ratio of PEG:nanoparticle of 1000:1 and 2500:1, the MPCs formed were unable to prevent against particle agglomeration during the purification by centrifugation step. This led to irreversible aggregated MPCs which were unable to dispersed in water contributing to a

markedly reduced in absorption spectra (Figure 2.8A–C). Long-chain PEGylated MPCs also showed similar red shift effect on the SPR peaks in response to a change in PEG:nanoparticle mole ratio and percentage of PEG_{5000}-COOH (Figure 2.7A–C). However, the long-chain PEGylated MPCs were stable against agglomeration due to their larger in size which requires less PEG molecules to form a protective monolayer over the surfaces of AuNPs.

Studies have shown that this change in the SPR peak can provide information about particle size, shape and concentration as well as the dielectric medium properties but not presence of biomolecules (El-Sayed, Huang & El-Sayed 2005; Murphy et al. 2008). BSA- and antibody-conjugated AuNPs were dispersed in PBS. Figure 2.8A showed red shift effect of SPR peaks from the UV-VIS absorbance spectra for both conjugated AuNPs due to the increase in particle size. Although the conjugation of biomolecules on AuNPs improved their stability in PBS, the removal of excess proteins and antibodies via repeated centrifuge purification results in a loss of AuNP where the pellet form at the bottom of centrifuge tubes cannot be re-suspended. This is evident in the lower absorption spectra observed for BSA-, CD31-, and CD31/CD11b-conjugated AuNPs compared to the unmodified citrate-coated AuNPs (Figure 2.8A). In addition, anti-CD31-AuNPs agglomerate over time and adhere to the wall of the low protein binding tubes (data not shown). Interestingly, conjugation of antibody on both short-chain and long-chain PEGylated MPCs did not result in the larger shift as observed from direct conjugation. Concentrations of unmodified AuNPs and MPCs

Elemental Au concentrations were quantified in AuNPs samples before and after PEGylation using ICP-MS (Table 2.3). According to the core size of AuNPs and elemental Au concentration, the number of nanosphere per mL and nanoparticle concentration can be theoretically calculated (assuming all particles were ~22 nm). Most of the preparation of MPCs and critical flocculation concentration experiments were based on the nanoparticle concentration of 2 nM.

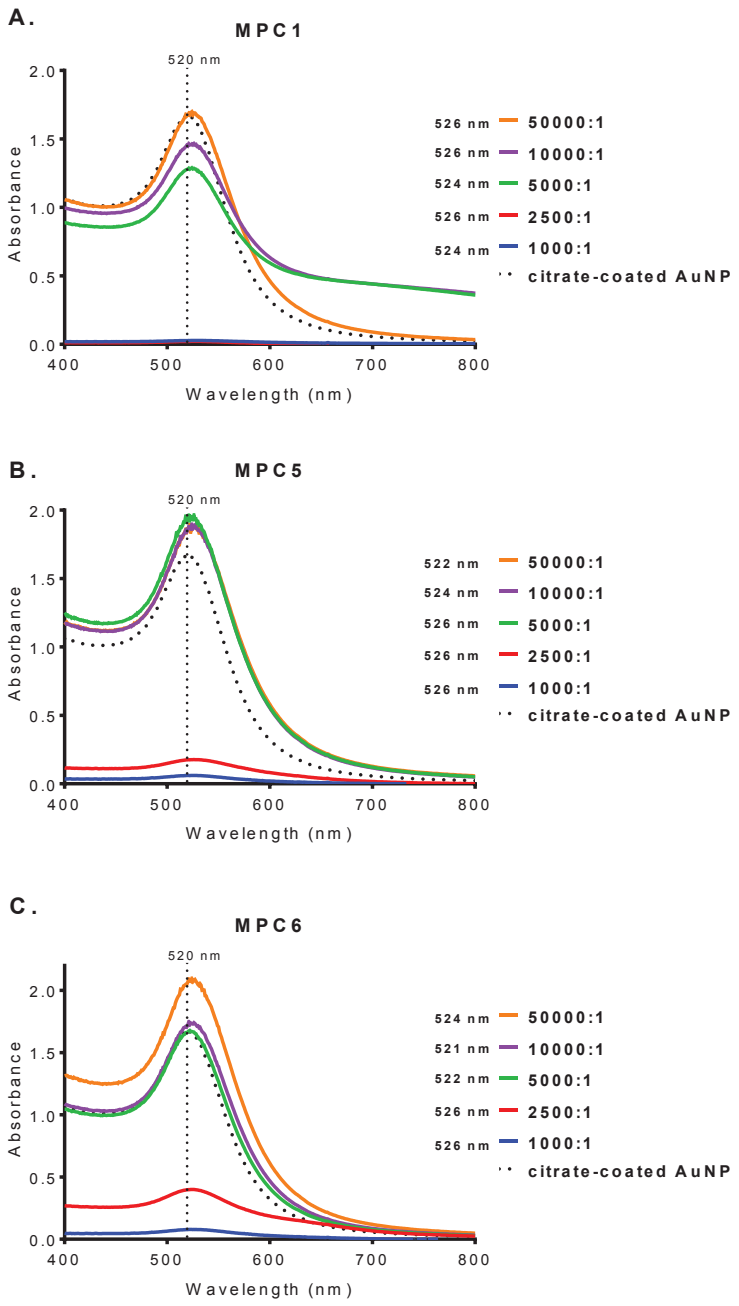

Figure 2.6 Optimization of short-chain PEG per nanoparticle ratio for MPC1, MPC5, and MPC6

UV-VIS absorption spectra and respective SPR peaks for MPC1 (A), MPC5 (B), and MPC6 (C) in MES buffer with decreasing short-chain PEG:nanoparticle mole ratio of 50000:1, 10000:1, 5000:1, 2500:1, 1000:1, and unmodified AuNPs (control, citrate-coated).

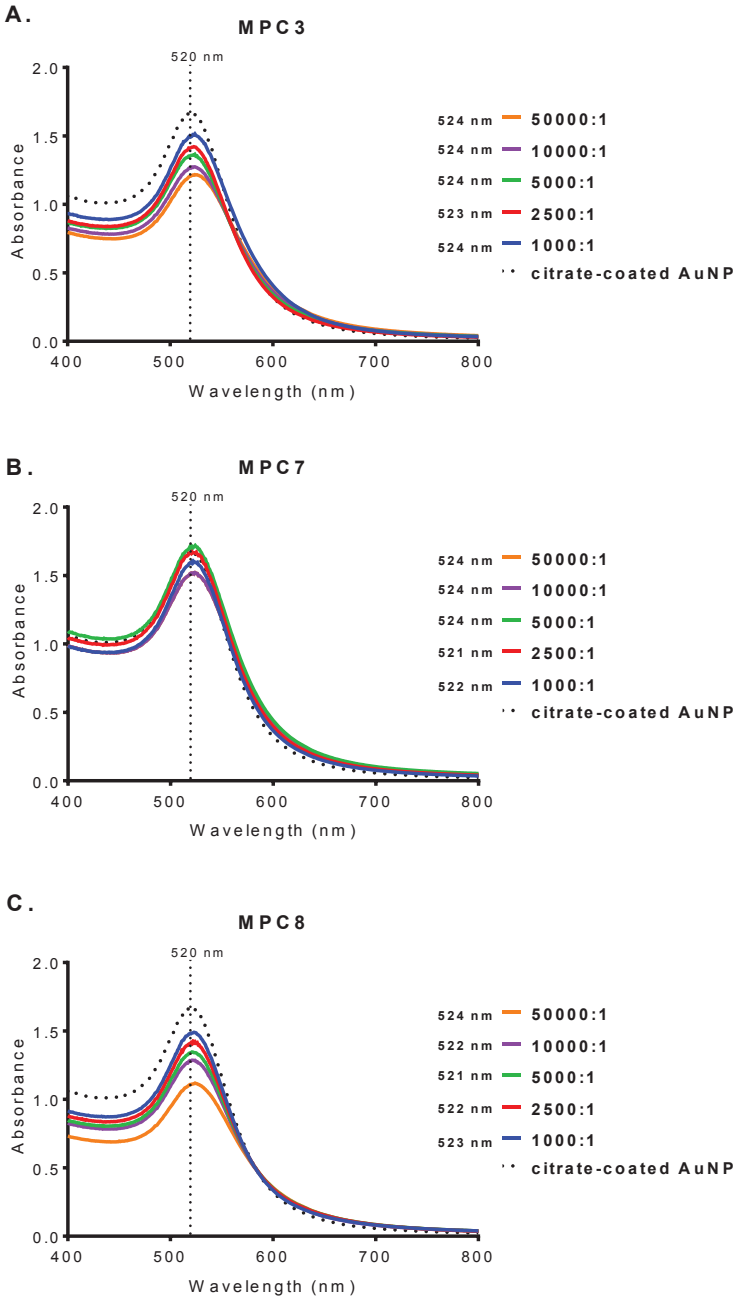

Figure 2.7 Optimization of long-chain PEG per nanoparticle ratio for MPC3, MPC7, and MPC8

UV-VIS absorption spectra and respective SPR peaks for MPC3 (A), MPC7 (B), and MPC8 (C) in MES buffer with decreasing long-chain PEG:nanoparticle mole ratio of 50000:1, 10000:1, 5000:1, 2500:1, 1000:1, and unmodified AuNPs (control, citrate-coated).

2.3.1.3 Critical flocculation concentration of unmodified AuNPs and MPCs

Critical flocculation concentration was employed to investigate the stability of the colloidal solutions under increased ionic strength. AuNPs and MPCs were diluted to a nanoparticle concentration of 1.7 nM with increasing NaCl concentration. The critical concentration of NaCl which caused the rapid aggregation of the particles was noted in Table 2.4. Unmodified AuNPs showed very poor stability against particle aggregation at high ionic strength environment with a critical flocculation concentration of ≤ 0.025M NaCl after 1 h and ≤ 0.015M NaCl at 72 h. The centrifuge purification of excess citrate slightly improved the critical flocculation concentration of unmodified AuNPs. AuNPs are sensitive to electrolytes because any electrolytes present constrict the ionic double layer and reduce electrostatic repulsion between the positively charged particles which results in particle aggregation. In comparison, all PEGylated MPCs exhibited exceptional stability up to 1 M of NaCl at 72 h.

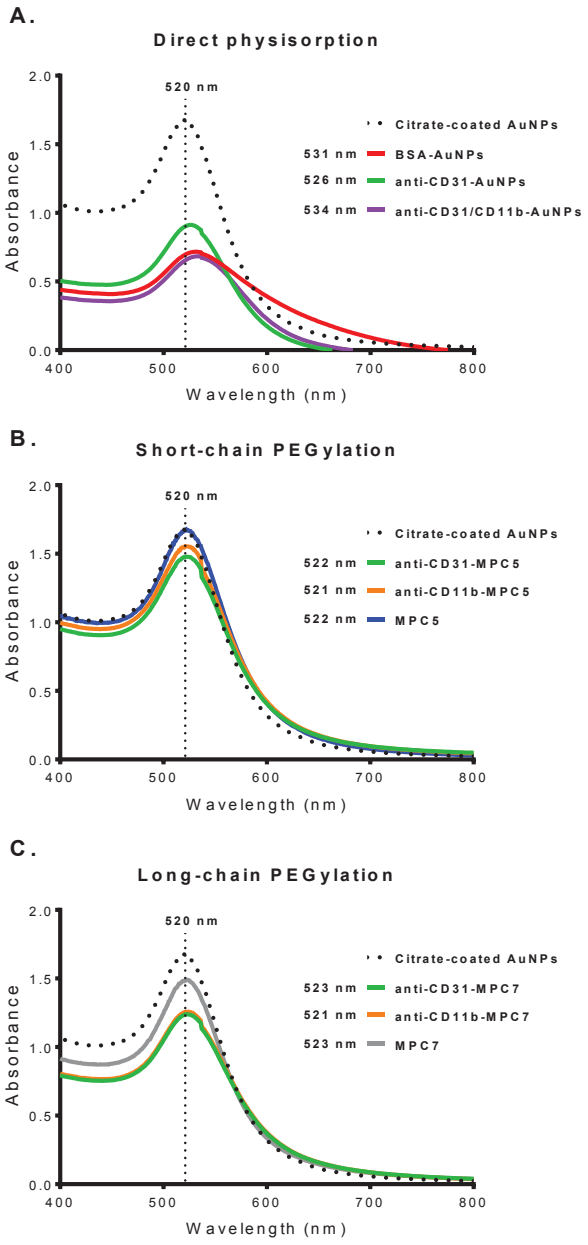

Figure 2.8 Shifting of SPR peak with biomolecule-conjugated AuNPs with/without PEGylation

UV-VIS absorption spectra and respective surface plasmon resonance peaks for colloidal suspension of various AuNPs in 1x PBS and citrate-coated AuNP in water. (A) direct conjugation of biomolecules on AuNPs, (B) immobilization of biomolecules on short-chain PEGylated MPCs, (C) immobilization of biomolecules on long-chain PEGylated MPCs. (A–C).

Table 2.3 Quantification of colloidal gold concentration before and after PEGylation using ICP-MS

Surface modification	Concentration of elemental Au (g/L) by ICP-MS	No. of Au nanosphere/mL	Nanoparticle concentration (nM)
Citrate			
AuNP (as synthesized)	0.1933	1.22×10^{18}	2.02
Short-chain PEGylated MPCs			
MPC1	0.1662	1.05×10^{18}	1.74
MPC2	0.1787	1.13×10^{18}	1.87
MPC5	0.2092	1.32×10^{18}	2.19
MPC6	0.1718	1.08×10^{18}	1.80
Long-chain PEGylated MPCs			
MPC3	0.1640	1.03×10^{17}	1.71
MPC4	0.1570	9.90×10^{17}	1.64
MPC7	0.2005	1.26×10^{18}	2.10
MPC8	0.1514	9.54×10^{17}	1.58

Table 2.4 Critical flocculation concentration of AuNPs before and after PEGylation

Surface modification	Critical flocculation concentration		
	1 h	18 h	3 days
Citrate			
AuNP (as synthesized)	≤ 0.025M NaCl	≤ 0.015M NaCl	≤ 0.015M NaCl
AuNP (centrifuged)	≤ 0.03 M NaCl	≤ 0.02 M NaCl	≤ 0.02 M NaCl
Short-chain PEGylation			
MPC1	> 1 M NaCl	> 1 M NaCl	> 1 M NaCl
MPC2	> 1 M NaCl	> 1 M NaCl	> 1 M NaCl
Long-chain PEGylation			
MPC3	> 1 M NaCl	> 1 M NaCl	> 1 M NaCl
MPC4	> 1 M NaCl	> 1 M NaCl	> 1 M NaCl

2.3.1.4 Surface potential and charge of unmodified AuNPs and MPCs

ζ potential is a physical property which is exhibited by any particle in suspension. Dissociation of acidic groups on the surface of a particle will give rise to a negatively charged surface. In the presence of high salt concentrations such as PBS, the zeta potential is reduced, thus not suited for the measurement of antibody-conjugated MPCs.

All ζ potential measurements were performed in water suspension. The as synthesized AuNPs showed a surface ζ potential of - 36.97 ± 1.05 due to the negatively charge of citrate capping, while removal of excess citrate in the suspension positively shifted ζ potential by approximately 6 mV (Table 2.5). Surface assembly of monolayer thiolated PEGs also positively shifts the ζ potential due to displacement of citrate from the surfaces of AuNPs. For short-chain PEGylated MPCs, increasing percentage of surface carboxyl groups showed an increased in ζ potential (Table 2.5). However, this trend was not observed in short-chain PEGylated MPCs due to the abundance of methyl groups which contributes to an overall positively charged surfaces (Table 2.5).

Table 2.5 Surface ζ potential measured using Malvern NanoZS

Surface modification	ζ potential (mV)
Water (background)	- 0.22 ± 0.28
Citrate	
AuNP (as synthesized)	- 36.97 ± 1.05
AuNP (centrifuge purified)	- 30.43 ± 0.72
Short-chain PEGylation	
MPC1 (100% -OH)	- 19.87 ± 0.92
MPC2 (100% -COOH)	- 44.27 ± 0.65
MPC5 (10% -COOH)	- 27.42 ± 1.57
MPC6 (50% -COOH)	- 28.62 ± 0.66
Long-chain PEGylation	
MPC3 (100% -CH3)	- 28.63 ± 0.68
MPC4 (100% -COOH)	- 28.49 ± 1.79
MPC7 (10% -COOH)	- 20.83 ± 1.59
MPC8 (50% -COOH)	- 29.57 ± 0.13

Data are expressed as mean ± S.E.M, n=6–9.

The overall surface charge for the antibody-conjugated MPCs suspended in PBS was measured using gel electrophoresis. The high salt content of PBS interferes with the measurement of ζ potential. Successful construction of anti-CD31-MPCs and AF594-MPCs was confirmed using gel electrophoresis (Figure 2.9). Lane 1–3 corresponds to the short-chain PEGylated MPCs with 10% carboxyl ends after conjugation to anti-CD31 only, dual AF594 cadeverine/anti-CD31, and AF594 cadeverine only, respectively. Lane 5 and 6 showed the short-chained PEGylated MPCs with 10% carboxyl ends without surface modification. Although both MPC5, the newly synthesized MPC5 in Lane 5 seems to be more negatively charged compared to MPC5 in Lane 6. The MPC5 before and after immobilization of anti-CD31 were found at similar positions, anti-CD31-MPC5 and AF594/anti-CD31-MPC5 had the a slightly

shifted bands towards the anode which may be due to aggregated dimers and trimers (Lane 1,2,6, Figure 2.9). However, AF594-MPC5 with an overall negative surface charges after AF594 immobilization, allowed them to run smoothly towards the anode compared to the unmodified MPC5 (Lane 3 *vs.* Lane 6, Figure 2.9). This effect was not observed in short-chain PEGylated MPC6 with 50% carboxyl ends before and after immobilization of AF594 (Lane 4 *vs.* Lane 7, Figure 2.9).

For long-chained PEGylated MPC7, all migrated from the cathode towards the anode indicating their overall positively charged surfaces (Lane 8–12, Figure 2.9). This was attributed to the deprotonation of methyl group in greater abundance of MPC7. Upon conjugation to anti-CD31 and AF594 cadevarine, the slight negatively charged biomolecules was unable to contribute to an overall shift in polarity for MPC7. In addition, the long-chain PEGylation on MPC7 contribute to a larger hydrodynamic diameter which unable to migrate smoothly from anode to cathode through the 1% agarose gel. The unmodified AuNPs rapidly precipitated in wells due to the high ionic strength of TBE 1x running medium (Lane 13, Figure 2.9).

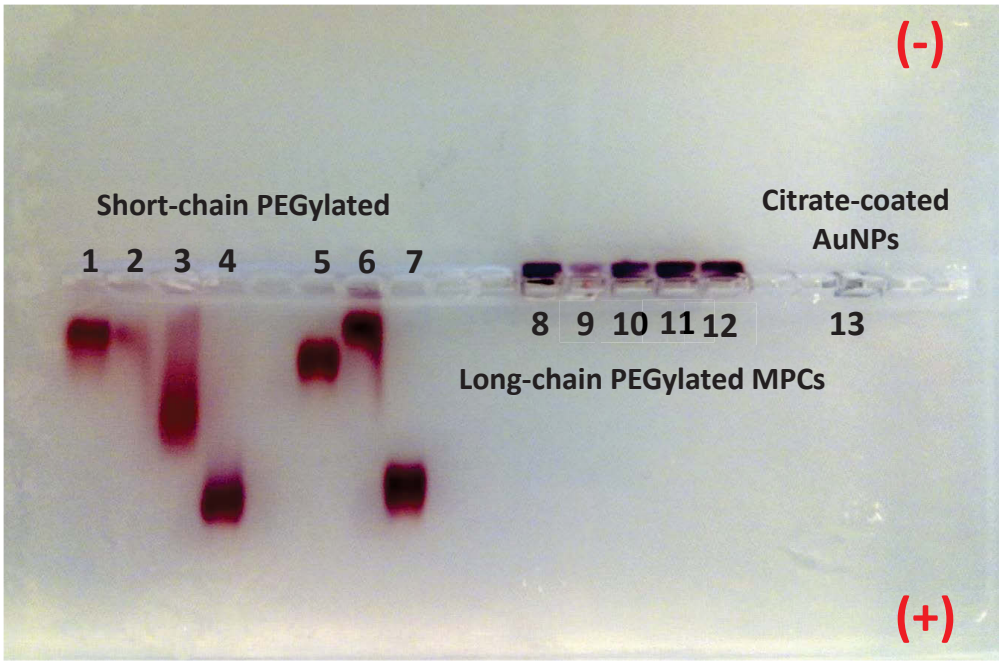

Figure 2.9 Migration of biomolecules and PEG-modified AuNPs determined using 1% agarose gel electrophoresis

Migration pattern for anti-CD31-MPC5 (lane 1), AF594/anti-CD31-MPC5 (lane 2), AF594-MPC5 (lane 3), AF594-MPC6 (lane 4), MPC5 (lane 5,6), MPC6 (lane 7), anti-CD31-MPC7 (lane 8), AF594/anti-CD31-MPC7 (lane 9), AF594-MPC7 (lane 10), MPC7 (lane 11,12), and citrate-coated AuNP (lane 13) in TBE 1x running buffer, pH 8. The electrophoresis separation caused migration of negatively charged MPCs from the cathode (-) to anode (+); while positively charged MPCs from the anode to cathode.

2.3.2 Cellular uptake and labelling of unmodified AuNPs and MPCs

The binding patterns on BAEC observed were different between the unmodified AuNPs and MPCs with/without anti-CD31 conjugation upon examination using HR-SEM (Figure 2.10). Figure 2.10A showed a typical BAEC without receiving any AuNP treatment. Figure 2.10B showed BAEC treated with citrate-coated AuNPs resulting in the formation of large aggregates deposited on cell surfaces surrounding the nucleus. This may be attributed to their instability in biological media with high ionic strength media. The non-targeting MPC5/MPC7 was not retained on BAEC whereas both of the CD31-targeting MPC5/MPC7 remained bound to BAEC after repeated washing (Figure 2.10C–F). Greater targeted accumulation of long-chain PEGylated anti-CD31-MPC7 was observed on BAEC compared to short-chain PEGylated anti-CD31-MPC5 which has an evidently smaller fraction of individual particles was observed (Figure 2.10E–F). Figure 2.11 showed high magnification HR-SEM images of anti-CD31-MPC5 binding to BAEC where both aggregated and non-aggregated AuNPs particles were observed. The EBSD analysis showed elemental peaks corresponding to gold from MPCs, carbon from carbon mesh coating, and silicon from wafer substrate (Figure 2.11D).

HCAEC were cultured on glass coverslips till confluent for immunofluorescence cell labelling by anti-CD31-MPC5 and anti-CD31-MPC6. Figure 2.12 showed immunofluorescence staining of anti-CD31 primary antibody compared to the anti-CD31-MPCs on HCAEC using Alexa Fluor 568 secondary antibody detection. Direct immunofluorescent staining of primary anti-CD31 showed bright orange/red staining of CD31 surface antigen. However, cell labelling using anti-CD31-MPCs of surface CD31 antigen on the HCAEC showed faintly stained red dots localized around the nucleus which is stained in blue. This observations from immunofluorescence microscopy corresponds to their localization observed using HR-SEM imaging. The differences in staining intensity was due to the high concentration of free anti-CD31 compared to the very low concentrations of anti-CD31 bound on the surfaces of MPCs. In addition, there seems to be greater binding affinity of anti-CD31-MPC6 compared to anti-CD31-MPC5 due to increased percentage of carboxyl group available for greater anchoring of anti-CD31.

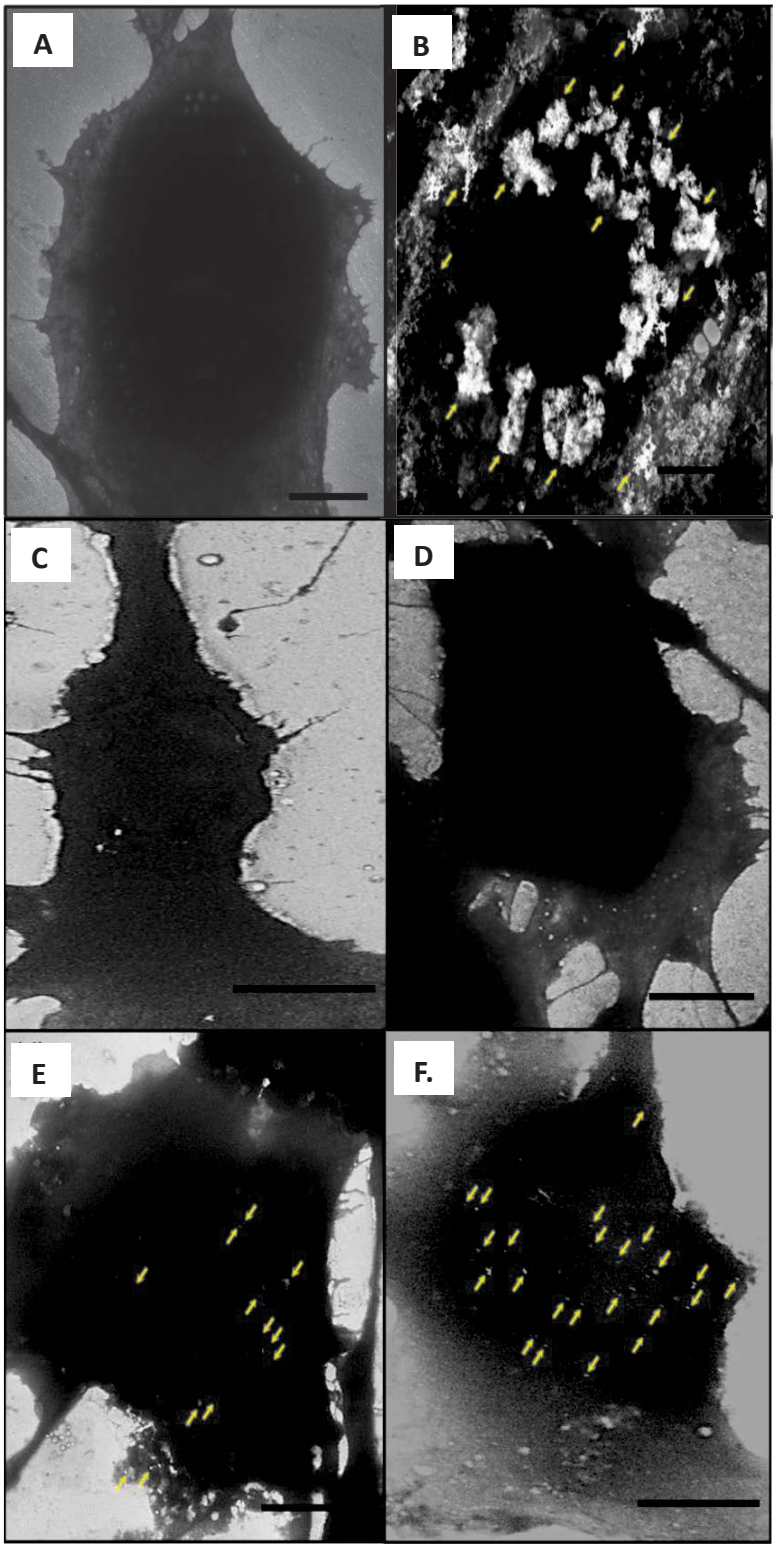

Figure 2.10 HR-SEM images of BAEC after 24 h treatment with various AuNPs

Representative HR-SEM in-lens mode images of BAEC treated with (A) PBS, (B) citrate-coated AuNP, (C) MPC5, (D) MPC7, (E) anti-CD31-MPC5, and (F) anti-CD31-MPC7. Arrows show aggregation of AuNPs. Scale bar = 10 μm.

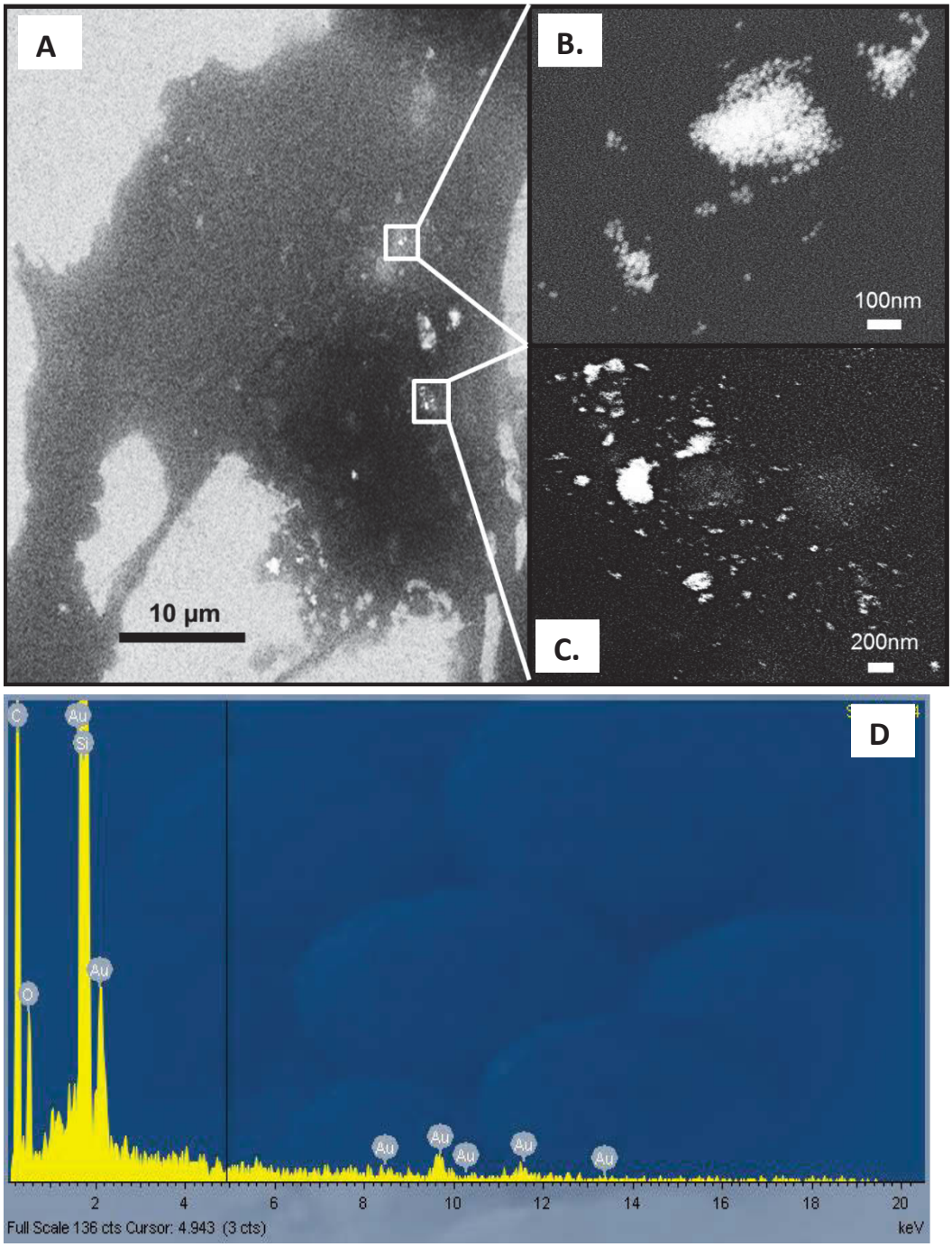

Figure 2.11 HR-SEM and EBSD analysis of BAEC treated with anti-CD31-MPC5 for 24 h.

(A) mixed in-lens/back-scatter mode HR-SEM image of BAEC for contrast localization of aggregated AuNPs. (B) high magnification back-scatter mode image of the indicated region. (C) high magnification back-scatter mode image of the indicated region revealing the distribution of aggregated and non-aggregated particles. (D) EBSD elemental analysis showing peaks corresponding to Au, C and Si.

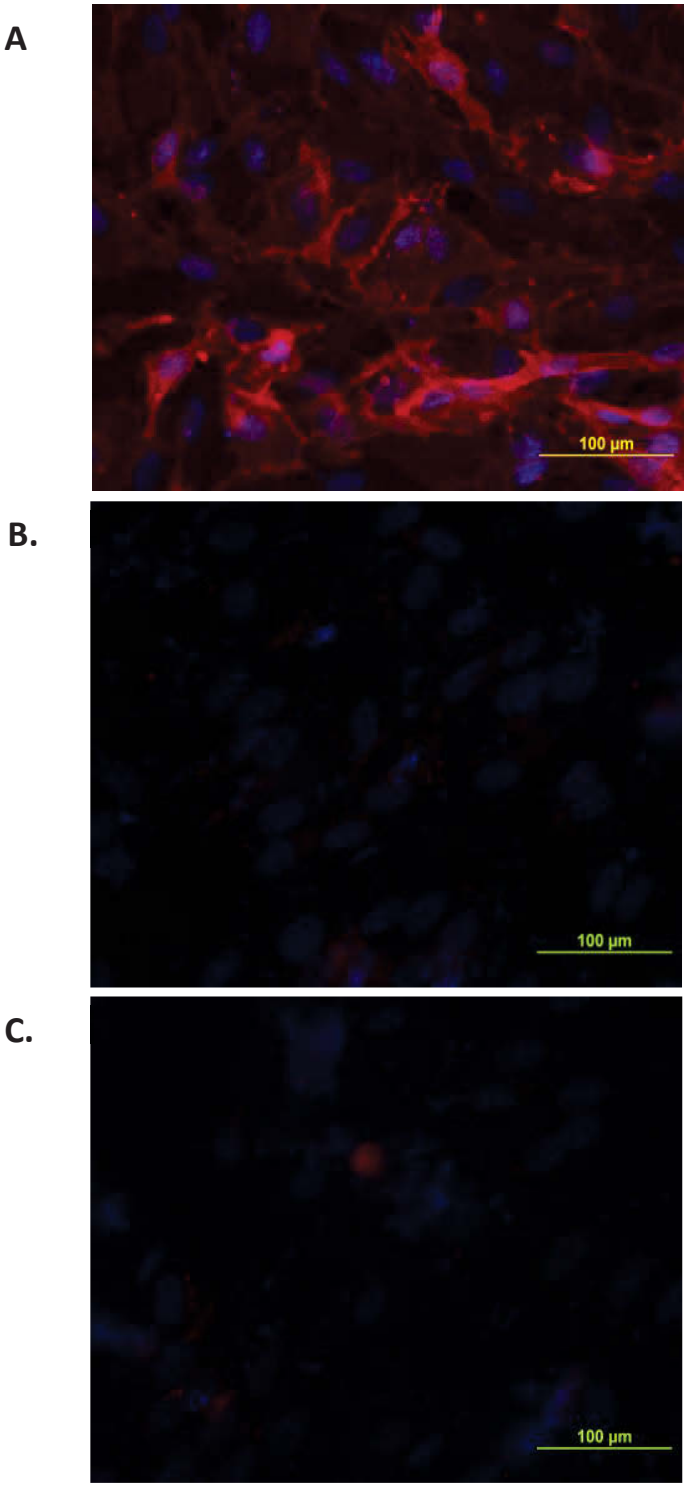

Figure 2.12 Immunofluorescence staining of HCAEC surface antigen CD31

HCAEC cultured on glass coverslips were labelled with (A) Anti-CD31, (B) anti-CD31-MPC6, (C) anti-CD31-MPC5 as primary antibodies, following detection with Alexa Fluor®568 secondary antibody (orange/red). Cell nuclei were stained with Dapi (blue).

2.3.3 Cellular toxicity of unmodified AuNPs and MPCs

Preliminary cytotoxic effect of the unmodified AuNPs and MPCs with or without anti-CD31 conjugation exposure on BAEC were determined using MTT assay at 24, 48, and 72 h (Figure 2.13). Figure 2.13 showed that BAEC treated with water (solvent control) induced mild cytotoxicity leading to a reduced in cell viability compared to PBS (solvent control) at all time points studied. In addition, the cell viability of BAEC treated with unmodified AuNPs also induced similar mild cytotoxicity as the water control at all time points studied.

At 24 h, no cytotoxicity was observed for all PEGylated MPCs (Figure 2.13A). However, pro-longed incubation of 48 h and 72 h showed mild cytotoxicity for all PEGylated MPCs similar to unmodified AuNPs (Figure 2.13B,C). This may be attributed to the cumulative cytotoxicity effect due to increased AuNP cellular uptake over time leading to cytotoxicity.

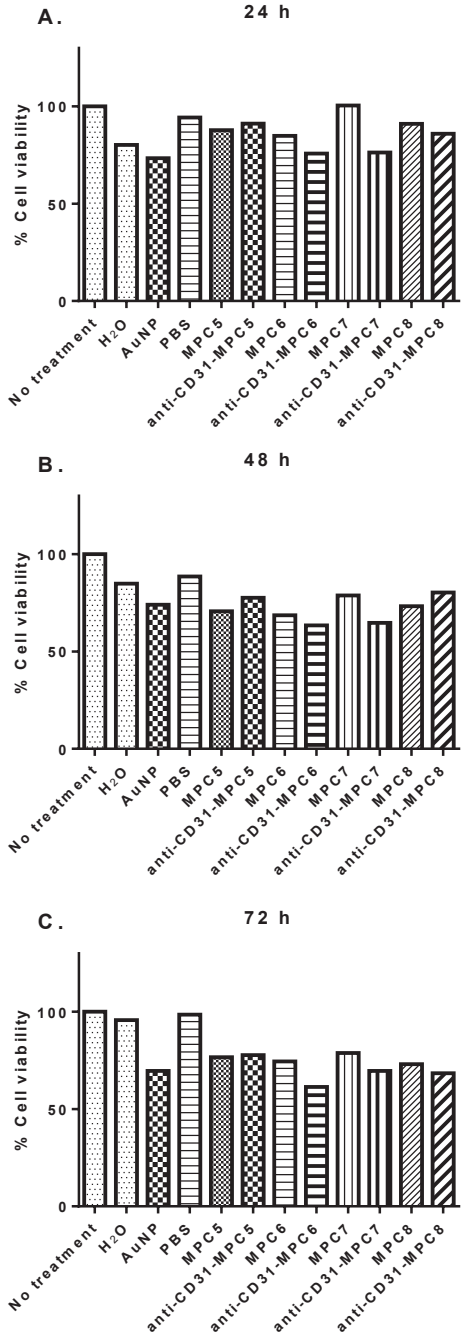

Figure 2.13 Preliminary cytotoxic effect of AuNP treatment on BAEC

Cell viability of BAEC treated with 50 µL of water (H_2O), PBS 1x, AuNPs, MPC5, anti-CD31-MPC5, MPC6, anti-CD31-MPC6, MPC7, anti-CD31-MPC7, MPC8, and anti-CD31-MPC8 at concentration of 1.7 nM for (A) 24, (B) 48, and (C) 72 h in replicate of five; n=1.

2.4 Discussion

The as synthesized citrate-coated AuNPs with a hydrodynamic diameter between 20–30 nm and with a SPR peak at 520 nm. The unmodified AuNPs are unstable in high ionic strength solvent such as PBS and precipitate immediately. Studies have shown that the presence of any electrolytes that constrict the ionic double layer and reduce electrostatic repulsion between the positively charged particles which results in particle aggregation (Hayat 1989). Our study showed that biological molecules such as proteins such as BSA (nonspecific binding) or antibodies (specific binding) can be used to functionalize the AuNPs for passive or active targeting, respectively. An increased in particle diameter as a result of direct conjugation of BSA or antibodies is observed accompanied by a red shift effect on SPR peaks in line with previous studies (El-Sayed 2001; Murphy et al. 2008). Both BSA- and antibody-conjugated AuNPs have slightly improved stability compared to unmodified AuNPs due to steric hindrance, however, a loss of nanoparticle-bound antibody in agglomeration was observed overtime.

In this study, methodology for preparation of mixed-hetero-bifunctionalized PEGylated MPCs with hydrodynamic diameters between 28–65 nm using varied lengths of PEG showed increased stability and were more resistant to agglomeration in biological environments and against protein adsorption. In addition, the overall surface charge of MPCs can be tuned by changing the ratio and density of the functional ends of the PEG and ligand conjugates. A red shift effect was also observed with the increment of particle size, altered surface ζ potential depending on surface function group, and critical flocculation concentration greater than 1 M of NaCl. The surfaces of carboxyl ends can support one or more ligand modification containing amine which can be covalently anchored onto MPCs via a strong amide bond. MPCs conjugated with endothelial specific anti-CD31, fluorophore AF594 cadeverine, and dual AF594/anti-CD31 was prepared and characterized. The primary antibody used in this study is CD31 also known as platelet endothelial cell adhesion molecule-1, expressed on the surface of endothelial cells, commonly used to label cell-cell adhesion and migration. Upon anti-CD31 immobilization on MPCs, there was an increase in the hydrodynamic size and a change in the absolute charge on the particles, yet the solutions remained stable as no change in SPR peak was observed before and after modifications.

Cellular uptake and labelling of MPCs with/without antibody conjugation was examined in BAEC using HR-SEM (in lens/backscatter mode) with electron backscatter detection analysis. The modified gold nanoparticles have shown significantly different behaviour in their interaction with the endothelial cells compared to the unmodified, as synthesized, citrate-coated AuNPs. In fact, aggregation of nanoparticles could influence their ability to interact with or enter into cells (Alkilany & Murphy 2010; Vesaratchanon, Nikolov & Wasan 2007). Studies have also shown cellular uptake depends of the sedimentation rate of colloidal gold to the bottom of culture wells and onto the surfaces of cells, followed by facilitated internalization via phagocytosis or pinocytosis, leading to cumulative cytotoxicity effects (Cho, Zhang & Xia 2011; Shukla et al. 2005; Vesaratchanon, Nikolov & Wasan 2007). We showed selective targeting of anti-CD31-MPCs and labelling of surface CD31 antigen of BAEC which was not observed for unconjugated MPCs. Immunofluorescence staining of anti-CD31-MPCs demonstrated high binding affinity at low concentrations to CD31 surface antigen on HCAEC. The localization of anti-CD31-MPCs observed using immunofluorescence coincides with the position of elemental gold accumulation from HR-SEM electron backscatter detection analysis. The differences between HCAEC fluorescence staining unconjugated anti-CD31 and MPC-conjugated anit-CD31, there would probably be a lot less of the anti-CD31 antibody on the MPCs than in the unconjugated solution, thus reducing the secondary antibody fluorescence in the images.

Our preliminary cytotoxicity study showed that prolonged exposure of both unmodified AuNPs and MPCs modified with or without anti-CD31 may induce an adverse effect compared to the endothelial cells receiving water or PBS treatment. Studies have shown that surface modification by PEGylation and antibody conjugation improved biocompatibility without inducing adverse nanotocity effect(Cho et al. 2010; Karakoti et al. 2011; Simpson et al. 2011). In this study, the anti-CD31 MPCs and MPCs showed no difference in cytotoxicity profile compared to the unmodified AuNPs. Here, we showed greater efficacy of non-specific accumulation of unmodified AuNPs on endothelial cells compared to the anti-CD31-MPCs which exhibited high selectivity and binding affinity to CD31 surface antigen of endothelial cells.

Although the MPCs have greater stability with an adaptable platform for targeted or non-targeted functionalization, they may be limited to *in vitro* cell labelling studies of angiogenesis due to the requirement of high concentration of MPCs administration for detectable cellular localization. By contrast, the unmodified AuNPs are inexpensive to synthesize and economical for upscale production without the cost of antibodies for both *in vitro* and *in vivo* studies. Therefore, the 21nm unmodified (citrate-coated) AuNPs although limited in their stability were a better candidate in this research project to further investigate on their potential therapeutic application for obesity and its related-metabolic syndrome.

CHAPTER 3

In Vitro *Study of the Effect of Gold Nanoparticles on Macrophages and Adipocytes*

3. *In vitro* study of the effect of gold nanoparticles on macrophages and adipocytes

3.1. Introduction

Adipocytes are the main cellular component making up to about 70% of adipose tissue while the other stromal vascular fraction, is composed of many heterogenous cell type including pre-adipocytes, fibroblasts, endothelial cells, and macrophages (Cawthorn & Sethi 2008; Heilbronn & Campbell 2008; Symonds 2011). During obesity, an increase of macrophages infiltration in adipose tissue and adipocyte hypertrophy results in elevated levels of pro-inflammatory cytokines and release of fatty acids (Ahima 2009). In addition to producing pro-inflammatory cytokines as part of their role in frontline host-defence, macrophages also engulf foreign materials via pinocytosis for particles smaller than 100 nm in diameter (e.g. nanoparticles) and by macropinocytosis or phagocytosis for particles larger than 100 nm (Shukla et al. 2005; Steirtman, Brodie & Cohn 1976). These characteristics of macrophages make them a suitable target for AuNPs.

In a recent study, Chen et al. (2013) have shown that a single intraperitoneal injection of 21 nm spherical "naked" AuNPs led to fat loss in lean C57BL/6 mice (Chen et al. 2013). The injected AuNPs were observed to accumulate in the abdominal fat tissues and significantly reduced mRNA expression of the pro-inflammatory cytokines, TNF-α and IL-6 in the abdominal fat tissue (Chen et al. 2013). It was therefore postulated that AuNP induced fat loss and inhibition of inflammatory cytokine production in the adipose tissue may be useful in the treatment of obesity and its related metabolic disorders.

Therefore, cellular uptake of "naked" AuNPs by macrophages may modulate macrophage activity and function, which in turn change local systemic immune responses. In particular, the current study focuses on the changes of pro-inflammatory cytokines including IL-1β, IL-2, IL-6, IL-8, interferon gamma (IFN-γ), TNF-α, and granulocyte-macrophage colony-stimulating factor (GM-CSF) which are responsible for

early responses and amplifying inflammatory reactions (Zhang & An 2007). On the other hand, IL-4 and IL-10 have been demonstrated to have anti-inflammatory activities, where they counteract inflammatory responses (Opal & DePalo 2000). Therefore, our *in vitro* studies of pro- and anti- inflammatory cytokines will provide critical insights into the mechanism of AuNP regulation of macrophage activity.

We therefore hypothesized that *in vitro* 21 nm spherical citrate-stabilized AuNPs can reduce macrophage pro-inflammatory cytokine production, which will in turn affect fat cell metabolism. The first aim was to study the impact of AuNPs on the inflammatory responses in both quiescent and activated macrophage cell-lines *in vitro*. The second aim was to study the impact of AuNPs on adipokine production and lipid metabolism by differentiated adipocyte cells *in vitro*. The third aim was to examine the effects of AuNPs on co-cultured macrophage-like cells and adipocytes, to model their co-localization within adipose tissue.

3.2. Methods

3.2.1. Cell culture and AuNP treatment

3.2.1.1. Materials

Cell culture was performed using a Class II Biosafety cabinet. Sterilisation of the biosafety cabinet work station was conducted by ultra-violet light illumination for 15–20 min, followed by 80% ethanol solution cleaning before and after use. All media and solutions were warmed to 37°C in a water bath prior to all cell culture work. All mammalian cell-lines were maintained in a 5% CO_2 humidified tissue culture incubator (MCO-17AI, Sanyo, Osaka, Japan) at 37°C and were routinely tested for mycoplasma. Cell concentration was determined using a Neubauer haemocytometer and adjusted as required for cell seeding in subsequent experiments. All the other materials used for cell culture in this chapter are listed in Table 3.1. The 21 nm "naked" AuNPs prepared in Chapter 2 were used in this study. The 31.5 μg/mL AuNPs dosage was chosen based on the preliminary findings in a study on U937 monocytic cell line carried by a previou

student Ms. Alicia Dorrigan in 2010 (unpublished). In this study, additional two concentration of 0.315 μg/mL and 3.15 μg/mL AuNPs were also investigated.

3.2.1.2. Murine RAW 264.7 macrophage-like cell line

Murine RAW264.7 macrophage-like cell line (RMΦ) was obtained from A/Prof. Bronwyn O'Brien at School of Life Sciences, University of Technology Sydney. RMΦ were maintained in DMEM supplemented with 10% FBS and 1% P/S at 37°C in a 5% CO_2 humidified atmosphere. The cells were routinely passaged at ~80% confluence by gently scraping the monolayer of adherent cells from the bottom of the tissue culture flask. The detached cells were then resuspended and seeded into 6-well or 96-well tissue culture plates at desired concentration and allowed to adhere overnight before all cell experiments.

RMΦ at density of ~1×10^6 cells/well in a 6-well plate or 1×10^4 cells/well in a 96-well plate, were treated with AuNPs of low dose (RMΦL, 0.315 μg/mL of AuNPs), high dose (RMΦH, 3.15 μg/mL of AuNPs) or extremely high dose (RMΦHH, 31.5 μg/mL of AuNPs) for 1, 24, and 72 h. Treatment with PBS was used as negative control (RMΦC), while treatment with LPS at a concentration of 1 ng/mL (RMΦLPSL) or 10 μg/mL (MΦLPSH) were used as positive controls for cell activation. The cell supernatant and whole cells were collected at the end of the incubation for western blot and real-time-polymerase chain reaction (RT-PCR) analysis.

Table 3.1 Details of materials used for macrophage and adipocyte cultures

Materials	Catalogue number/supplier
Mammalian cell lines:	
Murine RAW264.7 macrophage (RMΦ), adherent	CL-173, ATCC®
Human U937 monocyte (UMΦ), non-adherent	CRL-1593.2, ATCC®
Murine 3T3-L1 fibroblast, adherent	TIB-71, ATCC®
Culture media:	
Dulbecco's Modified Eagle's Medium (DMEM)	D5796, Sigma Aldrich
Roswell Park Memorial Institute (RPMI) 1640	11875-093, Life Technologies
Media supplements/chemicals:	
Heat-inactivated Fetal Bovine Serum (FBS)	10082-147, Life Technologies
Penicillin and Streptomycin (P/S, antibiotics)	5140-122, Life Technologies
Phorbol 12-Myristate 13-Acetate (PMA)	P8139, Sigma Aldrich
Lipopolysaccharide (LPS)	L7770, Sigma Aldrich
New Calf Serum (NCS), New Zealand	16010-159, Life Technologies
Insulin	I0516, Sigma Aldrich
Dexamethasone	D4902, Sigma Aldrich
3-Isobutyl-1-Methly-Xanthine	I5879, Sigma Aldrich
Biotin	B4639, Sigma Aldrich
Buffer solutions:	
Dulbecco's Phosphate Buffered Saline (DPBS)	14190-144, Life Technologies
Trypsin-Ethylene Diamine Tetraacetic Acid solution (Trypsin-EDTA)	15400-054, Life Technologies
N-2-Hydroxyethylpiperazine-N-2-Ethane Sulfonic acid buffer (HEPES)	15630-080, Life Technologies

ATCC®, Manassas, VA, USA; Sigma Aldrich, St. Louis, MO, USA; Life Technologies, Carlsbad, CA, USA

3.2.1.3. Human U937 monocyte cell line

Human U937 monocytes (UMΦ) were cultured in RPMI supplemented with 10% FBS and 10 mM of N-2-hydroxyethylpiperazine-N-2-ethane sulfonic acid (HEPES) buffer without antibiotics at 37°C in a 5% CO_2 humidified atmosphere as previously described (Passmore, Lukey & Ress 2001). The monocytes were maintained in their non-adherent and undifferentiated state in the tissue culture flasks and were routinely passaged every 3–4 days.

UMΦ can be induced to differentiate into a macrophage-like state using PMA. Following differentiation with PMA, the non-adherent monocytes became adherent, their size increased and morphology changed becoming elongated and spindle-shaped (Minta & Pambrun 1985). Briefly, the monocytes at a density of ~1×10^6 cells/well in a 6-well plate were treated with RPMI medium supplemented with 10% FBS, 10 mM HEPES and 160 nM PMA for 24 h. Then, UMΦat ~80–90% confluence were treated with AuNPs of low dose (UMΦL, 0.315 µg/mL of AuNPs), high dose (UMΦH, 3.15 µg/mL of AuNPs) or extremely high dose (UMΦHH, 31.5 µg/mL of AuNPs) with PBS only as negative control (UMΦC).

In another experimental setting, UMΦ were exposed to 10 µg/mL of LPS to induce inflammatory responses in the presence of AuNPs at high dose (UMΦH_LPS, 3.15 µg/mL of AuNPs) or extremely high dose (UMΦHH_LPS, 31.5 µg/mL of AuNPs) with PBS treatment as negative control (UMΦC_LPS). Cell supernatants were collected at 1, 24, and 72 h post-treatment for cytokine analysis.

3.2.1.4. Murine 3T3-L1 fibroblast cell line

Murine 3T3-L1 fibroblast (pre-adipocyte) cell line was obtained from Dr. Weihua Fei at the School of Biotechnology and Biomolecular Sciences, University of New South Wales. The 3T3-L1 pre-adipocytes were cultured in Basal Medium I, which is DMEM supplemented with 10% new calf serum (NCS), and 1% P/S at 37°C in a 5% CO_2 humidified atmosphere. The adherent cells were detached from the tissue culture flask

with 0.05% trypsin-EDTA and routinely passaged at ~80% confluence. The trypsin-EDTA detached cells were then resuspended and seeded in 6-well or 96-well tissue culture plates at the desired concentration and allowed to adhere to the plastic overnight before proceeding with cell differentiation treatment.

Figure 3.1 showed the morphologic changes of 3T3-L1 pre-adipocytes to mature adipocytes during differentiation are outlined, along with details of the respective differentiation medium used. The 3T3-L1 pre-adipocytes were differentiated into mature adipocytes according to pre-optimized protocols (Yamashita et al. 2007; Zebisch et al. 2012). Briefly, 3T3-L1 pre-adipocytes were seeded at $0.5–1\times10^5$ cells/well in a 6-well plate or $2–6\times10^3$ cells/well in a 96-well plate. The pre-adipocytes were cultured to reach 100% confluence in the Basal Medium I, after which, they were incubated for an additional 2 days in fresh Basal Medium I. The cells were then induced to differentiate into mature adipocytes by treating with Differentiation Medium I [DMEM supplemented with 5 µg/mL of insulin, 1 µM of dexamethasone, 0.5 mM of 3-isobutyl-1-methly-xanthine (IBMX), 100 ng/mL of biotin, 10% FBS, and 1% P/S] for 2 days. Afterwards, the cells were incubated in Differentiation Medium II [DMEM supplemented with 5 µg/mL insulin, 10% FBS and 1% P/S] and replaced with fresh media every 2 days. At day 6, Basal Medium II [DMEM supplemented with 10% FBS, and 1% P/S] was introduced to the adipocytes for another 2 days. Mature adipocytes are characterized with increased intracytoplasmic accumulation of lipid droplets and alteration of their morphology from fibroblastic elongated shape to a more rounded shape (Green & Meuth 1974). All cell experiments were conducted using mature adipocytes between Days 8–12, as the differentiated adipocytes tend to become hypertrophied and contain larger lipid droplets after 21 days of differentiation. At day 8, the cells were stained with Oil red O to demonstrate intracytoplasmic neutral lipid formation, a characteristic of mature adipocytes (Figure 3.1).

Differentiated 3T3-L1 adipocytes were then treated with AuNPs at low dose (AL, 0.315 µg/mL of AuNPs), high dose (AH, 3.15 µg/mL of AuNPs) or extremely high dose (AHH, 31.5 µg/mL of AuNPs) with PBS as control (AC). The cell supernatants and whole cells were harvested and collected at 1, 24, and 72 h post-treatment for RT-PCR and bioassay analyses. Neutral lipids in the adipocytes were stained using Oil red O and

cell nuclei were counterstained with Dapi stain (specific details in section 3.2.8). In another experiment, a high dose (3.15 μg/mL) of AuNPs was supplemented in the differentiation medium every second day to investigate their effect on adipocyte differentiation, in which cells were assessed by Oil red O staining at Days 2, 4, 6, 8, and 12 post-treatment.

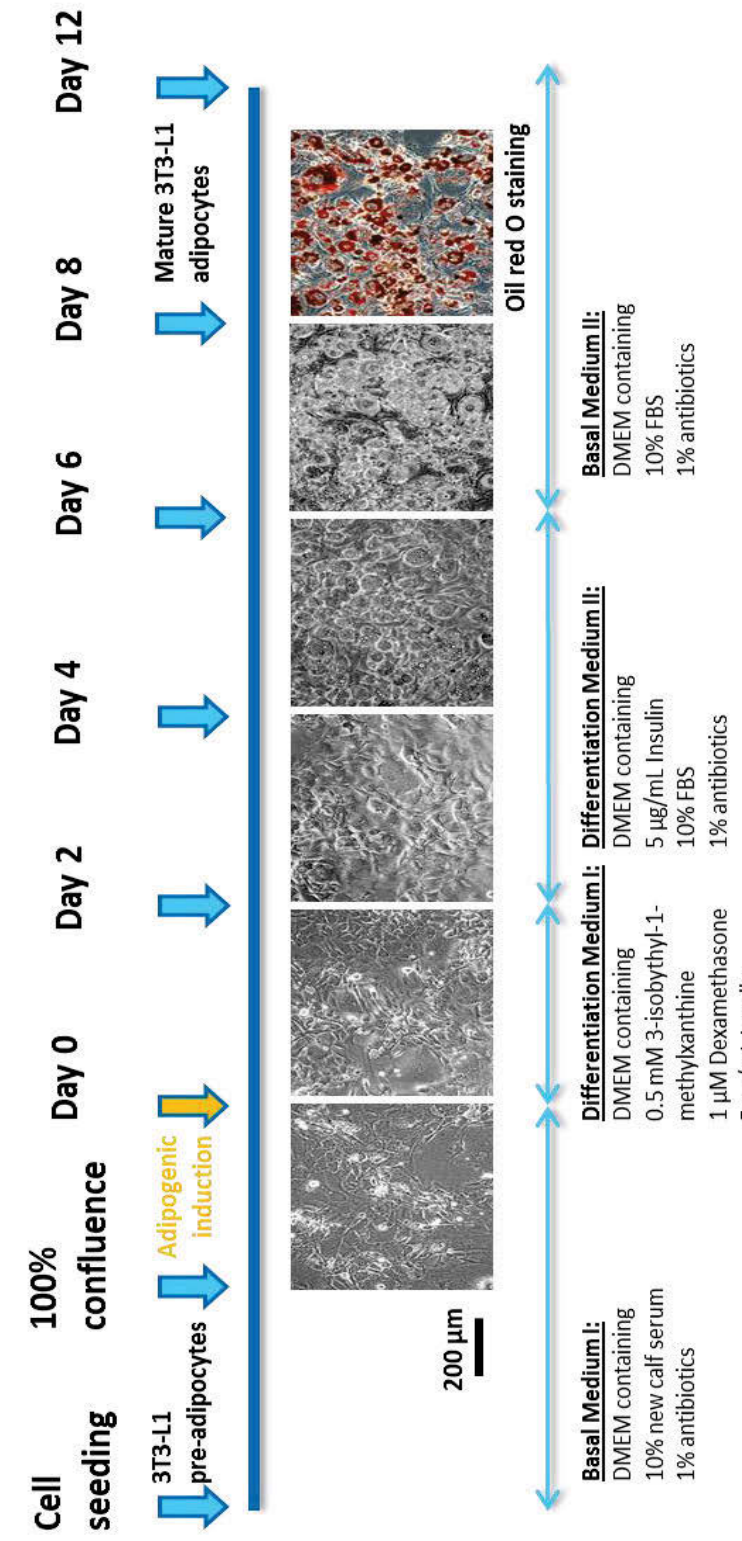

Figure 3.1 Visual images capture differentiation of 3T3-L1 pre-adipocytes into mature adipocytes. Images taken under 10 x magnification.

3.2.1.5. Co-culturing of murine mature adipocytes and macrophage cells

Murine 3T3-L1 mature adipocytes and RMΦ and were co-cultured in a contact system using a ratio of 15:1 of each cell type respectively as previously described (Suganami, Nishida & Ogawa 2005). Fewer RMΦ were added because they continue to proliferate while the adipocytes do not, while under physiological conditions the number of ATMs is also less than adipose tissue. Briefly, mature 3T3-L1 adipocytes were seeded ~1.5×10^6 cells/well in 6-well plate or ~1×10^4 cells/well in 96-well plate and serum starved overnight, followed by co-seeding with RMΦ at a concentration of ~1.5×10^5 cells/well in 6-well plate or ~1×10^3 cells/well in 96-well plate. The cells were then left to co-culture for 24 h at 37°C in a 5% CO_2 humidified atmosphere.

The co-culture system was then treated with AuNPs at low dose (ARMΦL, 0.315 µg/mL of AuNPs), high dose (AMΦH, 3.15 µg/mL of AuNPs) or extremely high dose (ARMΦHH, 31.5 µg/mL of AuNPs) or with PBS as negative control (ARMΦC). Cell supernatant and whole cells were harvested and collected at 1, 24, and 72 h for RT-PCR and bioassay analyses.

3.2.2. MTT assay

MTT cell proliferation assay was performed in a 96-well plate for all cell lines studied in this chapter as described in section 2.2.7.7. This assay measured the catalytic cellular activity of mitochondrial dehydrogenase which converts the water soluble MTT into insoluble formazan in water. In this chapter, a higher concentration of MTT (5 mg/mL) was added to each well containing cells in 100 µL of fresh culture media. The 96-well plates were then incubated at 37˚C in a 5% CO_2 humidified atmosphere for 2 h after which time the supernatants were discarded. The formazan formed were dissolved in dimethyl sulfoxide and absorbance read at 570 nm using Synergy HT microplate spectrophotometer (Bio-Tek Instrument Inc., Winooski, VT, USA). Results were expressed as the mean percentage of viability ± S.E.M relative to the control. The concentration of RAW 264.7 macrophages per well were determined by a standard curve ($R^2 = 0.9668$, Figure 3.2).

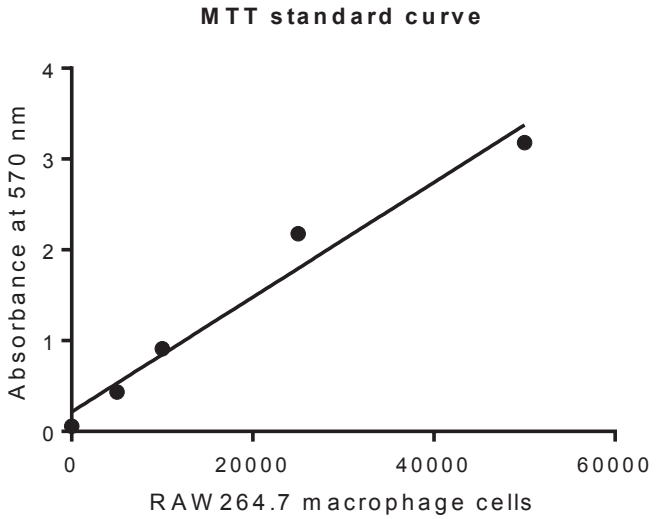

Figure 3.2 Standard curve of the MTT assay derived from titration of RAW 264.7 macrophages of known concentrations measured at 570 nm. Y = 0.0632X + 0.2142.

3.2.3. Intracellular reactive oxygen species (ROS) measurement

RAW macrophages and 3T3-L1 adipocytes treated with AuNPs (0.315 µg/mL, 3.15 µg/mL or 31.5 µg/mL) in 96-well plate were assessed for intracellular ROS, as an indication of oxidative stress. The concentration of ROS was determined using a 2',7'-dicholorofluorescein diacetate (H_2-DCFDA, D6883, Sigma Aldrich, St. Louis, MO, USA) method modified for fluorescent microplate reader as previously described (Wang & Joseph 1999). Briefly, the supernatants of cultured cells in 96-well plate were removed and the cells were washed with Dulbecco's Phosphate Buffered Saline (DPBS, Life Technology, Carlsbad, CA, USA) to remove residual serum. The cells were then incubated with 10µM of H_2-DCFDA in DPBS at 37˚C for 12 min in the dark. After being oxidized by various oxidants in the viable cells, the non-fluorescent H_2-DCFDA is converted to a highly fluorescent 2',7'-dicholorofluorescein (DCF). Subsequently, the staining solution was removed and the cells were washed with DPBS. In the final step, 100 µL of DPBS was added to each well and the fluorescence signals at 485 nm excitation and 530 nm (or 580 nm) emission were measured immediately with Infinite M200® Pro plate reader (Tecan Deutschland GmbH, Crailsheim, Germany). The fluorescence intensity of H_2-DCFDA detected was adjusted to the cell viability of

adjacent wells and the intracellular ROS measured were expressed as fold differences to the control.

3.2.4. Western blot analysis

3.2.4.1. Protein isolation

RAW246.7 macrophages were lysed in ice-cold RIPA lysis buffer containing 1% Nonidet P-40, 0.1% SDS, 0.5% deoxycholate, 150 mM NaCl, 50 mM Tris (pH 8), and protease inhibitor cocktail (P8340, Sigma Aldrich, St Louis, MO, USA). The protein lysates were extracted via centrifugation at 13,000 rpm for 15 min at 4°C and quantified using DC Protein Assay Kit II (500-0112, Bio-Rad, Hercules, CA, USA). Briefly, 5 µL of protein lysate was incubated with 25 µL reagent A and 200 µL of reagent B at room temperature for 15 min. The absorbance was then detected using Synergy HT microplate spectrophotometer (Bio-Tek Instrument Inc., Winooski, VT, USA) at 750 nm. The concentrations of the protein lysates were calculated according to a standard curve using known concentrations of BSA ($R^2 = 0.9821$, Figure 3.3).

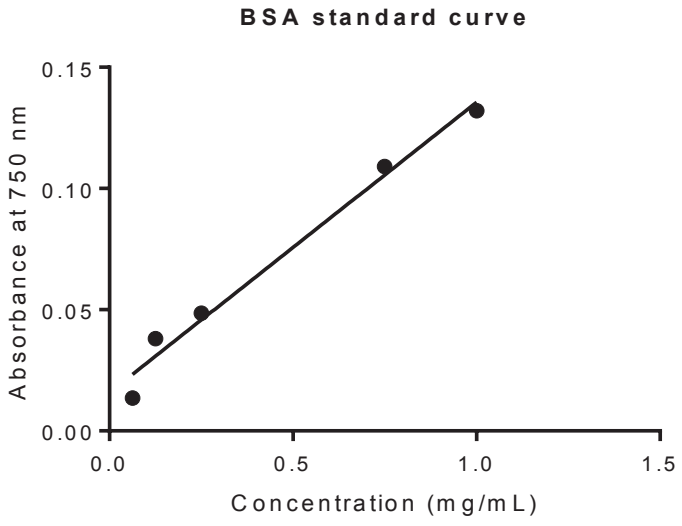

Figure 3.3 Standard curve derived from serial dilution of BSA of known concentration measured at Abs 750 nm, assayed using DC Protein Assay Kit II. Y = 0.1197*X + 0.01584.

3.2.4.2. Protein gel electrophoresis

Protein lysates containing 20 µg of protein were denatured at 95˚C for 5 min in 1x sample buffer [2% sodium dodecyl sulphate (SDS), 10% glycerol, 1% β-mercaptoethanol, 150 mM Tris, and 0.02 % of bromophenol blue (pH 6.8)]. Protein samples were separated on NuPAGE® 4–12% Bis Tris gel using SureLock™ gel electrophoresis system with NuPAGE® MES SDS running buffer (Life Technologies, Carlsbad, CA, USA) at 120 V for approximately 50 min or until the bromophenol blue dye indicator ran to the bottom of the gel. Separated protein samples were then transferred onto polyvinylidene difluoride membrane (PIE88518, Thermo Scientific, Waltham, MA) using TransBlot® Semi-Dry Electrophoretic Transfer Cell (Bio-Rad, Hercules, CA, USA) at 20V for 30 min. The protein membranes were blocked with tris-buffered saline containing tween-20 (0.01% v:v) (TBST) and 5% skim milk at room temperature for 2 h. The membranes were then washed with TBST and incubated overnight at 4°C with primary antibody in TBST containing 1% skim milk: rabbit monoclonal anti-TNF-α (1:1000, AB2148P, Merck Millipore, Billerica, MA, USA), mouse monoclonal anti-TLR-4 (1:500, sc-293072), rabbit polyclonal anti-inhibitory kappa kinase (IKK) α/β (1:500, sc-7607) or mouse monoclonal anti-β-actin (1:1000, sc-47778) from Santa Cruz Biotechnology, Dallas, TX, USA. Subsequently, membranes were washed and further incubated for 1 h at room temperature with secondary antibody in TBST containing 1% skim milk: goat polyclonal anti-rabbit-horseradish peroxidase (HRP) or goat polyclonal anti-mouse-HRP at 1:5000–10000 dilution from Santa Cruz Biotechnology, Dallas, TX, USA. Protein expression was measured using SuperSignal West Pico Chemiluminescence Substrate solution (PI-34087, Thermo Scientific, Waltham, MA, USA) and detected by LAS 3000 Image Analyzer (Fujifilm, Tokyo, Japan). The western blot bands were quantified by densitometry using Multi Gauge version 3.0 software (Fujifilm, Tokyo, Japan) where the relative protein expression was normalized by internal control, β–actin.

3.2.5. Gene expression analysis using RT-PCR

3.2.5.1. RNA isolation

TRIzol was used for RNA extraction, isolation, and purification as previously described (Chomczynski 1993; Simms, Cizdziel & Chomczynski 1993). The cultured cells were lysed in 500 μL of TRI reagent (T9424, Sigma-Aldrich, St. Louis, MO, USA) at room temperature for 10 min. Then, 0.1 ml of chloroform (>99.8%, BDH, Muskegon, MI, USA) was added to the samples, mixed well, and left at room temperature for 2–3 min before centrifugation at 13,000 g for 20 min at 4ºC. The sample mixtures were separated into 3 phases: a lower organic phase (containing protein), an intermediate phase (containing DNA), and an upper aqueous phase (containing RNA). The aqueous layer was transferred into a fresh Eppendorf tube and 0.25 mL of isopropanol (>99.5%, BDH1133, BDH, Muskegon, MI, USA) was added. The mixture was allowed to stand overnight at -20ºC for RNA precipitation. The precipitated RNA was extracted via centrifugation at 13,000 g for 15 min at 4ºC to form a pellet, rinsed with 75% ethanol, and dissolved in 0.1 mL DEPC-treated water containing DNase (1 U/μL, 18047-019, Life Technologies, Carlsbad, CA, USA). The reconstituted RNA samples were incubated at 37ºC for 10 min to remove possible DNA contamination and the DNAse was denatured by incubating the samples at 60ºC for 5 min. Total RNA concentrations was determined using an ND-1000 spectrometer (Thermo Fisher Scientific, Wilmington, DE, USA) and final concentration of samples diluted to 200 ng/μL.

3.2.5.2. cDNA synthesis

Purified total cellular RNA was used as template to generate first-strand cDNA using M-MLV Reverse Transcriptase, RNase H Minus, Point Mutant Kit (M3683, Promega, Madison, WI, USA) according to the manufacturer's instruction. Briefly, random primers were added to 1 μg of RNA and incubated using Mastercycler® Pro (Vapo.protect™ Technologies, Eppendorf, Hamburg, Germany) at 70ºC for 5 min, then cooled at 4ºC for 5 min. Master mix containing H-point mutant enzyme, dNTP and M-MLV reaction buffer was added to the RNA mixture and further incubated at room temperature for 10 min, 42ºC for 1.5 h, and finally at 70ºC for 15 min. cDNA were then

quantified using ND-1000 spectrometer (Thermo Fisher Scientific, Wilmington, DE, USA) and diluted to 200 ng/μL.

3.2.5.3. TaqMan® gene expression assay detection

Pre-optimized and validated TaqMan® gene expression assay probe/primers were used for the quantitative real-time PCR (Chen et al. 2011). The reagents for TaqMan® gene expression assay was listed in Table 3.2.

Table 3.2 Reagent composition for TaqMan® gene expression assay

Reagents	Single reaction
Platinum® quantitative PCR SuperMix-UDG	5 μL
FAM-labelled probe	0.5 μL
VIC-labelled probe	0.15 μL
ROX reference dye	0.2 μL
DEPC-treated deionised water	1.65 μL
cDNA (200 ng/μL)	2.5 μL
Total	10 μL

Briefly, 2.5 μL of cDNA (200 ng/μL) were thoroughly mixed and pipetted in duplicate onto 96 well twin-tec real-time PCR plate (0030132505, Eppendorf, Hamburg, Germany) using epMotion 5070 (Eppendorf, Wien, Austria) to reduce pipetting errors. Then 7.5 μL of PCR master mix solution containing 5 μL of Platinum® quantitative PCR SuperMix-UDG (11730-025, Life Technologies, Carlsbad, CA, USA), 0.5 μL of target gene (primer labelled with FAM,

Table 3.4), 0.15 μL of housekeeping gene (18s rRNA, labelled with VIC, Table 3.4), 0.2 μL of ROX dye, 1.65 μL of DEPC-treated deionised water was added. The RT-PCR amplifications were ran under the following cycling conditions in a Mastercycler® Ep Realplex^2 (Eppendorf, Hamburg, Germany): 50°C for 2 min and 95°C for 2 min incubations, followed by 40 cycles at 95°C for 15 sec, and 60°C for 30 sec (Table 3.3).

Table 3.3 RT-PCR amplification program for TaqMan® gene expression assay

Step	Temperature	Time	Cycle
Reaction mix incubation	50°C	2 min	1
Polymerase activation	95°C	2 min	1
Two-step amplification cycles:			
1. Denaturation	95°C	3 sec	40
2. Annealing/elongation	60°C	30 sec	

The pre-optimized oligonucleotide primers used in this study were of *Mus musculus* origin (Table 3.4). Gene expression was normalized against the housekeeping gene, 18s rRNA. A sample from the Control group was then arbitrarily assigned as a calibrator against which all other samples were expressed as fold change difference. The relative change in mRNA gene expression was determined by the ΔΔCT approach (Bustin 2000). The changes to mRNA expression of inflammatory markers including TNF-α, IL-6, IL-1β, and TLR-4 were determined for the AuNP-treated RAW246.7 macrophages. Whereas mRNA expression of adipokine markers including CPT-1α, ATGL, PPARγ, and GLUT-4 were determined for the AuNP-treated 3T3-L1 adipocytes. Both inflammatory and adipokine markers were investigated for the AuNP-treated adipocyte-macrophage co-cultures.

Table 3.4 Taqman® gene expression assay primer sequences

Marker	NCBI gene ref.	FAM-labelled probes (5’ →3’)	Assay ID
TNF-α	NM_001278601.1	GACCCTCACACTCAGATCATCTTCT	Mm00443258_m1
IL-6	NM_031168.1	TGAGAAAAGAGTTGTGCAATGGCAA	Mm00446190_m1
IL-1β	NM_008361.3	GACCCCAAAAGATGAAGGGCTGCTT	Mm00434228_m1
TLR-4	NM_021297.2	CCCTGCATAGAGGTAGTTCCTAATA	Mm00445273_m1
PPARγ	NM_0011273330.1	ATGCTGTTATGGGTGAAACTCTGG	Mm01184322_m1
ATGL	NM_025802.3	CCAAGACTGAATGGCTGGATGGCAA	Mm00503040_m1
CPT-1α	NM_013495.2	TCCAGGAGAATGCCAGGAGGTCATA	Mm00550438_m1
GLUT-4	NM_009204.2	GGCTCTGCTGCTGCTGGAACGGGTT	Mm00436615_m1
		VIC-labelled probes (5’ →3’)	
18S	X03205.1	ACCGCAGCTAGGAATAATGGA	4319413E

3.2.6. Cell supernatant analysis of secreted cytokines

Cell supernatants of UMΦ treated with AuNPs and/or LPS were used for the cytokine analysis. The concentration of inflammatory cytokines in cell supernatant were determined using a magnetic bead-based Bio-Plex® Pro human cytokine assay (8-plex panel, M50-000007A, Bio-Rad, Hercules, CA, USA) according to the manufacturer's instructions. Briefly, 8-plex cytokine assay kit is an immunoassay formatted on magnetic beads conjugated with monoclonal antibodies specific for IL-2, IL-4, IL-6, IL-8, IL-10, IFN-γ, TNF-α, and GM-CSF in a single well of 96-well plate. The magnetic beads coated with antibodies are useful for the capture and separation of targeted cytokines. In this assay, 50 µL of culture supernatant was reacted with the antibody-coupled beads. A series of washes were performed using an automated wash program on a Bio-Plex Pro wash station (Bio-Rad, Hercules, CA, USA) to remove any unbound proteins. The unwanted sample constituents such as large or fibrous particulates or viscous sample matrix may be washed away following a simple magnetic separation step. A biotinylated detection antibody was then added to create a sandwich complex which can be detected by the streptavidin-phycoerythrin conjugate with fluorescence.

The multi-plex beads were then assayed using the detection system Bio-Plex MAGPIX system (Bio-Rad, Hercules, CA, USA). Overall, highly efficient magnetic separation eliminates potential interfering molecules, allowing sensitive detection of targets. For each cytokine, nine standards ranging from 0.5 to 32,000 pg/ml were made to give standard curves with a minimum detectable concentration between 0.5 and 5 pg/ml. The standard curves and sample concentration of cytokines were generated by the Bio-Plex Manager 4.1 software (Bio-Rad, Hercules, CA, USA).

3.2.7. Biochemical assays

The cell culture supernatants and whole cell lysates extracted in water were used for various biochemical assay analysis according to manufacturer's instructions.

3.2.7.1. Non-esterified free fatty acids (NEFA) concentration

NEFA or free fatty acid concentration in the cell lysate was measured using NEFA-C kit (Wako Pure Chemicals Industries Ltd., Osaka, Japan) according to the manufacturer's instruction. The assay is based on an enzymatic colorimetric method as previously described (Chen et al. 2014). Briefly, 5 µL of cell lysate or supernatant were incubated with 100 µL of colour reagent solution A in a 96-well plate at 37˚C for 10 min. Subsequently, 200 µL of colour reagent solution B was added to the wells and further incubated at 37˚C for 10 mins to detect hydrogen peroxide produced which is proportional to the NEFA in the sample. The intensity of the colorimetric indicator was measured using a Synergy HT microplate spectrophotometer (Bio-Tek Instrument Inc., Winooski, VT, USA) at 550 nm. The concentration of NEFA in the sample was determined using a standard curve generated using the known concentration of NEFA ($R^2 = 0.9995$, Figure 3.4).

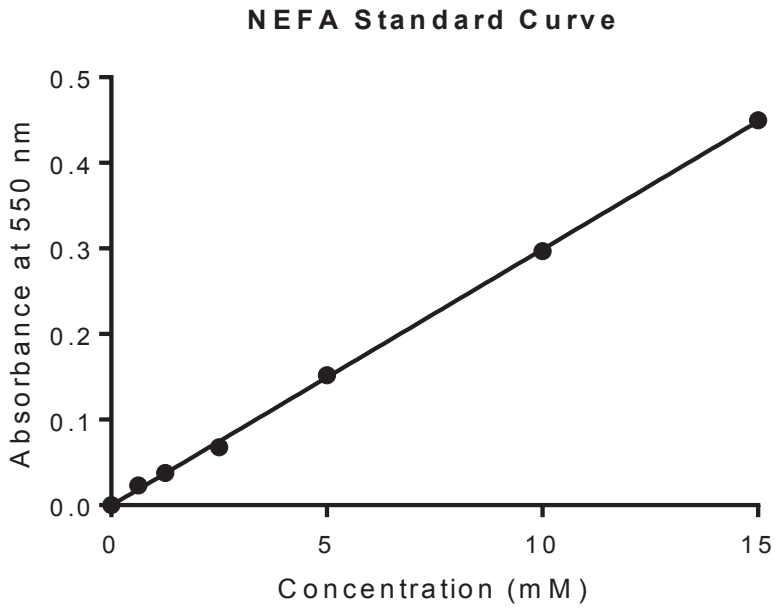

Figure 3.4 Standard curve derived from NEFA standards measured at 550 nm. Y = 0.0299X – 0.0002.

3.2.7.2. Cell Supernatant Triglyceride concentration

Triglyceride concentrations in the cell culture supernatant and cell lysates were measured using Triglyceride GPO-PAP reagent (Roche Diagnostics, Indianapolis, IN, USA) according to an in-house protocol. The assay is based on an enzymatic method where triglycerides are hydrolysed into glycerol and free fatty acids. Briefly, 10 µL of cell supernatant or cell lysate were incubated with 200 µL of triglyceride reagent at 37˚C for 5 min. The glycerol concentration is proportional to hydrogen peroxide formed where the colorimetric dye can be measured using a Synergy HT microplate spectrophotometer (Bio-Tek Instrument Inc., Winooski, VT, USA) at 490 nm. The concentration of triglyceride was determined by a standard curve generated using glycerol standards (G7793, Sigma Aldrich, St Louis, MO, USA, R^2 = 0.9953, Figure 3.5).

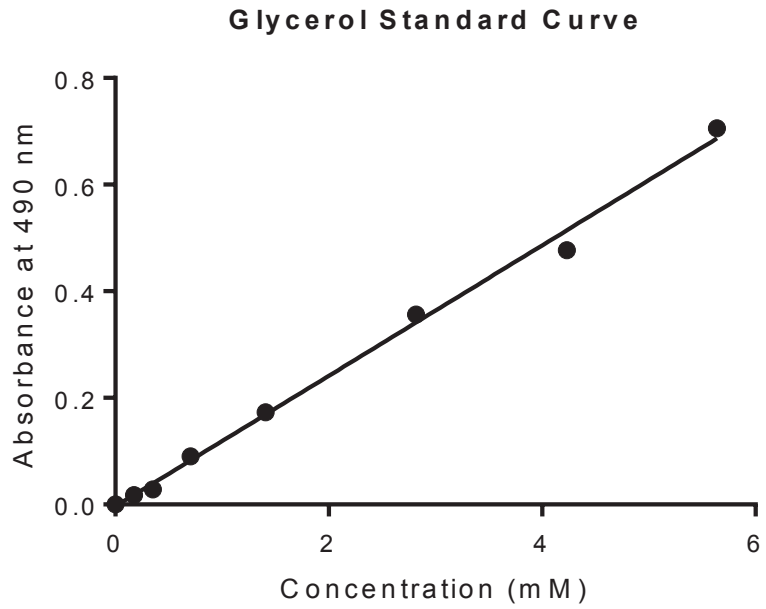

Figure 3.5 Standard curve derived glycerol standards measured at 490 nm. Y = 0.1224X – 0.00348.

3.2.8. Oil-red O staining of adipocytes

Oil red O is a lipid soluble dye commonly used as a fast and simple qualitative marker of cellular neutral lipids and cholesteryl esters (Green & Meuth 1974; Ramirez-Zacarias, Castro-Munozledo & Kuri-Harcuch 1992). The method for Oil red O staining was modified from a published protocol (Green & Kehinde 1975; Ramirez-Zacarias, Castro-Munozledo & Kuri-Harcuch 1992). A stock solution of 0.25% Oil red O was prepared by dissolving 0.5 g of Oil Red O powder (O0625, Sigma Aldrich, St. Louis, MO, USA) in 100 ml of 100% isopropanol (>99.5%, BDH1133, BDH, Muskegon, MI, USA) overnight at room temperature. The stock solution was then filtered through Whatman ashless qualitative filter paper (GE Healthcare Australia Pty. Ltd., Parramatta, NSW, Australia). The 0.1% Oil red O working solution was prepared by mixing 6 mL of stock solution with 4 mL deionised water, which was left standing overnight at 4°C and filtered using 0.2 μm disposable syringe filters (Gilson Scientific Ltd., Bedfordshire, UK) prior to use.

3T3-L1 pre-adipocytes and differentiated adipocytes were rinsed with PBS and fixed in ice-cold 4% paraformaldehyde for 30 min, then rinse with 100% isopropanol followed by 60% isopropanol. Then the cells were immersed in a 0.1% Oil red O working solution for 15 min and thoroughly rinsed with water. Adipocyte cell nuclei were counter stained with 300 nM of Dapi stain (4',6-diamidino-2-phenylindole dihydrochloride, D1306, Life Technology, Carlsbad, CA, USA) for 5 min and rinsed with water. Images of stained mature adipocytes were captured using an inverted light microscope (CKX31 Olympus Co., Tokyo, Japan) with a digital camera attached. More than 800 cells were quantified and analysed from the images using ImageJ (1.6.0_24, fiji.sc, National Institutes of Health, Bethesda, MD, USA).

The extent of adipocyte differentiation was quantified by extraction of Oil red O dye retained by the neutral lipids. The cultured cells were rinsed with PBS, fixed in ice-cold 4% paraformaldehyde for 30 min, and washed with 100% isopropanol and then 60% isopropanol. Fixed cells were stained by immersion in a 0.1% Oil red O working solution for 15 min and thoroughly rinsed with water. Then, the excess water was evaporated in an incubator at 32°C. The Oil red O dye was extracted via isopropanol dissolution. The extracted dye in solution was immediately collected and transferred into a 96-well plate. The absorbance was measured at 510 nm using a Synergy HT microplate spectrophotometer (Bio-Tek Instrument Inc., Winooski, VT, USA). Blank wells with no cells were stained with the dye and rinsed in the same manner and used as background controls.

3.2.9. Insulin-mediated glucose uptake

The efficiency of insulin mediated-glucose uptake by the 3T3-L1 mature adipocytes was determined using a modified 2-deoxyglucose uptake assay. Briefly, adipocyte cultures were pre-treated with PBS control (AC), 0.315 µg/mL AuNP (AL), 3.15 µg/mL AuNP (AH), and 31.5 µg/mL AuNP (AHH) in phenol-red free Dulbecco's Modified Eagle Medium (pf-DMEM) (D5030, Sigma Aldrich, St. Louis, MO, USA) supplemented with 25 mM D-glucose (Univar® Ajax Finechem Pty Ltd, Seven Hills, NSW, Australia), 10% FBS, and 1% P/S for 24 h at 37°C in a 5% CO_2 humidified atmosphere. The cells were gently washed three times with warm PBS. Then, the

adipocyte cultures were serum starved for 3 h in serum-free pf-DMEM (supplemented with 25 mM D-glucose and 1% P/S) at 37°C in a 5% CO_2 humidified atmosphere. Following that, the cells were washed once with glucose-free pf-DMEM containing 0.1% fatty acid free BSA (A7030, Sigma Aldrich, St. Louis, MO, USA). Then, the adipocytes cultures were incubated in DMEM containing 0.1% BSA and 100 nM of insulin with an increasing glucose concentration of 2 mM, 5 mM, or 10 mM at 37°C in a 5% CO_2 humidified atmosphere. Aliquots (50 µL) of cell supernatants were collected at 0 (baseline), 5, 20, and 60 min. The glucose levels in the cell supernatant were determined using an AccuCheck® Performa glucose meter (Roche, Branchburg, NJ, USA).

3.2.10. Statistical analysis

Results are expressed as mean ± S.E.M. Statistical analysis was performed using one- or two- way analysis of variance (ANOVA) followed by post hoc Bonferroni test to determine significant differences between groups (Prism version 6, GraphPad Software Inc, San Diego, CA, USA). $P < 0.05$ was considered statistically significant.

3.3. Results

3.3.1. Effect of AuNP treatment on RAW 264.7 macrophage-like cell line

Monocyte-derived macrophages play a crucial role in the innate immune system, providing a frontline of host-defence by initiation and resolution of inflammation (Janeway et al. 2001; Parihar, Eubank & Doseff 2010). Murine macrophage-like RAW264.7 cells are of monocyte-lineage and are often used to study cell surface receptors in response to microbial ligands and the production of cytokines when appropriately stimulated (Berghaus et al. 2010). Gram-negative bacterial endotoxin, containing LPS signals via a family of cell surface membrane receptors, including TLR-4 expressed by macrophages. This leads to activation of the NF-kB signalling pathway and cellular pro-inflammatory responses (Akira & Takeda 2004; Kawai & Akira 2007).Cell viability of RAW 264.7 macrophages following treatment with AuNPs

Cell viability at 3 different time points following treatment of the RAW 264.7 macrophages with 3 different doses (0.315 µg/mL, 3.15 µg/mL, and 31.5 µg/mL) of AuNPs are shown in . Our results showed that RMΦC groups had a rapid cell proliferation rate with a typical cell doubling time of approximately 12 h (B). At 72 h, the macrophage cells reached ~100% confluency in a standard 96-well tissue culture plate.

The RMΦL group showed no cytotoxicity at 1 h (A). Both RMΦH and RMΦHH cultures showed acute cytotoxicity resulting in significantly reduced cell viabilities compared to the RMΦC at 1 h ($P < 0.05$, A). Longer exposures of up to 24 and 72 h revealed significantly reduced cell viabilities in all AuNP-treated macrophage groups compared to RMΦC ($P < 0.01$, A). This suggests that cellular uptake of AuNPs at high concentrations likely induce cumulative cytotoxic effects which suppress the mitochondrial metabolic activity of macrophages.

Cell number in all AuNP-treated macrophages was not altered at 1 h in comparison to RMΦC (B). Our results revealed that higher concentrations of AuNP exposure

significantly reduced cell number in both RMΦH and RMΦHH cultures compared to RMΦC at 24 h and 72 h ($P < 0.05$, B). Prolonged exposure of cells to low concentrations of AuNP did not change the cell number nor the cell number at 24 h and 72 h. Therefore, AuNPs appear to suppress the number of macrophage cell at concentrations greater than 3.15 μg/mL.

3.3.1.1. ROS production by RAW 264.7 macrophages following treatment with AuNPs

Figure 3.7 showed the levels of oxidative stress in RAW264.7 macrophages exposed to 3 different doses of AuNPs were determined by measurement of intracellular ROS at 3 different time points. No change in ROS production was observed between RMΦL and RMΦC at all time points measured as shown in Figure 3.7. At 1 h, ROS levels in the macrophages treated with higher concentrations of AuNPs,, RMΦH and RMΦHH groups were also not significantly altered compare to RMΦC (Figure 3.7). At 24 h, there was increased overall oxidative stress index in both RMΦH and RMΦHH groups with significantly increased ROS production by 81% and 98%, respectively compared to the RMΦC ($P < 0.001$, Figure 3.7). Prolonged exposure to AuNP of up to 72 h, showed increased ROS generated by 35% in RMΦH ($P < 0.01$ *vs.* RMΦC) and 26% in RMΦHH ($P<0.05$ *vs.* RMΦC), suggesting a persistent cellular oxidative stress which may lead to cellular damage (Figure 3.7).

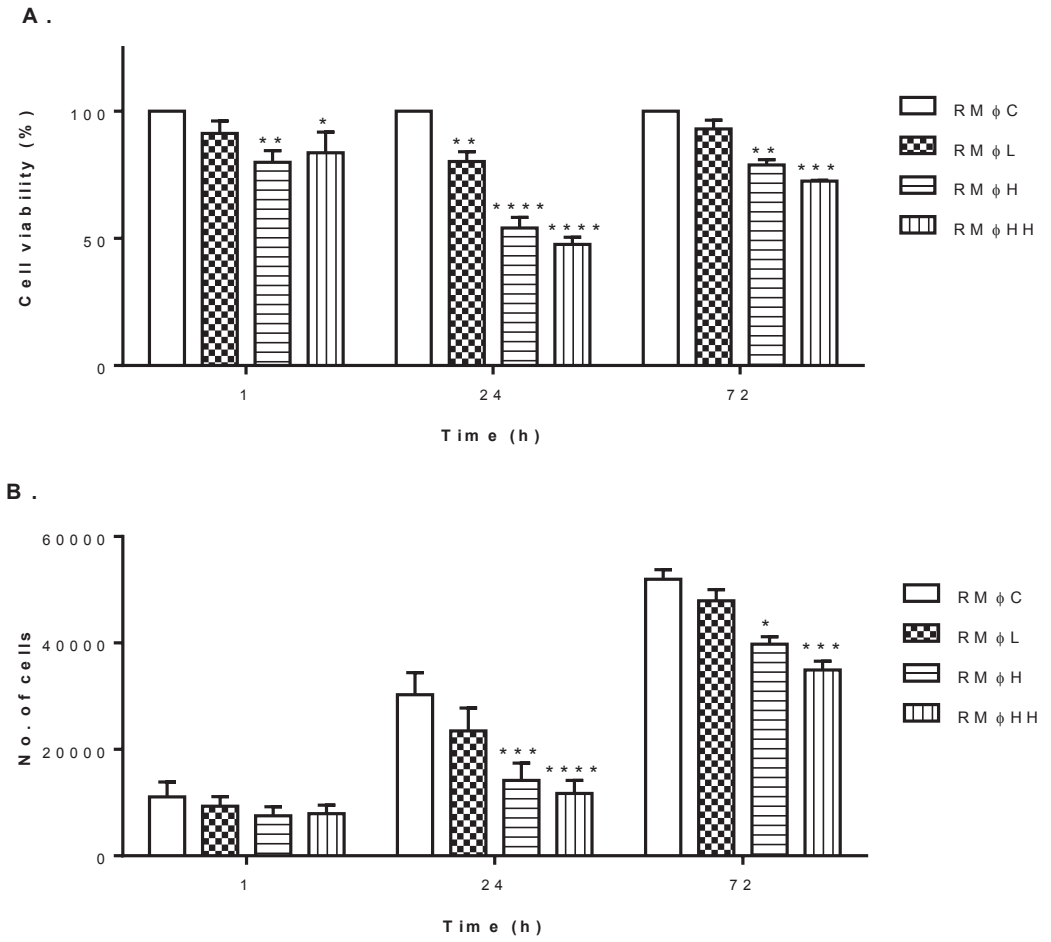

Figure 3.6 Effect of AuNP treatment on cell viability and cell number in RAW 264.7 macrophages

(A) cell viability and (B) the number of macrophage cells treated with PBS control (RMΦC), 0.315 µg/mL AuNP (RMΦL), 3.15 µg/mL AuNP (RMΦH), and 31.5 µg/mL AuNP (RMΦHH) at 1, 24, and 72 h. (A) Results are expressed as mean ± S.E.M.(B) Results are expressed as mean ± S.E.M. Data were analysed by two-way ANOVA followed by post hoc Bonferroni test, * $P < 0.05$, ** $P < 0.01$, *** $P < 0.005$, **** $P < 0.001$ *vs.* RMΦC; n=3–4

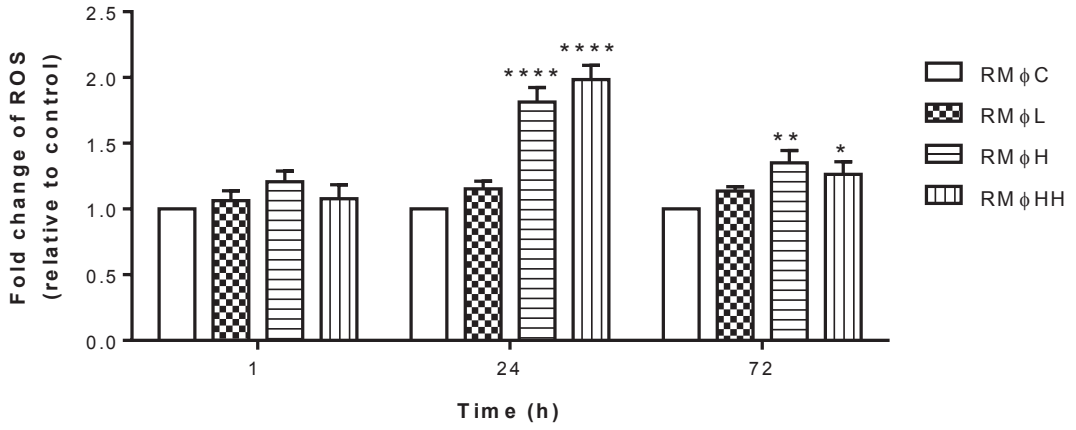

Figure 3.7 Effect of AuNP treatment on ROS production in RAW 264.7 macrophages

Fold change in ROS production adjusted by cell viability in PBS control (RMΦC), 0.315 μg/mL AuNP (RMΦL), 3.15 μg/mL AuNP (RMΦH), and 31.5 μg/mL AuNP (RMΦHH) groups at 1, 24, and 72 h. Results are expressed as mean ± S.E.M. Data were analysed by two-way ANOVA followed by post hoc Bonferroni test, * $P < 0.05$, ** $P < 0.01$, **** $P < 0.005$ *vs.* RMΦC; n=4.

3.3.1.2. Protein expression in RAW 264.7 macrophages following treatment with AuNPs

The alterations of intracellular protein levels for TLR-4 and TNF-α by AuNPs were examined via western blot, normalized against β-actin and expressed as fold change in protein concentration compared to RMΦC at each time point. Preliminary data on the effect of AuNP or LPS treatment on the induction of NF-κB signalling pathway through IKKα, and IKKβ was also included in this chapter. Figure 3.8 is a representative western blot showing TLR-4 and TNF-α protein levels in RAW 264.7 macrophages treated with either AuNPs or LPS after 72 h. LPS of 10 μg/mL induced pro-inflammatory responses with TLR-4 protein levels significantly increased by 50% ($P < 0.05$ for RMΦLPSH *vs.* RMΦC, Figure 3.8B) and TNF-α by 127-fold ($P < 0.001$ for RMΦLPSH *vs.* RMΦC, Figure 3.8C) at 72 h. Macrophage cells stimulated with 0.001

μg/mL LPS also resulted in significantly increased TNF-α protein expression by 30-fold ($P < 0.05$ for RMΦLPSL *vs.* RMΦC,

Figure 3.8B). At 72 h, no change was observed for TLR-4 protein expression between the AuNP-treated groups compared to control. Prolonged exposure to AuNPs resulted in no change to TLR-4 or TNF-α protein expression levels in all AuNP-treated macrophages compared to RMΦC at 72 h.

Figure 3.9 shows preliminary data of macrophages treated with 3 doses of AuNPs and 2 doses of LPS for 24 and 72 h. At 24 h, the protein expression of IKK complexes in RMΦLPSH group were lowered compared to RMΦC, while prolonged exposure showed almost no detectable protein expression of IKK complexes at 72 h (Figure 3.9C,D). No difference was observed in the protein expression of IKK complexes between all AuNPs-treated and RMΦLPSL compared to RMΦC at 24 h (Figure 3.9C,D). At 72 h, the alterations of IKKα protein level by AuNP treatment did not follow the trend of RMΦLPSL but were similar to control, while IKKβ protein expression were similar to the trend of RMΦLPSL and different to control (Figure 3.9C,D).

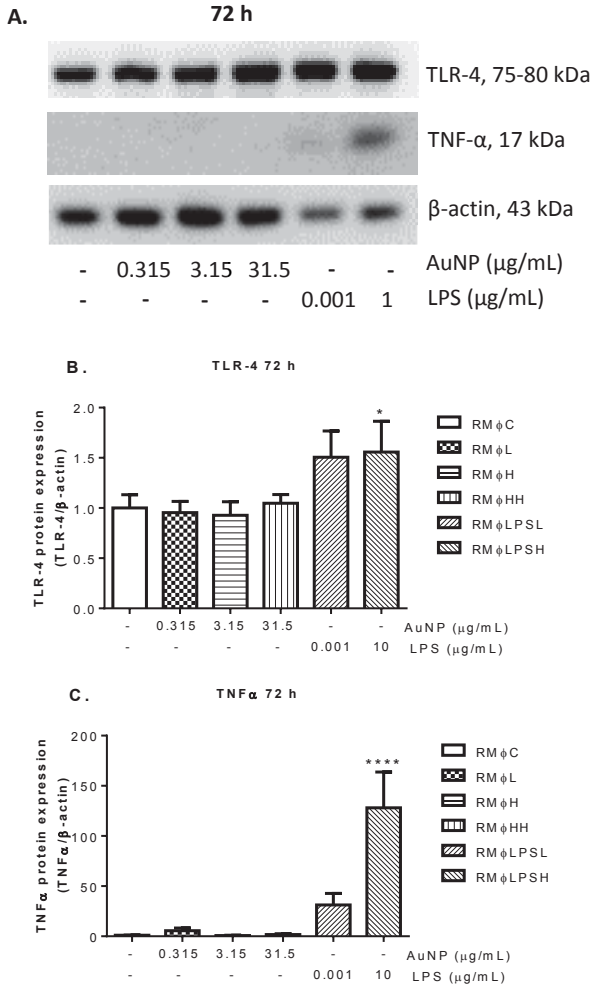

Figure 3.8 Effect of AuNPs treatment on TLR-4 and TNF-α protein expression in RAW 264.7 macrophages

Relative protein expression levels as determined by Western blot from RAW 264.7 treated with (+) or without (–) AuNP or LPS for 72 h. (A) representative western blot analysis for TLR-4, TNF-α, and β-actin at 72 h. The band densitometry was quantified using Fujiflim Multi Gauge version 3.0 software. Protein expression levels of TLR-4 (B) and TNF-α (C) relative to β-actin were semi-quantified for PBS control (RMΦC), 0.315 μg/mL AuNP (RMΦL), 3.15 μg/mL AuNP (RMΦH), 31.5 μg/mL AuNP (RMΦHH), 0.001 μg/mL LPS (RMΦLPSL), and 10 μg/mL LPS (RMΦLPSH) groups at 72 h. Results are expressed as mean ± S.E.M, normalized to RMΦC. Data were analysed by two-way ANOVA followed by post hoc Bonferroni test, * $P < 0.05$, **** $P < 0.001$ *vs.* RMΦC. n=4.

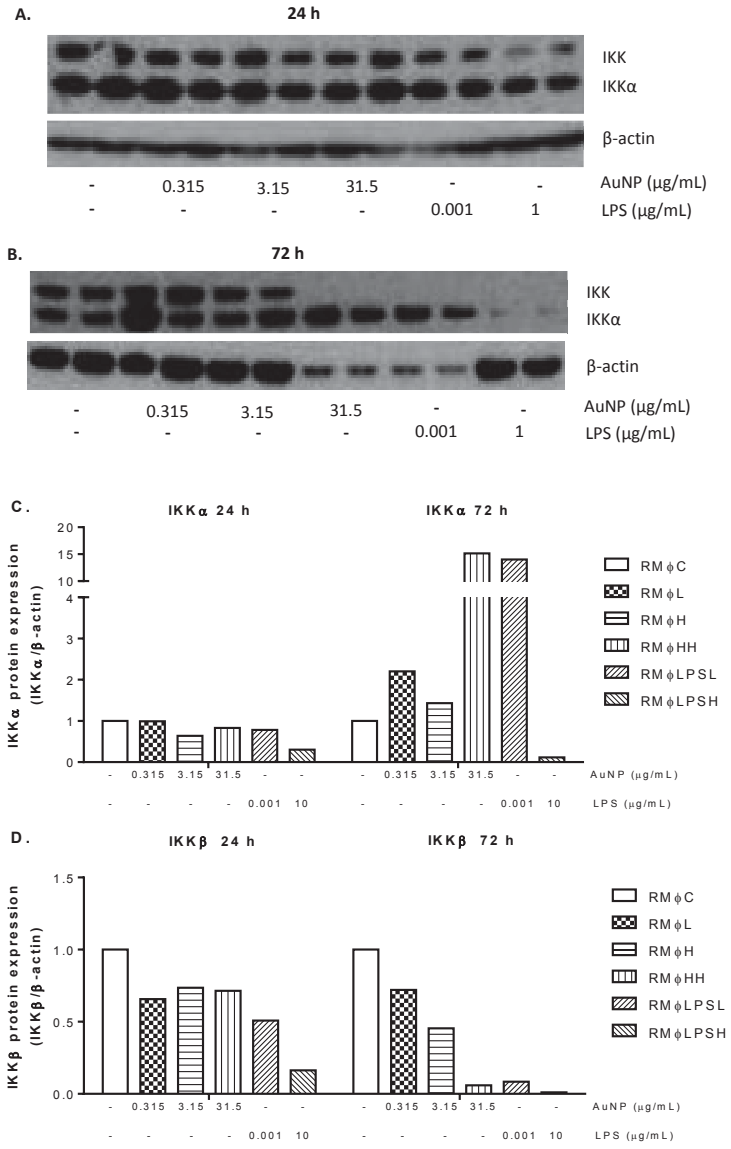

Figure 3.9 Effect of AuNPs treatment on IKKα and IKKβ protein expression in RAW 264.7 macrophages

Western blot analysis of RAW 264.7 whole cell lysates. Samples were from cultures grown in the presence (+) or absence (–) of AuNPs or LPS. Representative western blot at 24 h (A) and 72 h (B) in duplicate. Protein expression level of IKKα (C) and IKKβ (D) relative to β-actin for PBS control (RMΦC), 0.315 μg/mL AuNP (RMΦL), 3.15 μg/mL AuNP (RMΦH), 31.5 μg/mL AuNP (RMΦHH), 0.001 μg/mL LPS (RMΦLPSL), and 10 μg/mL LPS (RMΦLPSH) groups at 24 and 72 h. Results are expressed as a single sample at each time point measured.

3.3.1.3. mRNA expression of inflammatory markers in RAW 264.7 macrophages following treatment with AuNPs

In this study, the effect of AuNP exposure on the alteration of inflammatory marker mRNA levels were investigated since the activation of both canonical and alternative NF-κB signalling pathway commonly leads to downstream expression of pro-inflammatory genes. Figure 3.10 shows the mRNA expression profile of pro-inflammatory cytokines (TNF-α and IL-1β) and pro-inflammatory receptor (TLR-4) markers in RAW 264.7 macrophage cells treated with 3 different doses of AuNPs at 3 different time points.

Our results showed that pro-inflammatory TNF-α and IL-1β mRNA levels were no different in AuNP-treated cultures compared to the RMΦC at 1 h (Figure 3.10A,B). This suggests that AuNPs may regulate pro-inflammatory genes in a dose dependent manner in these cells. At 24 h, mRNA levels of TNF-α were significantly upregulated by 1.1-, 1.3-, and 3-fold in the RMΦL, RMΦH, and RMΦHH groups compare to the RMΦC, respectively ($P < 0.05$, Figure 3.10A). Similarly, mRNA of IL-1β was also significantly upregulated by 6 fold in the RMΦHH compared to RMΦC at 24 h ($P < 0.01$, Figure 3.10B). However, there were no differences observed in neither TNF-α nor IL-1β mRNA expression levels between all AuNP-treated macrophage cultures and RMΦC at 72 h (Figure 3.10A,B). This suggests that AuNPs may induce an acute pro-inflammatory response in macrophages, thereby inducing transient upregulation pro-inflammatory cytokine expression but without long-term effect.

The expression of pro-inflammatory receptor, TLR-4 was significantly downregulated in the RMΦH by 50% at 1 h ($P < 0.05$ *vs.* RMΦC, Figure 3.10C). At 24 h, mRNA levels of TLR-4 were not different between all groups (Figure 3.10C). Prolonged exposure to AuNPs showed no difference in the pro-inflammatory markers between RMΦL and RMΦHH compared to control at 72 h(Figure 3.10).

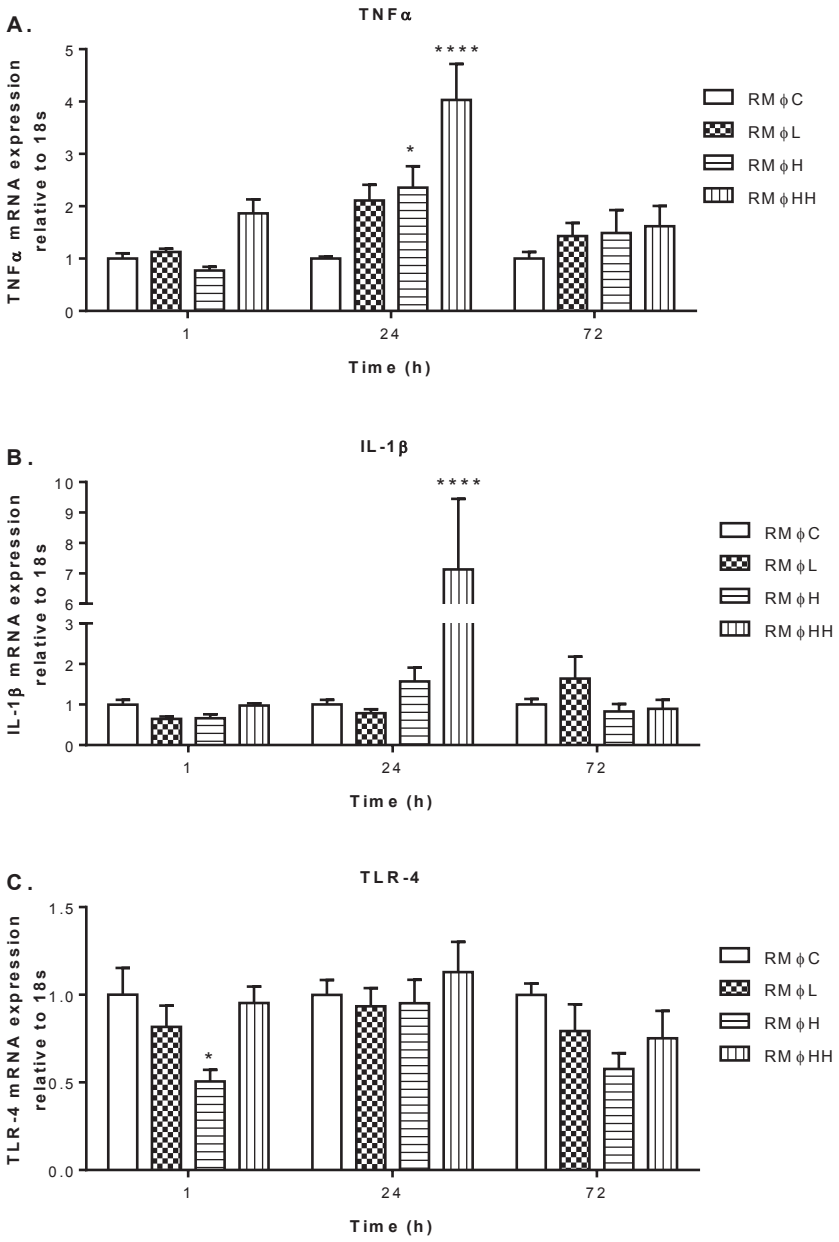

Figure 3.10 Effects of AuNP treatment on pro-inflammatory markers in RAW 264.7 macrophages

The mRNA expression levels of TNF-α (A), IL-1β (B), and TLR-4 (C) in PBS control (RMΦC), 0.315 μg/mL AuNP (RMΦL), 3.15 μg/mL AuNP (RMΦH), and 31.5 μg/mL AuNP (RMΦHH) groups at 1, 24, and 72 h. Results are expressed as mean ± S.E.M. Data were analysed by two-way ANOVA followed by post hoc Bonferroni test, *P < 0.05, **P < 0.01, ****P < 0.001 vs. RMΦC. n=8–12.

3.3.2. Effects of AuNP treatment on U937 monocytic cell-line

In this study, preliminary data of on pro- and anti- inflammatory effect of AuNP treatment on the human PMA-differentiated U937 macrophages exposed to AuNPs with or without LPS stimulationwere studied. The secreted levels of cytokines, including IL-2, IL-4, IL-6, IL-8, IL-10, IFN-γ, TNF-α, and GM-CSF in supernatant of PMA-differentiated U937 macrophages were determined using a magnetic-based multiplex immunoassay.

3.3.2.1. Cytokine profile response of PMA-differentiated U937 macrophage-like cells following treatment with AuNPs

Our preliminary data showed alterations in the levels of all secreted cytokines of PMA-differentiated U937 macrophage cultures at all 3 time points treated with AuNPs (Figure 3.11A–H). At 1 h, pro-inflammatory IL-8 levels showed elevation beyond the detection limit of the kit in the cell supernatant of UMΦH compared to UMΦC (Figure 3.11E). At 24 and 72 h, the IL-8 cytokine production measured in both AuNP-treated cultures and UMΦC were all above detection limit kit (Figure 3.11E). The levels of GM-CSF in all PMA-differentiated U937 macrophage cultures were below the detection limit of this assay due to the absence of potent stimulation, e.g. LPS.

Our results also showed no change in pro-inflammatory IL-2, IL-6, IFN-γ, and TNF-α cytokine levels between AuNP-treated cultures and UMΦC at 1 h (Figure 3.11A,B,D,E,H). At 24 h levels of pro-inflammatory cytokines IL-2, IL-6, IFN-γ, and TNF-α were increased in UMΦHH but not lower doses of AuNP-treated cultures (Figure 3.11A,B,D,E). Prolonged AuNP incubation up to 72 h showed a further increase in the levels of pro-inflammatory cytokines IL-2, IL-6, IFN-γ, and TNF-α in both UMΦH and UMΦHH cultures compared to the UMΦC at 72 h(Figure 3.11A,B,D,E).The anti-inflammatory IL-4 protein levels were below the detection limit at 1 h, however, IL-10 secretion were slightly suppressed in UMΦH and UMΦHH compared to UMΦC (Figure 3.11G,H). At 24 h, the supernatant levels of both IL-4 and IL-10 were elevated in UMΦH cultures compared to the UMΦC (Figure 3.11G,H). At

72 h, the secreted level of IL-4 cytokine was significantly increased in UMΦH; while the level of IL-10 cytokine was significantly increased in UMΦHH (Figure 3.11G,H).

3.3.2.2. Cytokine profile response of LPS stimulated PMA-differentiated U937 macrophage-like cells following treatment with AuNPs

In this preliminary study on secreted pro-inflammatory cytokines (IL-2, IL-6, IL-8, IFN-γ, TNF-α, and GM-CSF) or anti-inflammatory cytokines (IL-4 and IL-10) expression profile in PMA-differentiated U937 macrophages receiving both AuNPs treatment and LPS-stimulation are illustrated in Figure 3.12.

Our results showed that LPS induced a rapid activation of pro-inflammatory response where all pro-inflammatory cytokines measured were markedly higher in the supernatant of UMΦC_LPS compared to the non-stimulated controls from the former section (UMΦC, section 3.3.2.1) at all time points measured (Figure 3.12 A–H *vs.* Figure 3.11A–H). The majority of supernatant IL-8 and TNF-α levels in the LPS-stimulated UMΦ, were above the detection limit at all time points (Figure 3.12C,E).

UMΦ cultures with AuNPs treatment and LPS stimulation seem to behave in an opposite manner compared to AuNP-treated macrophage without LPS (section 3.3.2.1). Pro-inflammatory cytokines IL-2, IL-6, IFN-γ, and GM-CSF were significantly elevated in UMΦH_LPS culture at 1 h ($P < 0.05$ *vs.* UMΦC_LPS, Figure 3.12 A,B,D,F). At 24 h, there were no differences in pro-inflammatory cytokine secretion between all the groups. Prolonged AuNP exposure up to 72 h in the presence of LPS showed suppression of IL-2, IL-6, IFN-γ, and GM-CSF measured in UMΦHH_LPS culture compared to the UMΦC_LPS (Figure 3.12A,B,D,F). The suppression of IL-8 were also evident in UMΦHH_LPS culture, while the level of GM-CSF in AuNP-treated UMΦ fell below the detection limit at 72 h (Figure 3.12C,F). This suggests that long-term AuNP treatment can lower the pro-inflammatory response induced by LPS in UMΦ.

The levels of anti-inflammatory cytokines IL-4 and IL-10 showed a similar trend in the pro-inflammatory mediators following AuNP treatment and LPS stimulation. At 1 h,

UMΦH_LPS group showed slightly elevated levels of IL-4 and IL-10 cytokines in cell supernatant compared to UMΦC_LPS (Figure 3.12G,H). There was no difference in anti-inflammatory cytokines between all the groups at 24 h. At 72 h., the levels of IL-4 were suppressed in in both UMΦH_LPS and UMΦHH_LPS compared to UMΦC_LPS ($P < 0.05$, Figure 3.12G).The IL-10 secretion was slightly lowered in UMΦH_LPS but not UMΦHH_LPS cultures at 72 h (Figure 3.12H). This suggests that AuNPs did not affect the response of UMΦ to LPS over the longer term.

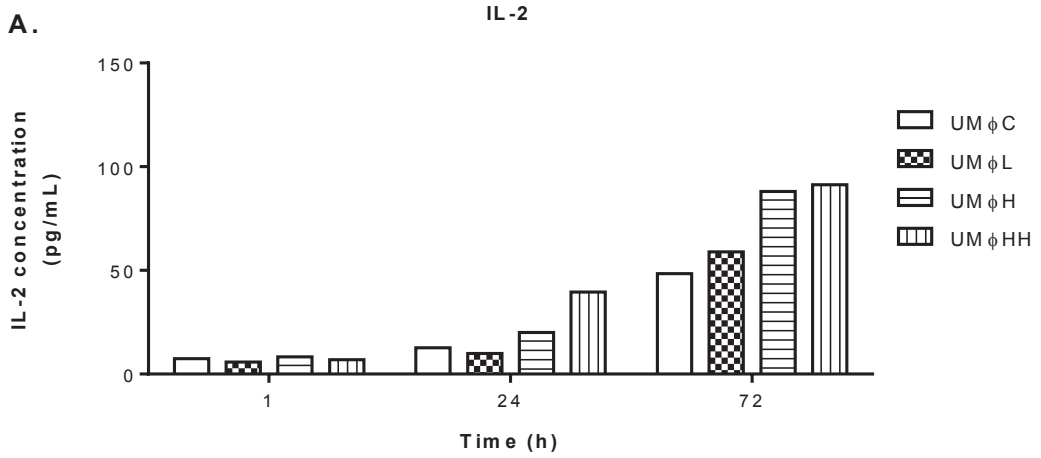
A.
IL-2
IL-2 concentration (pg/mL)
150
100
50
0
1
24
72
Time (h)
UMϕC
UMϕL
UMϕH
UMϕHH

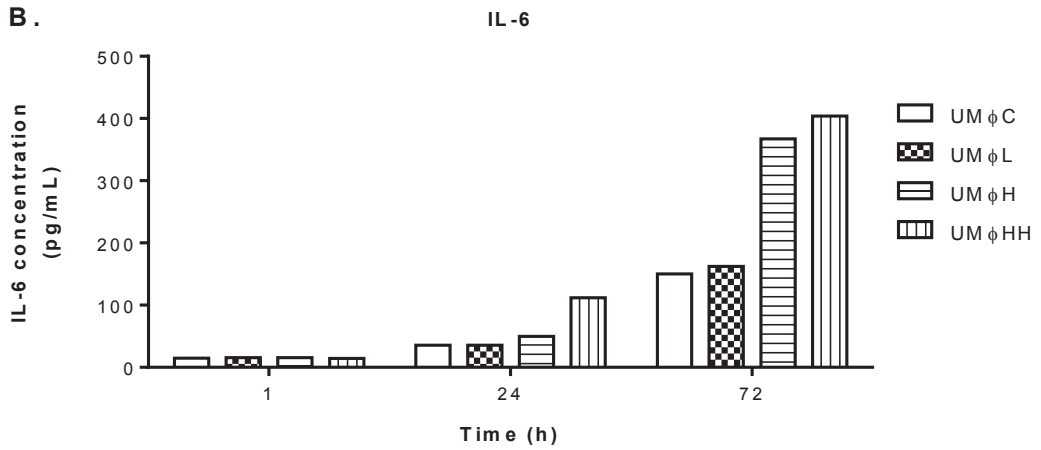
B.
IL-6
IL-6 concentration (pg/mL)
500
400
300
200
100
0
1
24
72
Time (h)
UMϕC
UMϕL
UMϕH
UMϕHH

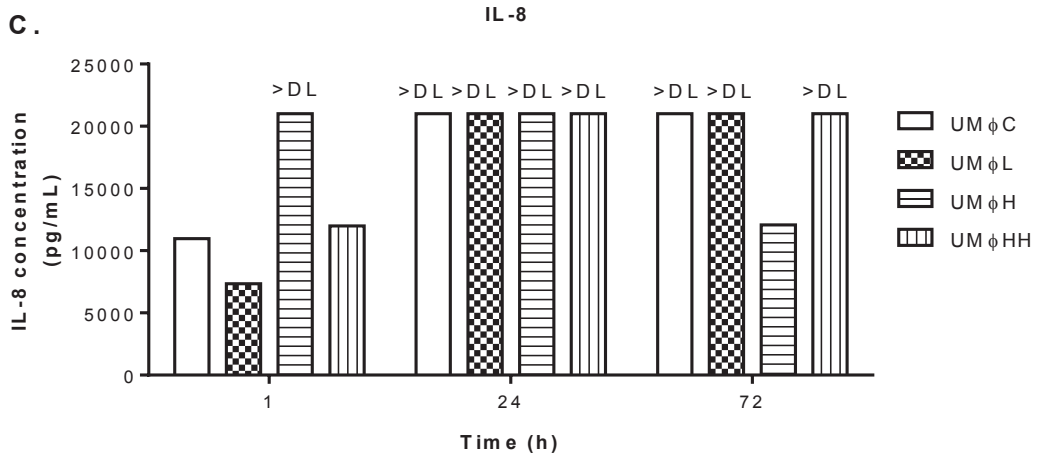
C.
IL-8
IL-8 concentration (pg/mL)
25000
20000
15000
10000
5000
0
>DL
>DL >DL >DL >DL
>DL >DL
>DL
1
24
72
Time (h)
UMϕC
UMϕL
UMϕH
UMϕHH

D.

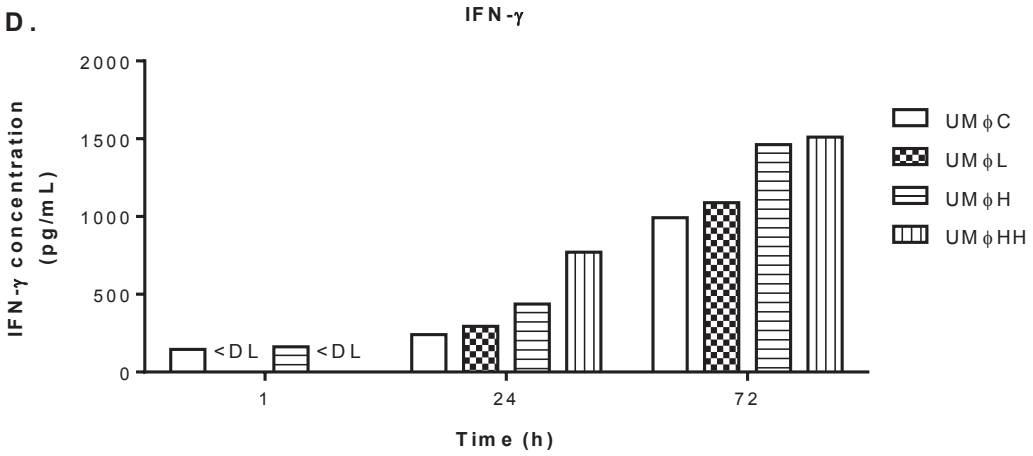
IFN-γ
IFN-γ concentration (pg/mL)
2000
1500
1000
500
0
<DL
<DL
1
24
72
Time (h)
UMϕC
UMϕL
UMϕH
UMϕHH

E.

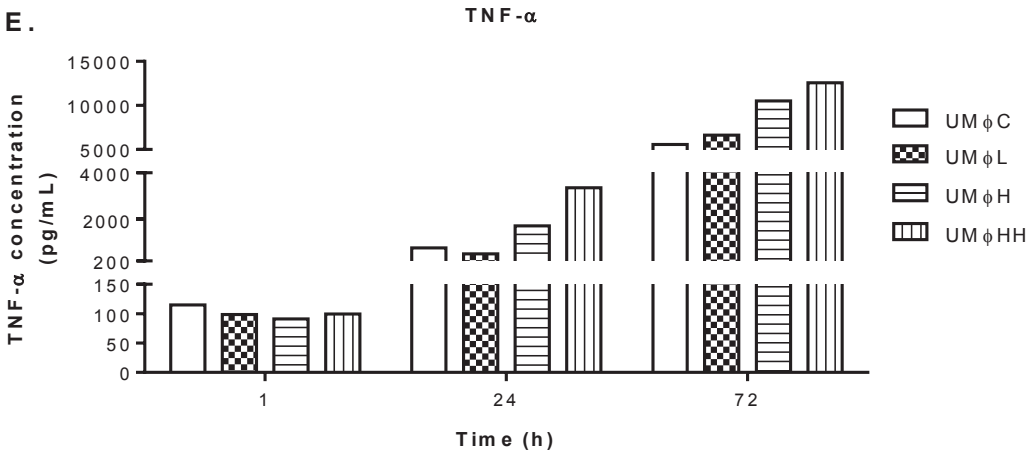
TNF-α
TNF-α concentration (pg/mL)
15000
10000
5000
4000
2000
200
150
100
50
0
1
24
72
Time (h)
UMϕC
UMϕL
UMϕH
UMϕHH

F.

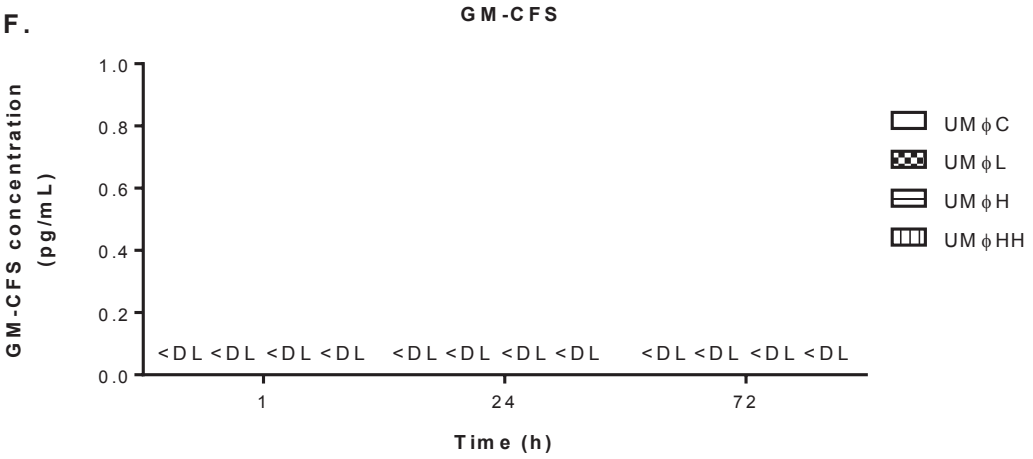
GM-CFS
GM-CFS concentration (pg/mL)
1.0
0.8
0.6
0.4
0.2
0.0
<DL <DL <DL <DL
<DL <DL <DL <DL
<DL <DL <DL <DL
1
24
72
Time (h)
UMϕC
UMϕL
UMϕH
UMϕHH

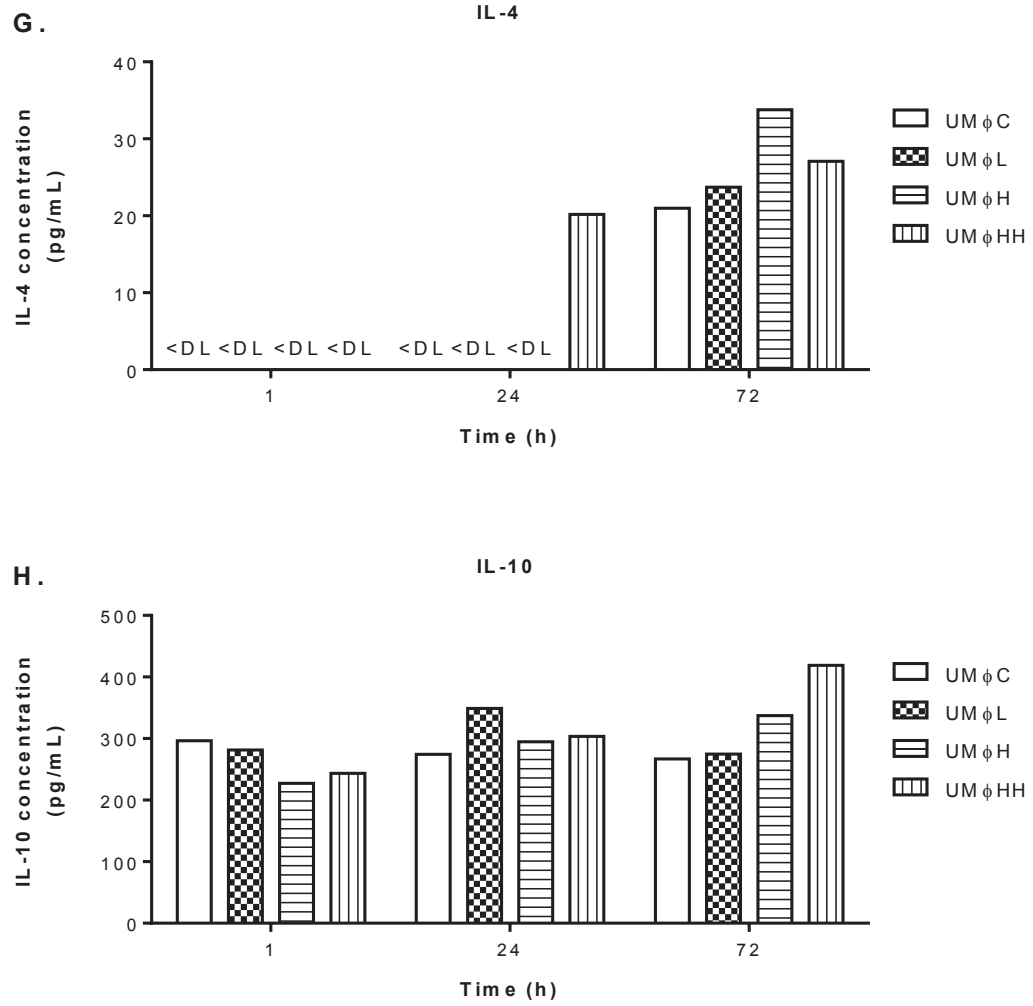

Figure 3.11 Effect of AuNP treatment on the cytokine production in PMA-differentiated U937 macrophage-like cells

Concentration of cytokines IL-2 (A), IL-6 (B), IL-8 (C), IFN-γ (D), TNF-α (E), and GM-CSF (F), IL-4 (G), and IL-10 (H) in the supernatant of PBS-treated control (UMΦC), 0.315 μg/mL AuNP (UMΦL), 3.15 μg/mL AuNP (UMΦH), and 31.5 μg/mL AuNP (UMΦHH) differentiated U937 macrophage-like cultures at 1, 24, and 72 h. <DL, below cytokine assay detection limit; >DL, above cytokine assay detection limit. Results are expressed as mean ± S.E.M. n=2.

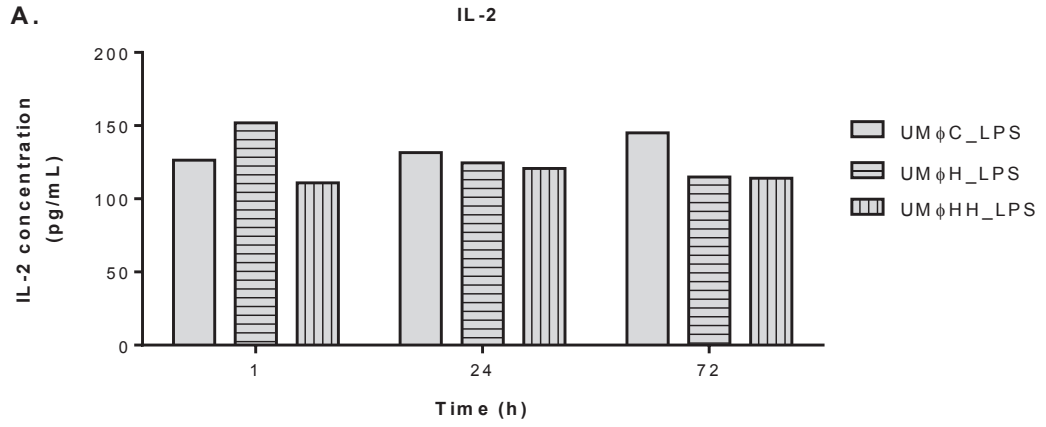
A.
IL-2
IL-2 concentration (pg/mL)
200
150
100
50
0
1
24
72
Time (h)
UMϕC_LPS
UMϕH_LPS
UMϕHH_LPS

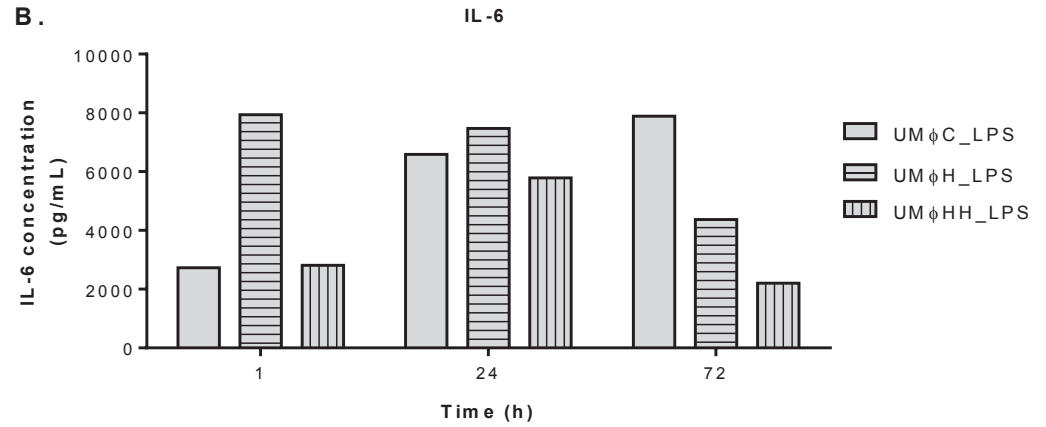
B.
IL-6
IL-6 concentration (pg/mL)
10000
8000
6000
4000
2000
0
1
24
72
Time (h)
UMϕC_LPS
UMϕH_LPS
UMϕHH_LPS

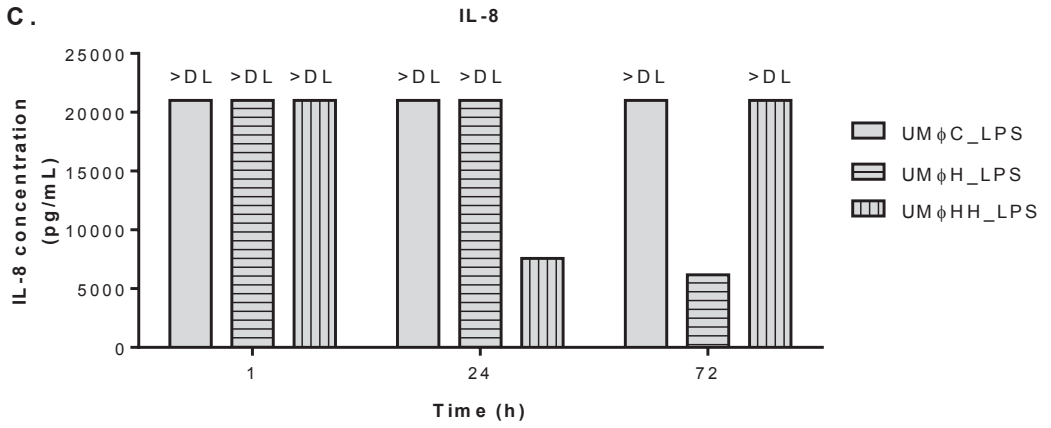
C.
IL-8
IL-8 concentration (pg/mL)
25000
20000
15000
10000
5000
0
>DL
1
24
72
Time (h)
UMϕC_LPS
UMϕH_LPS
UMϕHH_LPS

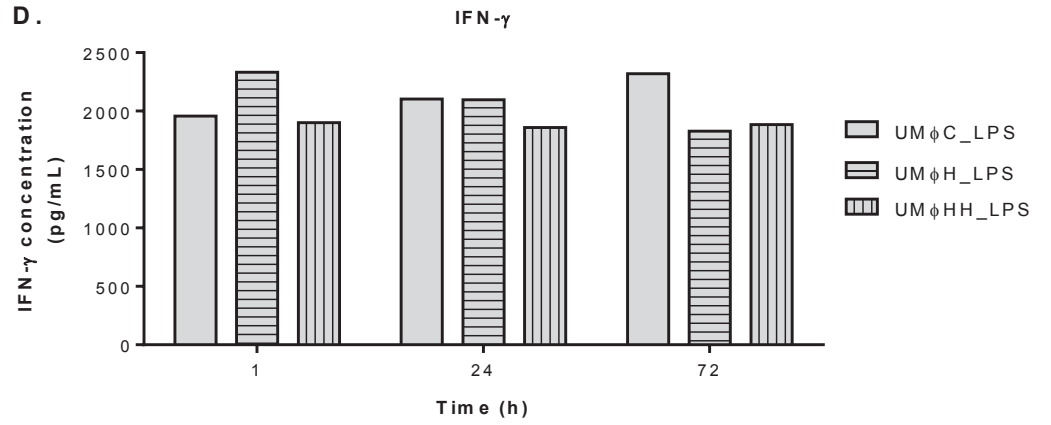
D.
IFN-γ
IFN-γ concentration (pg/mL)
2500
2000
1500
1000
500
0
1
24
72
Time (h)
UMϕC_LPS
UMϕH_LPS
UMϕHH_LPS

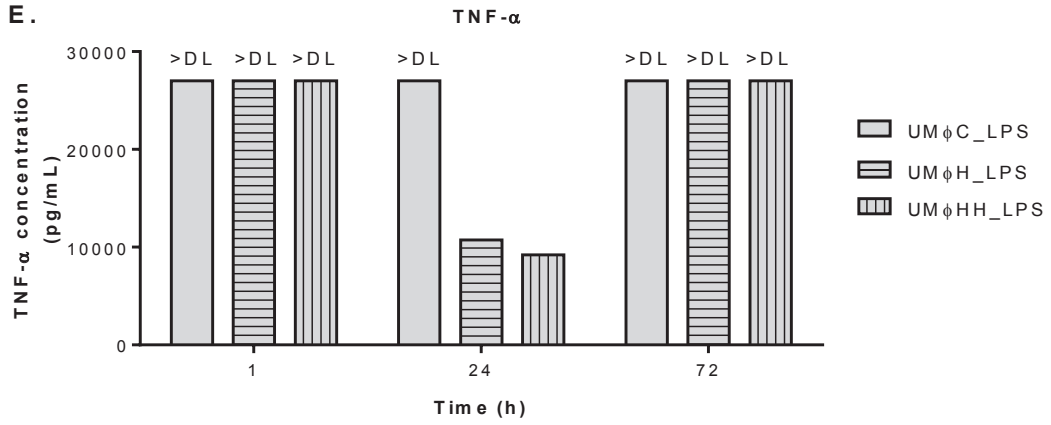
E.
TNF-α
TNF-α concentration (pg/mL)
30000
20000
10000
0
>DL >DL >DL >DL >DL >DL >DL
1
24
72
Time (h)
UMϕC_LPS
UMϕH_LPS
UMϕHH_LPS

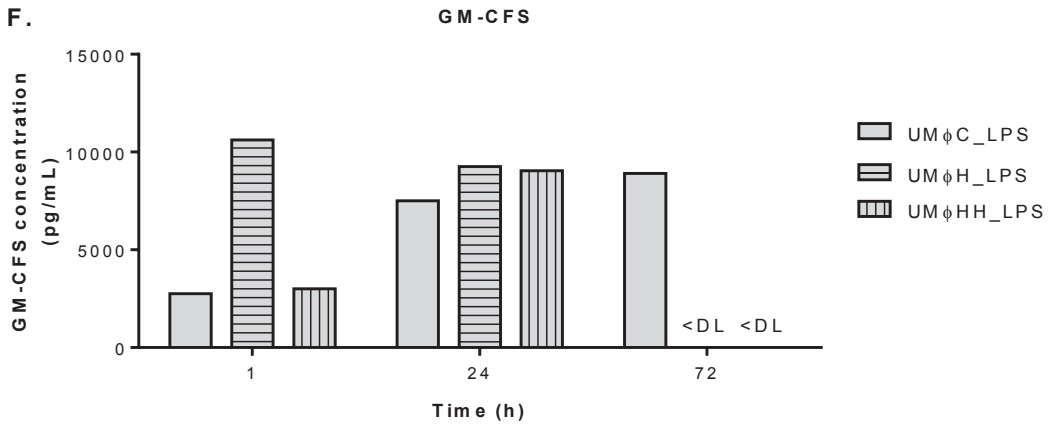
F.
GM-CFS
GM-CFS concentration (pg/mL)
15000
10000
5000
0
<DL <DL
1
24
72
Time (h)
UMϕC_LPS
UMϕH_LPS
UMϕHH_LPS

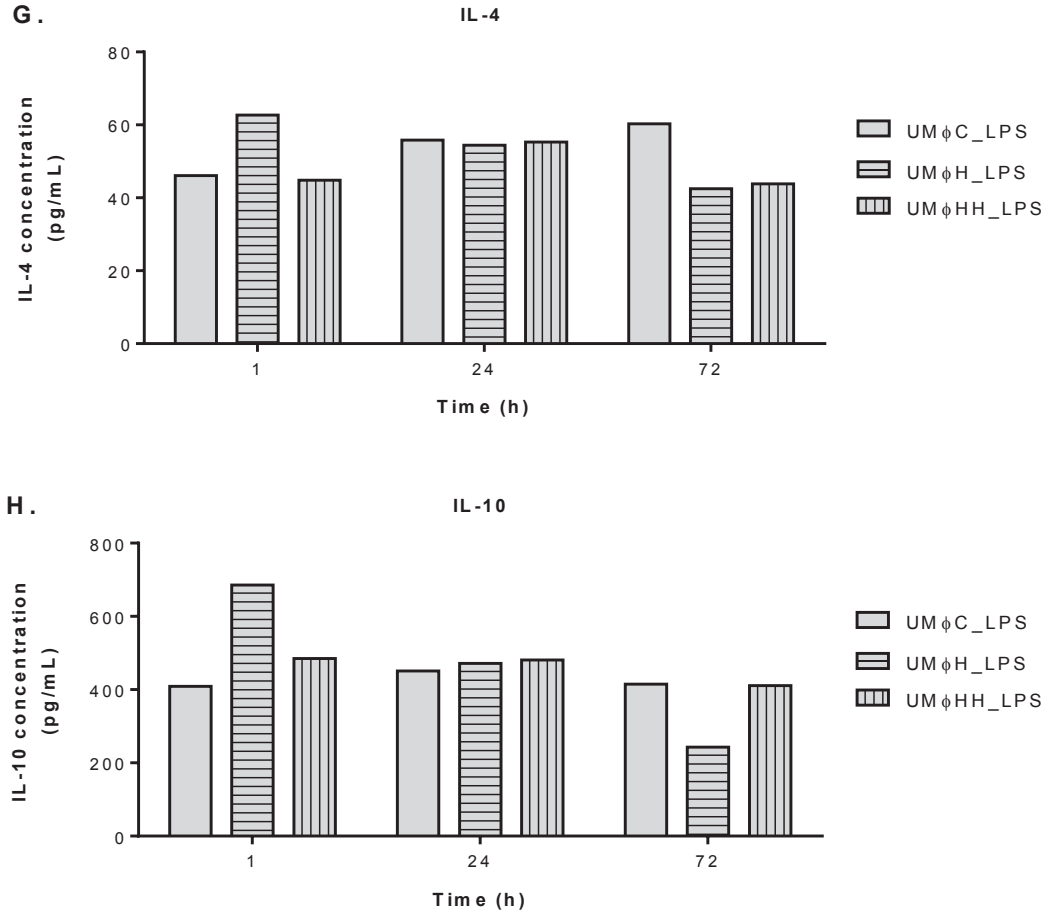

Figure 3.12 Effect of AuNP on the cytokine production in LPS-stimulated PMA-differentiated U937 macrophage-like cells

Concentration of secreted cytokines IL-2 (A), IL-6 (B), IL-8 (C), IFN-γ (D), TNF-α (E), and GM-CSF (F), IL-4 (G), and IL-10 (H) in the supernatant of PMA-differentiated U937 macrophage-like cells stimulated with 10 μg/mL LPS and PBS as control (UMΦC_LPS), 10 μg/mL LPS with 3.15 μg/mL AuNP (UMΦH_LPS), and 10 μg/mL LPS with 31.5 μg/mL AuNP (UMΦHH_LPS) at 1, 24, and 72 h. <DL, below cytokine assay detection limit; >DL, above cytokine assay detection limit. Results are expressed as mean ± S.E.M. n=2.

3.3.3. Effect of AuNP treatment on mature 3T3-L1 adipocytes

The murine 3T3-L1 fibroblast cell line is from a pre-adipocyte lineage which can undergo adipogenesis to develop many characteristics of mature adipose cells in vivo. They are often used as an in vitro model of adipocytes to study metabolism of triglycerides, fatty acids, and glucose (Gregoire, Smas & Sul 1998; Saltiel & Kahn 2001; Vankoningsloo et al. 2005). In the current study, the effect of AuNP treatment on adipocyte differentiation and alterations in lipid and glucose homeostasis were investigated. Adipogenesis of pre-adipocytes following treatment with AuNPs

During adipocyte differentiation, signalling through PPARγ is crucial to induce growth arrest in 3T3-L1 pre-adipocytes and initiate transcriptional regulation of most adipocyte-specific genes for the development of mature adipocytes (Altiok, Xu & Spiegelman 1997; Brun et al. 1996; Gregoire, Smas & Sul 1998). The confluent monolayers of 3T3-L1 fibroblasts at growth-arrest, undergo adipogenesis when treated with adipogenic inducers for 48 h, and are subsequently cultured in an insulin supplemented standard medium for an additional 96 h with 80–90% of differentiated cells exhibiting the adipocyte phenotype (Figure 3.1). During the initial 48 h of adipogenic induction, the cells assume a spindly shape with significantly decreased cell surface area (Figure 3.1, Day 1–2). Subsequently, the cells were transferred to drug free medium, where they regain their fibroblastic morphology of polygonal shapes and begin to accumulate insulin-mediated intracytoplasmic small lipid droplets (Figure 3.1, Day 3–4). The small lipid droplets then coalesce to form the central lipid droplet which occupies a major fraction with the cytoplasm, with the nucleus located at the cell periphery, as the cells become spherical in shape (Figure 3.1, Day 5–8).

A lipid soluble dye, Oil red O was used in this study for the staining of intracytoplasmic neutral lipids and cholesteryl esters in the differentiating and mature adipocytes. The extent of cell differentiation from pre-adipocytes into mature adipocytes, is directly proportional to the accumulation of intracytoplasmic lipid droplets which is insulin dependent (Green & Meuth 1974; Weyer et al. 2000). Figure 3.13 showed the effect of continuous AuNP treatment at a high dose of 3.15 μg/mL on the relative intracytoplasmic lipid accumulation during adipogenic induction assessed by Oil red O

staining. Our results showed that the neutral lipid droplets and triglycerides formed in differentiating mature adipocytes (AC) were positively stained by Oil red O, while the undifferentiated pre-adipocyte (PC) cultures were not stained (Figure 3.13). Exposure of the cells to 3.15 µg/mL of AuNP throughout the adipocyte differentiation did not inhibit adipogenesis, nor did it appear to affect the intracytoplasmic lipid accumulation, as illustrated by Oil red O staining (Figure 3.13).

3.3.3.1. Cell viability of adipocytes treated with AuNPs

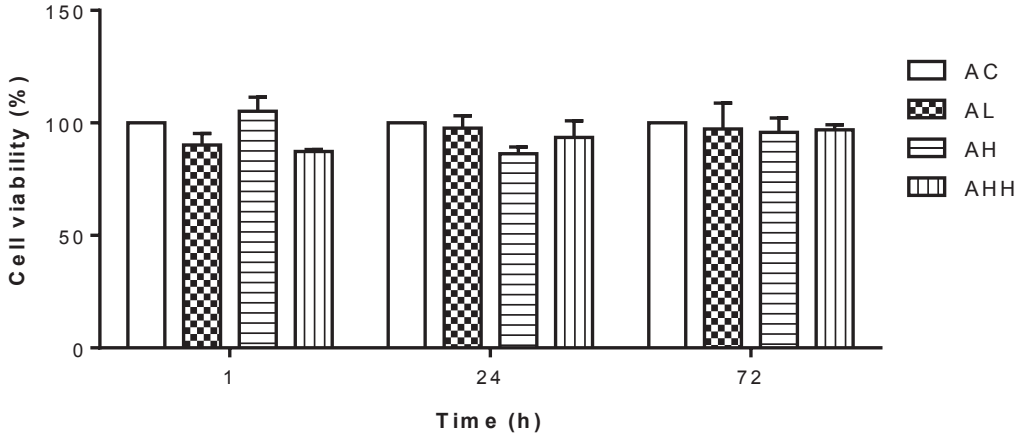

Figure 3.14 shows the cell viability of mature adipocytes exposed to 3 doses of AuNPs at 3 time points determined using MTT proliferation assay. The cell viability of control adipocytes (AC) treated with PBS were expressed as the percentage mean and used as the reference for all time points measured.

There was no difference observed in cell viability between all the AuNP-treated adipocytes and control group at all time points, suggested no cell cytotoxicity following prolonged AuNPs exposure for up to 72 h (Figure 3.14).

3.3.3.2. ROS production by adipocytes following treatment with AuNPs

The results showed no difference in the overall oxidative stress index between the AuNP-treated mature adipocytes and AC at 1 h (Figure 3.15). At 24 h, ROS generated in the adipocyte treated with AH and AHH were significantly increased by 1.8-, and 1.7-fold, respectively compared to AC ($P < 0.01$, Figure 3.15). However, ROS levels in

the adipocytes exposed to AL were not significantly altered at 24 h compared to AC. There was no difference in ROS levels between all groups at 72 h (Figure 3.15). This may indicate that increasing concentrations of AuNPs may induce acute oxidative stress in the cells.

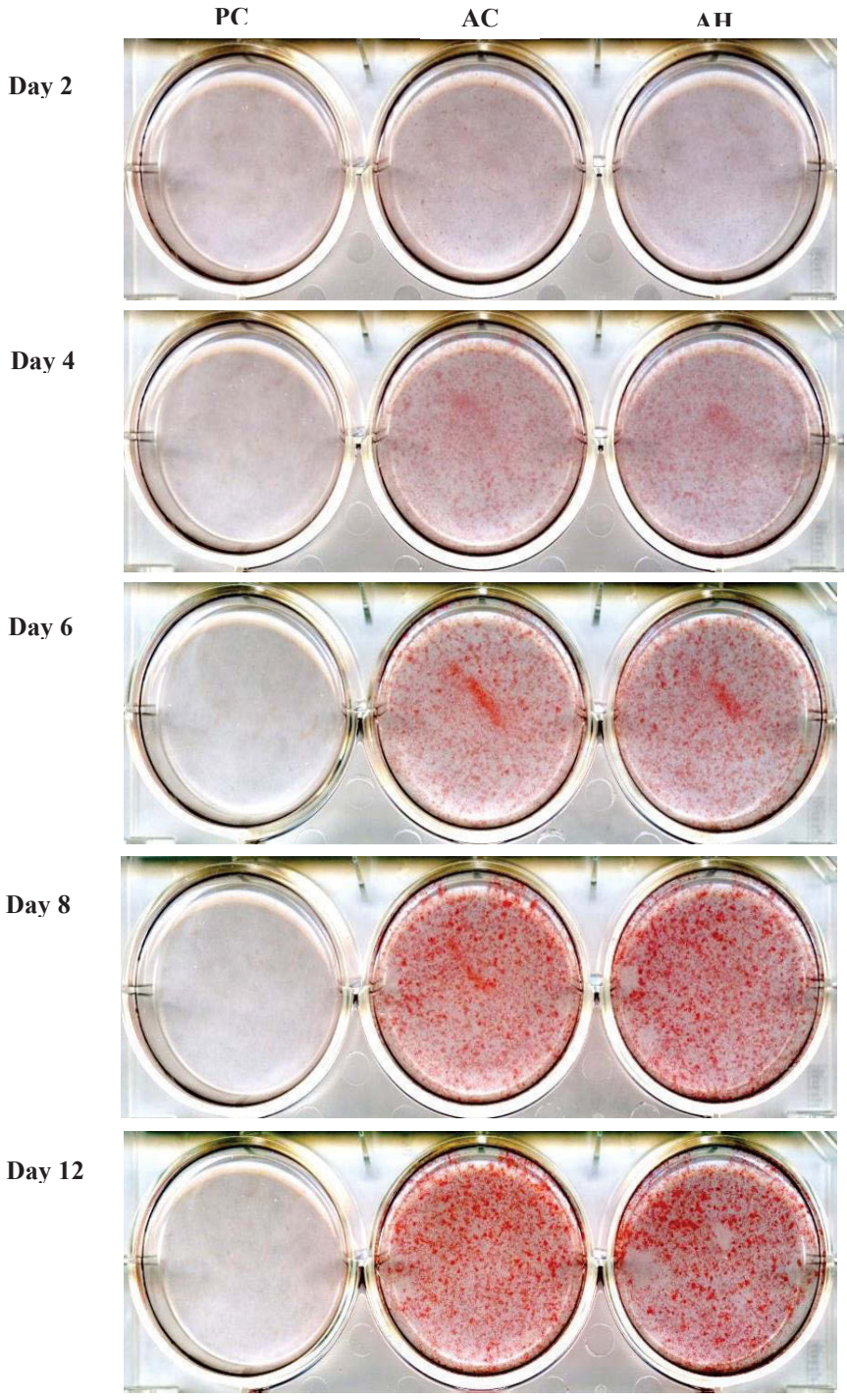

Figure 3.13 Effect of AuNP treatment on 3T3-L1 adipocyte differentiation

Representative cultures for 3T3-L1 pre-adipocytes control (PC, left), differentiating adipocytes treated with PBS (AC, middle), and differentiating adipocytes continuously treated with 3.15 µg/mL AuNP (AH, right). Culture well diameter = 3.4 cm. n=2.

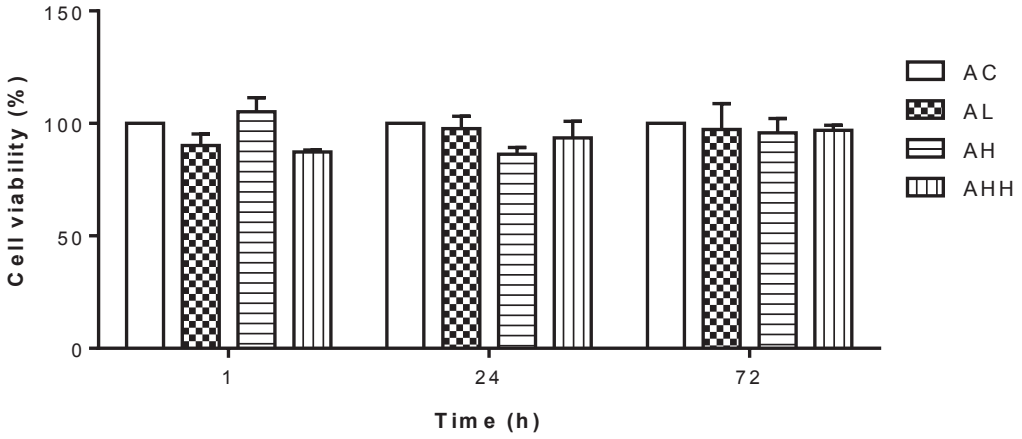

Figure 3.14 Effect of AuNP treatment on the cell viability of 3T3-L1 adipocytes

Cell viability in mature adipocytes treated with PBS control (AC), 0.315 μg/mL AuNP (AL), 3.15 μg/mL AuNP (AH), and 31.5 μg/mL AuNP (AHH) at 1, 24 and 72 h. Results are expressed as mean ± S.E.M. Data were analysed by two-way ANOVA followed by post hoc Bonferroni test. n=3.

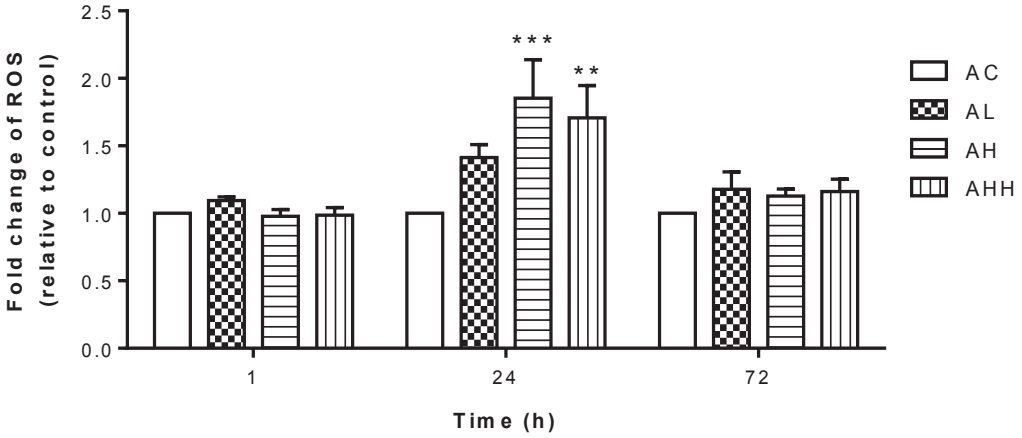

Figure 3.15 Effect of AuNP treatment on ROS production in 3T3-L1 adipocytes

Fold changes in ROS production adjusted by cell viability in PBS (AC), 0.315 μg/mL AuNP (AL), 3.15 μg/mL AuNP (AH), and 31.5 μg/mL AuNP (AHH) treated adipocytes at 1, 24, and 72 h. Results are expressed as mean ± S.E.M. Data were analysed by two-way ANOVA followed by post hoc Bonferroni test, ** $P < 0.01$, **** $P < 0.005$ *vs.* AC. n=3.

3.3.3.3. Lipid profiles of adipocytes following treatment with AuNPs

Figure 3.16 illustrates the overall and microscopic visualization of adipocytes treated with 3 different doses of AuNP for 3 different time points, with Oil red O staining for neutral lipid droplets. The effect of AuNP treatment on adipocyte size and neutral lipids accumulation were summarized in Table 3.5. At higher doses of AuNPs, no difference in the size of mature adipocytes was observed between AH and AHH cultures compared to AC at all time points. However, adipocyte size were significantly altered in AL group, where adipocytes were smaller in size at 1 h but at 72 h, the adipocytes were significantly larger in size compared to AC ($P < 0.05$, Table 3.5). This suggests that AuNPs affect adipocyte size at low concentration but not higher concentrations.

In this study, there seems to be a negative correlation between the number of lipid droplets and the average lipid droplet size for all AuNP-treated adipocytes compared to AC at 1 h ($P < 0.05$ for AHH, Table 3.5). At 24 h, AuNP treatment increased the formation of smaller sized lipid droplets at 24 h ($P < 0.05$ for AH and AHH, Table 3.5). Overtime, all the AuNP-treated adipocytes had fewer number of lipid droplets, however these were larger sized compared to the AC at 72 h ($P < 0.05$ for AH, Table 3.5). This suggests that AuNPs may affect the lipid homeostasis within the lipid droplets at higher but not low concentrations.

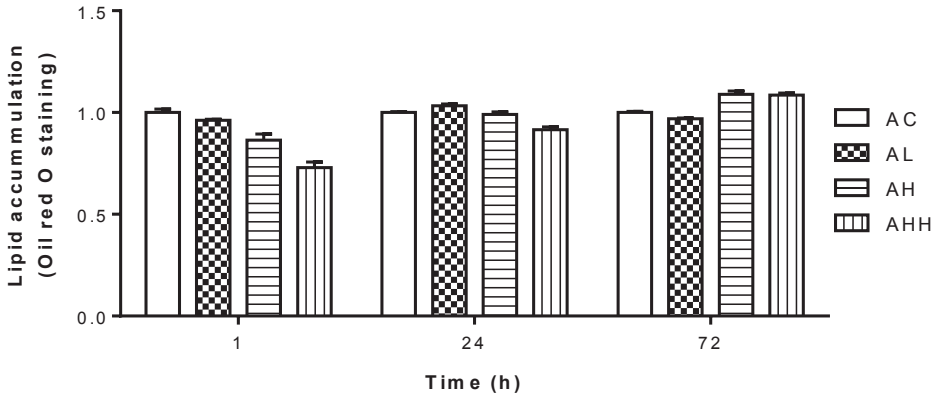

Figure 3.17 illustrated the quantitative total lipid accumulation in adipocyte treated with 3 different doses of AuNP at the 3 different time points. Total lipid accumulation were

not significantly altered in AuNP-treated adipocyte compared to the AC at all time point measured (Figure 3.17). This suggests that AuNP may transiently alter the adipocyte lipid homeostasis but with no long term effect.

Table 3.6 showed the effect of AuNPs on triglyceride and NEFA metabolism in 3T3-L1 adipocytes at 3 different doses measured at 3 different time points. Neither intracellular nor supernatant concentrations of triglyceride were significantly changed in all the AuNP-treated adipocytes at all time points compared to the AC (Table 3.6). This suggests that AuNP did not change the basal lipolysis and hydrolysis of triglyceride. Intracellular NEFA concentration observed in the AL and AH groups were not significantly different from the AC group at all time point measured. At 24 and 72 h, intracellular NEFA levels were significantly increased in the AHH ($P < 0.05$ *vs.* AC, Table 3.6). This suggests that AuNP at extremely high dose may suppress the accumulation of intracellular NEFA.

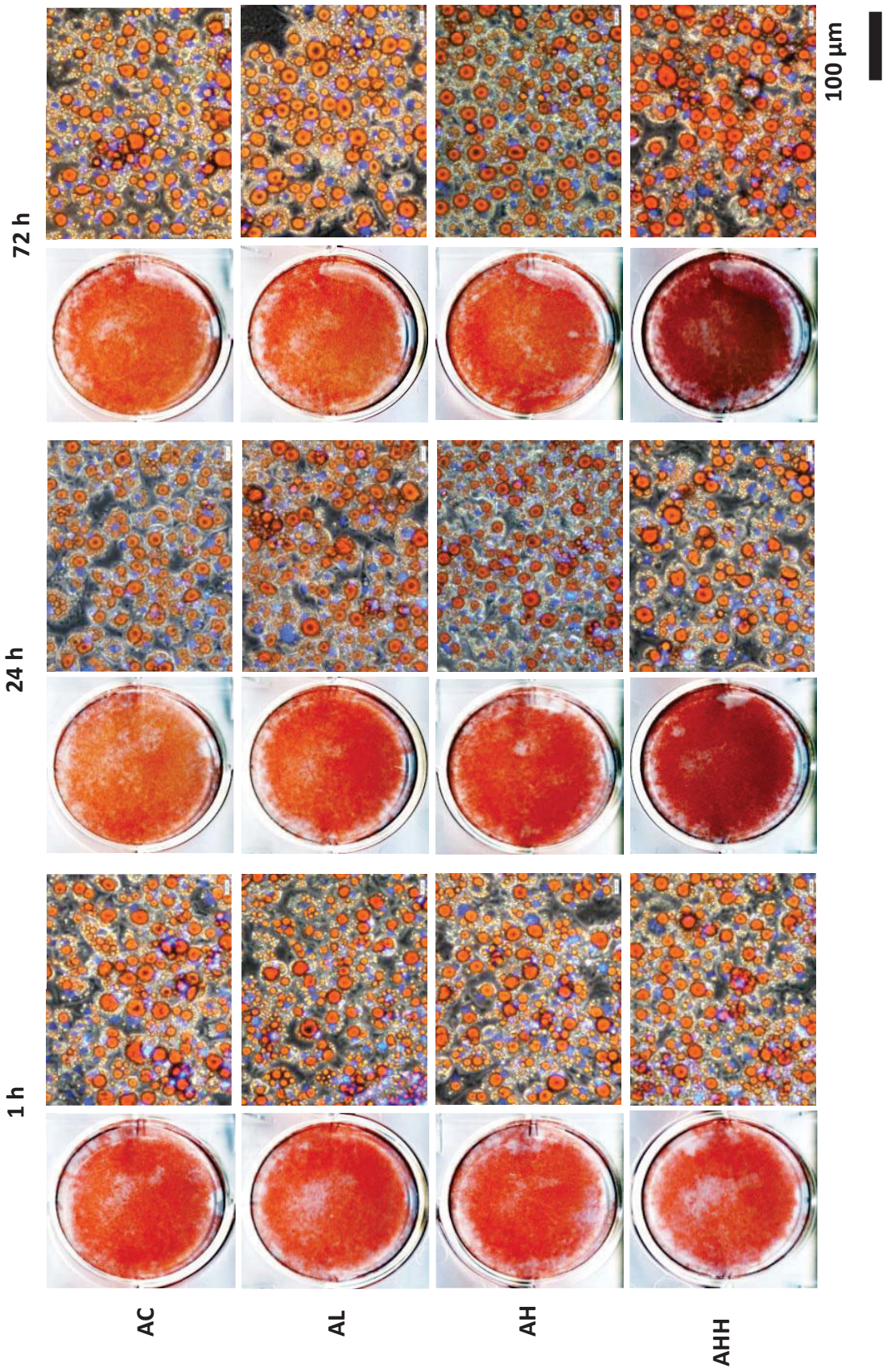
72 h
24 h
1 h
AC
AL
AH
AHH
100 µm

Figure 3.16 Effect of AuNP treatment on neutral lipids in 3T3-L1 adipocytes

Representative images of scanned 3T3-L1 mature adipocytes (left panel) and microscopic image of adipocyte morphology (right panel) stained with Oil red O in the PBS (AC), 0.315 μg/mL AuNP (AL), 3.15 μg/mL AuNP (AH), and 31.5 μg/mL AuNP (AHH) treated groups at 1, 24 and 72 h. Images taken under 20x phase contrast microscopic magnification. Culture well diameter = 3.4 cm, scale bar = 100 μm; n=3.

Table 3.5 Effect of AuNP treatment on the 3T3-L1 adipocytes (> 800 cells)

Time	AC	AL	AH	AHH
Diameter of the adipocytes (μm)				
1 h	34.29 ± 0.92	31.86 ± 0.60*	35.20 ± 0.88	34.63 ± 0.69
24 h	31.24 ± 1.01	33.23 ± 0.88	32.00 ± 1.00	37.73 ± 1.29
72 h	32.75 ± 0.62	36.22 ± 0.90*	33.30 ± 0.93	33.80 ± 0.91
Number of lipid droplets/cell				
1 h	4.5 ± 0.3	4.2 ± 0.3	3.8 ± 0.2	3.1 ± 0.2*
24 h	7.0 ± 0.5	8.4 ± 0.5	11.5 ± 0.7*	12.4 ± 1.1*
72 h	4.9 ± 0.3	5.8 ± 0.4	7.4 ± 0.5*	7.7 ± 0.6*
Diameter of lipid droplets/cell (μm)				
1 h	10.38 ± 0.62	9.68 ± 0.55	12.17 ± 0.61	14.73 ± 0.82*
24 h	6.01 ± 0.35	6.59 ± 0.38*	5.06 ± 0.25	5.26 ± 0.39
72 h	9.08 ± 0.40	9.12 ± 0.42	7.60 ± 0.52*	8.46 ± 0.74

Results are expressed as mean ± S.E.M. Data were analysed by one-way ANOVA followed by post hoc Bonferroni test.* $P < 0.05$ *vs.* AC; n=3.

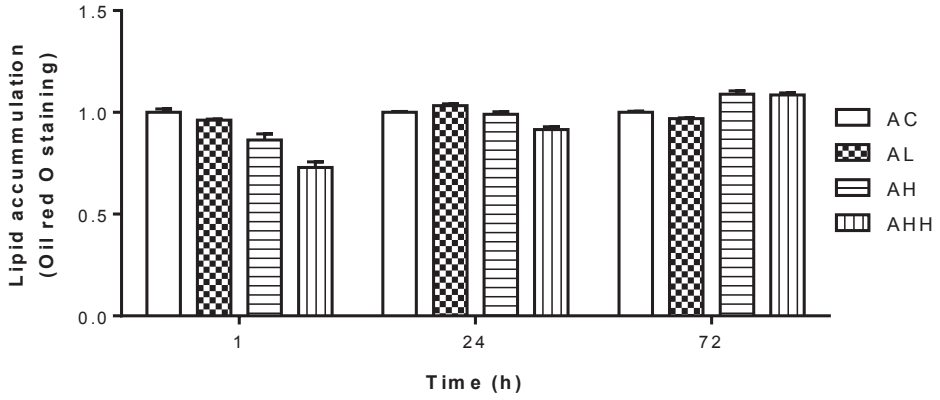

Figure 3.17 Effect of AuNP treatment on lipid accumulation in 3T3-L1 adipocytes

Quantification of lipid accumulation in PBS (AC), 0.315 μg/mL AuNP (AL), 3.15 μg/mL AuNP (AH), and 31.5 μg/mL AuNP (AHH) treated adipocytes by Oil red O staining at 1, 24, and 72 h. Results are expressed as mean ± S.E.M. n=2.

Table 3.6 Effect of AuNP treatment on lipid metabolism in 3T3-L1 adipocytes.

Time	AC	AL	AH	AHH
Intracellular triglyceride (mM)				
1 h	4.88 ± 0.63	4.72 ± 0.51	4.31 ± 0.37	5.15 ± 0.48
24 h	5.23 ± 0.41	5.96 ± 0.72	5.18 ± 0.60	5.56 ± 0.63
72 h	3.98 ± 0.33	4.51 ± 0.37	4.17 ± 0.35	4.39 ± 0.15
Supernatant triglyceride (mM)				
1 h	0.27 ± 0.04	0.21 ± 0.04	0.27 ± 0.03	0.27 ± 0.02
24 h	0.79 ± 0.10	0.64 ± 0.07	0.86 ± 0.12	0.83 ± 0.11
72 h	2.74 ± 0.34	2.71 ± 0.36	2.86 ± 0.54	2.90 ± 0.51
Intracellular NEFA (mM)				
1 h	10.58 ± 0.66	11.01 ±1.32	9.80 ± 0.64	10.72 ± 0.58
24 h	12.44 ± 1.02	12.20 ± 0.63	11.34 ± 0.77	16.79 ± 1.30*
72 h	8.54 ± 0.56	9.21 ± 0.78	8.35 ±0.77	13.23 ± 0.80*

Results are expressed as mean ± S.E.M. Data were analysed by one-way ANOVA followed by post hoc Bonferroni test.* $P < 0.05$ *vs.* AC; n=6–8.

3.3.3.4. Insulin-mediated glucose uptake in adipocytes following treatment with AuNPs

In this study, the mature adipocytes were pre-treated with 3 different doses of AuNPs and then stimulated with 100 nM insulin in varying glucose environments. The depletion of glucose from the culturing media over the 60 mins supported the efficiency of insulin-mediated uptake of glucose into the adipocytes.

Figure 3.18 showed the insulin-mediated glucose uptake in adipocyte cultures treated with 3 different doses of AuNPs within 60 min. No difference in insulin-mediated glucose uptake under all glucose conditions was observed between all the different AuNP-treated groups compared to AC group at 5 min post insulin stimulation (Figure 3.18). At 20 min, the glucose uptake was not significantly altered by AuNPs at different glucose conditions (Figure 3.18 A–C). Following prolonged AuNP exposure, the suppression of insulin-mediated glucose uptake into adipocytes was more significant in the AH and AHH cultures in the lower ambient glucose environment ($P < 0.05$ *vs.* AC, Figure 3.18). In the higher ambient glucose environment, the glucose uptake by AuNP were not significantly altered. This suggests that AuNPs may affect the insulin-mediated glucose uptake into the adipocytes.

3.3.3.5. mRNA expression of adipokine markers in adipocytes following treatment with AuNPs

Our results showed that AuNP treatment did not have any long-term impact on mRNA expression of CPT-1α, ATGL and PPARγ (Figure 3.19).

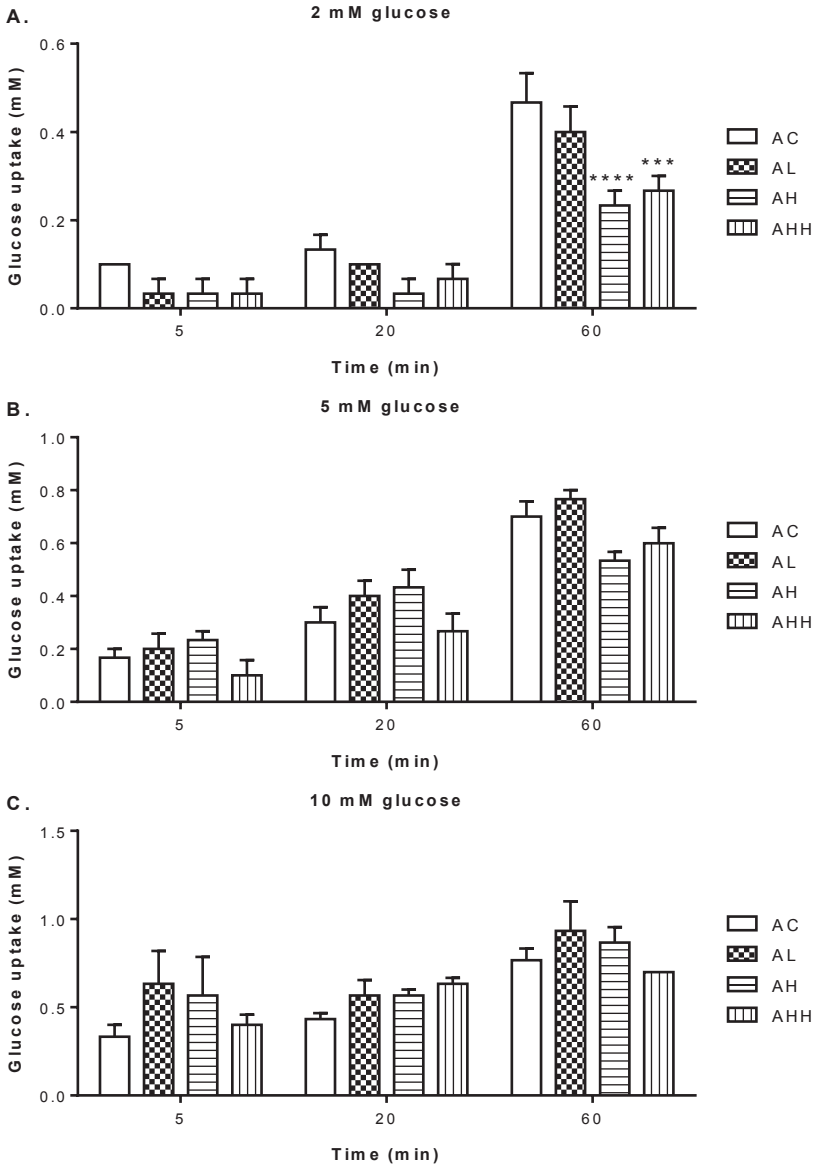

Figure 3.18 Effect of insulin-mediated glucose uptake in AuNP on 3T3-L1 adipocytes

Insulin simulated glucose uptake under glucose concentrations of 2 mM (A), 5mM (B), and 10 mM (C) for 0 (baseline), for 5, 20, and 60 min in mature adipocytes cultures were pre-treated with PBS control (AC), 0.315 µg/mL AuNP (AL), 3.15 µg/mL AuNP (AH), and 31.5 µg/mL AuNP (AHH) for 24 h. Results are expressed as mean ± S.E.M. Data were analysed by Two-way ANOVA followed by post hoc Bonferroni test, , *** P < 0.005, * P < 0.001 *vs.* AC. n=3.

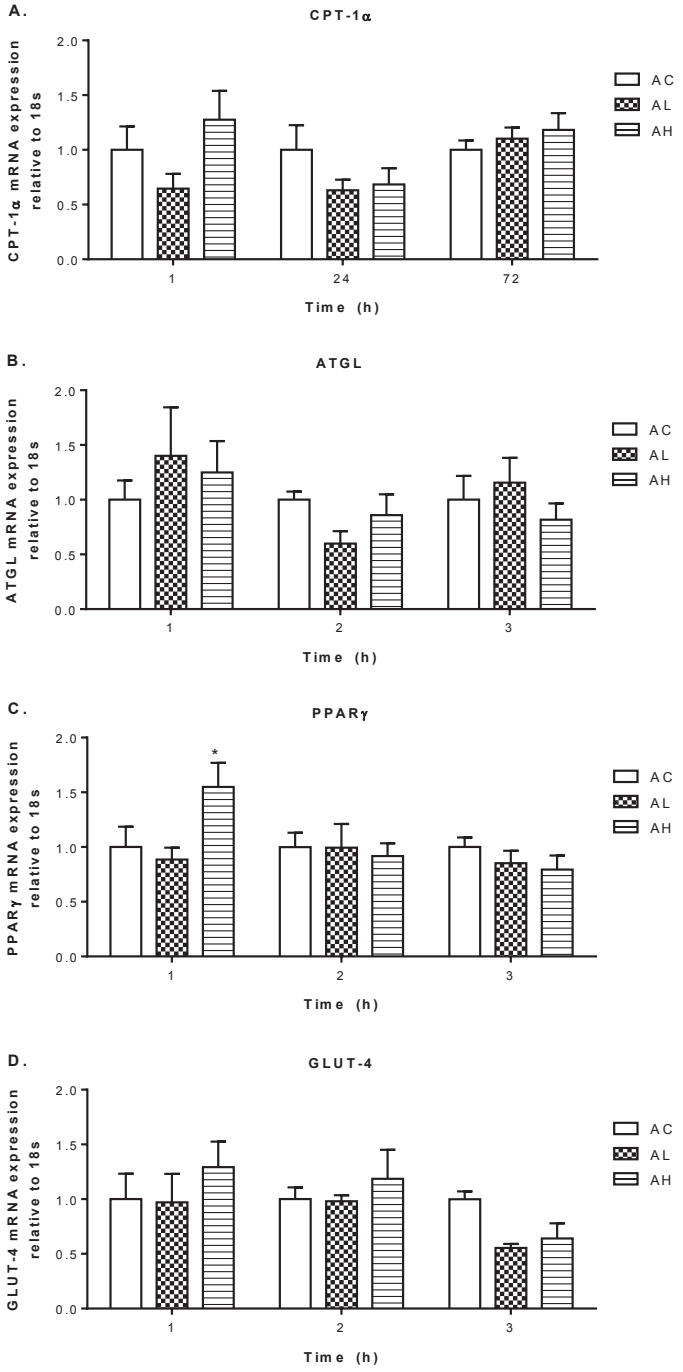

Figure 3.19 Effects of AuNP treatment on adipokine markers in 3T3-L1 adipocytes

mRNA expression of CPT-1α (A), ATGL (B), PPARγ (C), and GLUT-4 (D) in the control (AC), 0.315 µg/mL AuNP (AL), and 3.15 µg/mL AuNP (AH) treated groups at 1, 24, and 72 h. Results are expressed as mean ± S.E.M. Data were analysed by one-way ANOVA followed by post hoc Bonferroni test, *P < 0.05 *vs.* AC. n=5–8.

3.3.4. Effect of AuNP treatment on co-cultured adipocytes and macrophages

The inflammatory changes within the adipose tissue are highly dependent on the complex interactions between adipocytes and macrophages. It is, therefore, important to elucidate the underlying mechanism on how AuNPs may affect and alter lipid and/or glucose gene expression in adipocytes via a change in the local cytokine environment produced by macrophage cells. We aimed to investigate the effect of AuNPs in a setting which mimics the normal adipose tissue with an ATM infiltration. In this study, we employed a direct contact co-culture system of 3T3-L1 mature adipocytes and RAW 246.7 macrophages as our *in vitro* experimental model system.

3.3.4.1. Cell viability of adipocyte-macrophage co-cultures following treatment with AuNPs

Macrophage cells continued to proliferate while the differentiated mature adipocytes did not, at the 24 and 72 h time point studies. Figure 3.20 illustrates cell viability of co-cultured murine 3T3-L1 mature adipocyte and un-stimulated RAW 264.7. Our results showed that AuNP treatment did not affect cell viability of co-cultured cells compared to ARMΦC (Figure 3.20).

3.3.4.2. ROS production in co-cultured adipocytes-macrophages following their treatment with AuNPs

Our results showed that prolonged exposure of AuNPs do not induce oxidative stress in the co-cultured adipocytes and macrophages with no change in intracellular ROS production (Figure 3.21).

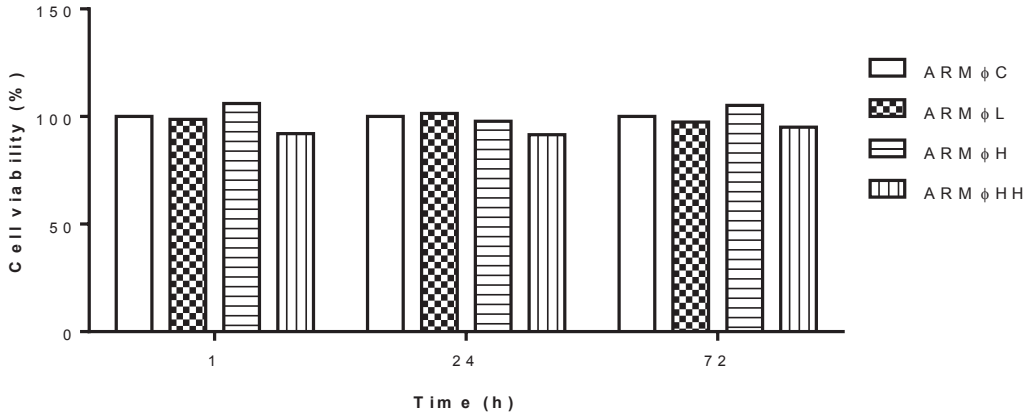

Figure 3.20 Effects of AuNP treatment on the cell viability of co-cultured adipocytes-macrophages.

Cell viability of co-cultured adipocytes-macrophages treated with either PBS (control) (ARMΦC), 0.315 μg/mL AuNP (ARMΦL), 3.15 μg/mL AuNP (ARMΦH), and 31.5 μg/mL AuNP (ARMΦHH) at 1, 24, and 72 h. Results are expressed as mean ± S.E.M. n=2.

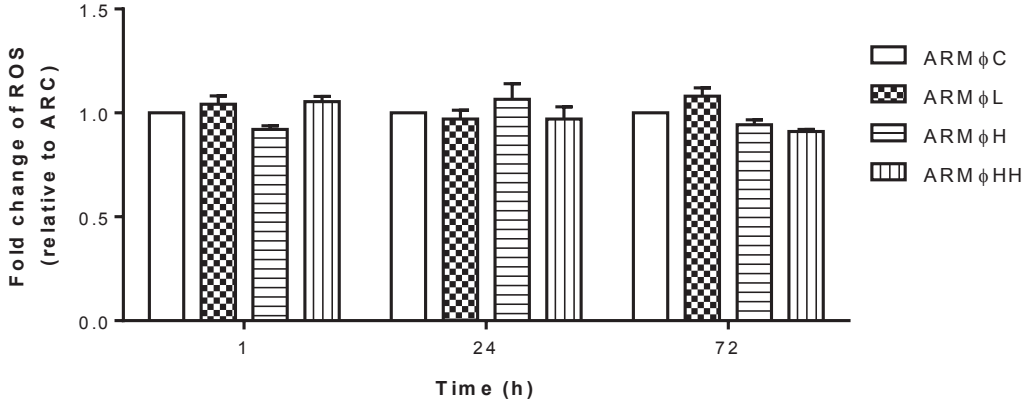

Figure 3.21 Effect of AuNP treatment on ROS production for adipocyte-macrophage co-cultures

Fold change in ROS productions in PBS control (ARMΦC), 0.315 μg/mL AuNP (ARMΦL), 3.15 μg/mL AuNP (ARMΦH), and 31.5 μg/mL AuNP (ARMΦHH) treated groups at 1, 24, and 72 h. Results are expressed as mean ± S.E.M. Data were analysed by two-way ANOVA followed by post hoc Bonferroni test. n=4.

3.3.4.3. mRNA expression of inflammatory and adipokine markers in co-cultured adipocyte-macrophages following AuNP treatment

AuNP treatment showed a trend of inhibition in adipocyte-related CPT-1α, ATGL, PPARγ, and GLUT-4 mRNA expression; while pro-inflammatory TNF-α, IL-6, and TLR-4 mRNA expression in ARMΦL and ARMΦH were not significantly altered at 1 h (Figure 3.22). mRNA expression of pro-inflammatory IL-1β was significantly downregulated by 63% in the ARMΦL compared to ARMΦC ($P < 0.05$) but not in the ARMΦH at 1 h (Figure 3.22F). This suggests that AuNPs may reduce the pro-inflammatory response in co-culture of adipocyte and macrophages.

At 24 h, AuNP treatment significantly increased adipocyte metabolic markers CPT-1α, ATGL, PPARγ and GLUT-4 mRNA in both ARMΦL and ARMΦH compared to ARMΦC ($P < 0.05$, Figure 3.22A–D). There was no difference in mRNA levels of pro-inflammatory TNF-α, IL-1β, and IL-6 in AuNP-treated co-cultures compared to ARMΦC at 24 h; while TLR-4 mRNA levels was significantly upregulated by 1.3-fold in ARMΦH ($P < 0.05$ *vs.* ARMΦC, Figure 3.22H). However, prolonged incubation of the co-cultured cells with AuNPs showed no effect on mRNA expression in all markers measured between groups at 72 h.

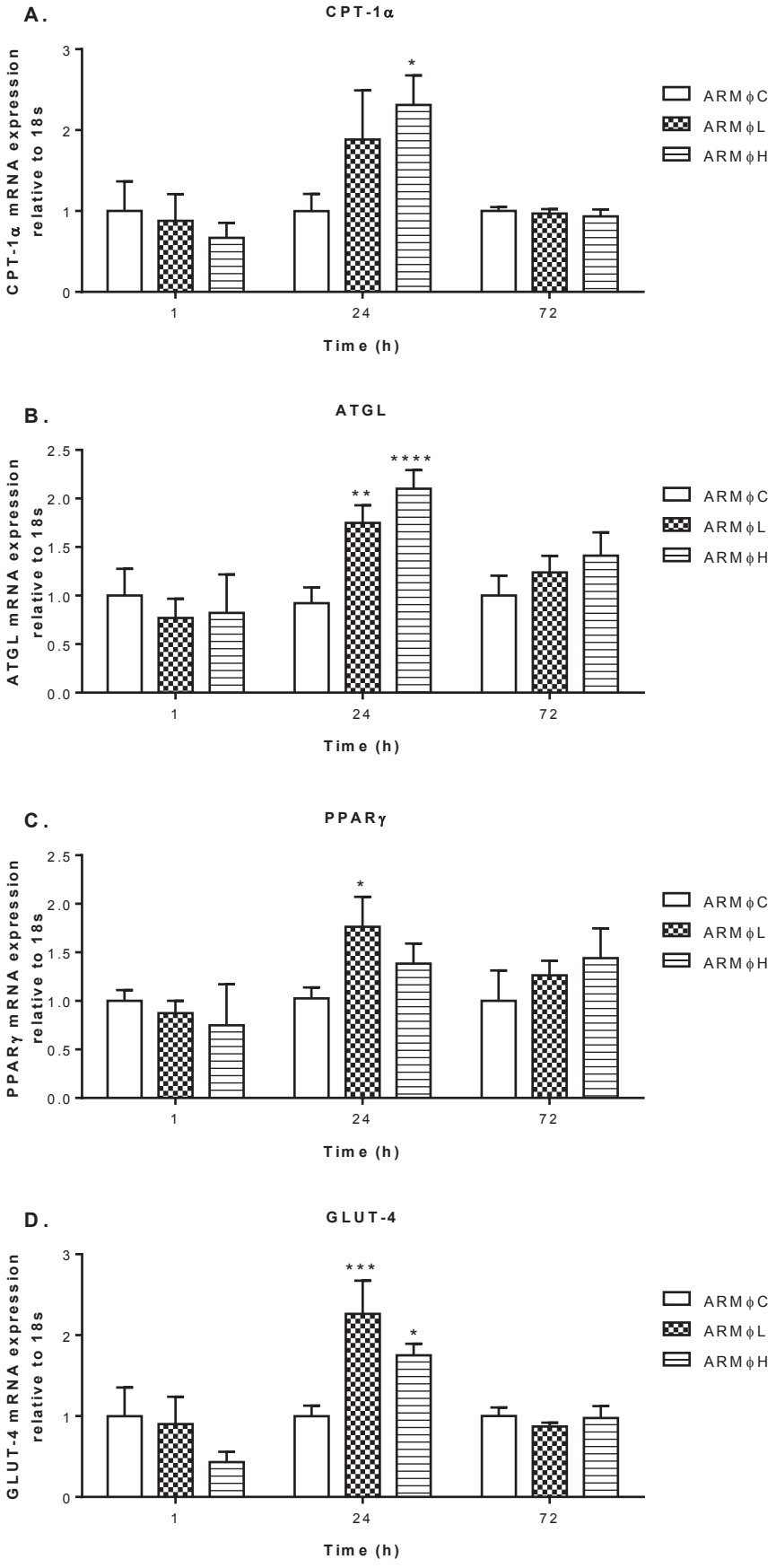
A.
CPT-1α
CPT-1α mRNA expression relative to 18s
3
2
1
0
*
1
24
72
Time (h)
ARMϕC
ARMϕL
ARMϕH
B.
ATGL
ATGL mRNA expression relative to 18s
2.5
2.0
1.5
1.0
0.5
0.0
**
****
1
24
72
Time (h)
ARMϕC
ARMϕL
ARMϕH
C.
PPARγ
PPARγ mRNA expression relative to 18s
2.5
2.0
1.5
1.0
0.5
0.0
*
1
24
72
Time (h)
ARMϕC
ARMϕL
ARMϕH
D.
GLUT-4
GLUT-4 mRNA expression relative to 18s
3
2
1
0
***
*
1
24
72
Time (h)
ARMϕC
ARMϕL
ARMϕH

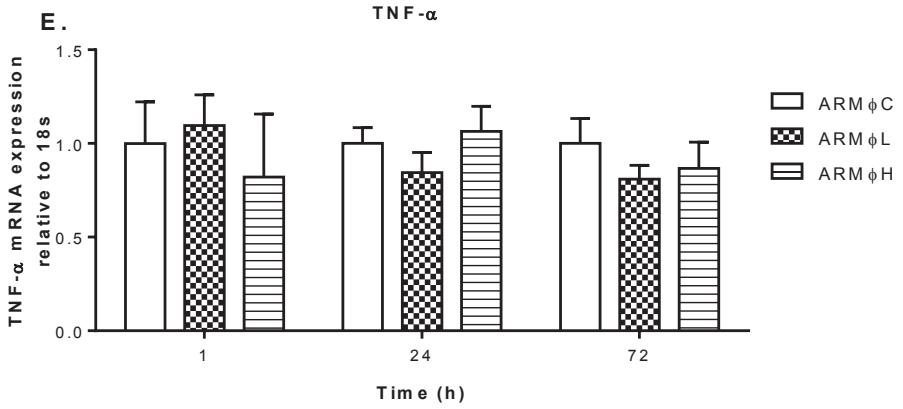
E.
TNF-α
TNF-α mRNA expression relative to 18s
1.5
1.0
0.5
0.0
1
24
72
Time (h)
ARMϕC
ARMϕL
ARMϕH

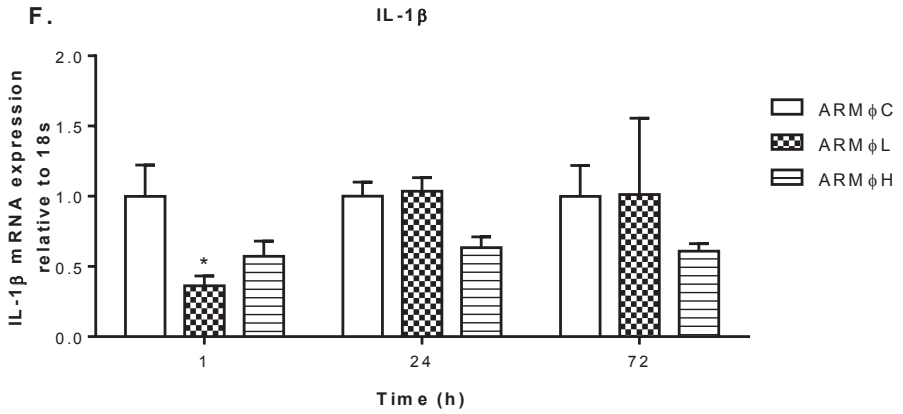
F.
IL-1β
IL-1β mRNA expression relative to 18s
2.0
1.5
1.0
0.5
0.0
*
1
24
72
Time (h)
ARMϕC
ARMϕL
ARMϕH

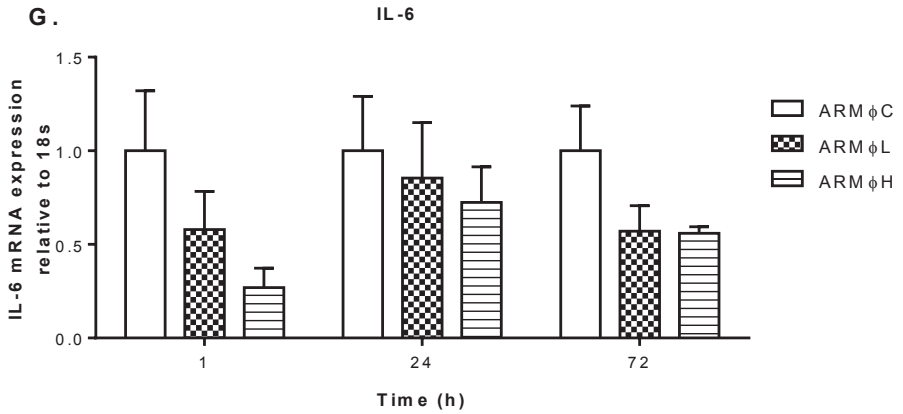
G.
IL-6
IL-6 mRNA expression relative to 18s
1.5
1.0
0.5
0.0
1
24
72
Time (h)
ARMϕC
ARMϕL
ARMϕH

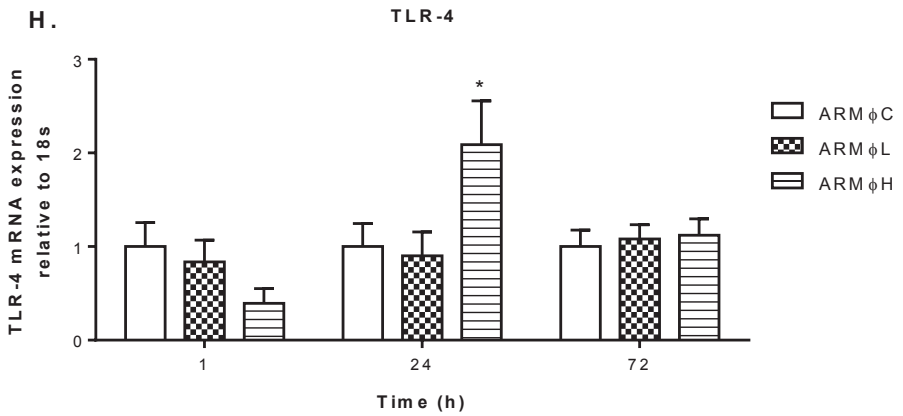
H.
TLR-4
TLR-4 mRNA expression relative to 18s
3
2
1
0
*
1
24
72
Time (h)
ARMϕC
ARMϕL
ARMϕH

Figure 3.22 Effect of AuNP treatment on adipokine and pro-inflammatory markers in co-cultured adipocyte-macrophage

mRNA expression of (A) CPT-1α, (B) ATGL, (C) PPARγ, (D) GLUT-4, (E) TNF-α, (F) IL-1β, (G) IL-6, and (H) TLR-4 in PBS (ARMΦC), 0.315 μg/mL AuNP (ARMΦL), and 3.15 μg/mL AuNP (ARMΦH) treated groups at 1, 24, and 72 h. Results are expressed as the mean ± S.E.M. Data were analysed by one-way ANOVA followed by post hoc Bonferroni test, *P < 0.05, *** P < 0.005 *vs.* ARMΦC. n=3–10.

3.4. Discussion

The major findings in this *in vitro* cell study are that 20–30 nm "naked" AuNPs can induce pro-inflammatory responses in un-stimulated quiescent macrophages, but suppress pro-inflammatory cytokine release in LPS-stimulated U937 macrophage-like cells. AuNPs can also alter lipid and fatty acid metabolic markers in adipocytes, however this only occurs in the presence of macrophages.

AuNPs can be toxic to the murine RAW264.7 macrophages as there was a significant decrease in cell viability observed in the lower doses of AuNP-treated cells as early as at 1 h, which was even more severe in high dose AuNP-treated cells. The opsonisation effect of serum proteins in the culture media onto the surfaces of "naked" AuNPs is well known to play a critical role in to their agglomeration, aggregation, and subsequence uptake into cells (Keene et al. 2012; Tsai et al. 2011). The uptake of the AuNPs into the endocytic compartments such as endosomes and lysozomes is via receptor mediated endocytosis (Steirtman, Brodie & Cohn 1976). The *in vitro* findings on the toxicity of "naked" AuNP have been contradictory and highly dependent on the particle size, shape and duration of exposure (Connor et al. 2005; Khan et al. 2007; Mironava et al. 2010; Pernodet et al. 2006; Yen, Hsu & Tsai 2009; Zhang et al. 2011). It is indeed difficult to compare AuNPs made by different laboratories and their cytotoxicity due to the numerous variations in method of synthesis, temperature, coating citrate ratio, purification, sterility, and possible endotoxin contamination. The AuNPs in our study were sterilized via autoclave to ensure sterility before addition to cell cultures and purified by centrifugation to remove excess citrate or Au ions from the suspension. At higher concentrations, AuNPs may possibly induce an adverse cellular toxic effect due to cumulative deposition and cellular uptake. Studies have similarly shown that increased cellular uptake into the phagocytic macrophages and other cells may thwart cell survival (Mironava et al. 2010; Pernodet et al. 2006; Yen, Hsu & Tsai 2009).

In this study, the same high concentrations of AuNPs did not show an overall cytotoxic effect on the mature adipocytes over time as was seen with the RAW264.7 cells. Interestingly, AuNP seems to lose their cytotoxic effect when applied to the un-stimulated macrophages co-cultured with mature adipocytes. These differences may be

attributed to certain chemicals produced by mature adipocytes that inhibit the cytotoxic effects of the AuNPs which warrants further investigation. Recently, Mironava et al. showed the endocytosis of 13 nm and 50 nm "naked" AuNPs disrupt multiple cellular processes crucial for cell proliferation including movement, cell division, and collagen contraction which interfered with the adipogenesis in human dermal fibroblast and adipose-derived stromal cells (Mironava et al. 2010; Mironava et al. 2014). In contradiction to Mironava et al. (2010, 2014), we showed that continuous exposure to AuNPs does not appear to inhibit adipogenesis or affect the intracytoplasmic neutral lipid formation during adipocyte differentiation. Interestingly, we did not see long term inhibition to adipogenesis and cytotoxicity in the adipocytes cultured independently or when in co-cultures.

In addition, our results showed that AuNP treatment in the un-stimulated RAW 264.7 macrophages caused increased levels of ROS production at 24 h resulting in potential oxidative damage to these cells. Here AuNPs also induced transient elevation of ROS levels in the 3T3-L1 mature adipocytes which after 72 h incubation of, were normalized to the control cells. ROS homeostasis is essential for normal cell growth and survival. Low levels of ROS can promote cell proliferation and differentiation, while excessive amounts of ROS can cause cellular oxidative damage, and depending on the severity and duration may elicit either cell survival or apoptotic mechanisms (Barrera 2012; Boonstra & Post 2004). Studies have shown that under stress, the typical cellular response is to exit the cell cycle and enter G0 or cell cycle arrest, where cells no longer divide. Therefore, the increase in cellular oxidative stress index following AuNP treatment at higher concentrations, may in turn inhibit macrophage cell cycling and cell proliferation, as evidenced in their cumulative cytotoxicity effect. However, in the co-cultured adipocyte-macrophage system, AuNPs suppressed the ROS production suggesting reduced oxidative stress. Such suppression of oxidative stress in the co-cultured conditions however only happened with high dose of AuNPs, not the lower doses.

A recent study by Li et al. (2010) demonstrated that 20 nm AuNP activated autophagic proteins and initiation of autophagy leading to oxidative stress by significant upregulation of several genes in the oxidative stress pathway in MRC-5 human lung

fibroblasts (Li et al. 2010). Zhang et al. (2011) showed that the AuNPs of 60 nm diameter did not induce cellular toxicity and oxidative stress with no change in either nitric oxide or ROS productions in RAW264.7 macrophages up to 24 h (Zhang et al. 2011). We showed that the intracellular ROS levels were proportional to the number of viable cells. Flow cytometry is commonly employed for measurements of ROS production using the H_2-DCFDA method as it selectively determines DCF fluorescence in the viable cell population, excluding the non-viable cell population. Using a modified method for microplate, it is therefore necessary to normalize the DCF fluorescence intensity to the viable cells as was done in our current study, however it is unclear if this was done in the study reported by Zhang et al. (2011). Even though our results may not fully be in agreement with the current literature, it is clear that the differences in size, concentration, and duration of AuNP exposure can affect their endocytic fate drastically leading to different cellular oxidative stress level in different cell lines.

Microbial products (e.g. LPS) and pro-inflammatory cytokines (e.g. IL-1 and TNF-α) typically activate the Nuclear factor kappaB (NF-κB) signalling pathway (Lawrence 2009). TLRs are family of membrane bound receptors, of which TLR-4 recognises LPS, triggering inflammatory pathways, leading to downstream expressions of pro-inflammatory genes including cytokines, chemokines, and adhesion molecules (Akira & Takeda 2004; Akira, Uematsu & Takeuchi 2006; Kawai & Akira 2007). Both IKKα and IKKβ are responsible for the phosphorylating IκB to activate the NF-κB signalling pathway leading to a pro-inflammatory response (Ghosh & Karin 2002; Guha & Mackman 2001; May & Ghosh 1999). Studies have shown the LPS and TNF-α activate IKKβ; while IKKα is required for activation of the alternative pathway. Therefore, IKKβ is a more potent IκB kinase than IKKα (Ghosh & Karin 2002; May & Ghosh 1999).

Pro-inflammatory TNF-α protein levels were not altered by AuNPs in the un-stimulated RAW264.7 macrophage-like cells; while LPS stimulation, as expected, significantly elevated TNF-α and TLR-4 proteins. This indicated that AuNPs may not induce NF-κB signalling pathway. However, mRNA levels for both TNF-α and IL-1β were increased by AuNPs in the un-stimulated RAW264.7 macrophage-like cells at 24 h. Contradictory to our findings, Yen et al. (2009) showed that 20–40 nm AuNP at an extremely low

concentration of 1 ppm increased mRNA expressions of IL-1, IL-6, and TNF-α which were reduced in the long term. Our findings also showed that despite the accumulation of cytoplasmic levels of TNF-α mRNA, cellular TNF-α protein secretion were below the detection limit in the un-stimulated RAW264.7 macrophages via western blot analysis, which is in line with previous reports (Bustin 2000). Our observation indicated the complex interaction between the AuNPs and macrophages in the cellular level at 24 and 72 h altering the pro-inflammatory marker expressions. Further studies on supernatant for secreted levels are required.to determine if the AuNPs induce a pro-inflammatory or anti-inflammatory response in the un-stimulated RAW 264.7 macrophages. Instead of using immortalized macrophage-like cells, an activated macrophage or primary macrophages isolated from peritoneal cavity may be a better *in vitro* model to examine the impact of AuNP on the alterations of inflammatory responses.

There is growing evidence that during obesity the ATMs exist in a pro-inflammatory M1 phenotype contributing to elevated local and systemic cytokine levels, which underlies the inflammatory status within the expanded adipose tissue (Lumeng et al. 2008). In this study, we also examined the impact of AuNP on inflammatory responses in individual cell types. PMA-differentiated U937 macrophage-like cells were used to represent the quiescent ATMs. Our results showed that AuNPs acutely (24 h) suppressed pro-inflammatory cytokine TNF-α protein secretion, however after longer exposure (72 h) they induced a pro-inflammatory reaction with elevation of IL-2, IL-6, IFN-γ and TNF-α cytokines. This may be due to particle aggregation within the cells in the long term whose properties were changed due to their enlarged size, which in turn activates the NF-κB signalling pathway.

On the other hand, LPS stimulated U937 macrophage-like cells showed hypersecretion of pro-inflammatory cytokines such as IL-8 (chemokine for neutrophils) and TNF-α into the cell supernatant in line with the classically activated macrophage pro-inflammatory M1 phenotype. Although AuNPs induced acute inflammatory responses in LPS stimulated U937 cells, at 72 h AuNPs showed an anti-inflammatory effect on LPS-stimulated macrophage-like cells. Therefore, it supports our hypothesis that AuNPs reduce pro-inflammatory responses in activated macrophages. This suggests that

cellular uptake of AuNPs may stimulate pro-inflammatory reactions of the quiescent macrophages. However, when macrophages are in an activated state, as simulated by exposure to LPS, AuNPs can inhibit their pro-inflammatory cytokine production. Studies using primary cells would be important for future studies as well as use of AuNPs in chronic inflammation at longer timeframes.

In this study, AuNP treatment did not show long term impact on adipocyte lipid homeostasis.We observed an increase in size of existing lipid droplets after a short 1 h exposure to AuNPs and an increased formation in the number of smaller sized lipid droplets formed around the central lipid at 24 h. The small lipid droplets seem to then coalescence resulting in larger in sized lipid droplets by 72 h in the AuNP-treated adipocytes. However, both intracellular and supernatant concentrations of triglycerides in adipocyte were not changed by AuNPs. mRNA expression of ATGL was also not affected by AuNP treatment, suggesting no change in triglyceride metabolism. ATGL is one of the many lipases essential for hydrolysis of triglycerides into fatty acids in the lipid droplets to maintain energy balance in adipocytes (Smirnova et al. 2006). AuNPs seem to affect the redistribution of lipids between the cytoplasm and lipid droplets independent of ATGL. In addition, long term exposure to high doses of AuNPs may affect fatty acid metabolism by significantly increasing intracellular NEFA levels. Previous study has shown correlation in the increased intracellular NEFA leves due to the reduction of fatty acid β-oxidation with reduced mRNA levels of CPT-1α (McGarry & Brown 1997). Although an increased intracellular NEFA levels was observed, our results showed that AuNPs did not alter mRNA expression of CPT-1α suggesting unchanged fatty acid β-oxidation. AuNPs also significantly downregulated GLUT-4 mRNA expression in adipocytes suggesting reduced insulin-mediated glucose metabolism. The reduced rate of glucose uptake by AuNPs was more pronounced under lower ambient glucose conditions.

Co-culturing of adipocytes and macrophages showed significantly upregulated mRNA expression levels of CPT-1α following AuNP treatment, which may in turn increase mitochondrial fatty acid β–oxidation and lower intracellular NEFA levels. At the same time, AuNP treatment also led to significantly increased expression of ATGL mRNA which may lead to an increased lipolysis, thereby reducing the lipid content in the

adipocytes grown in co-cultures. In the presence of macrophages, AuNP-treated adipocytes, also upregulated mRNA expression of PPARγ which is crucial for adipocyte growth and differentiation as well as systemic insulin sensitivity. GLUT-4 mRNA levels were also significantly upregulated which suggest an improved glucose uptake. If such an effect can be induced *in vivo*, it may also benefit body glycaemic control. AuNPs acutely reduce inflammatory responses in the co-cultured system at 1 and 24 h. This was in line with our single culture studies, where AuNPs selectively reduced pro-inflammatory responses of LPS-activated macrophages. Based on these findings, the effect of AuNPs appears to support an improvement in adipocyte metabolic markers and a reduction in inflammatory responses, which is also dependent upon the direct interaction between these two cell types - macrophages and adipocytes.

Our results clearly demonstrate the limitations in using single cell culture systems to try and elucidate complex multicellular interactions or test the efficacy of certain treatments. A major limitation however to the direct contact co-cultured model system is regulating the ratio of adipocytes to macrophages over time. This is due to the nature of the two cell types, where differentiated adipocytes do not proliferate, while macrophages continue to proliferate over time. In addition, both RAW 264.7 and U937 cells are immortalized cell lines which require appropriate stimulation to mimic physiological and cellular responses similar to those of ATMs with an M1 phenotype. Hence the use of primary macrophages isolated from peritoneal tissues that do not proliferate in culture and exhibit phenotypical heterogeneity would be superior. Therefore, further studies are necessary using primary peritoneal macrophages and adipocytes isolated from mice in order to further elucidate and corroborate our preliminary findings on the effects of AuNPs**.**

In summary, our *in vitro* study supports our hypothesis that AuNP treatment can lower inflammatory responses of activated macrophages, which in turn improves lipid and glucose metabolism of adipocytes in the presence of macrophages. Thus, 20–30 nm citrate-stabilized AuNPs possess therapeutic potential for the treatment of conditions due to inflammation and substrate metabolic disorders, such as obesity studied in Chapter 4 and Chapter 5.

CHAPTER 4

Treatment of HFD-induced Obesity in Mice Using Gold Nanoparticles

4. Treatment of HFD-induced obesity in mice using gold nanoparticles

4.1. Introduction

Obesity is associated with multiple metabolic disorders including glucose intolerance, hypertension and dyslipidaemia, rendering obese people more susceptible to developing type 2 diabetes, and subsequent macro- and micro-vascular diseases. In addition, there is increasing evidence that show obesity is associated with a markedly increased morbidity, premature mortality, impaired health-related quality of life and medical-care cost burden (Fontaine et al. 2003; Kolotkin, Meter & Williams 2001; Roth et al. 2004; Thompson & Wolf 2001). The current global surge in obesity has seen an staggering 800% increase in demand for weight loss surgical procedures over the last decade, as a means of controlling these metabolic disorders. This increase is also driven by the low success rate of currently available weight-loss medications and interventions, as well as the difficulties faced by individuals trying to maintain ideal body weight following initial weight loss. Therefore, there still remains an urgent and growing need for effective weight loss strategies to deal with the global obesity pandemic.

There has been very limited success in the development of anti-obesity therapeutic agents albeit the pursuit has lasted for more than half a century. Ideally, therapeutic agents for obesity should encompass the benefit of weight loss by decreasing food consumption, reducing food absorption, increasing energy expenditure with limited to no side effects. Advances in the area of energy homeostasis and neurobiology of appetite have led to the identification of numerous new molecular targets which allow better control of hyperlipidemia, hyperglycemia, hepatic steatosis and improved insulin sensitivity through the regulation of lipid and glucose metabolism. It is essential to develop new classes of therapeutic agents that are multi-targeted and which induce weight loss and inhibit weight gain with long-term safety.

The relative stability of individual's body weight and energy homeostasis indicates that energy balance is tightly regulated by a feedback loop, to maintain constancy of total

body energy stores and promote survival. In a state of weight gain or loss, the change in nutritional state is sensed by the hypothalamus, which in turn modulates energy intake and expenditure to resist change and maintain energy balance (Schwartz et al. 2003; Spiegelman & Flier 2001). Although genetics may play a major role in the regulation of body weight, various environmental factors can also exert constant pressure to increase dietary energy intake and decrease energy expenditure through changes in physical activity patterns. This persistent energy imbalance is the fundamental cause influencing a person's propensity to become overweight or obese and contributes to the rapid increase in the prevalence of obesity (ABS 2009; Bouchard & Tremblay 1997).

Since the 1970s, there has been a shift towards increased reliance upon processed foods, prepared meals and fast food with greater use of cheap edible oils, caloric sweeteners, flavouring enhancing additives and salt (Popkin, Adair & Ng 2012; Popkin & Nielsen 2003; Smith, Ng & Popkin 2013). This major dietary shift in both the quantity and quality of the fats consumed characterizes the "nutrition transition", where largely plant-based traditional diets have been promptly replaced by energy-dense and high-fat modern diets from animal sources (Fredrick 2006; Popkin 2004). High fat diet (HFD) consumption, increased lipid deposition and excess triglyceride storage in adipocytes, up-regulates ATGL to increase basal lipolysis which leads to increased intracellular and systemic levels of NEFA (Brown 2001; Gaidhu et al. 2010; Smirnova et al. 2006). Consequently, resident ATMs progressively change in polarization from an anti-inflammatory M2 phenotype to a pro-inflammatory M1 phenotype, along with infiltration of M1-polarized monocytes into the surrounding abdominal fat tissue (Lumeng et al. 2008; Mosser & Edwards 2008)(Cinti et al. 2005; Kosteli et al. 2010a).

This increased ATMs in an M1-state, promotes an inflammatory response in the adipose tissue by directly engaging TLRs to induce production of cytokines, such as TNFα and IL-6, contributing to a low-grade inflammation state associated with obesity (Nguyen et al. 2007)(Abdelhalim 2013). For these reasons, systemic levels of TNFα and IL-6 have been positively correlated with body mass index, hyperlipidemia, insulin resistance, and glucose intolerance (Bastard et al. 2000b; Cornelius et al. 1988a; Hauner, Petruschke, Russ, Röhrig, et al. 1995; Hu et al. 2004; Rosenson et al. 2004a; Semb et al. 1987b; Steinberg et al. 2006; Wunderlich et al. 2010). This highlights the essential roles of

ATM-related cytokines in the development of metabolic disorders in obesity. Interventions to reduce ATM recruitment were shown to partially protect mice from obesity-induced insulin resistance, while inhibition of cytokine release from ATMs increased fat loss and improved insulin sensitivity in obese mice (Kosteli et al. 2010a; Schenk, Saberi & Olefsky 2008b; Weisberg, Hunter, Huber, Lemieux, Slaymaker, Vaddi, Charo, Leibel & Ferrante Jr 2006). Thus, ATMs represent a promising target for reducing fat mass and improving metabolic disorders in obesity. In a recent study, lean mice treated with a single dose of AuNPs was shown to significantly reduced mRNA expression of TNF-α and IL-6 in adipose tissue due to reduced ATM activity, along with observations of weight loss and significant reduction in fat masses (Chen et al. 2013).

At present, C57BL/6 mice are probably the most common mouse model of dietary-induced obesity used for the investigation of metabolic disorders. In particular, 8 week old, male C57BL/6 mice fed a 8 week HFD have been shown to rapidly gain weight due to a chronic energy surplus and their susceptibility in the development of glucose intolerance and insulin resistance with age (Berger 2015). Other mouse strains including AKR/J, DBA/2J, 129X1, and FVB/N are also susceptible to varying degrees of HFD-induced obesity; however, C3H/HeJ, A/J, C57L/J, and BALB/c mice exhibit resistance and some protection from the detrimental effects of a HFD (Berger 2015; West et al. 1992). Interestingly, rodents and other animals have been shown to selectively prefer and overeat palatable HFD than normal rodent chow (West & York 1998). Consumption of HFD has been shown to increase total energy intake and greater efficiency in fat storage than similar excesses of dietary carbohydrate or protein diets (Hill et al. 1988; Hill, Melanson & Wyatt 2000; Sclafani 1989). Amongst the many commercially available HFD, the most common ones studied in rodents and other animals were originally developed by Surwit et al. (1988) which contain either 45% or 60% of calories from fat (Berger 2015; Surwit et al. 1988).

Our in vitro studies showed that AuNP treatment led to increased inflammatory markers in macrophages. However, in the adipocyte-macrophage co-cultures, exposure to AuNPs showed an increased lipid metabolic markers with some reduction in inflammatory markers which suggest a macrophage-dependent regulation of adipocytes

by AuNPs. Therefore, such observation forms the rationale of investigating the potential effect to promote lipid metabolism and fat loss in the animal model. This chapter describes the long-term safety of AuNP treatment in an *in vivo* mice model fed a HFD to induce dietary changes and development of obesity. In particular, two doses of spherical 21nm AuNPs were administered daily via IP injection into 7 week old, male, C56BL/6 mice fed a HFD for 9 weeks to examine their effect on the fat accumulation, glucose regulation, and related metabolic disorders.

4.2. Methods

4.2.1. Ethics approval

All procedures in this study were approved by the Animal Care and Ethics Committee at the University of Technology, Sydney (ethics approval number for this study ACEC#2011-403A) in accordance with Australian Code for the Care and Use of Animals for Scientific Purposes 8th Edition, 2013 by the National Health and Medical Research Council.

4.2.2. Animal experiment

Seven week old male C57BL/6 mice from the Animal Resource Centre, WA, Australia, were housed at 20±2°C on a 12:12 h light/dark cycle. Mice were fed standard rodent chow (13 kJ/g, 12% fat, 17.7% protein, Gordon's Specialty Stockfeeds, NSW, Australia), with *ad libitum* access to water during the acclimatization period. After a week of acclimatization, mice were ear notched for identification purposes following anesthetisation with 2% isofluorane and 1% oxygen inhalation. The mice were housed eight per cage with environmental enrichment. At time zero, the mice were fed either standard rodent chow or a HFD (20 kJ/g, 43% fat, 17% protein, SF03-020, Specialty Feeds, WA, Australia).

The mice were divided into 4 experimental groups with equal body weights (n=20, 20.2 ± 0.04 g). One group was fed standard chow and the other three groups were fed the HFD. Treatment consisted of a daily intraperitoneal injection (IP) with either vehicle

(water) control or AuNPs for 9 weeks. 21nm spherical "naked" AuNPs were prepared as described in Chapter 2 and the AuNP dose was determined from our previous study (Chen et al. 2013). Chen et al (2013) were investigating the effects of single dose of AuNPs at a concentration of 7.85 μg AuNPs/g mice in chow-fed mice. In this study, two doses of AuNPs at 0.785 μg AuNP/g mice and 7.85 μg AuNP/g mice were studied for daily intraperitoneal injection over a period of 8 weeks. We aimed to determine the minimum dosage for effective weight loss. Since long-term daily injection of AuNPs may leads to AuNPs aggregation in the abdominal fat, thus we propose that lower dose group may show a better effect. The maximum volume injected into the mice did not exceed 200 μL.

The control group on standard chow (Chow-C) was injected daily with PBS (vehicle only) solution, as was one of the HFD control group (HFD-C). Of the remaining two groups on the HFD, one received injections at a low dose AuNP concentration (HFD-LAu) (0.785 μg AuNP/g mice, daily IP), and the final group received injections at a high dose AuNP concentration (HFD-HAu) (7.85 μg AuNP/g mice, daily IP). Body weights were measured and recorded weekly and energy consumption (kJ/mouse/24 h) was measured between 10:00 and 11:00 am fortnightly before the AuNP treatment. Measurement of food intake was determined by subtracting the weight of food remaining in the lid of the cage and any collected from within the cage, after 24 h from the time pre-weighed food was originally placed on the lid of the cage. The energy consumption was calculated according to Table 4.1.

Table 4.1 Summary of animal feed composition according to manufacturer.

	Manufacturer	Energy (kJ/g)	Protein per gram	Fat per gram	Protein per kJ	Fat per kJ
Chow	Gordon's Specialty Stockfeeds	13	23%	6%	17.7%	12%
HFD	Specialty Feeds, SF03-020	20	19.4%	23%	17%	43%

4.2.2.1. Tissue and blood sample collections

At the end of week 9, the mice (n=6) were euthanized using Pentothal (0.1mg/g, IP, Abbott Diagnostics, Kurnell, NSW, Australia) injection. Once the mice fell into a deep sleep and lost consciousness, blood was collected via cardiac puncture using 24G needle and syringe. Endpoint blood glucose was determined using an AccuCheck® Performa glucose meter (Roche, Branchburg, NJ, USA) by pipetting 10 uL of blood onto the test strips. Blood was immediately centrifuged at 15,000 rpm, for 6 min. The plasma was stored at -20°C for bioassay analyses. Tissues such as heart, spleen, kidneys, liver, and abdominal fat pads were harvested and weighed. The hypothalamus and soleus muscles were also dissected and collected. The fat pads and organs were either fixed in 10% formalin or snap frozen in liquid nitrogen and then stored at -80°C for further analysis.

4.2.3. Glucose tolerance test

At week 8 of treatment, the mice were fasted for 5 h after which time an intraperitoneal glucose tolerance test (IPGTT) was performed following glucose challenge as previously described (Chen et al. 2011). All mice were administered with D-glucose (2 g/kg, Univar® Ajax Finechem Pty Ltd, Seven Hills, NSW, Australia) by IP injection with a 26G syringe needle. Tail tip blood was collected at 0 time prior to glucose injection (baseline), then at 15, 30, 60, and 90 min after glucose administration. Blood glucose levels were measured using an AccuCheck® Performa glucose meter (Roche, Branchburg, NJ, USA). The trapezoid method was used to calculate the area under the curve (AUC) corresponding to the blood glucose levels over the monitoring period obtained for each animal.

4.2.4. Biochemical assays

The blood plasma and liver tissue lysate were used for various biochemical assay analyses according to manufacturer's instructions.

4.2.4.1. Determination of plasma NEFA concentration

Plasma NEFA was measured using NEFA-C kit (Wako Pure Chemicals Industries Ltd., Osaka, Japan) according to the manufacturer's recommendations detailed in section 3.2.7.1.

4.2.4.2. Determination of plasma and liver tissue triglyceride concentrations

Liver tissue triglycerides were isolated and purified according to extraction method previously described (Folch, Lees & Sloane-Stanley 1957). Briefly, 1 mL of chloroform:methanol (2:1 v/v, BDH, Muskegon, MI, USA) solution was added to a known amount of liver sample (approximately 50 mg) and homogenized using Precelleys®24 (Bertin Technologies, Carlsbad, CA, USA) with ceramic beads (Sarstedt, Nümbrecht, Germany). The homogenised tissue was then washed with an additional 3 mL of choloform:methanol solution and transferred to 15 mL falcon tubes to be rotated overnight at room temperature for the extraction of triglycerides. The next day, 2 mL of sodium chloride (0.6% w/v) was added to each tube to be mixed thoroughly by vortexing and centrifuged at 850 g for 10mins, room temperature. The lower organic phase containing the triglycerides was transferred to a glass vial to be dried in the fume cupboard. Finally, the triglyceride extract was reconstituted in 3 mL of absolute ethanol and assayed.

The liver tissue lysate and plasma triglyceride concentrations were measured using Triglyceride GPO-PAP reagent (Roche Diagnostics, Indianapolis, IN, USA) as per protocol detailed in section 3.2.7.2.

4.2.4.3. Determination of plasma insulin concentration

Plasma insulin was measured using a mouse Insulin Enzyme-Linked Immunosorbent Assay kit (KA3812, Abnova, Taipei, Taiwan) according to manufacturer's instruction based on a sandwich antibody-protein-antibody detection method. Briefly, 50 µL of test sample was added into the test wells of monoclonal anti-insulin antibody pre-coated 96-well plate. Then 50 µL of HRP-conjugated polyclonal anti-insulin antibody was added

into the test wells except the control wells. Following that, the sample plate was incubated at 37˚C for 60 min and thoroughly washed with wash buffer. Subsequently, 50 µL of TMB substrate A and 50 µL of TMB substrate B were added and the sample plate gently vortexed on a shaker for 30 sec, and then incubated in the dark at 37˚C for 60 min. This enzymatic catalytic activity of HRP forms a blue colour solution that quickly changed yellow upon final addition of 50 µL of stop solution from the assay kit which contains sulphuric acid. The amount of insulin in plasma sample is proportional to the optical density of yellow colour measured at 450 nm using Synergy HT microplate spectrophotometer (Bio-Tek Instrument Inc., Winooski, VT, USA). The concentration of insulin was determined by a standard curve (R^2 = 0.9986, Figure 4.1).

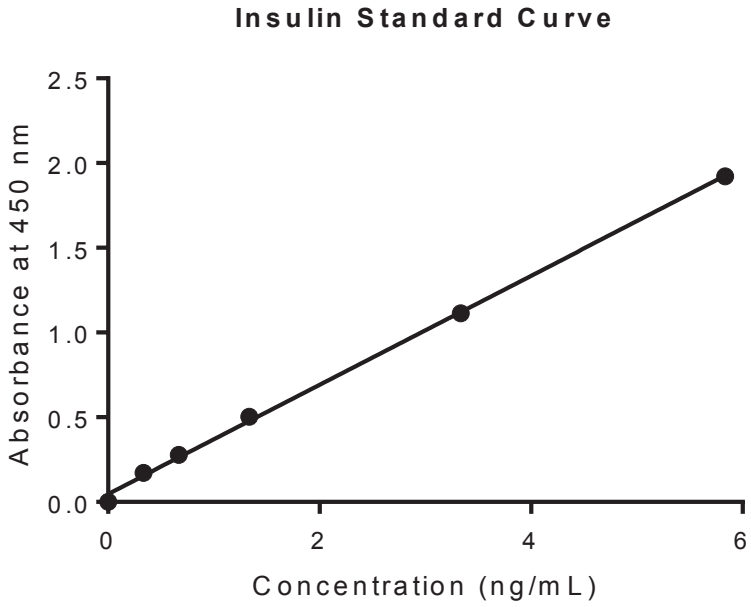

Figure 4.1 Standard curve derived from titration of insulin using mouse insulin Enzyme-Linked Immunosorbent Assay kit. Y = 0.3219X + 0.04768.

4.2.4.4. Determination of plasma cholesterol concentration

Plasma cholesterol concentration was measured using Cholesterol Flurometric assay kit (1007640, Cayman Chemical, Ann Arbor, MI, USA) according to manufacturer's instruction. This assay is a simple enzyme-coupled flurometric detection method for the sensitive quantification of cholesterol in serum and plasma. Briefly, 50 µL of plasma

samples (diluted in 1:200) were added into test wells of a black 96-well solid plate (400017, Cayman Chemical, Ann Arbor, MI, USA) in duplicate. The Assay Cocktail containing 4.724 mL of assay buffer, 150 µL of cholesterol detector, 50 µL of HRP, 50 µL of cholesterol oxidase, and 5µL of cholesterol esterase were prepared. Assay enzymatic reactions were initiated by the addition of 50 uL of freshly prepared Assay Cocktail into all the test wells and incubated at 37˚C for 30 min with plate cover in dark. In this assay, the cholesterol and cholesterol ester in the samples were hydrolysed by cholesterol esterase into cholesterol, and then oxidised by cholesterol oxidase to produce hydrogen peroxide. In the presence of HRP, the hydrogen peroxide reacts with a highly sensitive and stable detection probe to yield a highly fluorescent resorufin. This fluorescence indicator can be measured at 530 nm excitation and 590 nm emission wavelengths using Infinite M200® Pro plate reader (Tecan Deutschland GmbH, Crailsheim, Germany).The concentration of cholesterol was determined by a standard curve plotted from known Cholesterol assay standards (10008053, Cayman Chemical, Ann Arbor, MI, USA) (R^2 = 0.9989, Figure 4.2).

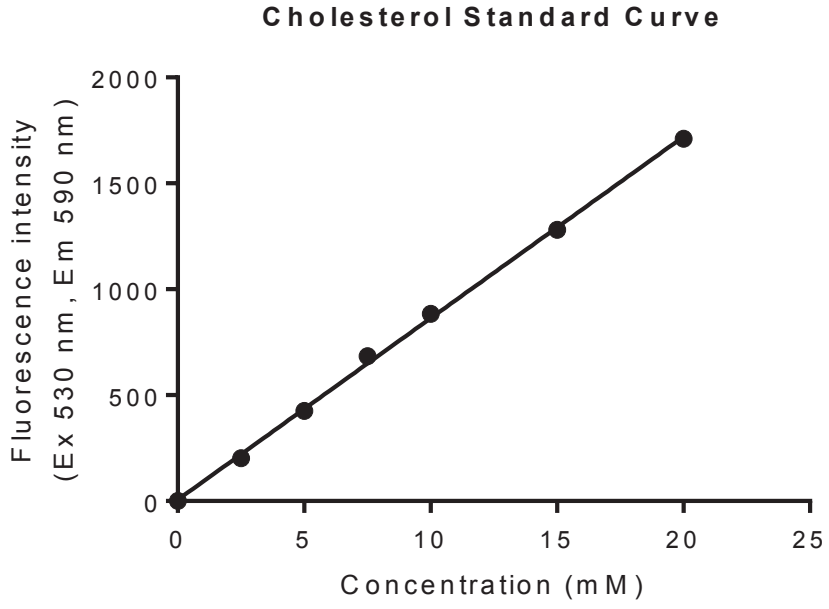

Figure 4.2 Standard curve derived from titration cholesterol using Cholesterol Flurometric assay kit. Y = 85.71*X + 6.290.

4.2.4.5. Determination of plasma alanine aminotransferase (ALT) concentration

Plasma ALT also known as glutamate pyruvate transaminase was measured using ALT reagent kit (D94620, Dialab Ltd, Vienna, Austria). Briefly, 20 µL of sample was incubated with 100 uL of Reagent 1 at 37˚C (room temperature) for 5 min. Then, 25 µL of Reagent 2 was added to test wells and the plate was gently shaken for 5 sec to mix. Immediately after that, the optical density at 340 nm was read at 0 (initial read against air) and repeated after 1, 2, and 3 mins at 37˚C using a Synergy HT microplate spectrophotometer (Bio-Tek Instrument Inc., Winooski, VT, USA). Serum ALT concentration in each well was calculated from the average difference between the absorbance measured per minute, multiplied by a sample start factor constant of 1745 (Δ Absorbance/min x Factor).

4.2.4.6. Determination of plasma aspartate aminotransaminase (AST) concentration

Plasma AST also known as glutamate oxaloacetate transaminase was measured using a AST reagent kit (D94620, Dialab Ltd, Vienna, Austria). Briefly, 20 µL of sample was incubated with 100 uL of Reagent 1 at 37˚C (room temperature) for 5 min. This was followed by addition of 25 µL of Reagent 2 to test wells, after which the sample plate was gently shaken for 5 sec to mix. Immediately after that, the optical density at 340 nm was read at 0 (initial read against air) and repeated after 1, 2, and 3 mins at 37˚C using Synergy HT microplate spectrophotometer (Bio-Tek Instrument Inc., Winooski, VT, USA). Serum AST concentration in each well was calculated from the average difference between the absorbance measured per minute, multiplied by a sample start factor constant of 1745 (Δ Absorbance/min x Factor).

4.2.5. Histological analysis

4.2.5.1. Tissue specimen preparation

Formalin fixed adipose tissue samples were placed in a tissue embedding cassette and covered with 70% ethanol for 72 h. The adipose tissue was then processed using a Shandon Excelsior^{TM} Tissue Processor (Thermo Fisher Scientific Inc., Wilmington, MA, USA) following a standard protocol. Briefly, the cassettes were processed through a series of graded alcohol at 70%, 95% (JJ00ABS95/5), 100% (JJ008) and xylene (JJ028/5) from Thermo Fisher Scientific Inc., Wilmington, MA, USA. Following the dehydration process, the cassettes were embedded in paraffin wax by heating to the 50–54˚C melting point (Paraplast X-tra, P3808-1KG, Sigma Aldrich, St. Louis, MO, USA) in a Shandon Histocentre 3 Embedding Station (Thermo Fisher Scientific Inc., Wilmington, MA, USA). The cassettes were then removed and the paraffin-embedded tissues were sectioned at 5 μm thickness using a HM 325 Rotary Microtome (Thermo Fisher Scientific Inc., Wilmington, MA, USA). The tissue sections were floated on a water bath at a temperature below the wax melting temperature of 43˚C before transferred onto histology glass slides and dried in an incubator at 60˚C overnight.

4.2.5.2. Harris haematoxylin and eosin (H&E) tissue staining

The adipose tissue sections were stained using H&E to examine the morphology and size of the lipid droplets. Briefly, the sectioned slides were deparaffinized using xylene (2 x 10 min), then rehydrated using a graduated series of alcohol washes; 100% absolute ethanol (2 x 5 min), 95% ethanol (2 x 5 min), and 70% ethanol (2 x 5 min). Subsequently, the slides were rinsed with deionised water to remove any remaining fixative. The rehydrated tissue sections were then stained with Harris haematoxylin solution (HHS-128, Sigma Aldrich, St. Louis, MO, USA) for 1 min and washed under running tap water. The sections were subsequently differentiated in 1% acid alcohol (1 mL of 37% concentrated HCl solution and 99 mL of 70% ethanol solution) to remove excess dye and thoroughly washed in running water. The sections were counterstained with Eosin solution (E4009, Sigma Aldrich, St. Louis, MO, USA) for 1 min then dehydrated through a series of washes starting with 95% ethanol (2 x 5 min), 100%

absolute ethanol (2 x 5 min), and then xylene (2 x 5min). The stained tissue sections were mounted in DPX mounting medium (06522, Sigma Aldrich, St. Louis, MO, USA) and covered with glass coverslips. Digital photomicrographs of stained tissue sections were captured with an inverted light microscope (CKX31 Olympus Co., Tokyo, Japan) using a digital camera (Olympus) using cellSens software (version 1.7). For each mouse, 800–1000 adipocytes were quantified from 6 different region of interest using ImageJ software (1.6.0_24, fiji.sc, National Institutes of Health, Bethesda, MD, USA).

4.2.6. Gene expression analysis using RT-PCR

4.2.6.1. RNA isolation and cDNA synthesis

Snap frozen fat and liver tissue samples (50–100 mg) were homogenized in 2 mL polypropylene cryovials containing ceramic beads (Sarstedt, Nümbrecht, Germany) and 1 mL of TRI reagent (T9424, Sigma-Aldrich, St Louis, MO, USA) using Precelleys®24 (Bertin Technologies, Carlsbad, CA, USA). The RNA extraction, isolation, and purification were prepared according to the TRIzol method as outlined in section 3.2.5.1. The purified total cellular RNA at 200 ng/µL was used for first-strand cDNA library synthesis detailed in section 3.2.5.2. The synthesized cDNA was diluted to 200 ng/µL and used for gene expression assay detection.

4.2.6.2. Taqman® and SYBR ® Green gene expression assay

mRNA expression of a number of genes was determined from the retroperitoneal fat and liver tissue samples collected following 9 weeks of HFD intervention. These markers included macrophage markers CD68 and F4/80, inflammatory cytokines TNFα, IL-6, TLR-4, IL-1R and IL-1β. Markers related to glucose metabolism (GLUT-4, PEPCK and FOX-O1), lipid metabolism (ATGL, CPT-1α, SREBP-1c, FASN) and other adipokine (PPARγ, adiponectin, serum alpha amyloid A (SAA)-1 and leptin) were also determined.

Primers and probes of TaqMan® gene expression assays of Mus musculus origin were used (Table 4.2). The reagents composition and RT-PCR amplification program for

TaqMan® gene expression assay detection were outlined in section 3.2.5.3 (Table 3.2 and Table 3.3). Gene expression was normalized against housekeeping gene, 18s rRNA and the relative change in mRNA gene expression was determined by the ΔΔCT approach (Bustin 2000). The SYBR® Green gene expression assays of Mus musculus origin were optimised for target genes listed in Table 4.3 according to RT-PCR protocol previously described (McGrath et al. 2014). Table 4.4 showed the reagent composition used for single reaction in the SYBR® Green gene expression assay. Briefly, 2.5 µL of cDNA (200 ng/µL) were thoroughly mixed and pipetted in duplicate onto 96 well twin-tec real-time PCR plate (Eppendorf, Hamburg, Germany) using epMotion 5070 (Eppendorf, Wien, Austria). Then, 12 µL of PCR master mix solution containing 7.5 µL of iQ SYBR® Green Supermix (1708880, BioRad, Carlsbad, CA, USA), 0.6 µL of forward primer sequence of target gene (Table 4.3), 0.6 µL of reverse primer sequence of target gene (Table 4.3), 3.3 µL of diethylpyrocarbonate (DEPC)-treated deionised water were accurately was added. The RT-PCR amplifications were ran under the following the cycling conditions in Mastercycler® Ep Realplex^2 (Eppendorf, Hamburg, Germany): 50°C for 2 min and 95°C for 3 min incubations, followed by 50 cycles at 95°C for 10 sec, 60°C for 10 sec, and 72°C for 10 sec (Table 4.4). In addition, a dissociation or melting curve analysis was performed at the completion of the RT-PCR amplification cycles to reveal the purity of the amplified product yielded for each reaction (Table 4.4). For not validated markers, a standard curve was prepared by serial dilution of cDNA at undiluted, 1:10, 1:100, 1:1000, 1:10,000, and 1:100,000 dilutions (n=7) to assess the primer efficiency on the respective fat and liver tissues samples prior to the RT-PCR analysis. Gene expression was normalized against housekeeping gene, 18s rRNA and the relative change in mRNA gene expression was determined by the ΔΔCT approach (Bustin 2000).

Table 4.2 TaqMan® gene expression assay primer sequences

Marker	NCBI gene ref.	FAM-labelled probes (5’→3’)	Assay ID
CD68	NM_009853.1	GCTTAAAGAGGGCTTGGGGCATATC	Mm03047340_m1
TNF-α	NM_001278601.1	GACCCTCACACTCAGATCATCTTCT	Mm00443258_m1
IL-6	NM_031168.1	TGAGAAAAGAGTTGTGCAATGGCAA	Mm00446190_m1
IL-1β	NM_008361.3	GACCCCAAAAGATGAAGGGCTGCTT	Mm00434228_m1
IL-1R	NM_001123382.1	AGCTGACCCAGGATCAATGATACAA	Mm00434237_m1
TLR-4	NM_021297.2	CCCTGCATAGAGGTAGTTCCTAATA	Mm00445273_m1
PPARγ	NM_0011273330.1	ATGCTGTTATGGGTGAAACTCTGG	Mm01184322_m1
ATGL	NM_025802.3	CCAAGACTGAATGGCTGGATGGCAA	Mm00503040_m1
CPT-1α	NM_013495.2	TCCAGGAGAATGCCAGGAGGTCATA	Mm00550438_m1
GLUT-4	NM_009204.2	GGCTCTGCTGCTGCTGGAACGGGTT	Mm00436615_m1
Leptin	NM_008493.3	TCACACACGCAGTCGGTATCCGCCA	Mm00434759_m1
		VIC-labelled probe (5’→3’)	
18S	X03205.1	ACCGCAGCTAGGAATAATGGA	4319413E

Table 4.3 SYBR® Green gene expression assay primer sequences

Marker	NCBI gene ref.	Forward primer sequence (5'→3')	Reverse primer sequence (5'→3')
Adiponectin	NM_009605.4	CCACTTTCTCCTCATTTCTG	CTAGCTTCAGTTGTAGTAAC
SREBP-1c	NM_011480.3	AATAAATCTGCTGTCTTGCG	CCTTCAGTGATTTGCTTTTG
FASN	NM_007987.2	TGAATGCCTCAAATCTTAGC	TTTTAGCTTCCTGGATTGTC
FOX-O1	NM_019739.3	AAACACATATTGAGCCACTG	TCTACTCTGTTTGAAGGAGG
PEPCK	NM_011044.2	GGTGTTTACTGGGAAGGCATC	CAATAATGGGGCACTGGCTG
F4/80	X93328.1	CTCCAAGCCTATTATCTATACC	CTTCCACAATCTCAC
SAA-1	NM_000331	TGACCAGGAAGCCAA	GTAGGAAGAAGCCCA

Table 4.4 Reagent composition for SYBR® Green gene expression assay

Reagents	Single reaction
iQ SYBR Green Supermix	7.5 µL
Forward primer sequence	0.6 µL
Reverse primer sequence	0.6 µL
DEPC-treated deionised water	3.3 µL
cDNA (200 ng/µL)	3 µL
Total	15 µL

Table 4.5 RT-PCR amplification program for SYBR® Green gene expression assay

Step	Temperature	Time	Cycle
Reaction mix incubation	50°C	2 min	1
Polymerase activation	95°C	3 min	1
Three-step amplification cycles:			
1. Denaturation	95°C	10 sec	
2. Annealing	60°C	10 sec	50
3. Elongation	72°C	10 sec	
Dissociation/melting curve:			
1. Heating	95°C	1 min	1
2. Cooling	55°C	1 min	1
3. Dissociation of the DNA strands	60–94.5°C*	10 min	70

* increase set point temperature after cycle 2 by 0.5°C

4.2.7. Tissue preparation and digestion for ICP-MS analysis

Mouse tissue and organs including fat, liver, spleen, kidney, heart, lung and brain were assayed for elemental gold content. Briefly, tissue samples (approximately 0.02–0.1 g) were incised, weighed and dehydrated with a series of grated alcohols (70%, 95%, and 100%) from Thermo Fisher Scientific Inc., Wilmington, MA, USA. The tissue samples

were then placed in 1.5 mL polypropylene sample tubes and further dehydrated using an Alpha 1-2 LDplus freeze dryer (CHRIST® GmbH, Osterode am Harz, Germany) under vacuum pressure of 0.017 mBAR at - 93°C for more than 24 h. Thereafter, the dried tissue pellets were weighed again before grinding into a course powder to facilitate subsequent acid digestion (1:2:1 v:v:v of nitric acid: hydrochloric acid:hydrogen peroxide). The powdered samples were then digested and heated intermittently at 80°C in acid solution comprised of a mixture of 100 µL of concentrated nitric acid (67–69%, S020101-CHEF03, Baseline® Seastar Chemicals Inc., Sidney, BC, Canada) and 200 µL concentrated 37% hydrochloric acid (32–35%, S020401-SSEP03, Baseline® Seastar Chemicals Inc., Sidney, BC, Canada). Upon acid digestion to white ash, samples were cooled to room temperature and 100 µL concentrated hydrogen peroxide (30–31%, S021001-CHEF04, Baseline® Seastar Chemicals Inc., Sidney, BC, Canada) was added, then heated intermittently to 60°C to ensure complete digestion of tissue. Subsequently, the digested tissue samples were diluted with 600 µL volume of purified water and stored in 4°C for analysis using ICP-MS (Agilent 7500 CE series, Agilent Technologies Inc., Forrest Hill, VIC, Australia) detailed in section 2.2.7.3. Reagent blanks were analysed for baseline control on the digestion procedures. Calibration curves were constructed with known concentrations (0.2–0.5 µg/L) of the gold standard solution (Choice Analytical, Thornleigh, NSW, Australia) and the results analysed using Agilent Technologies MassHunter Workstation software.

4.2.8. Statistical analysis

Results are expressed as mean ± S.E.M. IPGTT analysis were performed using one-way ANOVA with repeated measures followed by post hoc Bonferroni test (Prism version 6, GraphPad Software Inc, San Diego, CA, USA). All other analyses in this study were performed using one-way ANOVA followed by post hoc Bonferroni test. $P < 0.05$ was considered statistically significant.

4.3. Results

4.3.1. Effect of HFD consumption

4.3.1.1. Body measurements

Prior to HFD feeding, there were no differences in energy consumption, nor body weight amongst the four groups of mice at week 0 (Figure 4.3A,B). The difference in the average energy consumption between the Chow-C mice and HFD-C mice throughout the 9 weeks of study were not significant (Figure 4.3A and Table 4.6). However, the body weight trajectory of the HFD-C mice was significantly higher than the Chow-C group one week after the dietary intervention ($P < 0.05$, Figure 4.3B). Over time, this difference became more pronounced (Figure 4.3B) with the HFD-C mice becoming 35% heavier than the Chow-C mice ($P < 0.05$, Table 4.6) after 9 weeks.

HFD consumption significantly increased the body weight of the HFD-C group and their organ masses including fat mass, liver, kidney and heart ($P < 0.05$ *vs.* Chow-C, Table 4.6). Retroperitoneal, epididymal and mesenteric adipose tissue masses in the HFD-C group were 6.9, 4, and 1.5-fold greater than the Chow-C group, respectively ($P < 0.05$, Table 4.6). When the fat masses were standardised against body weight, the differences remained significantly different ($P < 0.05$, HFD-C *vs.* Chow-C, Table 4.6).

IPGTT results are shown in Figure 4.4. The blood glucose levels in HFD-C mice was constantly higher than the Chow-C mice at 15, 30, 60 and 90 min post glucose injection ($P < 0.05$, Figure 4.4A). The AUC of the HFD-C mice was also 60% higher compared to the Chow-C mice ($P < 0.005$, Figure 4.4B). The endpoint blood glucose level of the HFD-C group was still significantly higher compared to the Chow-C group suggesting impaired glucose metabolism ($P < 0.05$, Table 4.7). Interestingly, non-fasting plasma insulin level was not significantly different between the HFD-C group and Chow-C group (Table 4.7).

At the endpoint, the concentration of plasma NEFA was significantly elevated by 77% ($P < 0.05$) in the HFD-C mice compared to the Chow-C mice (Table 4.7). Plasma

cholesterol was also significantly increased in the HFD-C mice by 78% ($P < 0.05$) without a difference in triglyceride levels (HFD-C *vs.* Chow-C, Table 4.7). The HFD-C mice had a 4.3-fold increase of liver triglyceride concentration compared to the Chow-C mice ($P < 0.05$, Table 4.5), suggesting liver steatosis.

Plasma ALT and AST, indicators of liver function, are normally increased when liver cell damage has occurred. Long-term HFD feeding resulted in significantly higher plasma ALT (2.2-fold, $P < 0.05$), and AST levels (3.9-fold, $P < 0.05$) in HFD-C mice compared to Chow-C mice (Table 4.5).

At 9 weeks, the HFD-C mice had significantly hypertrophied adipocytes in mesenteric adipose tissue compared to the Chow-C mice (2144 ± 48 μm^2 HFD-C *vs.* 909 ± 13 μm^2 Chow-C, $P < 0.001$, Figure 4.5E).

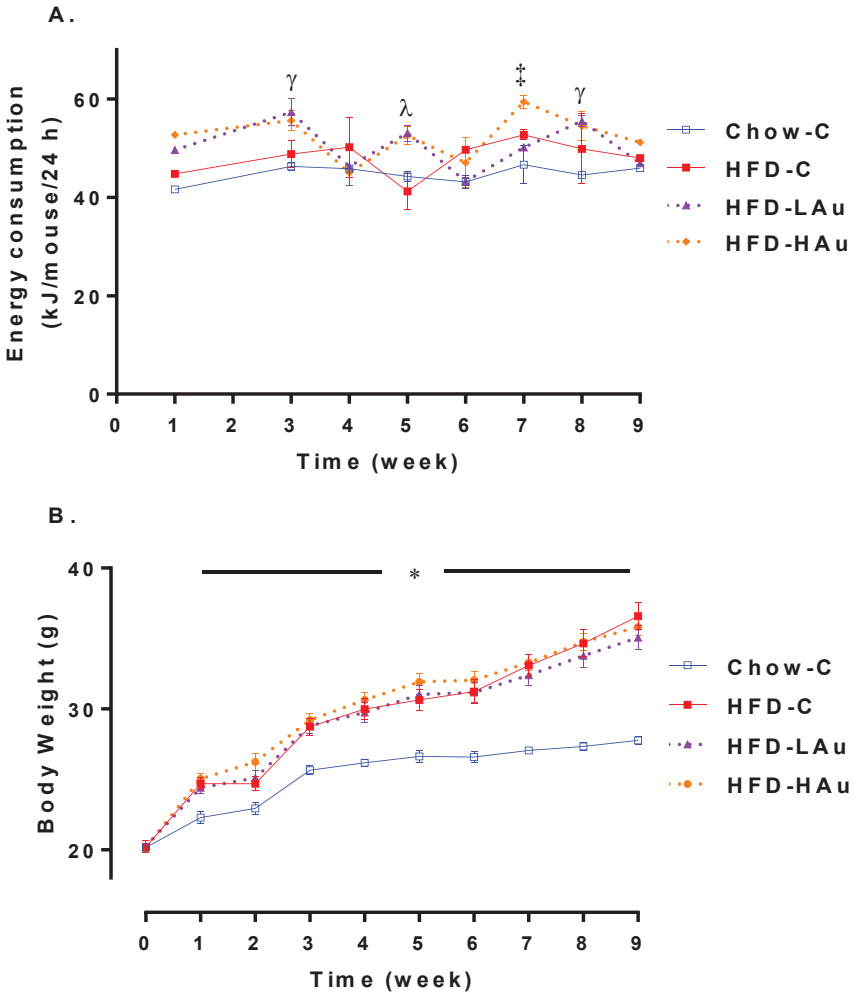

Figure 4.3 Effects of 9 weeks HFD and AuNP treatment on energy consumption and body weight of C57Bl/6 mice.

Energy consumption (A) and body weight (B) in Chow-C (water, daily IP), HFD-C (water, daily IP), HFD-LAu (0.785 µg AuNP/g mice, daily IP), and HFD-HAu (7.85 µg AuNP/g mice, daily IP) for 9 weeks. Results are expressed as mean ± S.E.M. Data were analysed by two-way ANOVA followed by post hoc Bonferroni test. γ $P < 0.05$ Chow-C *vs.* HFD-LAu & HFD-HAu; λ $P < 0.05$ Chow-C *vs.* HFD-LAu and HFD-C *vs.* HFD-LAu & HFD-HAu; ‡ $P < 0.05$ Chow-C *vs.* HFD-HAu; * $P < 0.05$ Chow-C *vs.* all the other groups. n=12–20.

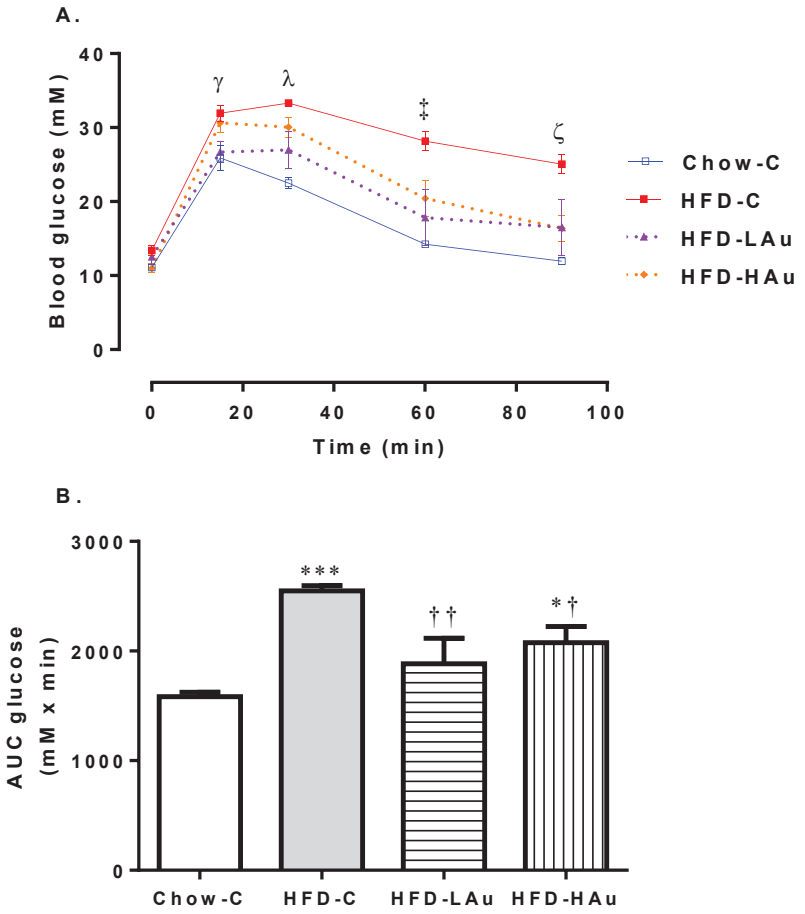

Figure 4.4 Effects of 9 weeks HFD and AuNP treatment on glucose tolerance

(A) Change in blood glucose level during IPGTT in Chow-C (water, daily IP), HFD-C (water, daily IP), HFD-LAu (0.785 µg AuNP/g mice, daily IP), and HFD-HAu (7.85 µg AuNP/g mice, daily IP) for 9 weeks. (B) area under the curve (AUC) of (A). Results are expressed as mean ± S.E.M. Data in (A) were analysed by two-way ANOVA with repeated measures followed by post hoc Bonferroni test. Data in (B) were analysed by one-way ANOVA followed by post hoc Bonferroni test. (A) γ $P< 0.05$ HFD-C *vs.* Chow-C & HFD-LAu at 15min; λ $P< 0.05$ Chow-C *vs.* HFD-HAu, HFD-C *vs.* Chow-C & HFD-LAu at 30mins; ‡ $P< 0.05$ Chow-C *vs.* HFD-HAu, HFD-C *vs.* Chow-C, HFD-LAu & HFD-HAu at 60min; ζ $P< 0.05$ Chow-C *vs.* HFD-HAu, HFD-C *vs.* Chow-C, HFD-LAu & HFD-HAu at 90mins. (B) * $P < 0.05$ *vs.* Chow-C; *** $P < 0.005$ *vs.* Chow-C; † $P < 0.05$ *vs.* HFD-C; †† $P < 0.01$ *vs.* HFD-C; n=4–6.

Table 4.6 Effect of 9 weeks HFD and AuNP treatment on body morphometry

	Chow-C	HFD-C	HFD-LAu	HFD-HAu
Body weight initial (g)	20.2 ± 0.3	20.2 ± 0.3	20.3 ± 0.2	20.2 ± 0.3
Body weight final (g)	27.7 ± 0.3	37.6 ± 1.3*	34.6 ± 0.8*†	35.8 ± 0.6*†
Energy intake (kJ/d)	44.9 ± 0.6	48.4 ± 1.4	50.5 ± 1.4*	52.3 ± 1.4*†
Liver (g)	1.34 ± 0.03	1.90 ± 0.10*	1.47 ± 0.04†	1.54 ± 0.04*†
Liver (%)	4.86 ± 0.08	5.03 ± 0.12	4.27 ± 0.07*†	4.30 ± 0.10*†
Retroperitoneal fat (g)	0.097 ± 0.006	0.771 ± 0.057*	0.649 ± 0.042*†	0.616 ± 0.048*†
Retroperitoneal fat (%)	0.35 ± 0.02	2.01 ± 0.10*	1.86 ± 0.11*	1.77 ± 0.09*†
Mesenteric fat (g)	0.372 ± 0.018	0.935 ± 0.048*	0.725 ± 0.087*†	0.691 ± 0.029*†
Mesenteric fat (%)	1.35 ± 0.06	2.46 ± 0.14*	2.07 ± 0.28*†	1.97 ± 0.07*†
Epididymal fat (g)	0.405 ± 0.013	2.059 ± 0.19*	1.76 ± 0.08*	1.80 ± 0.09*
Epididymal fat (%)	1.43 ± 0.06	5.38 ± 0.35*	5.07 ± 0.14*	4.98 ± 0.19*
Heart (g)	0.135 ± 0.002	0.149 ± 0.004*	0.136 ± 0.007†	0.141± 0.004
Heart (%)	0.49 ± 0.01	0.40 ± 0.01*	0.39 ±0.02*	0.40 ± 0.01*
Kidney (g)	0.165 ± 0.004	0.191 ± 0.005*	0.178 ± 0.009*	0.188 ± 0.005*
Kidney (%)	0.59 ± 0.01	0.51 ± 0.02*	0.49 ± 0.02*	0.53 ± 0.02*
Muscle (g)	0.046 ± 0.002	0.048 ± 0.002	0.044 ± 0.002	0.047 ± 0.001
Muscle (%)	0.17 ± 0.01	0.13 ±0.01*	0.13 ±0.01*	0.13 ± 0.01*

Chow-C (water, daily IP), HFD-C (water, daily IP), HFD-LAu (0.785 µg AuNP/g mice, daily IP), and HFD-HAu (7.85 µg AuNP/g mice, daily IP) for 9 weeks. Results are expressed as mean ± S.E.M. Data were analysed by one-way ANOVA followed by post hoc Bonferroni test.* $P < 0.05$ *vs.* Chow-C; † $P < 0.05$ *vs.* HFD-C; n=12–20.

Table 4.7 Effect of 9 weeks HFD and AuNP treatment on mice body metabolic parameters in non-fasting state

	Chow-C	HFD-C	HFD-LAu	HFD-HAu
Plasma glucose (mM)	12.1 ± 0.28	15.2 ± 0.31*	14.7 ± 0.56*	15.8 ± 0.46*
Plasma insulin (ng/mL)	0.041 ± 0.005	0.043 ± 0.005	0.062 ± 0.008*†	0.043 ± 0.002
Plasma NEFA (mM)	2.54 ± 0.16	4.51 ± 0.54*	2.9 ± 0.24†	3.14 ± 0.35†
Plasma triglyceride (mM)	0.75 ± 0.05	0.86 ± 0.05	0.67 ± 0.04†	0.69 ± 0.05†
Plasma cholesterol (mM)	6.24 ± 0.31	11.14 ± 0.36*	9.40 ± 0.29*†	9.46 ± 0.41*†
Plasma ALT (U/L)	17.3 ± 6.2	55.9 ± 13*	25.5 ± 6.9†	26.3 ± 2.4†
Plasma AST (U/L)	6.33 ± 2.16	31.4 ± 7.1*	16.9 ± 3.9†	12.1 ± 2.2†
Liver triglyceride (mM/mg)	0.023 ± 0.005	0.124 ± 0.019*	0.139 ± 0.007*	0.145 ± 0.010*

Chow-C (water, daily IP), HFD-C (water, daily IP), HFD-LAu (0.785 µg AuNP/g mice, daily IP), and HFD-HAu (7.85 µg AuNP/g mice, daily IP) for 9 weeks. Results are expressed as mean ± S.E.M. Data were analysed by one-way ANOVA followed by post hoc Bonferroni test.* $P < 0.05$ *vs.* Chow-C; † $P < 0.05$ *vs.* HFD-C; n=4–17.

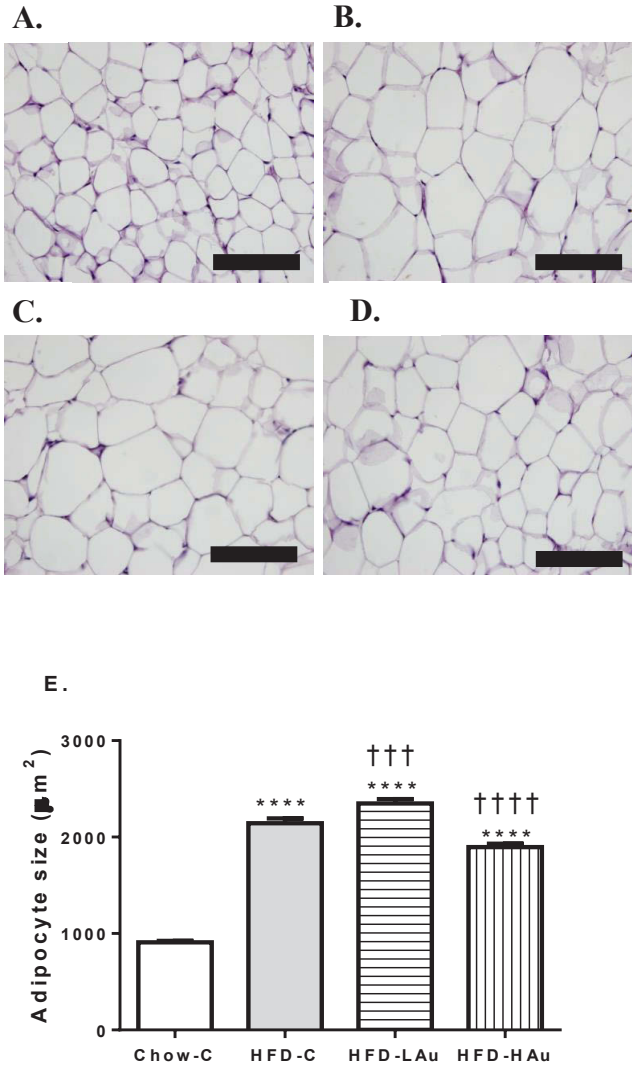

Figure 4.5 Effects of 9 weeks HFD and AuNP treatment on the adipose size in mesenteric adipose tissue determined by H&E staining

Representative image of mesenteric adipose tissue section stained with H&E after 9 weeks of (A) Chow-C (water, daily IP), (B) HFD-C (water, daily IP), (C) HFD-LAu (0.785 µg AuNP/g mice, daily IP), and (D) HFD-HAu (7.85 µg AuNP/g mice, daily IP) treatment. Images were taken at 40x magnification, scale bar=100 µm for (A-D). (E) Adipocyte size measured from H&E stained tissue sections; where 800–1000 adipocytes were measured from 6 different region of interest per group using ImageJ softwareResults are expressed as mean ± S.E.M. Data were analysed by one-way ANOVA followed by post hoc Bonferroni test. **** $P < 0.001$ *vs.* Chow-C; ††† $P < 0.005$ *vs.* HFD-C; †††† $P < 0.001$ *vs.* HFD-C; n=3.

4.3.1.2. mRNA expression of inflammatory and adipokine in the adipose tissue

At 9 weeks, there was no significant change in mRNA expression of macrophage markers CD68 and F4/80 (Figure 4.6A,B) in the fat tissue of the HFD-C group. mRNA levels of TLR-4 and TNF-α were significantly upregulated in the HFD-C compared to the Chow-C by 2.4-fold ($P < 0.01$) and 7.5-fold ($P < 0.01$) respectively (Figure 4.6C,D). mRNA levels of IL-6 (46%, $P < 0.05$) and IL-1R (79%, $P < 0.001$) were downregulated in the fat cells of the HFD-C group compared to the Chow-C (Figure 4.6E,G). No difference in the IL-1β mRNA expression was observed between HFD-C and Chow-C mice (Figure 4.6F). mRNA expression of SAA-1 was not significantly altered (Figure 4.6H).

HFD consumption significantly upregulated lipolysis marker, ATGL by 2.6-fold ($P < 0.05$) and fatty acid oxidation marker, CPT-1α by 1.1-fold in the fat ($P < 0.05$ HFD-C *vs.* Chow-C, Figure 4.7A,B). Fat hormone, leptin was significantly upregulated by 5.9-fold in mice consuming a HFD ($P < 0.005$ HFD-C *vs.* Chow-C, Figure 4.7C). Adipose tissue specific hormone, adiponectin mRNA expressions was significantly downregulated by 77% and GLUT-4 mRNA expression was significantly downregulated by 73% suggesting impaired glucose uptake and insulin sensitivity in HFD-C mice ($P < 0.05$ *vs.* Chow-C, Figure 4.7D,E). No difference was observed on markers involving gluconeogenesis (FOX-O1), adipogenesis (PPARγ), and lipogenesis (SREBP-1c and FASN) in the adipose tissue between the HFD-C mice and Chow-C mice (Figure 4.7F–I).

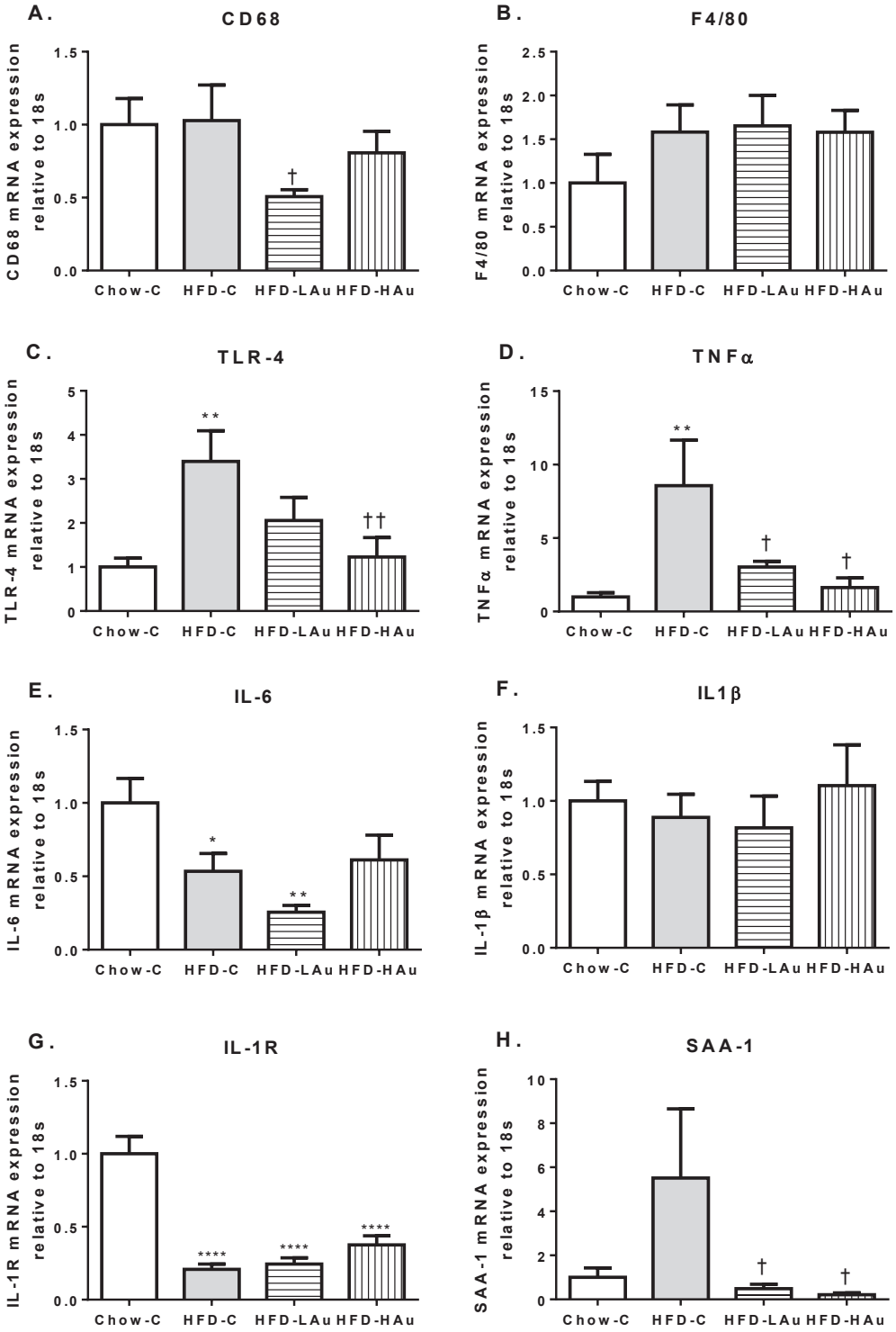
A.
CD68
CD68 mRNA expression relative to 18s
1.5
1.0
0.5
0.0
†
Chow-C
HFD-C
HFD-LAu
HFD-HAu
B.
F4/80
F4/80 mRNA expression relative to 18s
2.5
2.0
1.5
1.0
0.5
0.0
Chow-C
HFD-C
HFD-LAu
HFD-HAu
C.
TLR-4
TLR-4 mRNA expression relative to 18s
5
4
3
2
1
0
**
††
Chow-C
HFD-C
HFD-LAu
HFD-HAu
D.
TNFα
TNFα mRNA expression relative to 18s
15
10
5
0
**
†
†
Chow-C
HFD-C
HFD-LAu
HFD-HAu
E.
IL-6
IL-6 mRNA expression relative to 18s
1.5
1.0
0.5
0.0
*
**
Chow-C
HFD-C
HFD-LAu
HFD-HAu
F.
IL1β
IL-1β mRNA expression relative to 18s
1.5
1.0
0.5
0.0
Chow-C
HFD-C
HFD-LAu
HFD-HAu
G.
IL-1R
IL-1R mRNA expression relative to 18s
1.5
1.0
0.5
0.0
****
****
****
Chow-C
HFD-C
HFD-LAu
HFD-HAu
H.
SAA-1
SAA-1 mRNA expression relative to 18s
10
8
6
4
2
0
†
†
Chow-C
HFD-C
HFD-LAu
HFD-HAu

Figure 4.6 Effects of 9 weeks HFD and AuNP treatment on macrophage and inflammatory markers in abdominal fat

Fat mRNA expression of CD68 (A), F4/80 (B), TLR-4 (C), TNFα (D), IL-6 (E), IL-1β (F), IL-1R (G), and SAA-1 (H) in Chow-C (water, daily IP), HFD-C (water, daily IP), HFD-LAu (0.785 μg AuNP/g mice, daily IP), and HFD-HAu (7.85 μg AuNP/g mice, daily IP) for 9 weeks. Results are expressed as mean ± S.E.M. Data were analysed by one-way ANOVA followed by post hoc Bonferroni test. * $P < 0.05$ *vs.* Chow-C; ** $P < 0.01$ *vs.* Chow-C; **** $P < 0.001$ *vs.* Chow-C; † $P < 0.05$ *vs.* HFD-C; †† $P < 0.01$ *vs.* HFD-C; n=4–8.

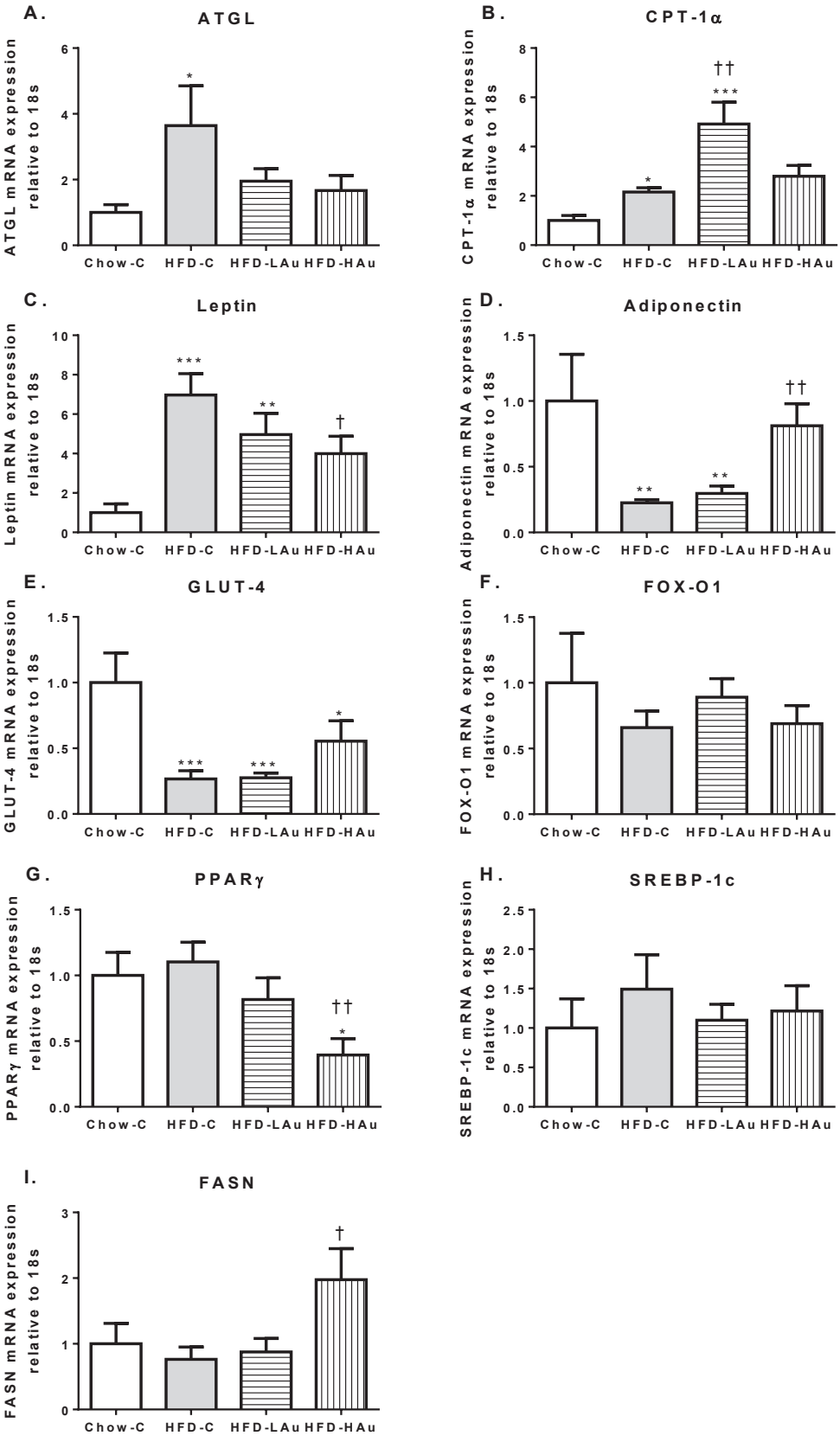
A.
ATGL
ATGL mRNA expression relative to 18s
Chow-C
HFD-C
HFD-LAu
HFD-HAu
B.
CPT-1α
CPT-1α mRNA expression relative to 18s
C.
Leptin
Leptin mRNA expression relative to 18s
D.
Adiponectin
Adiponectin mRNA expression relative to 18s
E.
GLUT-4
GLUT-4 mRNA expression relative to 18s
F.
FOX-O1
FOX-O1 mRNA expression relative to 18s
G.
PPARγ
PPARγ mRNA expression relative to 18s
H.
SREBP-1c
SREBP-1c mRNA expression relative to 18s
I.
FASN
FASN mRNA expression relative to 18s

Figure 4.7 Effects of 9 weeks HFD and AuNP treatment on lipid and glucose metabolic markers in abdominal fat

Fat mRNA expression of ATGL (A), CPT-1α (B), leptin (C), adiponectin (D), GLUT-4 (E), FOX-O1 (F), PPARγ (G), SREBP-1c (H), and FASN (I) in Chow-C (water, daily IP), HFD-C (water, daily IP), HFD-LAu (0.785 μg AuNP/g mice, daily IP), and HFD-HAu (7.85 μg AuNP/g mice, daily IP) for 9 weeks. Results are expressed as mean ± S.E.M. Data were analysed by one-way ANOVA followed by post hoc Bonferroni test. * $P < 0.05$ *vs.* Chow-C; ** $P < 0.01$ *vs.* Chow-C; *** $P < 0.005$ *vs.* Chow-C; † $P < 0.05$ *vs.* HFD-C; †† $P < 0.01$ *vs.* HFD-C; n=4–8.

4.3.1.3. mRNA expression of inflammatory, lipid, and glucose markers in the liver

In the liver, CD68 levels were significantly downregulated by 44% ($P < 0.05$) with no difference in F4/80 mRNA expression in the HFD-C mice compared to the Chow-C mice (Figure 4.8A,B). Liver TNF-α mRNA expression was also upregulated by 2.1-fold ($P < 0.01$, Figure 4.8D) in HFD-C group; while mRNA expressions of IL-6, IL-1β, and IL-1R were significantly downregulated by 70%, 71%, and 49%, respectively ($P < 0.001$ HFD-C *vs.* Chow-C, Figure 4.8E–G). The mRNA level of SAA-1 in the liver was not significantly altered in the HFD-C group compared to Chow-C group (Figure 4.8H). No difference in mRNA expression of TLR-4 was observed in the liver between the HFD-C and Chow-C group (Figure 4.8C).

In the liver, HFD consumption did not alter mRNA levels of ATGL but significantly downregulated CPT-1α by 31% ($P < 0.01$ *vs.* Chow-C, Figure 4.9A,B). GLUT-4 mRNA expressions was significantly upregulated by 11.2-fold in HFD-C mice compared to Chow-C mice ($P < 0.01$, Figure 4.9C). Liver mRNA expression of gluconeogenesis marker, PEPCK was significantly downregulated by 34% ($P < 0.05$) in HFD-C group; however, its upstream signalling FOX-O1 mRNA level was not significantly altered (Figure 4.9D,E). mRNA expression of SREBP-1c was also upregulated by 97% ($P < 0.01$) with a slight increase in downstream signalling FASN mRNA expression (HFD-C *vs.* Chow-C, Figure 4.9G,H).

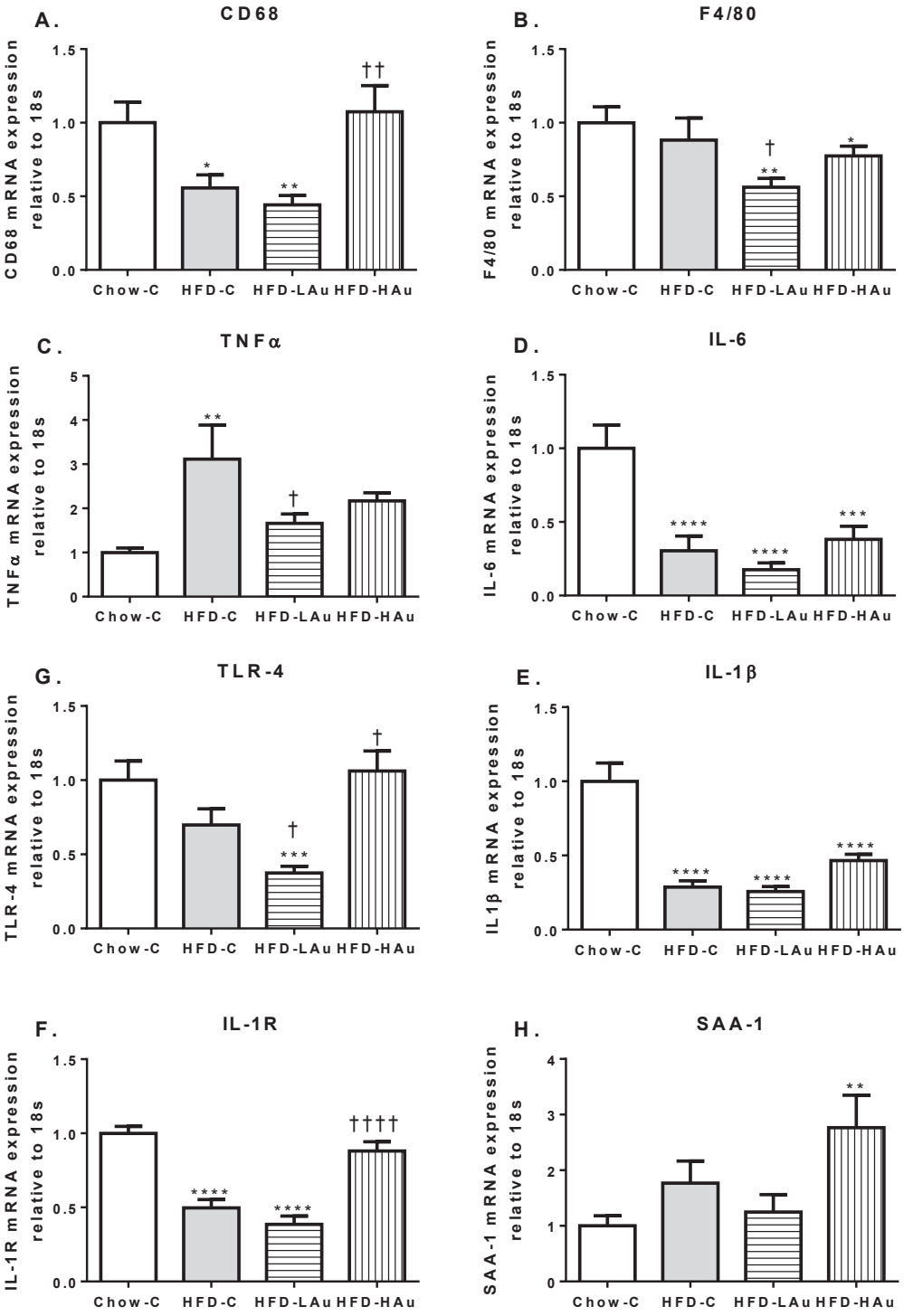
A.
CD68
CD68 mRNA expression relative to 18s
1.5
1.0
0.5
0.0
*
**
††
Chow-C
HFD-C
HFD-LAu
HFD-HAu
B.
F4/80
F4/80 mRNA expression relative to 18s
1.5
1.0
0.5
0.0
†
**
*
Chow-C
HFD-C
HFD-LAu
HFD-HAu
C.
TNFα
TNFα mRNA expression relative to 18s
5
4
3
2
1
0
**
†
Chow-C
HFD-C
HFD-LAu
HFD-HAu
D.
IL-6
IL-6 mRNA expression relative to 18s
1.5
1.0
0.5
0.0
****
****
***
Chow-C
HFD-C
HFD-LAu
HFD-HAu
G.
TLR-4
TLR-4 mRNA expression relative to 18s
1.5
1.0
0.5
0.0
†
***
†
Chow-C
HFD-C
HFD-LAu
HFD-HAu
E.
IL-1β
IL1β mRNA expression relative to 18s
1.5
1.0
0.5
0.0
****
****
****
Chow-C
HFD-C
HFD-LAu
HFD-HAu
F.
IL-1R
IL-1R mRNA expression relative to 18s
1.5
1.0
0.5
0.0
****
****
††††
Chow-C
HFD-C
HFD-LAu
HFD-HAu
H.
SAA-1
SAA-1 mRNA expression relative to 18s
4
3
2
1
0
**
Chow-C
HFD-C
HFD-LAu
HFD-HAu

Figure 4.8 Effects of 9 weeks HFD and AuNP treatment on macrophage and inflammatory markers in the liver

Liver mRNA expression of CD68 (A), F4/80 (B), TNFα (C), IL-6 (D), IL-1β (E), IL-1R (F), TLR-4 (G), and SAA-1 (H) in Chow-C (water, daily IP), HFD-C (water, daily IP), HFD-LAu (0.785 μg AuNP/g mice, daily IP), and HFD-HAu (7.85 μg AuNP/g mice, daily IP) for 9 weeks. Results are expressed as mean ± S.E.M. Data were analysed by one-way ANOVA followed by post hoc Bonferroni test. * $P < 0.05$ *vs.* Chow-C; ** $P < 0.01$ *vs.* Chow-C; *** $P < 0.005$ *vs.* Chow-C; **** $P < 0.001$ *vs.* Chow-C; † $P < 0.05$ *vs.* HFD-C; n=6–12.

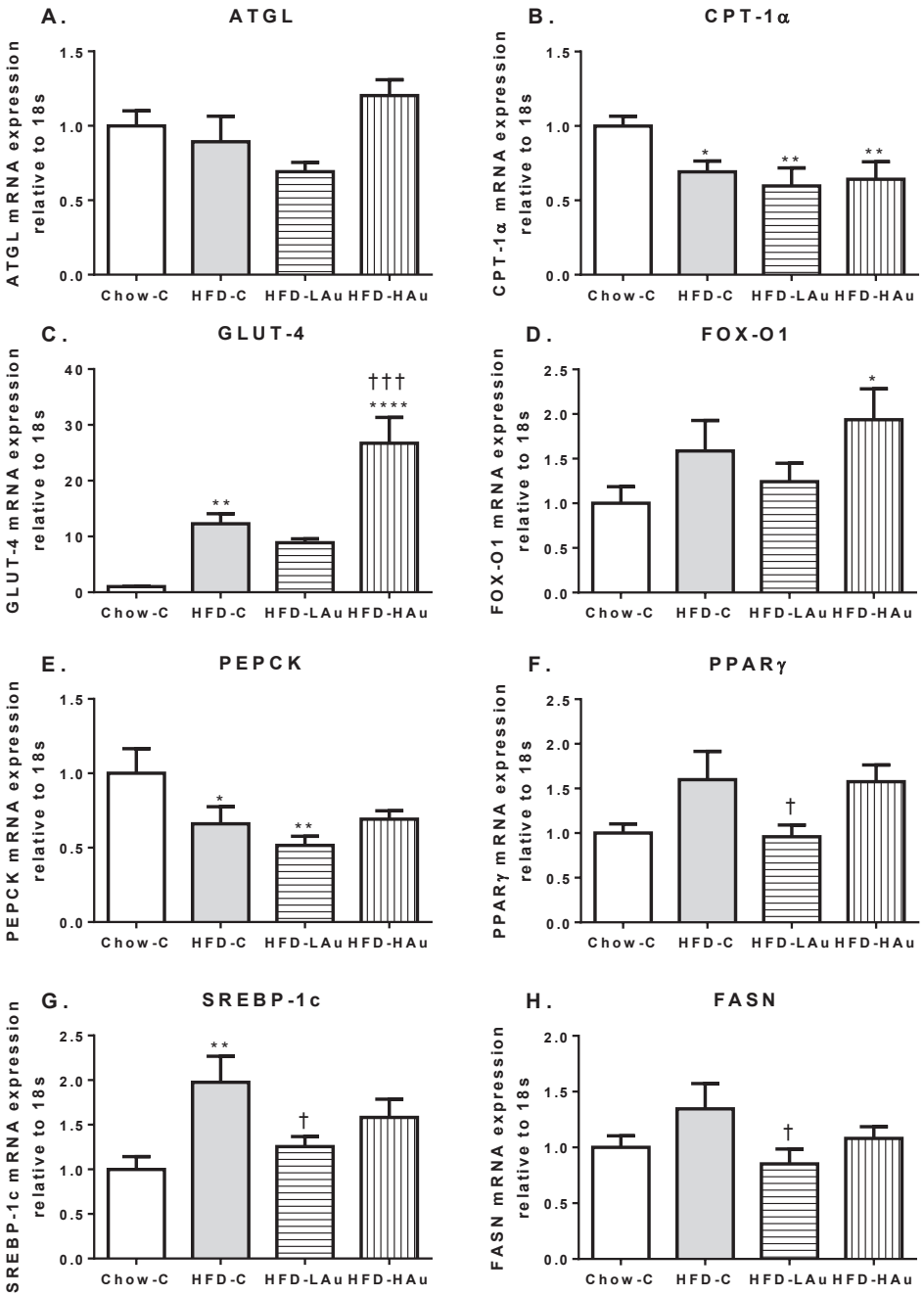
A.
ATGL
ATGL mRNA expression relative to 18s
1.5
1.0
0.5
0.0
Chow-C
HFD-C
HFD-LAu
HFD-HAu
B.
CPT-1α
CPT-1α mRNA expression relative to 18s
*
**
**
C.
GLUT-4
GLUT-4 mRNA expression relative to 18s
40
30
20
10
0
**
†††
****
D.
FOX-O1
FOX-O1 mRNA expression relative to 18s
2.5
2.0
1.5
1.0
0.5
0.0
*
E.
PEPCK
PEPCK mRNA expression relative to 18s
*
**
F.
PPARγ
PPARγ mRNA expression relative to 18s
†
G.
SREBP-1c
SREBP-1c mRNA expression relative to 18s
**
†
H.
FASN
FASN mRNA expression relative to 18s
†

Figure 4.9 Effects of 9 weeks HFD and AuNP treatment on lipid and glucose metabolic markers in the liver

Liver mRNA expression of ATGL (A), CPT-1α (B), GLUT-4 (C), FOX-O1 (D), PEPCK (E), PPARγ (F), SREBP-1c (G), FASN (H) in Chow-C (water, daily IP), HFD-C (water, daily IP), HFD-LAu (0.785 μg AuNP/g mice, daily IP), and HFD-HAu (7.85 μg AuNP/g mice, daily IP) for 9 weeks. Results are expressed as mean ± S.E.M. Data were analysed by one-way ANOVA followed by post hoc Bonferroni test. * $P < 0.05$ *vs.* Chow-C; ** $P < 0.01$ *vs.* Chow-C; *** $P < 0.005$ *vs.* Chow-C; † $P < 0.05$ *vs.* HFD-C; †† $P < 0.01$ *vs.* HFD-C; n=7–12.

4.3.2. Effect of AuNP treatment

4.3.2.1. Body measurements of HFD mice with AuNP treatment

Mice treated with AuNPs showed no signs of reduced daily activities and interactions with the housemates, or change in fur conditions, but there was a change in their appetite. In fact, both HFD-LAu and HFD-HAu groups consumed more energy than the HFD-C and Chow-C groups receiving vehicle treatment (Table 4.6). The total daily energy consumption of HFD-LAu and HFD-HAu groups were significantly increased by 4% and 8%, respectively compared to the HFD-C group ($P < 0.05$, Table 4.6).

However, body weights of the AuNP-treated mice did not increase as expected with the increased energy consumption. Instead, the HFD-LAu and HFD-HAu groups weighed 8% (ΔBW 3.1 g, $P < 0.05$) and 5% (ΔBW 1.8 g, $P < 0.05$) less, respectively compared to the HFD-C group (Table 4.6). Nevertheless, both HFD-LAu and HFD-HAu mice were still 25% (ΔBW 6.8 g, $P < 0.05$) and 29% (ΔBW 8.1 g, $P < 0.05$) heavier than the Chow-C, respectively (Table 4.6).

In correlation to reduced weight gain by AuNP treatment, significantly reduced organ mass and adiposity were also observed in the AuNP-treated mice. The liver, heart, retroperitoneal and mesenteric adipose tissue masses were significantly less in both HFD-LAu and HFD-HAu groups compared to the HFD-C group ($P < 0.05$, Table 4.6). Upon standardisation to body weight, the significant difference remains (liver and mesenteric HFD-C vs. HFD-LAu & HFD-HAu, retroperitoneal HFD-C *vs*. HFD-HAu, $P < 0.05$). While the weights of the other organs including kidney and epididymal fat tissues were significantly different compared to Chow-C group but not to HFD-C group (Table 4.6).

Glucose clearance during IPGTT was significantly improved in AuNP-treated mice. Blood glucose levels during IPGTT in the HFD-LAu group were similar as the Chow-C group (Figure 4.4A, $P < 0.05$). The HFD-HAu group also had a significantly improved glucose clearance compared with HFD-C group at 60 and 90 min ($P < 0.05$, Figure 4.4A). Similarly, AUC values for both AuNP-treated groups were significantly lower compared to the HFD-C mice ($P < 0.05$, Table 4.7).

AuNP-treated mice were as hyperglycaemic as the HFD-C group during their non-fasting state ($P < 0.05$, Table 4.7). Additionally, plasma insulin concentration of HFD-LAu group was significantly elevated in comparison to the HFD-C and Chow-C (32% and 37%, respectively $P < 0.05$, Table 4.7) but not in the HFD-HAu group.

Treatment with AuNP improved hyperlipidaemia in HFD-fed mice. The concentrations of plasma NEFA were significantly reduced by 36% and 30% in the HFD-LAu and HFD-HAu groups, respectively ($P < 0.05$ *vs.* HFD-C, Table 4.7). Similarly, HFD-LAu and HFD-HAu also markedly reduced the levels of plasma triglyceride (22% and 20%, respectively $P < 0.05$) and cholesterol (15% and 15%, respectively $P < 0.05$) compared to the HFD-C group (Table 4.7). Notably, plasma NEFA and triglyceride concentrations were similar between the Chow-C and AuNP-treated mice (Table 4.7).

The level of liver enzyme ALT was significantly lowered by AuNP treatment by 46% in HFD-LAu group and 61% in HFD-HAu group compared to the HFD-C group ($P < 0.05$, Table 4.7). Similarly, liver AST concentrations were also significantly reduced by 54% and 52%, respectively for HFD-LAu and HFD-HAu groups ($P < 0.05$ *vs.* HFD-C, Table 4.7). Liver triglyceride concentration was not significantly changed by AuNP treatment (Table 4.7).

At 9 weeks, the size of adipocytes in epididymal adipose tissue of HFD-LAu group were significantly increased by 9.5% ($P < 0.005$ *vs.* HFD-C, Figure 4.5E). However, the adipocytes in epididymal adipose tissue of HFD-HAu group was significantly smaller in size by 11.6% ($P < 0.001$ *vs.* HFD-C, Figure 4.5E).

4.3.2.2. mRNA expression of inflammatory and adipokine markers in the adipose tissue

Treatment with low dose of AuNP significantly downregulated mRNA expression of fat CD68 was by 51% compared to the vehicle-treated HFD-C mice ($P < 0.05$, Figure 4.6A), with no difference in F4/80 marker expression (Figure 4.6B). Fat inflammatory TNFα mRNA expression was significantly reduced by 65% in the HFD-LAu group ($P < 0.05$ *vs.* HFD-C, Figure 4.6D), while mRNA expression of TLR-4 and IL-6 were

slightly reduced without significance (Figure 4.6C,E). No difference was observed in IL-1β and IL-1R mRNA expression between the HFD-LAu and HFD-C groups in the fat (Figure 4.6F,G). Due to the large error bar for HFD-C, the increased in fat SAA-1 may not play a significant physiological role. Additionally, fat CPT-1α mRNA expression was significantly upregulated by 1.2-fold in the HFD-LAu group ($P < 0.05$ *vs.* HFD-C, Figure 4.7B). While fat mRNA expression of ATGL, leptin, and PPARγ showed a trend of reduction in HFD-LAu group which was not significantly different compared to HFD-C group (Figure 4.7A,C,G). No change was observed in fat adiponectin, GLUT-4, FOX-O1, SREBP1-c, and FASN mRNA expression levels between the HFD-LAu and HFD-C groups (Figure 4.7D–F,H–I).

By contrast, in the HFD-HAu mice mRNA expression of CD68 and F4/80 in the fat were similar as the HFD-C mice (Figure 4.6A,B). Fat TLR-4 mRNA expression was significantly reduced by 64% in the HFD-HAu group ($P < 0.05$ *vs.* HFD-C, Figure 4.6C). This was accompanied by 81% downregulation of fat TNFα mRNA expression ($P < 0.05$ *vs.* HFD-C, Figure 4.6D). No change was observed in inflammatory IL-6, IL-1β, and IL-1R mRNA levels in the fat between HFD-HAu and HFD-C groups (Figure 4.6E–G). Similarly, fat SAA-1 was also significantly downregulated by 96% in the HFD-HAu mice ($P < 0.05$ *vs.* HFD-C, Figure 4.6H), suggesting no nanoparticle-induced adverse inflammatory reaction. There was no difference observed in mRNA levels of ATGL, CPT-1α, GLUT-4, and FOX-O1 between the HFD-LAu and HFD-C groups in the fat (Figure 4.7A,B,E,F). mRNA expression of fat hormones, leptin was significantly reduced by 43% while adiponectin was significantly upregulated by 2.6-fold in HFD-HAu mice ($P < 0.05$ *vs.* HFD-C, Figure 4.7C,D). Adipogenic marker, PPARγ mRNA level was significantly reduced by 64% ($P < 0.05$, HFD-HAu *vs.* HFD-C, Figure 4.7G) suggesting reduced adipocyte differentiation in the abdominal fat. The mRNA expression of lipogenic marker, FASN was significantly upregulated by 1.5-fold in HFD-HAu group compared to the HFD-C group ($P < 0.05$, Figure 4.7I) without any change in its upstream regulator SREBP-1c mRNA levels (Figure 4.7H).

4.3.2.3. mRNA expression of inflammatory lipid and glucose markers in the liver

Liver F4/80 mRNA expression was significantly downregulated by 36% in HFD-LAu group ($P < 0.05$ *vs.* HFD-C, Figure 4.8B) but CD68 was not changed (Figure 4.8A). Both liver TLR-4 and TNFα mRNA expression was also significantly reduced by 46% ($P < 0.05$ *vs.* HFD-C, Figure 4.8C,D) with no change in mRNA levels of the other inflammatory marker IL-6, IL-1β, IL-1R, and SAA-1 (Figure 4.8E–H). Liver ATGL, CPT-1α, GLUT-4, FOX-O1, and PEPCK were not significantly changed in HFD-LAu group compared with HFD-C group (Figure 4.9A–E). mRNA expression of insulin sensitive marker in the liver, PPARγ was reduced significantly in the HFD-LAu group compared to the HFD-C group ($P < 0.05$, Figure 4.9F). HFD-LAu mice showed significantly downregulated liver lipogenic markers, SREBP-1c and FASN by 36% and 37%, respectively ($P < 0.05$ *vs.* HFD-C, Figure 4.9G,H) suggesting reduced lipid synthesis in the liver.

In the liver, mRNA expression of CD68 was significantly upregulated by 93% ($P < 0.01$ *vs.* HFD-C, Figure 4.8A) with no change in F4/80 in the HFD-HAu mice (Figure 4.8B). TLR-4 mRNA expression was significantly increased by 52% in the liver of HFD-HAu mice ($P < 0.05$ *vs.* HFD-C, Figure 4.8C). TNFα and SAA-1 mRNA expression was not significantly altered in the HFD-HAu mice compared to the HFD-C mice. There was no difference observed in IL-6, IL-1β, and IL-1R mRNA expressions in the liver between HFD-HAu and HFD-C groups (Figure 4.8D-H). Liver ATGL, CPT-1α, FOX-O1, PEPCK, PPARγ, SREBP-1c, and FASN were not significantly altered by high dose of AuNP treatment (Figure 4.9 A–B,D–H). Interestingly, mRNA expression of GLUT-4 was increased by 1.1-fold in the HFD-HAu group ($P < 0.05$ *vs.* HFD-C, Figure 4.9C).

4.3.2.4. Distribution of the Au in body organs

After daily IP injection of AuNPs for 9 weeks, the level of accsumulated elemental gold in a number of different tissues was determined by ICP-MS analysis (Table 4.8). In the Chow-C and HFD-C groups receiving vehicle injection, a low but detectable concentration of Au was measured in all organs assessed. AuNP-treated mice had an increased gold concentration in their abdominal fat, livers and spleens compared to both Chow-C and HFD-C groups (Table 4.8). The total gold deposited in decreasing order were abdominal fat, liver, spleen, kidney, and brain in dose-dependent manner except for the heart. There seems to be an increased accumulation of Au in the kidney and brain at higher dose of AuNP injection compared to the Chow-C and HFD-C group due to agglomeration of AuNPs ($P < 0.05$, Table 4.8).

Table 4.8 Concentration of gold measured in the organs after 9 weeks of AuNPs treatment

µg Au/g tissue	Chow-C	HFD-C	HFD-LAu	HFD-HAu
Fat	0.1 ± 0.0	4.7 ± 1.4	7253 ± 3784	29883 ± 3154*†‡
Liver	2.4 ± 0.6	2.1 ± 0.6	128 ± 31	1792 ±1297
Spleen	5.1 ± 2.4	3.8 ±0.9	628 ± 148*†	1943 ± 196*†‡
Kidney	6.6 ± 1.8	1.3 ± 0.0	9.9 ± 1.7	23.8 ± 5.3*†‡
Brain	1.9 ± 1.0	1.1 ± 0.2	2.7 ± 1.6	12.1 ± 4.9*†‡
Heart	0.5 ± 0.2	0.3 ± 0.2	3.3 ± 2.2	± 0.5

Chow-C (water, daily IP), HFD-C (water, daily IP), HFD-LAu (0.785 µg AuNP/g mice, daily IP), and HFD-HAu (7.85 µg AuNP/g mice, daily IP) for 9 weeks. Results are expressed as mean ± S.E.M. Data were analysed by one-way ANOVA followed by post hoc Bonferroni test.* $P < 0.05$ *vs.* Chow-C; † $P < 0.05$ *vs.* HFD-C; ‡ $P < 0.05$ *vs.* HFD-LAu. n=3.

4.4. Discussion

The major finding in this present study was that a daily injection of AuNPs into HFD-fed mice can significantly reduce blood lipid levels and prevent the development of glucose intolerance. The reduction in localised inflammation in the fat and liver and ATM macrophage numbers are the proposed mechanisms.

In this study, adult C57BL/6 mice fed a long term HFD developed glucose intolerance and dyslipidaemia with increased fat accumulation and weight gain. Long term treatment with AuNP did not produce any mortality or any symptoms of toxicity (e.g. reduced social and physical activities, loss of appetite and change in fur conditions), but did result in slowing of weight gain. The weight difference between the AuNP-treated and HFD mice may be small, however, clinical research suggests that weight loss of as little as 5% of initial body weight, can reduce the risk of developing diabetes by 58% (Anderson, Kendall & Jenkins 2003). Indeed, this has been clearly supported by our current study. With 9% less body weight in the HFD-LAu group, mice had normal glucose tolerance; while in the HFD-HAu group with 5% less body weight, their glucose intolerance due to HFD consumption was significantly improved.

In addition, treatment with AuNPs also improved fat deposition and lipid metabolism reflected by the increased adipocyte storage capacity and normalization of circulating blood lipid, which potentiate their amelioration of hyperlipidaemia in mice with HFD intervention. In a recent study with FDA approved prescription anti-obesity drug, Contrave, prescribed to obese and overweight patients shown that 55–60% of patients lost more than 5% of their body weight after 52 weeks of treatment (Wadden et al. 2011). Notably, this prescribed weight-loss drug acts on appetite regulation commonly accompanied with various side effects including nausea, headache, constipation, dizziness, and dry mouth as well as a strict adherence to a low fat diet (Greenway et al. 2010). We have shown a similar pattern of weight loss with AuNPs in mice feeding a HFD. Therefore, the injectable AuNPs without the painful dietary restriction may offer a promising alternative for the management of obesity, glucose and lipid disorders.

Furthermore, it seems that the low dose of AuNP treatment exerted a better effect for reducing HFD-induced weight gain and euglycaemic control than the high dose. This

may be due to the aggregative nature of injected AuNPs at high concentration, leading to less “free” individual AuNPs. It is noted that cellular interactions of AuNPs is highly size dependent (Chithrani, Ghazani & Chan 2006b; Fischer & Chan 2007). This is due to the fact that aggregated AuNPs lose their usual interaction with surrounding cells, as observed in Chapter 2 of this thesis. It is interesting to observe increased energy intake in AuNP-treated mice, which can be an adaptation in response to reduced fat mass and weight loss. This leaves a future research question whether controlling energy intake during AuNP treatment would achieve an even better control of adiposity, hyperlipidaemia and euglycaemia in dietary obesity.

During obesity, excessive production of TNFα and IL-6 by ATMs in a pro-inflammatory M1-state, contributes to the local and systemic inflammatory state, driving the development of obesity-related metabolic disorders (Kosteli et al. 2010a; Tilg & Moschen 2008). The increased insulin level in HFD-LAu mice may lead to an increase in glucose uptake by the tissues resulting in improved glucose tolerance. In addition, previous studies have shown improved insulin sensitivity and glucose uptake in peripheral tissues through neutralizing the systemic pro-inflammatory cytokine TNFα (Hotamisligil 2006a; Hotamisligil, Shargill & Spiegelman 1993b). In this study, mRNA expressions of fat TNFα and its upstream regulator TLR-4 was markedly downregulated in the adipose tissue of AuNP-treated mice suggesting suppressed inflammatory response in ATMs. In fact, the levels of TNFα were not different between the Chow-C and AuNP-treated mice. This can in turn improve insulin sensitivity in the peripheral tissues to improve glucose clearance as well. Our finding was consistent with our previous acute study in lean mice (Chen et al. 2013). It is also noteworthy that studies have shown that weight loss may also be a contributing factor of decreased inflammatory gene expression in the fat (Vemuri, Janero & Makriyannis 2008). Thus, alteration of the ATM inflammatory responses may be a key approach to regulating inflammatory processes in the body, and AuNPs appear to be highly suited to carry out this task. However, we do not observe a linear response of the various markers with increasing concentration of AuNPs. This is not an unusual observation with the complex inflammatory environment in adipose tissue and liver during obesity where various up and down regulators are in play.

The liver has also been known to be highly susceptible in ectopic fat and lipid deposition due to increased circulating NEFA levels during HFD consumption (Browning & Horton 2004). This leads to the activation of hepatic resident macrophage-like cells, Kupffer cells, contributing to local inflammation (Olefsky & Glass 2010). Importantly, studies have shown the existence of a strong correlation between Kupffer cell activation with steatosis and hepatic insulin resistance as well as the associated risk of cardiovascular mortality independent of inflammation in the adipose tissue (Lanthier et al. 2010; Targher et al. 2005). Our data showed that under conditions of over-nutrition, the expression of TNFα was significantly upregulated in the liver, suggesting increased liver inflammation in HFD mice. Contrary to that, low dose AuNP-treated mice had a significant downregulation of both TNFα and TLR-4 mRNA expression accompanied by the downregulation of F4/80 Kupffer cells. This suggests that low dose AuNP may suppress the microphage number in the liver. Upregulated TLR-4 in the liver from mice with high dose AuNP may be due the coagulation nature of AuNP at high dose. The AuNP clusters can induce inflammatory response due to the increase in size compared with the single AuNP. ” In addition, liver AST and ALT levels were significantly reduced in the HFD AuNP-treated mice, suggesting improved liver function and integrity. Therefore, these protective and anti-inflammatory effects of AuNPs may serve one of the mechanisms underlying improved glucose and lipid metabolism in AuNP-treated mice.

Our data showed an increased CPT-1α mRNA expression by 1.1-fold in the adipose tissue of HFD mice while an additional 1.1-fold upregulation in the adipose tissue of low dose AuNP-treated mice. This suggests that improved mitochondrial fatty acid oxidation could lead to a reduction of whole body lipid accumulation since adipose tissue makes up a large proportion of body mass. Studies have shown that reduction in CPT-1α expression can reduce mitochondrial fatty acid oxidation and increase intracellular NEFA, ultimately resulting in triglyceride accumulation leading to hyperlipidaemia, which is one of the key contributors to insulin resistance (Leinonen et al. 2003). Therefore, lower fat masses and euglycaemic state in AuNP-treated mice receiving HFD may be attributed to the reduced TNFα and NEFA levels, since both played a major role in the development of hyperlipidaemia and obesity-related insulin resistance.

PPARγ is the main target of the anti-diabetic drug class of thiazolidinediones (TZDs) used to increase insulin sensitivity to treat type 2 diabetes (Berger & Moller 2002). PPARγ regulates the expression of genes encoding protein for lipid uptake crucial for adipocyte growth and differentiation (Sárvári et al. 2015). In this study, expression of fat PPARγ was significantly downregulated in HFD-HAu mice, which suggests reduced fat cell differentiation. In the liver, PPARγ is normally expressed at very low levels but overexpressed in mice models that are insulin resistant and have hepatic steatosis (Edvardsson et al. 1999; Steel & Whitehead 1994). Treatment with low dose AuNPs normalised liver PPARγ mRNA expression comparable to mice fed a normal diet, which may further suggest improved insulin sensitivity by AuNPs to improve glucose metabolism.

Therefore, leptin mRNA expression in AuNP-treated mice was noticeably lowered than the vehicle-treated HFD mice, in correlation with their significantly reduced fat masses. Patients with excess visceral adiposity show reduced mRNA and serum levels of adiponectin due to the inflammatory states which inhibits adipocyte adiponectin production (Kuri-Harcuch & Green 1978; Sorisky, Molgat & Gagnon 2013; Tilg & Moschen 2008). In fact, studies have shown an inverse correlation between weight loss or treatment with insulin-sensitising drugs and serum levels of adiponectin, owing to the improved insulin sensitivity (Kershaw & Flier 2004; Osborn & Olefsky 2012). In this study, mRNA expression of adiponectin was significantly upregulated upon high dose AuNP treatment indicating improved insulin sensitivity which contributes to greater glucose tolerance.

In this study, liver SREBP-1c and FASN mRNA expression levels were downregulated in AuNP-treated mice suggesting suppression of *de novo* fatty acid biosynthesis, liver lipogenesis, and lipid accumulation in the face of HFD intervention. However, our data showed no difference in the mRNA expression of PEPCK between the HFD and AuNP-treated groups, suggesting no change in hepatic *de novo* glucose synthesis. Insulin sensitive genes, adiponectin was significantly upregulated in the adipose tissue and GLUT-4 upregulated in the liver of HFD mice compared to control. However, high dose AuNP-treated mice showed markedly increased fat adiponectin and liver GLUT-4 mRNA expression levels along with low levels of plasma insulin indicate improved

insulin sensitivity contributing to the improved IPGTT in those mice. Therefore, AuNP treatment which suppresses liponeogenesis and increased insulin sensitivity may significantly reduce the risk of developing other obesity-related complications including type 2 diabetes.

In line with previous studies, we have demonstrated the uptake of AuNPs into the surrounding abdominal fat after repeated IP administration and systemic clearance into the liver from the peritoneal cavity (Balasubramanian et al. 2010; Chen et al. 2013). The clearance of AuNPs larger than the renal filtration fenestrations which are approximately 15 nm for kidney glomerulus are not excreted from the urine, instead they are eliminated from the blood by the reticuloendothelial system (Abdelhalim 2013; Balasubramanian et al. 2010; Sarin 2010). Short-term repeated AuNP injection has been shown to have no proportional increase in gold levels in the blood (Lasagna-Reeves et al. 2010). Gold levels were highest in the fat upon long-term repeated IP administration of AuNPs suggesting the movement of AuNPs from the peritoneal cavity into the surrounding adipose tissue, which were further absorbed into the circulation and distributed to other tissues. Due to the size of the AuNPs administered, they have very limited excretion via the renal system but cleared via the liver and spleen. This is also evident by an increased accumulation and retention of gold in the liver and spleen compared to the kidney. The bioavailability of AuNPs in the systemic circulation and constant flow through of blood, gold was also detectable in the heart independent of dose administered. Detectable amount of gold were found in the brain tissue in a dose dependent manner suggesting a non-saturable retention of gold in the blood vessels (Lasagna-Reeves et al. 2010). Intriguingly, there was no indication of liver toxicity or cell damage in AuNP-treated mice, with no elevation of liver AST or ALT levels.

In summary, our results indicate that inhibition of the local inflammatory environment due to changes in macrophage activity caused by AuNPs may be one of the key underlying mechanisms for reduced weight gain in this study. Specifically, we have demonstrated the possible anti-inflammatory effect of AuNPs protecting mice against the development of HFD-induced glucose intolerance. Additionally, AuNPs seems to have a dose dependent mechanism of action in regulating adipokine and lipid metabolism. This novel therapeutic treatment strategy using AuNP serves a new

paradigm in preventing obesity-related metabolic disorders. In the next chapter, we will further investigate the potential use of AuNPs as in subjects with existing obesity to further elude the action of AuNPs in ameliorating obesity-related metabolic disorders.

CHAPTER 5

Treating Obesity in Mice using

Gold Nanoparticles

5. Treating obesity in mice using gold nanoparticles

5.1. Introduction

The obesity epidemic was first noted in the U.S. at 1970 and concurrently in the UK and most industrialized countries in the 1980s; since then, many middle- and low-income developing countries have joined the surge in obesity prevalence (WHO 2014a, 2014b). This phenomenon seems to be driven mainly by the swift changes in the global food system, which is manufacturing more processed, affordable, and effectively marketed food (Swinburn et al. 2011). In addition, the lack of physical exercise and overconsumption of diets that are high-fat and high-carbohydrate, further contribute to the development of obesity-related complications. According to Gardner et al. (2000), the number of people who are overfed and overweight in the world has overtaken the number of those underfed and underweight, for the first time in history (Gardner, Halweil & Peterson 2000).

Obesity can be categorized into 3 classes according to the increasing BMI levels and the associated health risk: class I (moderately obese, BMI 30–34.9 kg/m^2), class II (severely obese, BMI 35–39.9 kg/m^2) and class III (morbidly obese, BMI $\geq$ 40 kg/m^2) by the WHO (NHLBI 1998; WHO 1995, 2015a). There is increasing evidence that obesity is associated with a markedly increased morbidity, premature mortality, impaired health-related quality of life and medical-care cost burden (Fontaine et al. 2003; Kolotkin, Meter & Williams 2001; Roth et al. 2004; Thompson & Wolf 2001). Obesity is now considered a chronic disease, which requires long-term therapy, education, modification to lifestyle and/or obesogenic environment.

There is an urgent need of new treatment strategies which facilitate an effective and sustained weight loss for patients with moderate or less severe obesity, which are not prioritized for such invasive surgical interventions. Currently, there is lack of evidence of sustained weight loss following discontinuation of anti-obesity therapeutic drug interventions; instead, patients usually regain some or all of the weight that was originally lost (Ioannides-Demos, Piccenna & McNeil 2010; Rodgers, Tschöp &

Wilding 2012). Bariatric surgery although effective for long term weight loss, has been reserved for morbidly obese patients as a last resort .

In chronic obesity, a state of chronic low-grade inflammation in the adipose tissue is characterized by the recruitment and infiltration of ATMs in the pro-inflammatory M1-state (Weisberg et al. 2003; Wellen & Hotamisligil 2003). Most of the ATMs in obese mice and in humans, scatter between the hypertrophied adipocytes and completely surrounds necrotic adipocytes, forming crown-like structures (CLS) (Alkhouri et al. 2010; Cinti et al. 2005; Murano et al. 2008; Weisberg et al. 2003). Thus, increased pro-inflammatory M1 ATMs mediate a pro-inflammatory response via the secretion of the pro-inflammatory cytokines, TNFα and IL-6, which has significant implications for insulin resistance and metabolic disease associated with obesity. As shown in Chapter 4, mice with HFD-induced obesity, have increased ATM activity which can impair the insulin response in adipocytes and dysregulate basal lipolysis leading to glucose intolerance and hyperlipidaemia, which eventually contributes to insulin resistance and non-alcoholic fatty liver disease (Hill, Reid Bolus & Hasty 2014).

Non-alcoholic fatty liver diseases are an ectopic accumulation of fat in the liver due to non-alcoholic causes leading to steatosis. Non-alcoholic fatty liver diseases is the most common asymptomatic liver disease found in morbidly obese patients with central adiposity and insulin resistance (Gaggini et al. 2013; Musso, Gambino & Cassader 2010; Perlemuter et al. 2007; Sanyal et al. 2001). Other organs including the heart, kidneys, pancreas, and muscles are also susceptible to fat accumulation. Liver steatosis also induces a low grade inflammatory response through the activation of Kupffer cells and production of pro-inflammatory TNFα, similar to that seen in adipose tissue after long term HFD feeding (Cai et al. 2005; Olefsky & Glass 2010). Studies have shown that elevated hepatic TNFα signalling is essential for the progression of non-alcoholic fatty liver diseases to non-alcoholic steatohepatitis and liver fibrosis leading to cirrhosis (Das & Kar 2005; Tomita et al. 2006).

In Chapter 4 of this thesis, we demonstrated the beneficial effects of simultaneous treatment of mice with AuNPs while also being exposed to a HFD, leading to induced obesity. Our results showed these AuNP treated mice had significantly improved body

anthropometry, reduced pro-inflammatory ATM activity, improved glucose tolerance and blood lipid profiles. Therefore, it was of interest to study the effect of AuNPs in mice with chronic obesity. In this chapter, we aimed to further evaluate the impact of spherical 21 nm AuNPs and optimize the dosage of treatment using a mouse model of existing obesity, glucose intolerance and non-alcoholic fatty liver disease. Specifically, 8 week old male C56BL/7 mice were fed a HFD for 10 weeks to induce obesity, this was then followed by daily IP injection of AuNPs at three different doses for 5 weeks to examine their effects on fat reduction, amelioration of glucose intolerance and hepatic steatosis. An additional dosage of AuNPs, at an extremely low concentration were added in this study to investigate whether they will exert an equivalent or better effect compared with the two doses studied in the previous chapter.

5.2. Methods

5.2.1. Ethics approval

All procedures in this study were approved by the Animal Care and Ethics Committee at the University of Technology Sydney (ACEC#2011-403A) in accordance with the Australian Code for the Care and Use of Animals for Scientific Purposes 8th Edition, 2013 by the National Health and Medical Research Council.

5.2.2. Animal experiment

Seven week old male C57Bl/6 mice from Animal Resource Centre, WA, Australia, were housed at 20±2°C on a 12:12 h light/dark cycle. Mice were fed standard rodent chow with *ad libitum* access to water during the acclimatization

At week zero, the mice were divided into 5 groups with equal body weights (n=16); one group was fed a rodent chow and the other four period. Then, mice were housed and ear marked as described in section 4.2.2. groups were fed a HFD for 10 weeks to induce obesity. At week 10, the chow-fed (Chow-C) group received a 5 weeks of daily vehicle (water) IP injection without dietary modification. One of the four HFD-induced obesity (OB-C) group also received a 5 weeks of daily vehicle IP injection and continued

feeding on HFD. The remaining three HFD-induced obesity groups, one received injections at an extremely low dose AuNP (OB-EAu) (0.0785 μg of Au/g mice, daily IP), one received injections at a low dose AuNP (OB-LAu) (0.785 μg of Au/g mice, daily IP), and the last group received injections at a high does AuNP (OB-HAu) (7.85μg of Au/g mice, daily IP) for 5 weeks. The AuNP-treated mice were fed HFD throughout the 5 weeks treatment. The extremely low dose was included in this study with modification from the study in Chapter 4. The AuNP used in this study were prepared as described in Chapter 2, and injection was performed at 10 am daily. The maximum volume injected into the mice did not exceed 200 μL/mouse.

Body weights were measured weekly; while energy consumptions (kJ/mouse/24 h) was measured fortnightly before the AuNP treatment. During the 5 weeks of AuNP treatment, body weight was monitored 3 times a week and energy consumption was measured weekly. The energy consumption was calculated according to the animal feed composition as described in section 4.2.2.

5.2.2.1. Tissue and blood sample collections

At the end of 15 weeks, the mice were euthanized by Pentothal (0.1mg/g, IP, Abbott Diagnostics, Kurnell, NSW, Australia). Once the mice fell into a deep sleep and lost consciousness, blood was collected via cardiac puncture using a 24G needle and syringe. The endpoint non-fasting blood glucose was determined using an AccuCheck® Performa glucose meter (Roche, NJ, USA) by pipetting 10 uL of blood onto the test strips. Blood was immediately collected and separated by centrifugation at 15,000 rpm, for 6 min. The plasma faction was stored at -20°C for bioassay analyses. Tissues such as heart, spleen, kidneys, liver, and abdominal fat pads were harvested and weighed. The hypothalamus and soleus muscles were also dissected and collected. The fat pads and organs were either fixed in 10% formalin or snap frozen in liquid nitrogen and then stored at -80°C for further analysis.

5.2.3. Glucose tolerance test

At week 14, the mice (n=8) were fasted for 5 h after which time an IPGTT was performed following glucose challenge as outlined in section 4.2.3. All mice were administered D-glucose (2g/kg, Univar, Ajax Chemicals Ltd, Australia) and blood glucose levels were measured at 0, 15, 30, 60 and 90 min using an AccuCheck® Performa glucose meter (Roche, NJ, USA). The AUC was calculated as described in section 4.2.3.

5.2.4. Biochemical assays

The plasma and liver tissue lysate were used for biochemical assays to determine concentration of NEFA and triglyceride as described in section 3.2.7.1 and section 4.2.4.2, respectively according to manufacturer's instruction. Plasma concentrations of insulin, AST and ALT in were measured according to manufacturer's protocol detailed in section 4.2.4.

5.2.4.1. Determination of plasma cholesterol high density lipoprotein (HDL-C) concentration

Plasma HDL-C concentration was measured using the Cholesterol HDL-C kit (D00127, Dialab Ltd., Vienna, Austria) according to manufacturer's protocol. Briefly, 50 µL of plasma sample was incubated at room temperature for 10 min and then precipitated by centrifugation at 4000 g for 10 min to separate the non-HDL-C lipoproteins. Following that, 20 µL of precipitated plasma sample and 200 µL of reagent were incubated in 96-well plate for 10 min at 37˚C. The colourimetric indicator was measured with Synergy HT microplate spectrophotometer (Bio-Tek Instrument Inc., Winooski, VT, USA) at 500 nm. The concentration of cholesterol was determined using a standard curve made from Cholesterol standards (D95114, Dialab Ltd., Vienna, Austria) plotted against Abs at 500 nm (R^2 = 0.9878, Figure 5.1).

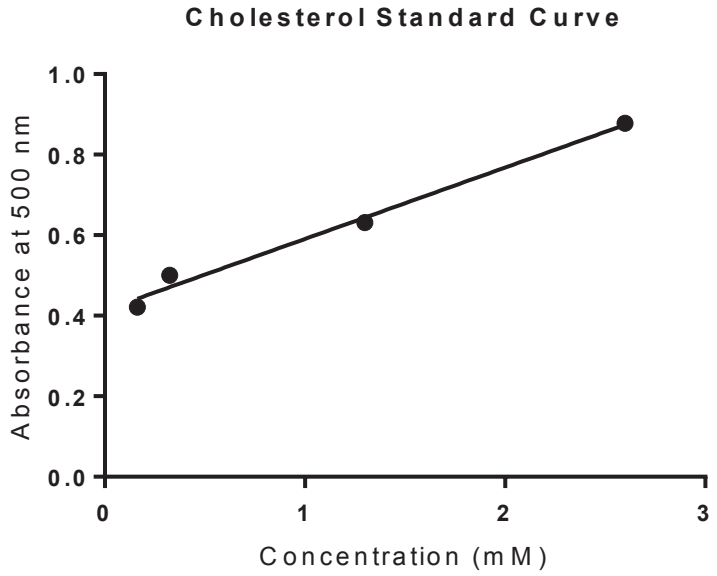

Figure 5.1 Standard curve derived from cholesterol standards (Y = 0.1772X + 0.4135).

5.2.5. Histological analysis

Formalin fixed adipose tissue samples were embedded in paraffin and sectioned at 5 μm thickness, then transferred on histology glass slides according to the protocol outlined in section 4.2.5.1.

5.2.5.1. H&E staining

The paraffin-embedded adipose tissue sections were stained with Harris haematoxylin and counterstained with eosin to examine the general morphology and size of the lipid droplets as described in section 4.2.5.2. Digital photomicrographs of stained tissue sections were captured with an inverted light microscope (BX51 Olympus Co., Tokyo, Japan) using a digital camera (Olympus) using cellSens software (version 1.7). For each mouse, 800–1000 adipocytes were quantified from 6 different regions using ImageJ (1.6.0_24, fiji.sc, National Institutes of Health, Bethesda, MD, USA).

5.2.5.2. Immunohistochemistry staining

Immunohistochemistry staining was carried out using serial sections corresponding to H&E-stained tissue sections. The sectioned slides were deparaffinized by xylene (2 x 10 min) wash, then rehydrated with graduated series of alcohols, 100% absolute ethanol (2 x 5 min), 95% ethanol (2 x 5 min), and 70% ethanol (2 x 5 min). Subsequently, the slides were rinsed with deionised water and microwaved in antibody retrieval buffer (Tris/EDTA, pH 9.0) for 20 min. After heat-induced epitope retrieval, tissue sections were stained for macrophage marker F4/80 using VECTASTAIN Universal Elite ABC Kit (PK-6200, Vector Laboratories, Burlingame, CA, USA). Briefly, the samples slides were washed in Tris buffered saline containing 0.05% (v:v) tween-20 (TBST) and outlined with PAP pen (S2002, DakoCytomation, Glostrup, Denmark). Then, the sample slides were exposed to hydrogen peroxide solution for 5 min, washed in TBST (2 x 5 min), and blocked with protein solution for another 5 min. Then, the sample slides were incubated with rabbit monoclonal F4/80 (SP115) antibody (1:250, NBP2-12506, Novus Biologicals, Littleton, CO, USA) at 4˚C overnight and washed in TBST (3 x 5 min). Then the slides were incubated with biotinylated goat anti-rabbit secondary antibody (1:1000, BA1000, Vector Laboratories, Burlingame, CA, USA) at room temperature for 1 h and washed in TBST (3 x 5 min). The target proteins binding with the primary and secondary antibody were incubated using with avidin/biotinylated HRP reagent mix from ABC kit for 30 min and washed in TBST (3 x 5 min). Thereafter, 3,3'-diaminobenzidine tetrahydrochloride (DAB, D5905, Sigma Aldrich, St. Louis, MA, USA) chromogen peroxidase substrate was added to the sections for 5 min and rinsed in running tap water. This was followed by steps of dehydration with 95% ethanol (2 x 5 min), 100% absolute ethanol (2 x 5 min), and xylene (2 x 5 min). The tissue sections were not counterstained with hematoxylin due to signal interference. The sections were then mounted in DPX mounting medium (06522, Sigma Aldrich, St. Louis, MO, USA) with glass coverslips. Adjacent serial sections were prepared without primary antibody as negative controls. Images of stained tissue sections were captured with an inverted light microscope (BX51 Olympus Co., Tokyo, Japan) using a digital camera (Olympus) using cellSens software (version 1.7). Quantifications of CLS that positively stained with F4/80 expressing ATMs were manually counted and expressed as the number of CLS per mm^2 of tissue at 10x magnification.

5.2.6. Gene expression analysis using RT-PCR

5.2.6.1. RNA extraction and cDNA synthesis

Snap frozen fat and liver tissue samples (50–100 mg) were homogenized in 2 mL polypropylene tubes containing ceramic beads (Sarstedt, Nümbrecht, Germany) and 1 mL of TRI reagent (T9424, Sigma Aldrich, St. Louis, MO, USA) using Precelleys®24 (Bertin Technologies, Carlsbad, CA, USA). RNA isolation and purifications steps were prepared as outlined in section 3.2.4.1. The purified total RNA at 200 ng/µL was used for cDNA synthesis according to section 3.2.4.2. The synthesized cDNA was diluted to 200 ng/µL and used for gene expression assay detection.

5.2.6.2. Gene expression assays

mRNA expression of target genes was determined in the retroperitoneal fat and liver, including macrophage markers CD68 and F4/80, inflammatory cytokines TNFα, IL-6, TLR-4, IL-1R and IL-1β. Markers related to glucose metabolism (GLUT-4, PEPCK and FOX-O1), lipid metabolism (ATGL, CPT-1α, SREBP-1c, FASN) and other adipokine (PPARγ, adiponectin, SAA-1 and leptin) were also determined. mRNA levels were measured with TaqMan® or SYBR Green II assays (Life Technologies, Carlsbad, CA, USA) using the quantitative real-time PCR as described in section 4.2.6.1. The sequences of the primers and probes used in this study were of Mus musculus origin (section 4.2.6.2, Table 4.2 and Table 4.3).

5.2.7. Tissue preparation and digestion for ICP-MS analysis

The fat, liver, spleen, kidney, heart, lung and brain tissues were prepared and acid digested to assay for the concentration of elemental gold using ICP-MS as described in section 4.2.7.

5.2.8. Statistical analysis

Results are expressed as mean ± S.E.M. IPGTT analysis was performed using one-way ANOVA with repeated measures followed by post hoc Bonferroni test (Prism version 6, GraphPad Software Inc, CA, USA). All other analyses in this study were performed using one-way ANOVA followed by post hoc Bonferroni. $P < 0.05$ was considered statistically significant.

5.3. Results

5.3.1. Effects of HFD consumption

5.3.1.1. Body measurements of obese mice

Prior to the HFD intervention, body weight and food intake were no different among all the groups as shown in Figure 5.2 and Table 5.1. The effect of 10 weeks HFD feeding on body weight was similar among the four HFD-induced obesity groups, which was significantly greater than the Chow-C group shortly after the diet commenced ($P < 0.05$, Figure 5.2B), which was similar to the results in the cohort in Table 4.6 of Chapter 4 (see section 4.3.1.1).

At week 10, the body weight of all the HFD-induced obesity groups reached 44.3 ± 0.1 g (Figure 5.2B and Table 5.1). At the end of the 15 weeks of HFD intervention, there was a 24% greater energy consumption in the OB-C group compared with the Chow-C group ($P > 0.05$, Table 5.1). The end-point body weight of OB-C group was 52% greater than the Chow-C group ($P < 0.05$, Table 5.1) after 15 week of HFD intervention.

The organ masses of the OB-C group were also significantly greater than the Chow-C group in line with the increased body weight, including fat, liver, kidney and heart ($P < 0.05$, OB-C *vs.* Chow-C, Table 5.1). Liver mass in the OB-C group was twice as much as the Chow-C group; while the retroperitoneal, epididymal and mesenteric adipose tissues were 5, 2.5 and 4 times greater than the control group, respectively (all $P < 0.05$,

Table 5.1). When the liver and fat masses were standardised by the body weight, the differences remained significant ($P < 0.05$, OB-C *vs.* Chow-C, Table 5.1).

IPGTT results at week 14 were shown in Figure 5.3. The blood glucose levels in OB-C group was consistently higher than the Chow-C group at 15, 30, 60 and 90 min post glucose injection ($P < 0.05$, Figure 5.3A). The AUC of the OB-C was also bigger than the Chow-C group by 56% ($P < 0.001$, Figure 5.3B). At 15 weeks, plasma insulin was significantly increased in the OB-C mice ($P < 0.05$, Table 5.2); while no difference in non-fasting glucose concentration was observed between the OB-C and Chow-C groups at the end-point.

Plasma NEFA concentration was significantly elevated (63%, $P < 0.05$) after 15 weeks of HFD consumption without difference in plasma triglyceride and HDL–C levels between OB-C and Chow-C mice (Table 5.2). However, liver triglyceride concentration was significantly increased by 11-fold in the OB-C mice compared to the Chow-C mice ($P < 0.05$, Table 5.2) indicating fatty liver. Plasma ALT and AST levels were also significantly elevated by 2.1-fold and 5.7-fold, respectively, suggesting some level of liver cell damage ($P < 0.05$, OB-C *vs.* Chow-C, Table 5.2).

Figure 5.4 showed the histologic analysis of epididymal adipose tissue. Long term HFD treatment resulted in adipocytes hypertrophy by 42% (2698.8 ± 55.71 μm^2 OB-C *vs.* 1899.23 ± 33.73 μm^2 Chow-C, $P < 0.05$, Figure 5.4K) in the OB-C mice compared to the Chow-C mice, contributing to the significantly increased fat pad size. Moreover, quantification of F4/80 expressing ATMs which form CLS around dead adipocytes was significantly increased by 3.5 times in the OB-C mice compared to the Chow-C mice ($P < 0.005$, Figure 5.4L).

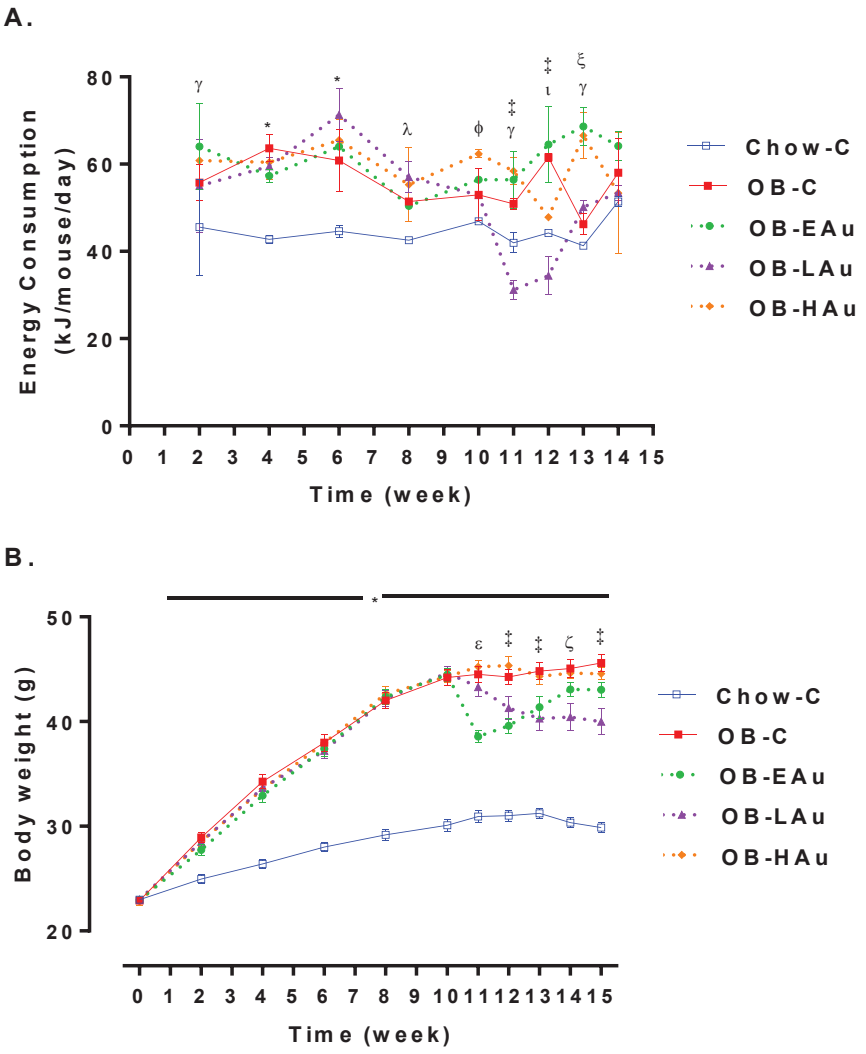

Figure 5.2 Effects of 15 weeks HFD with 5 weeks AuNP treatment on food intake and body weight in male mice.

Energy consumption (A) and body weight (B) at week 15 in Chow-C (water, daily IP), OB-C (water, daily IP), OB-EAu (0.0785 µg AuNP/g mice, daily IP), OB-LAu (0.785 µg AuNP/g mice, daily IP), and OB-HAu (7.85 µg AuNP/g mice, daily IP) for 5 weeks. Results are expressed as mean ± S.E.M. Data were analysed by one-way ANOVA followed by post hoc Bonferroni test. γ $P < 0.05$ Chow-C *vs.* OB-EAu & OB-LAu; * $P < 0.05$ Chow-C *vs.* all other groups; λ $P < 0.05$ Chow-C *vs.* OB-LAu; ϕ $P < 0.05$ Chow-C *vs.* OB-HAu; ‡ $P < 0.05$ OB-C *vs.* OB-EAu & OB-LAu; τ $P < 0.05$ Chow-C *vs.* OB-C & OB-EAu; ξ $P < 0.05$ OB-C *vs.* OB-EAu & OB-HAu; ε $P < 0.05$ OB-C *vs.* OB-EAu; ζ $P < 0.05$ OB-C *vs.* OB-LAu; n=13–16.

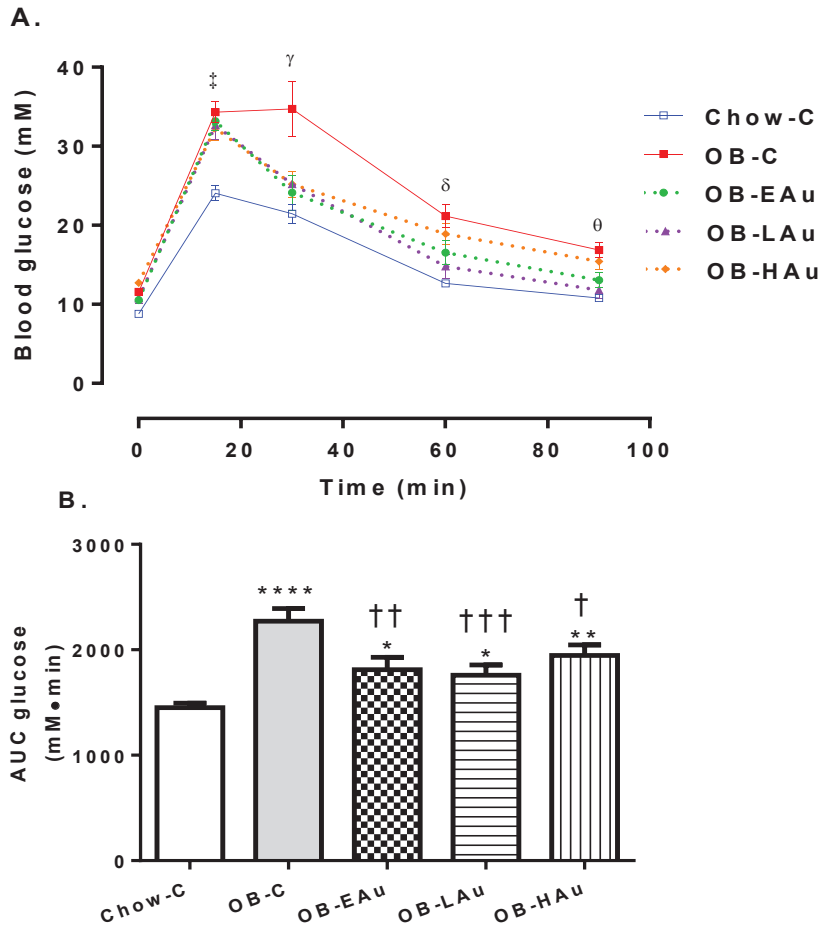

Figure 5.3 Effect of 15 weeks HFD with 5 weeks AuNP treatment on glucose tolerance

(A) Fasting blood glucose levels during IPGTT at week 14 in Chow-C (water, daily IP), OB-C (water, daily IP), OB-EAu (0.0785 µg AuNP/g mice, daily IP), OB-LAu (0.785 µg AuNP/g mice, daily IP), and OB-HAu (7.85 µg AuNP/g mice, daily IP) for 5 weeks. (B) area under the curve (AUC) of (A). Results are expressed as mean ± S.E.M. Data in (A) were analysed by one-way ANOVA with repeated measures. Data in (B) were analysed by one way ANOVA followed by post hoc Bonferroni test. (A) ‡ $P< 0.05$ Chow-C *vs.* all other 4 groups at 15min; γ $P< 0.05$ OB-C *vs.* all other 4 groups at 30mins; δ $P< 0.05$, Chow-C *vs.* OB-C & OB-HAu, OB-C *vs.* OB-EAu & OB-LAu at 60mins; θ $P< 0.05$, Chow-C *vs.* OB-C & OB-HAu, OB-C *vs.* OB-LAu at 90mins. (B) * $P < 0.05$ *vs.* Chow-C; † $P < 0.05$ *vs.* OB-C; n=7–9.

Table 5.1 Effect of 15 weeks of HFD with 5 weeks of AuNP treatment on body morphometry

	Chow-C	OB-C	OB-Eau	OB-Lau	OB-HAu
Body weight initial (g)	23.0 ± 0.3	22.9 ± 0.3	23.0 ± 0.3	23.0 ± 0.3	22.9 ± 0.4
Body weight at 10 weeks (g)	30.1 ± 0.6	44.2 ± 0.8*	44.2 ± 0.6*	44.7 ± 0.6*	44.3 ± 0.6*
Body weight at 15 weeks (g)	29.9 ± 0.5	45.6 ± 0.8*	43.0 ± 0.7*†	40.0 ± 1.2*†	44.6 ± 0.5*
Energy intake (kJ/d)	44.6 ± 1.0	55.7 ± 1.9*	60.6 ± 1.9*	51.6 ± 4.1*	59.0 ± 2.0*
Liver (g)	1.41 ± 0.04	2.85 ± 0.19*	2.64 ± 0.12*	2.10 ± 0.13*†	2.66 ± 0.12*
Liver (%)	4.74 ± 0.13	6.20 ± 0.31*	6.10 ± 0.22*	5.20 ±0.19†	5.94 ± 0.23*
Retroperitoneal fat (g)	0.138 ± 0.018	0.713 ± 0.041*	0.564 ± 0.035*†	0.51 ± 0.05*†	0.62 ± 0.02*
Retroperitoneal fat (%)	0.46 ± 0.06	1.56 ± 0.08*	1.30 ± 0.07*†	1.23 ± 0.09*†	1.38 ± 0.04*
Mesenteric fat (g)	0.430 ± 0.029	1.115 ± 0.044*	1.192 ± 0.065*	1.023 ± 0.086*	1.201 ± 0.041*
Mesenteric fat (%)	1.45 ± 0.08	2.44 ± 0.10*	2.76 ± 0.13*	2.53 ± 0.17*	2.69 ± 0.08*
Epididymal fat (g)	0.510 ± 0.035	2.076 ± 0.082*	2.431 ±0.078*†	1.810 ± 0.122*†	2.251 ± 0.083*
Epididymal fat (%)	1.17 ± 0.12	4.57 ± 0.21*	5.66 ± 0.19†	4.54 ± 0.29*	5.05 ±0.19*
Heart (g)	0.147 ± 0.005	0.161 ± 0.006*	0.140 ± 0.003†	0.143 ± 0.004†	0.151 ± 0.006
Heart (%)	0.49 ± 0.01	0.35 ± 0.01*	0.33 ± 0.01*	0.36 ± 0.01*	0.34 ± 0.01*
Kidney (g)	0.174 ± 0.004	0.193 ± 0.007*	0.184 ± 0.006	0.173 ± 0.007†	0.182 ± 0.006
Kidney (%)	0.58 ± 0.01	0.42 ± 0.02*	0.43 ± 0.01*	0.43 ± 0.01*	0.41 ± 0.01*
Muscle (g)	0.093 ± 0.004	0.100 ± 0.004	0.096 ± 0.002	0.093 ± 0.003	0.095 ± 0.004
Muscle (%)	0.31 ± 0.01	0.22 ± 0.01*	0.22 ± 0.01*	0.23 ± 0.01*	0.21 ± 0.01*

Chow-C (water, daily IP), OB-C (water, daily IP), OB-EAu (0.0785 µg AuNP/g mice, daily IP), OB-LAu (0.785 µg AuNP/g mice, daily IP), and OB-HAu (7.85 µg AuNP/g mice, daily IP) for 5 weeks. Results are expressed as mean ± S.E.M. Data were analysed by one-way ANOVA followed by post hoc Bonferroni test.* $P < 0.05$ *vs.* Chow-C; † $P < 0.05$ *vs.* OB-C. n=9–15.

Table 5.2 Effect of 15 weeks of HFD with 5 weeks of AuNP treatment on mice body metabolic parameters in non-fasting state

	Chow-C	OB-C	OB-Eau	OB-Lau	OB-HAu
Plasma glucose (mM)	13.7 ± 0.48	12.1 ± 0.56	13.7 ± 1.34	13.6 ± 0.62	12.4 ± 0.50
Plasma insulin (ng/mL)	0.012 ± 0.001	0.032 ± 0.007*	0.039 ± 0.011*	0.028 ± 0.004	0.035 ± 0.007*
Plasma NEFA (mM)	2.07 ± 0.16	3.38 ± 0.31*	2.63 ± 0.21	2.56 ± 0.23†	2.83 ± 0.35*
Plasma triglyceride (mM)	0.74 ± 0.10	0.54 ± 0.09	0.37 ± 0.04*	0.38 ± 0.07*	0.40 ± 0.06*
Plasma HDL-C (mM)	1.27 ± 0.34	2.01 ± 0.30	3.40 ± 0.34*†	2.79 ± 0.20*	3.00 ± 0.23*†
Plasma ALT (U/L)	6.40 ± 0.68	20.01 ± 3.18*	12.08 ± 2.90	23.85 ± 3.32*	25.35 ± 4.41*
Plasma AST (U/L)	7.45 ± 1.35	50.14 ± 9.41*	41.94 ± 2.87*	25.30 ± 5.17†	23.46 ± 2.70†
Liver triglyceride (mM/mg tissue)	0.05 ± 0.01	0.60 ± 0.07*	0.55 ± 0.04*	0.58 ± 0.05*	0.44 ± 0.05*†

Chow-C (water, daily IP), OB-C (water, daily IP), OB-EAu (0.0785 μg AuNP/g mice, daily IP), OB-LAu (0.785 μg AuNP/g mice, daily IP), and OB-HAu (7.85 μg AuNP/g mice, daily IP) for 5 weeks. Results are expressed as mean ± S.E.M. Data were analysed by one-way ANOVA followed by post hoc Bonferroni test.* $P < 0.05$ *vs.* Chow-C; † $P < 0.05$ *vs.* OB-C. n=4–15.

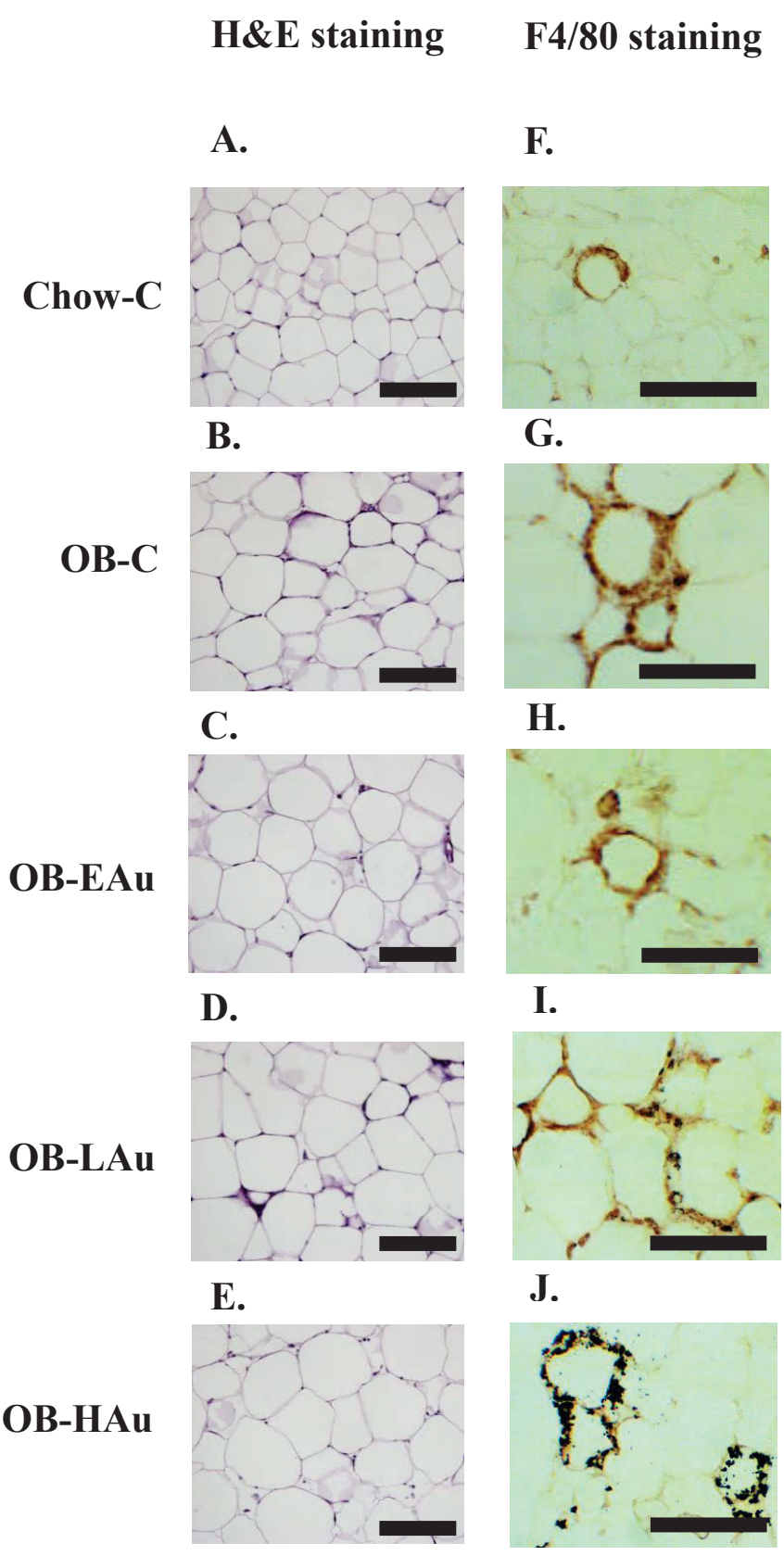
H&E staining
F4/80 staining
A.
F.
Chow-C
B.
G.
OB-C
C.
H.
OB-EAu
D.
I.
OB-LAu
E.
J.
OB-HAu

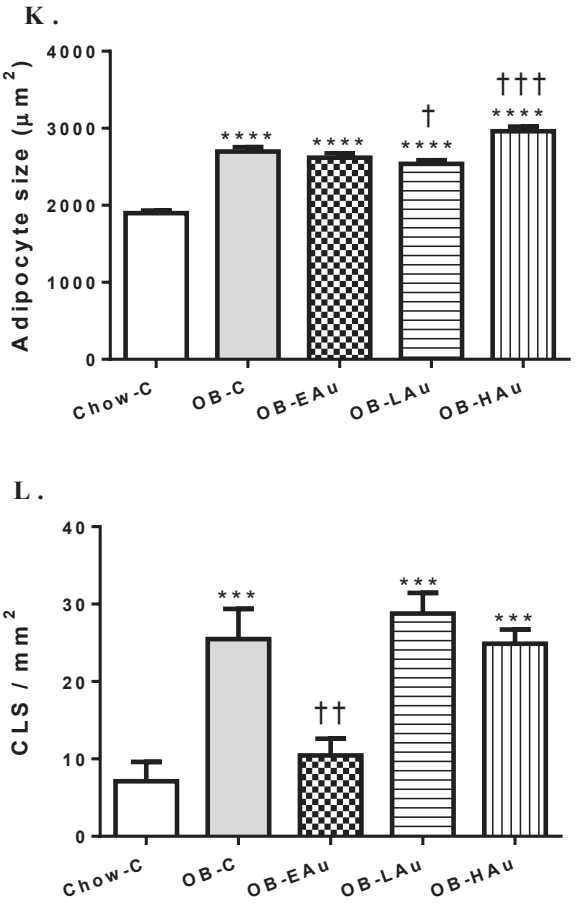

Figure 5.4 Effects of 15 weeks HFD with 5 weeks AuNP treatment on adipose size in the epididymal adipose tissue determined by H&E and F4/80 staining for CLS

Representative images of H&E staining and F4/80 positively CLS in epididymal adipose tissue sections at 15 weeks for (A,F) Chow-C (water, daily IP), (B,G) OB-C (water, daily IP), (C,H) OB-Eau (0.0785 µg AuNP/g mice, daily IP), (D,I) OB-LAu (0.785 µg AuNP/g mice, daily IP), and (E,J) OB-HAu (7.85 µg AuNP/g mice, daily IP) for 5 weeks. (A–J) Images were taken at 40x magnification, scale bar = 100 µm. (K) adipocyte size measured from H&E stained tissue sections; where 800–1000 adipocytes were measured from 6 different region of interest per group using ImageJ software. (L) number of CLS per mm^2 of adipose tissue. Results are expressed as mean ± S.E.M. Data were analysed by one-way ANOVA followed by post hoc Bonferroni test. *** $P < 0.005$ *vs.* Chow-C; **** $P < 0.001$ *vs.* Chow-C; † $P < 0.05$ *vs.* OB-C; †† $P < 0.01$ *vs.* OB-C; ††† $P < 0.005$ *vs.* OB-C; n=3.

4.4.1.1. mRNA expression of inflammatory and adipokine markers in the adipose tissue

At 15 weeks, there was increased mRNA expression of CD68 (5.6-fold, $P < 0.005$, Figure 5.5A) and F4/80 (2.1-fold, $P < 0.01$,

Figure 5.5B) in the OB-C group in comparison to Chow-C group, suggesting increased macrophage infiltration in the retroperitoneal fat. TNF-α and IL-1β mRNA levels in retroperitoneal fat were not significantly altered between the OB-C group and Chow-C group(Figure 5.5C,E). HFD consumption significantly upregulated TLR-4 mRNA expression by 2.3-fold ($P < 0.01$, Figure 5.5F) in the OB-C group compared to the Chow-C. There was also a significant almost 25-fold overexpression of fat SAA-1 mRNA in the OB-C group ($P < 0.05$ *vs.* Chow-C, Figure 5.5G).

As shown in Figure 5.6, long term HFD consumption led to a global increase in adipokine mRNA expression in the retroperitoneal adipose tissue. Lipid and fatty acid metabolic markers including ATGL, SREBP-1c and FASN mRNA expression were markedly increased by 3-fold in the OB-C group ($P < 0.05$ *vs.* Chow-C, Figure 5.6A,C,D). Adipogenesis marker, PPARγ mRNA expression was also significantly upregulated by 3-fold ($P < 0.01$ OB-C *vs.* Chow-C, Figure 5.6E). Moreover, markers involved in glucose metabolism including GLUT-4, adiponectin, and FOX-O1 mRNA expressions were also upregulated by 2-fold, 1-fold, and 2.6-fold, respectively in the OB-C group compared to the Chow-C group (Figure 5.6F–H). Adipose hormone leptin mRNA expression was 8-fold overexpressed in the OB-C mice compared to the Chow-C mice ($P < 0.001$, Figure 5.6I).

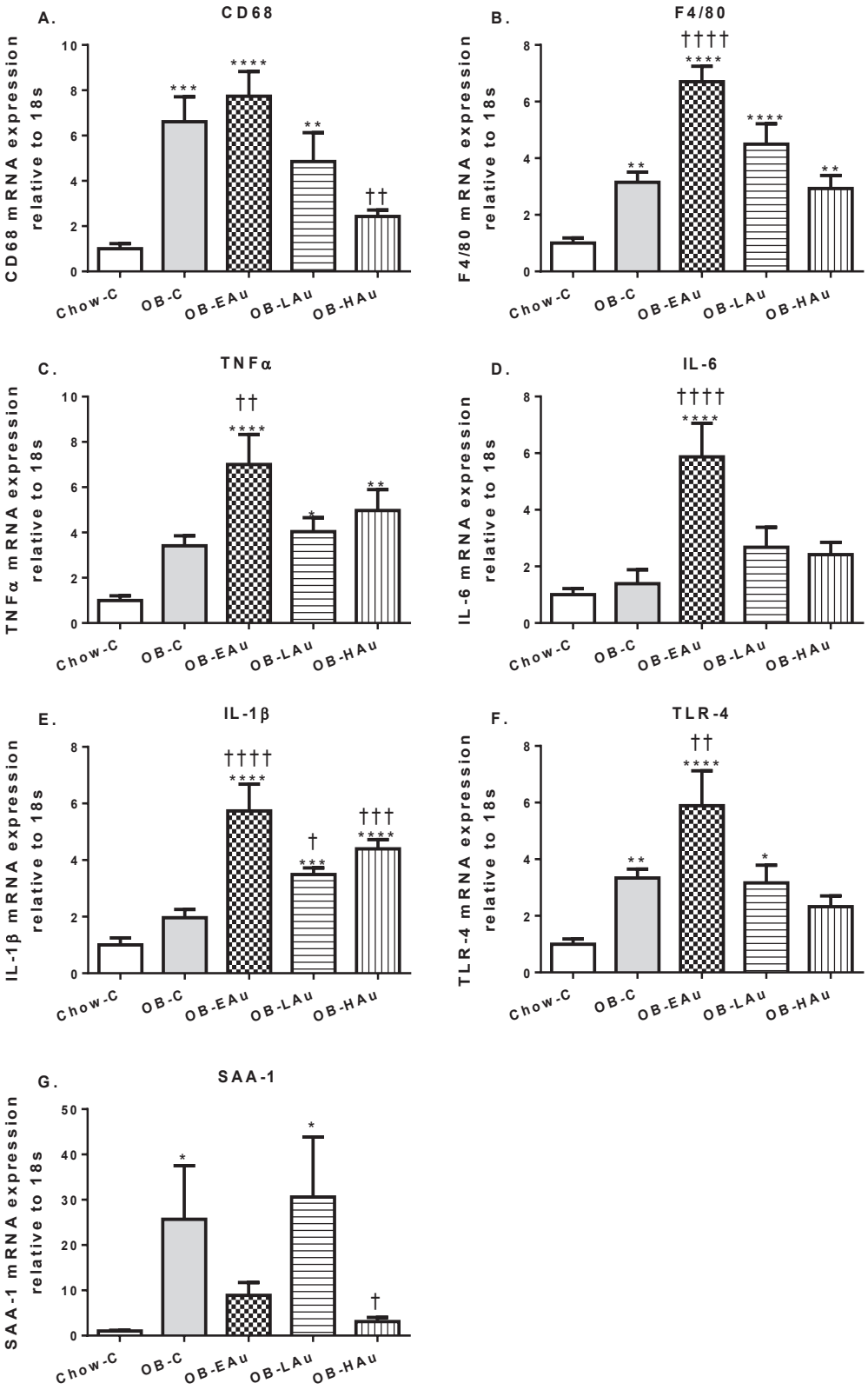
A.
CD68
CD68 mRNA expression relative to 18s
B.
F4/80
F4/80 mRNA expression relative to 18s
C.
TNFα
TNFα mRNA expression relative to 18s
D.
IL-6
IL-6 mRNA expression relative to 18s
E.
IL-1β
IL-1β mRNA expression relative to 18s
F.
TLR-4
TLR-4 mRNA expression relative to 18s
G.
SAA-1
SAA-1 mRNA expression relative to 18s
Chow-C
OB-C
OB-EAu
OB-LAu
OB-HAu

Figure 5.5 Effect of 15 weeks HFD with 5 weeks AuNP treatment on macrophage and inflammatory markers in retroperitoneal fat

Fat mRNA expression of CD68 (A), F4/80 (B), TNF-α (C), IL-6 (D), IL-1β (E), TLR-4 (F), and SAA-1 (G) at 15 weeks in Chow-C (water, daily IP), OB-C (water, daily IP), OB-EAu (0.0785 μg AuNP/g mice, daily IP), OB-LAu (0.785 μg AuNP/g mice, daily IP), and OB-HAu (7.85 μg AuNP/g mice, daily IP) for 5 weeks. Results are expressed as mean ± S.E.M. Data were analysed by one-way ANOVA followed by post hoc Bonferroni test. * $P < 0.05$ vs. Chow-C; ** $P < 0.01$ vs. Chow-C; *** $P < 0.005$ vs. Chow-C; **** $P < 0.001$ vs. Chow-C; † $P < 0.05$ vs. OB-C; †† $P < 0.01$ vs. OB-C; ††† $P < 0.005$ vs. OB-C; †††† $P < 0.001$ vs. OB-C.. n=5–8.

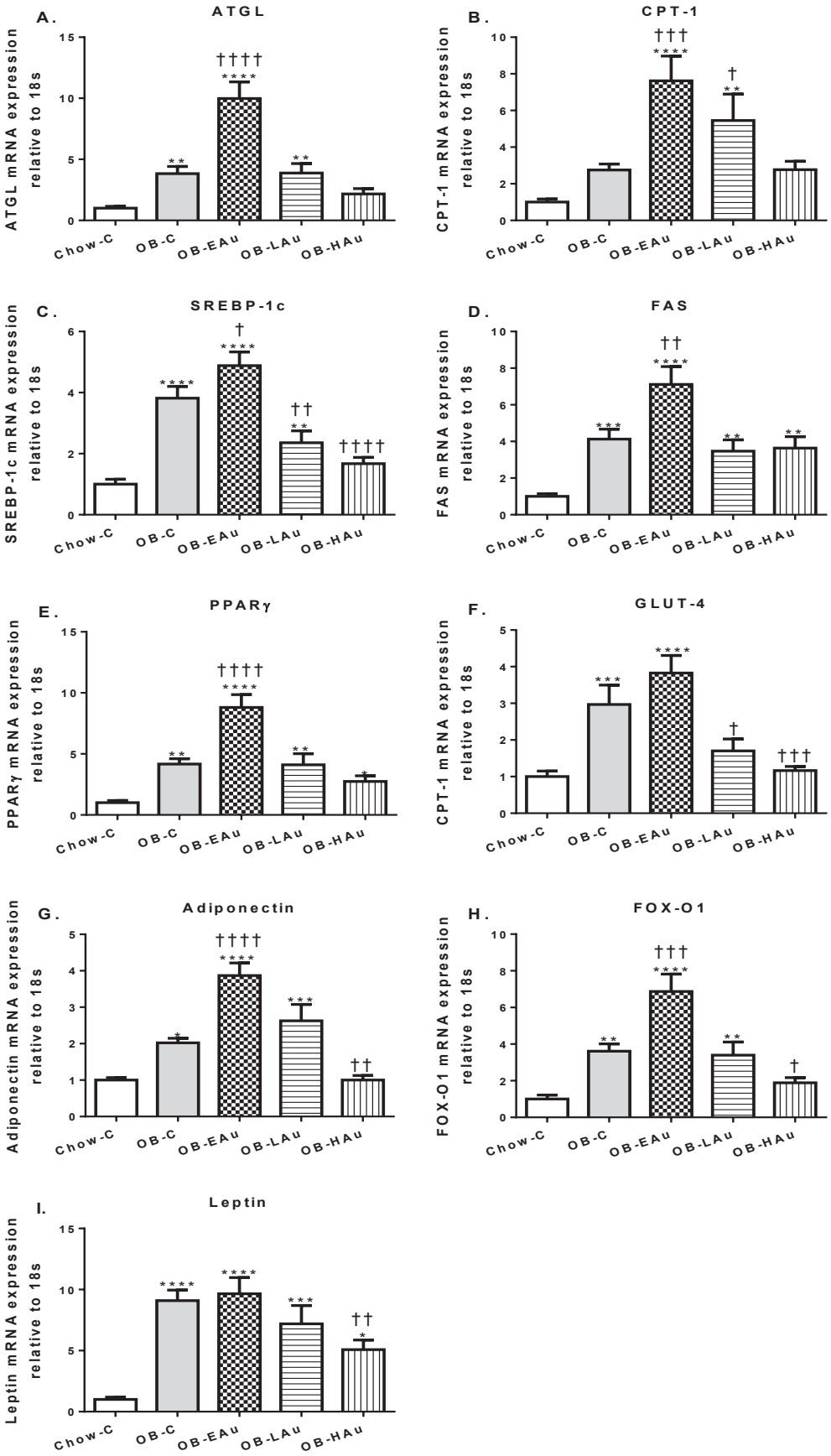
A.
ATGL
ATGL mRNA expression relative to 18s
B.
CPT-1
CPT-1 mRNA expression relative to 18s
C.
SREBP-1c
SREBP-1c mRNA expression relative to 18s
D.
FAS
FAS mRNA expression relative to 18s
E.
PPARγ
PPARγ mRNA expression relative to 18s
F.
GLUT-4
CPT-1 mRNA expression relative to 18s
G.
Adiponectin
Adiponectin mRNA expression relative to 18s
H.
FOX-O1
FOX-O1 mRNA expression relative to 18s
I.
Leptin
Leptin mRNA expression relative to 18s
Chow-C
OB-C
OB-EAu
OB-LAu
OB-HAu

Figure 5.6 Effect of 15 weeks HFD with 5 weeks AuNP treatment on lipid and glucose metabolic markers in retroperitoneal fat

Fat mRNA expression of ATGL (A), CPT-1α (B), SREBP-1c (C), FASN (D), PPARγ (E), GLUT-4 (F), adiponectin (G), FOX-O1 (H), and leptin (I) at 15 week in Chow-C (water, daily IP), OB-C (water, daily IP), OB-EAu (0.0785 μg AuNP/g mice, daily IP), OB-LAu (0.785 μg AuNP/g mice, daily IP), and OB-HAu (7.85 μg AuNP/g mice, daily IP) for 5 weeks. Results are expressed as mean ± S.E.M. Data were analysed by one-way ANOVA followed by post hoc Bonferroni test. * $P < 0.05$ vs. Chow-C; ** $P < 0.01$ vs. Chow-C; *** $P < 0.005$ vs. Chow-C; **** $P < 0.001$ vs. Chow-C; † $P < 0.05$ vs. OB-C; †† $P < 0.01$ vs. OB-C; ††† $P < 0.005$ vs. OB-C; †††† $P < 0.001$ vs. OB-C. n=6–8.

5.3.1.2. mRNA expression of inflammatory, lipid, and glucose markers in the liver

Liver CD68 and F4/80 mRNA expressions were significantly upregulated by 2.6-fold ($P < 0.001$) and 1.3-fold ($P < 0.005$), respectively in mice consuming HFD (Figure 5.7A,B). Both TNF-α and IL-1β mRNA expression was markedly increased by 1.6-fold and 1.5-fold; while TLR-4 mRNA expression was increased by 3.8-fold in the liver (all $P < 0.001$, OB-C *vs.* Chow-C, Figure 5.7C,E,F).

Lipid and glucose metabolic markers were also significantly increased in the liver of obese mice as shown in Figure 5.8. mRNA expression of liver ATGL and CPT-1α were significantly increased by 1.8-fold and 1-fold in the OB-C group compared to the Chow-C group ($P < 0.001$, Figure 5.8A,B). Liver lipogenic markers, SREBP-1c and FAS were also markedly increased which are commonly associated with obesity-related steatosis ($P < 0.001$ *vs.* Chow-C, Figure 5.8C,D). Additionally, PPARγ mRNA expression was also significantly increased by 3.5-fold along with GLUT-4 by 5.5-fold in the liver of the OB-C mice ($P < 0.001$ vs. Chow-C, Figure 5.8E,F). In the OB-C mice, also had gluconeogenesis markers PEPCK and FOXO-1 were significantly upregulated by 49% and 90%, respectively compared to the Chow-C mice ($P < 0.001$, Figure 5.8G,H).

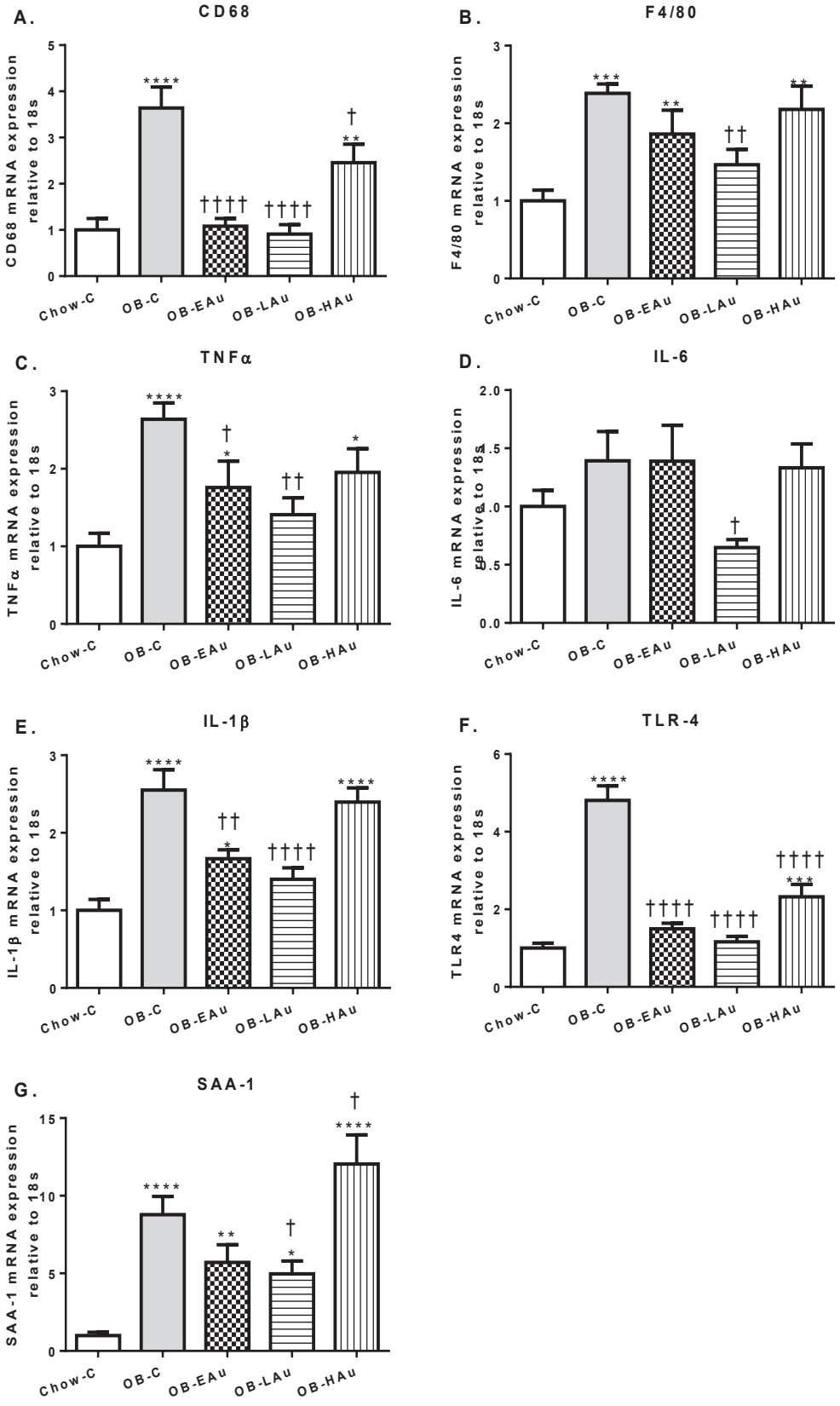
A.
CD68
CD68 mRNA expression relative to 18s
B.
F4/80
F4/80 mRNA expression relative to 18s
C.
TNFα
TNFα mRNA expression relative to 18s
D.
IL-6
IL-6 mRNA expression relative to 18s
E.
IL-1β
IL-1β mRNA expression relative to 18s
F.
TLR-4
TLR4 mRNA expression relative to 18s
G.
SAA-1
SAA-1 mRNA expression relative to 18s
Chow-C
OB-C
OB-EAu
OB-LAu
OB-HAu

Figure 5.7 Effect of 15 weeks HFD with 5 weeks AuNP treatment on macrophage and inflammatory markers in the liver

Liver mRNA expression of CD68 (A), F4/80 (B), TNF-α (C), IL-6 (D), IL-1β (E), TLR-4 (F), and SAA-1 (G) at 15 weeks in Chow-C (water, daily IP), OB-C (water, daily IP), OB-EAu (0.0785 μg AuNP/g mice, daily IP), OB-LAu (0.785 μg AuNP/g mice, daily IP), and OB-HAu (7.85 μg AuNP/g mice, daily IP) for 5 weeks. Results are expressed as mean ± S.E.M. Data were analysed by one-way ANOVA followed by post hoc Bonferroni test. * $P < 0.05$ vs. Chow-C; ** $P < 0.01$ vs. Chow-C; *** $P < 0.005$ vs. Chow-C; **** $P < 0.001$ vs. Chow-C; † $P < 0.05$ vs. OB-C; †† $P < 0.01$ vs. OB-C; †††† $P < 0.001$ vs. OB-C. n=6–8.

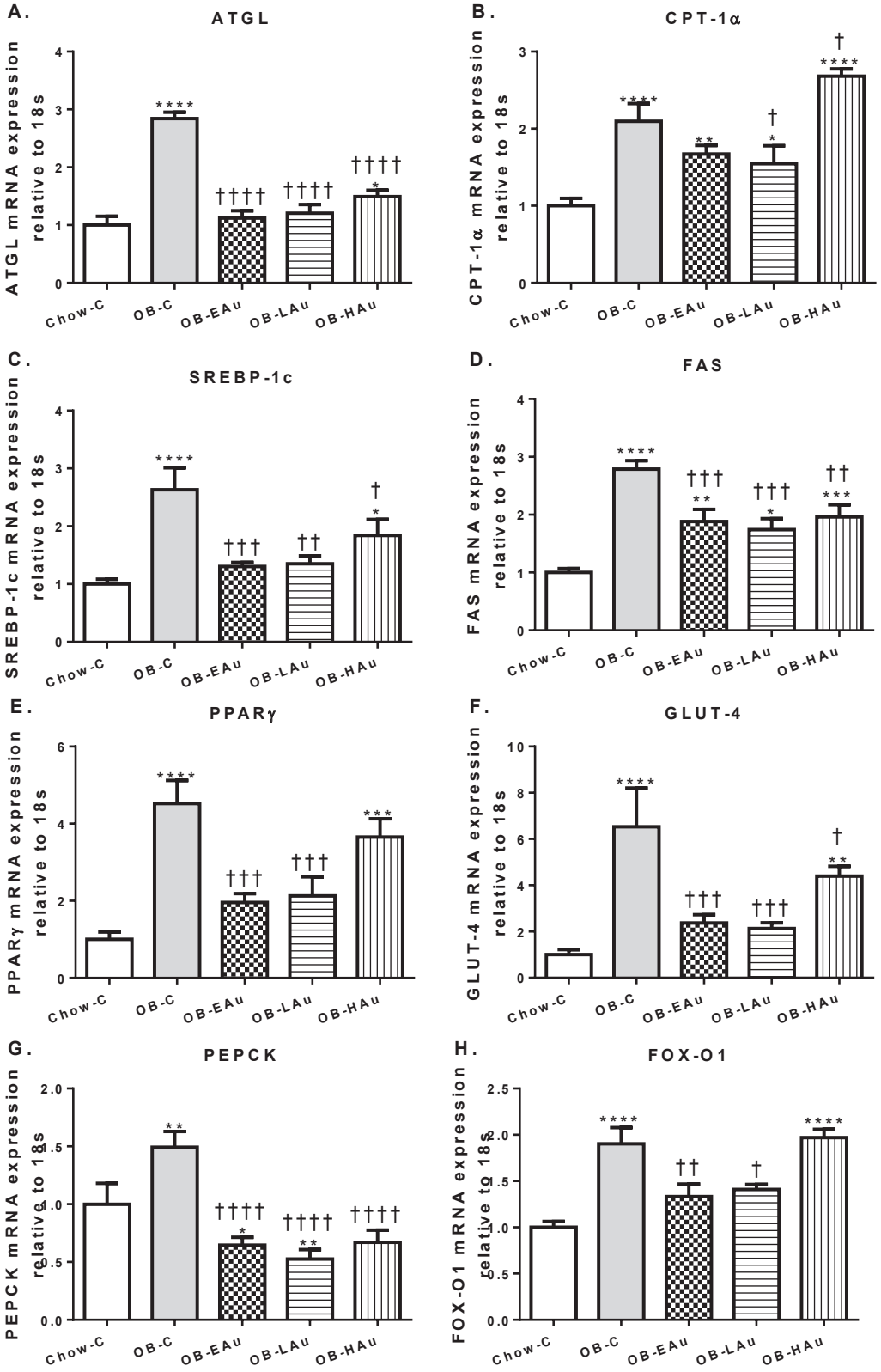
A.
ATGL
ATGL mRNA expression relative to 18s
B.
CPT-1α
CPT-1α mRNA expression relative to 18s
C.
SREBP-1c
SREBP-1c mRNA expression relative to 18s
D.
FAS
FAS mRNA expression relative to 18s
E.
PPARγ
PPARγ mRNA expression relative to 18s
F.
GLUT-4
GLUT-4 mRNA expression relative to 18s
G.
PEPCK
PEPCK mRNA expression relative to 18s
H.
FOX-O1
FOX-O1 mRNA expression relative to 18s
Chow-C
OB-C
OB-EAu
OB-LAu
OB-HAu

Figure 5.8 Effect of 15 weeks HFD with 5 weeks AuNP treatment on lipid and glucose metabolic markers in the liver

Liver mRNA expression of ATGL (A), CPT-1α (B), SREBP-1c (C), FASN (D), PPARγ (E), GLUT-4 (F), PEPCK (G), FOX-O1 (H) at 15 weeks in Chow-C (water, daily IP), OB-C (water, daily IP), OB-EAu (0.0785 µg AuNP/g mice, daily IP), OB-LAu (0.785 µg AuNP/g mice, daily IP), and OB-HAu (7.85 µg AuNP/g mice, daily IP) for 5 weeks. Results are expressed as mean ± S.E.M. Data were analysed by one-way ANOVA followed by post hoc Bonferroni test. * $P < 0.05$ vs. Chow-C; ** $P < 0.01$ vs. Chow-C; *** $P < 0.005$ vs. Chow-C; **** $P < 0.001$ vs. Chow-C; † $P < 0.05$ vs. OB-C; †† $P < 0.01$ vs. OB-C; ††† $P < 0.005$ vs. OB-C; †††† $P < 0.001$ vs. OB-C. n=5–8.

5.3.2. Effects of AuNP treatment

5.3.2.1. Body measurements of obese mice with AuNP treatment

AuNP-treated mice showed no signs of fatigue or change in fur conditions after 5 weeks of daily AuNP injection along with HFD consumption. The OB-LAu and OB-HAu mice had a sudden reduction in daily energy consumption in the initial 2 weeks of AuNP treatment which gradually returned to their previous levels (Figure 5.2A). OB-EAu mice continually increased daily energy consumption throughout the 5 weeks (Figure 5.2A). However, the average daily energy consumption of the AuNP-treated mice was not different from the OB-C group and was significantly higher than the Chow-C group (Table 5.1).

After 1 week of AuNP treatment, both OB-EAu and OB-LAu groups were weighted 13% (ΔBW 5.9 g) and 3% (ΔBW 1.4 g) smaller than the OB-C group, respectively at week 11 (Figure 5.2B). However, the body weight of the OB-EAu group gradually increased over the remaining 4 weeks of treatment; while the OB-LAu group maintained their body weight (Figure 5.2B). At the endpoint, the body weight of the OB-EAu and OB-LAu groups weighed 5% (ΔBW 2.6 g, $P < 0.05$) and 12% (ΔBW 5.6 g, $P < 0.05$) less compared to the OB-C group, respectively (Table 5.1). The body weight of the OB-HAu group was not different from the OB-C group (Table 5.1). Nevertheless, all the AuNP-treated groups were still significantly heavier than the Chow-C group ($P < 0.05$ OB-EAu, OB-LAu and OB-HAu *vs.* Chow-C, Table 5.1).

In the OB-EAu and OB-LAu groups, a significant difference in organ masses and adiposity was observed compared with the OB-C group (Table 5.1). The liver, heart, kidney, retroperitoneal and epididymal adipose tissue masses were all significantly smaller in the OB-LAu group compared to the OB-C group ($P < 0.05$, Table 5.1). However, there seems to be a redistribution of abdominal fat pads in the OB-EAu group with significantly reduced retroperitoneal fat mass but increased epididymal fat masses compared to the OB-C group ($P < 0.05$, Table 5.1). When standardised by the body weight, only the percentage of the liver and retroperitoneal adipose tissue remained significant in the OB-LAu group ($P < 0.05$ vs. OB-C, Table 5.1); while the percentage

of adipose tissue masses was not different in OB-EAu group compared with the OB-C group. The percentages of all organs measured in the AuNP-treated mice were still significantly greater than Chow-C group ($P < 0.05$, Table 5.1).

Fig 5.3A showed that during IPGTT, blood glucose levels of the AuNP-treated mice peaked at 15 min post-glucose injection at a similar level to the Chow-C mice. At 30 min, the levels of glucose were significantly lower in the obese mice treated with AuNPs compared with non-treated mice ($P < 0.05$, Figure 5.3A). It is noteworthy that the blood glucose level measured at 30 mins was not different between the Chow-C and all AuNP-treated groups (Figure 5.3A). Blood glucose levels of the OB-LAu group were significantly lower than OB-C group at both 60 and 90 min post-injection ($P < 0.05$, Figure 5.3A). The AUC values for the AuNP-treated mice groups were significantly lower compared to the OB-C mice ($P < 0.05$, Figure 5.3B). However, end-point non-fasting plasma glucose and insulin levels were not different between OB-C and AuNP-treated groups.

AuNP Treatment improved lipid profile in the obese mice. The concentrations of plasma NEFA were significantly reduced in the OB-LAu group by 24% ($P < 0.05$ *vs.* OB-C) but not significantly altered in the OB-EAu and OB-HAu groups compared to OB-C group (Table 5.2). The levels of HDL-C were significantly elevated in OB-EAu and OB-HAu groups compared to OB-C group ($P < 0.05$, Table 5.2). However, the AuNP-treated groups showed a trend of reduction in plasma of triglyceride concentrations without significance (Table 5.2).

The levels of liver enzyme AST were significantly lower by 49% ($P < 0.05$) in the OB-LAu and 53% ($P < 0.05$) in the OB-HAu mice compared to the OB-C mice (Table 5.2). However, plasma ALT concentrations were not significantly altered by AuNP treatment. Liver TG concentration was not significantly changed by AuNP treatment (Table 5.2).

AuNP treatment did not affect HFD-induced adipocyte hypertrophy in the epididymal fat of the obese mice; however, there seems to be a dose independent alteration in adipocyte size (Figure 5.4C–E). The adipocytes in the OB-HAu group were 9.7% larger

than OB-C group (2961.1 ± 60.3 μm^2 in the OB-HAu *vs.* 2698.8 ± 55.7 μm^2 in the OB-C, $P < 0.005$, Figure 5.4K); while the adipocytes of the OB-LAu group were 6.0% smaller than OB-C group (2537.1 ± 47.1 μm^2 in the OB-LAu *vs.* 2698.8 ± 55.7 μm^2 in the OB-C, $P < 0.05$, Figure 5.4K). Histological analysis only showed the localisation of aggregated AuNPs at the peripheral of the fat tissue, but not visible deep into tissue sections of both OB-LAu and OB-HAu mice. AuNPs mainly accumulated in the connective tissue around the adipocytes or inside the macrophages formed CLS (Figure 5.4I,J). However, the number of CLS in the adipose tissue of both OB-LAu and OB-HAu groups were not different from the OB-C group (Figure 5.4L). By contrast, OB-EAu mice had significantly lowered CLS density in the adipose tissue compared to the OB-C mice ($P < 0.01$, Figure 5.4L) with no difference from the Chow-C mice.

5.3.2.2. mRNA expression of inflammatory and adipokine markers in the adipose tissue

In the fat issue, mRNA expression of both macrophage and pro-inflammatory markers F4/80, TNF-α, IL-6, IL-1β, and TLR-4 were significantly upregulated in the OB-EAu mice by 53%, 51%, 321% 192% and 76% in comparison to the OB-C mice (all $P < 0.05$, Figure 5.5B–F). However, no difference in mRNA expression of F4/80, TNF-α, IL-6, and TLR-4 was observed for in the adipose tissue of OB-LAu and OB-HAu mice compared to the OB-C mice (Figure 5.5). Fat IL-1β mRNA expression was significantly upregulated by 77% and 123% in the OB-LAu and OB-HAu groups, respectively ($P < 0.05$ *vs.* OB-C, Fig 5.5E). Interestingly, fat CD68 and SAA-1 mRNA expressions were significantly downregulated in the OB-HAu mice by 63% ($P < 0.01$ *vs.* OB-C, Figure 5.5A) and 87% ($P < 0.05$ vs. OB-C, Figure 5.5G), respectively, but not in the OB-Lau mice.

Adipokine mRNA expression levels of ATGL, CPT-1α, SREBP-1c, FASN, PPARγ, adiponectin, and FOX-O1 were significantly upregulated in the OB-EAu group by 160%, 176%, 27%, 72%, 110%, 91% and 189%, respectively ($P < 0.05$ vs. OB-C, Figure 5.6A–E,G–H). However, an opposite effect was observed at higher concentrations of AuNP treatment. In the OB-LAu mice, mRNA expression levels of SREBP-1c and GLUT-4 were downregulated by 42% and 38%, respectively but fat

CPT-1α was significantly upregulated by 97% ($P < 0.05$ *vs.* OB-C, Figure 5.6B,C,F). In the OB-HAu mice, mRNA expressions of SREBP-1c, GLUT4, adiponectin, FOX-O1, and leptin were significantly downregulated by 60%, 56%, 50%, 47%, and 44%, respectively ($P < 0.05$ *vs.* OB-C, Figure 5.6C,F–I).

5.3.2.3. mRNA expression of inflammatory, lipid, and glucose markers in the liver

Liver macrophage and inflammatory markers were significantly downregulated in all AuNP-treated mice. Liver CD68, TNF-α, IL-1β and TLR-4 mRNA expression levels were downregulated by 70%, 33% and 34% and 68% in the OB-EAu group compared to the OB-C group ($P < 0.05$, Figure 5.7A,C,E,F). In the OB-LAu mice, mRNA expressions of CD68, F4/80, TNF-α, IL-6, IL-1β, and TLR-4 were 74%, 38%, 46%, 53%, 45% and 75% lower than the OB-C group ($P < 0.05$, Figure 5.7A–F). In the OB-HAu mice, liver CD68 and TLR-4 mRNA expressions were selectively downregulated by 32% and 52% compared to the OB-C mice ($P < 0.05$, Figure 5.7A,F). Interestingly, SAA-1 mRNA expression was significantly downregulated in the OB-LAu mice by 43% ($P < 0.05$) and significantly upregulated in the OB-HAu mice by 37% ($P < 0.05$), with no difference observed between OB-EAu and OB-C groups (Figure 5.7G).

Most of the lipid and glucose metabolic markers measured in the liver were also significantly downregulated in all AuNP-treated mice. In the OB-EAu mice, ATGL, SREBP-1c, FASN, PPARγ, GLUT-4, PEPCK, and FOX-O1 mRNA expressions in the liver were significantly downregulated (all $P < 0.05$ *vs.* OB-C, Figure 5.8A,C–H). Similarly, liver ATGL, SREBP-1c, FAS, PPARγ, GLUT-4, PEPCK, and FOX-O1 mRNA levels were significantly reduced in the OB-LAu group compared to the OB-C group ($P < 0.05$, Figure 5.8A,C–H). In the OB-HAu mice, mRNA expressions of ATGL, SREBP-1c, FASN, GLUT-4, and PEPCK were also significantly downregulated by 47%, 30%, 29%, 32%, and 55%, respectively compared to the OB-C mice (all $P < 0.05$, Figure 5.8A, B). Interestingly, liver CPT-1α mRNA expression was significantly decreased in OB-LAu mice by 26% ($P <0.05$) but significantly increased in the OB-HAu mice by 27% ($P < 0.05$) compared to the OB-C mice (Figure 5.8B).

5.3.2.4. Distribution of gold in the organs

Trace amount of gold was detected in all the organs of the Chow-C and OB-C groups receiving vehicle injection (Figure 5.3). All AuNP-treated mice had significantly increased gold concentrations in the abdominal fat, liver, spleen, kidney, heart and brain in decreasing order compared to both the Chow-C and OB-C groups (Table 5.3). Five weeks of daily IP injection of AuNPs resulted in a dose-dependent increase in Au concentration in the abdominal fat, liver, and spleen as shown in Table 5.3. Significantly elevated Au levels were found in the spleen and liver compared to the Chow-C and OB-C (Table 5.3). Au was also detectable in the heart and kidneys. Negligible amounts of gold were detected in the brain of AuNP-treated mice due to possible retention of nanoparticles in the blood vessels as the mice were not perfused prior to organ collection.

Table 5.3 Concentration of Au in the organs after 5 weeks of AuNPs treatment

µg Au/g tissue	Chow-C	OB-C	OB-EAu	OB-LAu	OB-HAu
Fat	0.22 ± 0.01	1.89 ± 0.49	36.91 ± 14.61	750 ± 187	10692 ± 2207*†ζ‡
Liver	0.42 ± 0.05	0.54 ± 0.14	14.83 ± 3.52	624 ± 311	3052 ± 1959*†ζ
Spleen	1.57 ± 0.87	0.69 ± 0.28	3.28 ± 0.65	21.41 ± 6.63	236.1 ± 113.6*†ζ‡
Kidney	0.16 ± 0.07	0.07 ± 0.01	0.16 ± 0.02	0.93 ± 0.17	2.73 ± 0.95*†ζ‡
Heart	0.01 ± 0.01	0.01 ± 0.00	0.06 ± 0.01	0.42 ± 0.13	2.64 ± 1.25*†ζ‡
Brain	0.12 ± 0.04	0.05 ± 0.01	0.08 ± 0.01	0.09 ± 0.01	0.28 ± 0.14*†ζ‡

Chow-C (water, daily IP), OB-C (water, daily IP), OB-EAu (0.0785 µg AuNP/g mice, daily IP), OB-LAu (0.785 µg AuNP/g mice, daily IP), and OB-HAu (7.85 µg AuNP/g mice, daily IP) for 5 weeks. Results are expressed as mean ± S.E.M. Data were analysed by one-way ANOVA followed by post hoc Bonferroni test.* $P < 0.05$ *vs.* Chow-C; † $P < 0.05$ *vs.* OB-C; ζ $P < 0.05$ *vs.* OB-EAu; ‡ $P < 0.05$ *vs.* OB-LAu. n=3.

5.4. Discussion

The major findings in this study are that daily IP AuNP injections in mice with existing dietary obesity can significantly improve lipid and glycaemic control, possibly via the alteration of inflammatory cytokines in the fat and liver as proposed in Chapter 4.

In this study, adult C57BL/6 mice were fed a HFD over a 10 week term to induce dietary obesity and subsequently developed metabolic disorders including glucose intolerance, dyslipidaemia, hyperphagia, excessive weight gain, and increased fat mass. The reduction in body weight in the obese mice negatively correlates with dose administered without any significant alteration to energy consumption. Mice treated with AuNPs did not exhibit symptoms of toxicity in the face of weight loss. Based on the clinical data, it is suggested that a weight loss of 5-10% can favourably improve glycaemic control and life quality in obese individuals who also have a high risk of diabetes and cardiovascular diseases (Anderson, Kendall & Jenkins 2003; Blackburn 1999). In a recent trial of the latest approved injectable weight loss medication, Liraglutide (Saxenda®) has been shown to induce 6.2% of total body weight loss in users after one year, compared to the placebo group (Wadden et al. 2013). However, this significant weight loss requires adherence to a strict low-caloric diet to prevent weight gain and ongoing support by dieticians, making its implementation difficult to achieve in reality (Wadden et al. 2013).

The OB-EAu group had a weight loss of 13% after the initial week of treatment. After the first week of drastic weight loss, the OB-EAu mice gradually regained their body weight throughout the remaining 4 weeks of AuNP injection and at the endpoint, they lost a total of 5% of their initial body weight. This may be a physiological adaptation to protect against vigorous weight loss which is critical and beneficial especially during periods of nutrient scarcity for survival (Schwartz et al. 2003; Sumithran & Proietto 2013). The OB-LAu group had 3% weight loss in the first week of treatment, following a slight reduction in daily energy intake resulting in 12% loss from initial body weight. The weight loss in the OB-EAu and OB-LAu mice also resulted in smaller fat masses compared with non-treated obese mice. Surprisingly, the body weight of the OB-HAu

mice was not significantly altered after the treatment consistent with previous study in Chapter 4.

The repeated AuNP IP injections at high concentration may increase their possibility of agglomeration and aggregation due to the high ionic strength of peritoneal fluids (Vesaratchanon, Nikolov & Wasan 2007). In addition, the adsorption of "free" soluble proteins from the peritoneal fluids onto the surfaces of the unmodified citrate-coated AuNPs could influence their ability to interact with surrounding cells and subsequently retard their movement into surrounding tissues (Keene et al. 2012). Herein, we speculate that AuNP treatment at lower doses are less likely to aggregate upon IP administration, thus, maintaining their physiological advantages at the nano-scale. It is noteworthy that the weight loss observed, occurred without any dietary restriction and interference throughout the 5 weeks of AuNPs treatment. Therefore, this raises a future research question as to whether the combination of switching to a healthy diet (normal rodent chow) and AuNPs treatment of the extreme low and low doses would achieve a more robust weight control.

In line with the weight gain, the vehicle-treated obese mice developed glucose intolerance with significantly elevated insulin levels after 15 weeks of HFD consumption compared to the lean mice. Interestingly, all AuNP-treated obese mice demonstrated significantly improved glucose metabolism, along with reduction in plasma NEFA levels independent of the body weight alterations. A recent study by BarathManiKanth et al. (2010) also demonstrated that biologically synthesized 50 nm AuNPs exhibit anti-hyperglycaemic properties in a diabetic mice model (BarathManiKanth et al. 2010). However, no information was provided on body weight and organ mass changes in the AuNP-treated mice. Therefore, there is great potential to use AuNPs as a promising anti-hyperglycaemic treatment strategy in addition to its weight loss effect.

ATMs comprise a significant proportion of the cellular component of adipose tissue. ATMs have been identified primarily through immunohistochemical analysis using macrophage marker, F4/80 (or F4/80^{+}) (Lumeng et al. 2007; Weisberg et al. 2003). The infiltrated ATMs in a M1-state selectively forms CLS around the apoptotic adipocytes,

producing elevated levels of pro-inflammatory cytokines. The density of fat CLS in the obese subject also indirectly reflects the extent of adipocyte hypertrophy and necrosis (Cinti et al. 2005; Weisberg et al. 2003). In addition, the presence of CLS is the hallmark of local inflammation, leading to increased systemic inflammation and consequently the development of insulin resistance and glucose intolerance (Alkhouri et al. 2010; Murano et al. 2008). In this study, all the obese mice were found to have significantly hypertrophied adipocytes and the presence of CLS in comparison to lean mice, which is consistent with the current literature (Cinti et al. 2005; Murano et al. 2008).

Interestingly, CLS density in the OB-EAu mice was significantly reduced, albeit an overall upregulation of macrophage and pro-inflammatory marker in the adipose tissue. Our result showed that this overall increased in macrophage and pro-inflammatory markers in OB-EAu mice were more significant than OB-C, although weight loss was observed in the OB-EAU mice. Further experiments are required to measure the protein level of cytokines to determine whether the upregulated mRNA expression is due to negative feedback of suppressed protein transcription." ATMs did not form CLS due to less adipocyte apoptosis although rapid weight loss happened in the first week treatment. Kosteli et al. (2010) also showed an increased number of ATMs during weight loss where the adipocytes shrank by losing their lipid content but did not die (Kosteli et al. 2010a). However, the CLS density was not altered in both OB-LAu and OB-HAu mice, suggesting that AuNPs cannot change adipocyte necrosis. This is also consistent with mRNA expressions of pro-inflammatory cytokines in those animals which were not different from vehicle-treated obese controls. However, there seems to be a lower abundance in $CD68^{+}$ macrophages, which is derived from monocytes in the OB-HAu mice but not OB-LAu mice. Thus, AuNPs treatment may alter ATMs inflammatory responses with a dose independent manner either through the reduction of CLS at extremely low dose or potentially reduce recruitment of monocyte at high dose.

The accumulation of excess lipids in the hepatocytes correlates with the increase in adiposity leading to liver steatosis, commonly accompanied with long term HFD-induced obesity (Shoelson, Herrero & Naaz 2007). Similar to that in adipocytes, steatosis also induced low grade inflammatory response and activation of Kupffer cell

(liver resident macrophages) in the liver of the obese mice (Cai et al. 2005; Olefsky & Glass 2010). Expressions of liver macrophage markers, CD68 and F4/80 as well as pro-inflammatory cytokines including TNF-α, IL-1β, IL-6, TLR-4, and SAA-1 were all significantly upregulated vehicle-treated obese mice indicating an activation of liver Kupffer cells, consistent with hepatic steatosis. The heterogeneity of Kupffer cells depends on their size and/or location in the liver. According to Kinoshita et al. (2010), most $F4/80^+$ Kupffer cells in normal mice are mainly $CD68^+$ with potent phagocytic and ROS-producing activities, while the $CD11b^+$ $F4/80^+$ Kupffer cells showed a strong cytokine-producing capacity (Kinoshita et al. 2010). Interestingly, expression of both populations of Kupffer cells was supressed by AuNP treatment. In line with that, liver TNF-α, IL-1β, and TLR-4 mRNA expression levels were also significantly downregulated in the OB-EAu and OB-LAu groups that experienced weight loss but not OB-HAu group. Therefore, AuNPs treatment at lower doses may improve inflammation in the liver which is a critical component of hepatic steatosis.

Long term chronic energy surplus often contributes to dyslipidaemia commonly associated with metabolic disorders such as, insulin resistance and cardiovascular disease risk (Bays et al. 2008; Bergman et al. 2001). In the present study, AuNPs regulate various adipokine mRNA levels that were evaluated in the adipose tissue of the obese mice. The expression of adipose-specific hormone, leptin was selectively reduced in OB-HAu mice but not OB-EAu or OB-LAu groups in this study albeit significant fat loss in the latter. This may suggest that AuNP somewhat stimulate leptin production, which may play a role in reduced fat mass and improved lipid metabolism. Both OB-LAu and OB-HAu mice showed significantly downregulated SREBP-1c mRNA expressions in the adipose tissue, suggesting a reduction of *de novo* lipid and fatty acid biosynthesis. Moreover, the expression of CPT-1α mRNA was significantly upregulated in both OB-EAu and OB-LAu mice, suggesting an improved mitochondrial fatty acid oxidation. Thus, AuNPs be improve lipid metabolism in obese mice allowing better control of dyslipidaemia, which may in turn reduce the risk of cardiovascular diseases in the obese mice.

The fatty liver is likely to contribute to insulin resistance (Browning & Horton 2004; Roden 2006). Studies have shown amelioration of hepatic insulin resistance in HFD-fed

rats through the reduction in of liver fat accumulation or hepatic steatosis (Samuel et al. 2004). In the vehicle treated-obese mice, mRNA expression of SREBP-1c and FASN which are crucial for lipogenesis and fatty acid biogenesis respectively was significantly upregulated indicative of the development of liver steatosis; while hepatic PEPCK and FOXO1 mRNA levels were also significantly upregulated suggesting an increase in gluconeogenesis. In response to the chronic excessive circulating lipid and glucose levels, liver ATGL, CPT-1α, PPARγ, and GLUT-4 mRNA levels were elevated in the vehicle-treated obese mice. In AuNP-treated obese mice, lipogenic gene expression such as SREBP-1c and FASN was significantly downregulated, suggesting reduced hepatic *de novo* synthesis of lipid and fatty acids. The significant downregulation of liver PEPCK and FOXO1 mRNA expression by AuNP also suggests a reduced in hepatic gluconeogenesis and improved glycaemic control. Consistent with previous animal work, the restorative effect of AuNP treatment on the liver against the adverse effect of HFD feeding was remarkable with an improvement in liver enzymatic AST levels. Taken together, these findings suggest that AuNP treatment can restore liver integrity through amelioration of hepatic steatosis and thereby hepatic insulin resistance. Therefore, AuNPs may significantly lower the risk of developing obesity-related complications such as type 2 diabetes.

Due to the size of AuNP, they were preferentially eliminated via the reticuloendothelial system such as liver and spleen, while limited excretion through the renal system by kidneys, consistent with previous animal study (Abdelhalim 2013; Balasubramanian et al. 2010). Highest Au levels were found in the abdominal fat suggesting that injected AuNPs were absorbed from the peritoneal cavity into the surrounding adipose tissue and then distributed to the other tissue via the circulation (Abdelhalim 2013; Chen et al. 2013). Most importantly, AuNP-treatment did not cause measureable liver toxicity or cell damage.

In summary, our results suggest AuNPs may regulate macrophage recruitment to reduce local inflammation which may be one of the key mechanisms in improved lipid and glucose metabolic markers in adipose tissue and liver in the mice with pre-existing obesity. The positive outcomes observed in this study entails further investigation to confirm the therapeutic value of AuNPs and their anti-obesity and anti-diabetic

properties in ob/ob and db/db obese mice models. The AuNP treatment strategy is promising for managing body weight and glucose control in the obese and diabetic populations.

CHAPTER 6

Future Studies and Conclusions

6. Future studies and conclusions

In this work, 21 nm citrate-stabilized, unmodified or "naked" AuNPs were robustly synthesized using a citrate sol method. The "naked" AuNPs used were spherical in shape, exhibited a surface plasmon resonance peak of 520 nm, core particle size of 22.33 ± 1.45 nm, and a hydrodynamic diameter of 20–30 nm.

In this study, surface modified AuNPs using short-chain and long-chain heterobifunctionalized PEGs also known as MPCs exhibited increase colloidal stability with functional ends that allow anti-CD31 antibody conjugation. Our results showed that both the anti-CD31 conjugated MPCs were more target specific in the labelling of endothelial cells surface antigen CD31, while the unmodified AuNPs showed non-specific accumulation and cellular uptake by endothelial cells. No difference were observed in the cytotoxicity and biocompatibility between the modified and unmodified AuNPs. In fact, there has been an increased exploitation of "naked" AuNPs in biomedical applications attributed to their unique ability of non-selectively accumulate and internalized by all the cell types studied. Due to the multi-step surface modification, anti-CD31 conjugated MPCs showed significant a batch-to-batch variation on the upscale production. There needs to be more studies will be required to further control the monolayer self-assembly of mixed hetero-bifunctionalized PEGs and characterize the available functional ends for biomolecules conjugation.

Our *in vitro* studies suggest that the cellular uptake of AuNPs may induced an inflammatory response in un-stimulated/quiescent RAW264.7 macrophages, but suppressed inflammatory responses in LPS-stimulated PMA-differentiated U937 macrophage-like cells. Both the murine RAW264.7 and human U937 cells are immortalized monocytic cell lines that require activation to become macrophage-like *in vitro* capable of secreting inflammatory cytokine. Therefore, a tissue-derived activated macrophages may be a better *in vitro* model to examine the impact of AuNP on the alterations of inflammatory responses. We propose the use of primary macrophages isolated from peritoneal cavity with AuNPs in the future where the secreted levels of pro-inflammatory and anti-inflammatory cytokines in supernatant are collected and analyzed.

In Chapter 3, the improved adipocyte metabolic markers and reduced inflammatory responses by AuNPs observed in adipocyte-macrophages co-cultures but not adipocyte only cultures, further highlight the complex interaction between adipocyte-macrophage *in vitro*. Here, we showed the limitations in the use of single cell lines to investigate cellular responses to AuNP and it would be beneficial to repeat in future using a co-culture setting, more closely resembles a physiological *in vivo* system. In order to corroborate our preliminary findings and further elucidate the effect by AuNPs, further co-culture studies using primary peritoneal macrophages and adipocytes isolated the peritoneal cavity are essential. Overall consideration of our cell studies, led to our hypothesis that daily treatment with AuNPs can potentially alter the inflammatory response and regulate lipid and glucose metabolism associated with obesity using an in vivo mice model.

In our first animal study (Chapter 4), we have demonstrated that 9 weeks daily IP injection of AuNPs can protect mice against the development of HFD-induced glucose intolerance and improve their blood lipid profile. The results suggest that the alterations of ATM activity and local inflammatory environment may be the key underlying reduced adipose tissue mass and weight reduction observed in the HFD-fed mice receiving concurrent daily AuNP treatment. Further analysis are required to understand the impact of AuNPs on the chronic systemic inflammation in HFD-induced obesity mice by measurement of serum levels of C-reactive protein (CRP) and pro-inflammatory cytokines, such as TNFα and IL-6. In the future, we could potentially further investigate the AuNPs in other inflammatory conditions, such as rheumatoid arthritis. In addition, we could employ a TNFa knockout system to see if the effect of AuNPs in altering the inflammatory environment is dependent to TNFa. However, we do not negate that it is possible that some other mechanism is in play causing the improved glucose and lipid metabolism, as well as reduced inflammation.

Our study was the first to study 9 weeks continuous daily administration of AuNPs. Although our results showed that AuNPs do not induce toxicity in the liver but seem to exert a protective effect against the adverse effect of HFD in the HFD-fed mice, it should be emphasized that AuNPs are not biodegradable. Therefore, the biodistribution and excretion kinetics have to be studied comprehensively to further determine the

long-term safety of AuNPs. In the future, other organs including excretions (urine and feaces) should also be collected for whole organ dissolution and measurement of gold ion concentrations. In particular, the functionality of the kidney can be determined by measuring the metabolites such as urea nitrogen and creatinine, while the hepatic and biliar functionality can be tested by measuring the total bilirubin and alkaline phosphatase in blood.

In our second animal study (Chapter 5), all obese mice would have developed chronic obesity with glucose intolerance and non-alcoholic fatty liver disease at 15 weeks of HFD feeding. Our results showed a significant weight loss effects at lower doses (OB-EAu and OB-LAu group) but not in high doses (OB-HAu) of AuNP treatment. There are no signs of fatigues or changes in fur conditions, therefore, it is unlikely that those mice were ill during the treatment.. It is noteworthy that the weight reductions observed with AuNP treatment were without any dietary interventions. This raises the future research question, whether controlling energy intake by switching to a healthy diet (normal rodent chow) during AuNP treatment could achieve an even better weight loss effect.

All the AuNP-treated obese mice in this study showed an improved glucose and lipid markers expression in the liver and amelioration of glucose intolerance. The reduced hepatic inflammation seems to be the key underlying mechanism of AuNPs for the improved lipid and glucose metabolic marker in the liver, whereby improving glucose tolerance and preventing the onset of obesity-related metabolic diseases such as Type 2 diabetes and cardiovascular diseases. Therefore, it is necessary to examine the liver and skeletal muscle of AuNP-treated obese mice further to confirm if there is a reduced hepatic steatosis and insulin sensitivity. In addition, more experiments are necessary to understand the changes observed in the adipose tissue. Furthermore, it would also be interesting further elucidate if this promising anti-obesity and anti-diabetic effect of AuNPs on the HFD-induced obese model can be replicated in genetic modified models of obesity such as ob/ob and db/db mice.

In conclusion, our results have highlighted the key mechanisms by which AuNPs alter macrophage activity to reduce the local pro-inflammatory cytokine environment,

resulting in effective weight loss in the obese mice and amelioration of obesity related glucose and lipid disorders. Therefore, this novel treatment with AuNPs serves as a new paradigm for the prevention of obesity-related metabolic disorders and weight control.

CHAPTER 7

References

7. References:

Abdelhalim, M.A.K. 2013, 'Uptake of gold nanoparticles in several rat organs after intraperitoneal administration in vivo: a fluorescence study', *BioMed Research International*, vol. 2013, p. 353695.

ABS 2009, *Australian Social Trends, Smoking, risky drinking, and obesity*, Austrlia Bureau of Statistics (ABS), Canberra.

ABS 2012, *Australian health survery: First results, 2011-12*, Australian Bureau of Statistics (ABS), Canberra.

Adams, T.D., Gress, R.E., Smith, S.C., Halverson, R.C., Simper, S.C., Rosamond, W.D., LaMonte, M.J., Stroup, A.M. & Hunt, S.C. 2007, 'Long-term mortality after gastric bypass surgery', *New England Journal of Medicine*, vol. 357, no. 8, pp. 753-61.

Ahima, R.S. 2009, 'Connecting obesity, aging and diabetes', *Nature Medicine*, vol. 15, no. 9, pp. 996-7.

Aiello, L.P., Avery, R.L., Arrigg, P.G., Keyt, B.A., Jampel, H.D., Shah, S.T., Pasquale, L.R., Thieme, H., Iwamoto, M.A. & Park, J.E. 1994, 'Vascular endothelial growth factor in ocular fluid of patients with diabetic retinopathy and other retinal disorders', *New England Journal of Medicine*, vol. 331, no. 22, pp. 1480-7.

Aillon, K.L., Xie, Y., El-Gendy, N., Berkland, C.J. & Forrest, M.L. 2009, 'Effects of nanomaterial physicochemical properties on in vivo toxicity', *Advanced Drug Delivery Reviews*, vol. 61, no. 6, pp. 457-66.

Akira, S. & Takeda, K. 2004, 'Toll-like receptor signalling', *Nature Reviews Immunology*, vol. 4, no. 7, pp. 499-511.

Akira, S., Uematsu, S. & Takeuchi, O. 2006, 'Pathogen recognition and innate immunity', *Cell*, vol. 124, no. 4, pp. 783-801.

Alberti, K.G.M., Zimmet, P., Shaw, J. & Group, I.E.T.F.C. 2005, 'The metabolic syndrome—a new worldwide definition', *The Lancet*, vol. 366, no. 9491, pp. 1059-62.

Alkhouri, N., Gornicka, A., Berk, M.P., Thapaliya, S., Dixon, L.J., Kashyap, S., Schauer, P.R. & Feldstein, A.E. 2010, 'Adipocyte apoptosis, a link between obesity, insulin resistance, and hepatic steatosis', *Journal of Biological Chemistry*, vol. 285, no. 5, pp. 3428-38.

Alkilany, A.M. & Murphy, C.J. 2010, 'Toxicity and cellular uptake of gold nanoparticles: what we have learned so far?', *Journal of Nanoparticle Research*, vol. 12, no. 7, pp. 2313-33.

Altiok, S., Xu, M. & Spiegelman, B.M. 1997, 'PPARγ induces cell cycle withdrawal: inhibition of E2F/DP DNA-binding activity via down-regulation of PP2A', *Genes & Development*, vol. 11, no. 15, pp. 1987-98.

Anderson, J.W., Kendall, C.W.C. & Jenkins, D.J.A. 2003, 'Importance of weight management in type 2 diabetes: review with meta-analysis of clinical studies', *Journal of the American College of Nutrition*, vol. 22, no. 5, pp. 331-9.

Aslan, K., Lakowicz, J.R. & Geddes, C.D. 2005, 'Plasmon light scattering in biology and medicine: new sensing approaches, visions and perspectives', *Current Opinion in Chemical Biology*, vol. 9, no. 5, pp. 538-44.

Balasubramanian, S.K., Jittiwat, J., Manikandan, J., Ong, C.-N., Yu, L.E. & Ong, W.-Y. 2010, 'Biodistribution of gold nanoparticles and gene expression changes in the liver and spleen after intravenous administration in rats', *Biomaterials*, vol. 31, no. 8, pp. 2034-42.

BarathManiKanth, S., Kalishwaralal, K., Sriram, M., Pandian, S.R.K., Youn, H.-s., Eom, S. & Gurunathan, S. 2010, 'Anti-oxidant effect of gold nanoparticles restrains hyperglycemic conditions in diabetic mice', *Journal of Nanobiotechnology*, vol. 8, no. 16, pp. 1-15.

Barrera, G. 2012, 'Oxidative stress and lipid peroxidation products in cancer progression and therapy', *ISRN Oncology*, vol. 2012.

Bastard, J.-P., Jardel, C., Bruckert, E., Blondy, P., Capeau, J., Laville, M., Vidal, H. & Hainque, B. 2000a, 'Elevated levels of interleukin 6 are reduced in serum and subcutaneous adipose tissue of obese women after weight loss', *J Clin Endocrinol Metab*, vol. 85, no. 9, pp. 3338-42.

Bastard, J.-P., Jardel, C., Bruckert, E., Blondy, P., Capeau, J., Laville, M., Vidal, H. & Hainque, B. 2000b, 'Elevated Levels of Interleukin 6 Are Reduced in Serum and Subcutaneous Adipose Tissue of Obese Women after Weight Loss 1', *The Journal of Clinical Endocrinology & Metabolism*, vol. 85, no. 9, pp. 3338-42.

Bauer, S.M., Bauer, R.J. & Velazquez, O.C. 2005, 'Angiogenesis, vasculogenesis, and induction of healing in chronic wounds', *Vascular & Endovascular Surgery*, vol. 39, no. 4, pp. 293-306.

Bays, H.E., González-Campoy, J.M., Bray, G.A., Kitabchi, A.E., Bergman, D.A., Schorr, A.B., Rodbard, H.W. & Henry, R.R. 2008, 'Pathogenic potential of adipose tissue and metabolic consequences of adipocyte hypertrophy and increased visceral adiposity', *Expert Review of Cardiovascular Therapy*, vol. 6, no. 3, pp. 343-68.

Berger, J. & Moller, D.E. 2002, 'The mechanisms of action of PPARs', *Annual Review of Medicine*, vol. 53, no. 1, pp. 409-35.

Berger, N.A. 2015, 'Murine Models, Energy Balance, and Cancer', *Energy*.

Berghaus, L.J., Moore, J.N., Hurley, D.J., Vandenplas, M.L., Fortes, B.P., Wolfert, M.A. & Boons, G.-J. 2010, 'Innate immune responses of primary murine macrophage-lineage cells and RAW 264.7 cells to ligands of Toll-like receptors 2, 3, and 4', *Comparative Immunology, Microbiology and Infectious Diseases*, vol. 33, no. 5, pp. 443-54.

Bergman, R.N., Van Citters, G.W., Mittelman, S.D., Dea, M.K., Hamilton-Wessler, M., Kim, S.P. & Ellmerer, M. 2001, 'Central role of the adipocyte in the metabolic syndrome', *Journal of Investigative Medicine*, vol. 49, no. 1, pp. 119-26.

Blackburn, G.L. 1999, 'Benefits of weight loss in the treatment of obesity', *American Journal of Clinical Nutrition*, vol. 69, no. 3, pp. 347-9.

Boisselier, E. & Astruc, D. 2009, 'Gold nanoparticles in nanomedicine: preparations, imaging, diagnostics, therapies and toxicity', *Chemical Society Reviews*, vol. 38, no. 6, pp. 1759-82.

Boonstra, J. & Post, J.A. 2004, 'Molecular events associated with reactive oxygen species and cell cycle progression in mammalian cells', *Gene*, vol. 337, pp. 1-13.

Bouchard, C. & Tremblay, A. 1997, 'Genetic influences on the response of body fat and fat distribution to positive and negative energy balances in human identical twins', *Journal of Nutrition*, vol. 127, no. 5, pp. 943S-7S.

Bray, G.A. & Ryan, D.H. 2014, 'Update on obesity pharmacotherapy', *Annals of the New York Academy of Sciences*, vol. 1311, no. 1, pp. 1-13.

Brown, D.A. 2001, 'Lipid droplets: Proteins floating on a pool of fat', *Current Biology*, vol. 11, no. 11, pp. R446-R9.

Browning, J.D. & Horton, J.D. 2004, 'Molecular mediators of hepatic steatosis and liver injury', *Journal of Clinical Investigation*, vol. 114, no. 2, pp. 147-52.

Brun, R.P., Kim, J.B., Hu, E., Altiok, S. & Spiegelman, B.M. 1996, 'Adipocyte differentiation: a transcriptional regulatory cascade', *Current Opinion in Cell Biology*, vol. 8, no. 6, pp. 826-32.

Bryant, N.J., Govers, R. & James, D.E. 2002, 'Regulated transport of the glucose transporter GLUT4', *Nature Reviews Molecular Cell Biology*, vol. 3, no. 4, pp. 267-77.

Buchwald, H., Avidor, Y., Braunwald, E., Jensen, M.D., Pories, W., Fahrbach, K. & Schoelles, K. 2004, 'Bariatric surgery: a systematic review and meta-analysis', *Journal of American Medical Association*, vol. 292, no. 14, pp. 1724-37.

Bustin, S.A. 2000, 'Absolute quantification of mRNA using real-time reverse transcription polymerase chain reaction assays', *Journal of molecular endocrinology*, vol. 25, no. 2, pp. 169-93.

Cai, D., Yuan, M., Frantz, D.F., Melendez, P.A., Hansen, L., Lee, J. & Shoelson, S.E. 2005, 'Local and systemic insulin resistance resulting from hepatic activation of IKK-β and NF-κB', *Nature Medicine*, vol. 11, no. 2, pp. 183-90.

Cai, Q.Y., Kim, S.H., Choi, K.S., Kim, S.Y., Byun, S.J., Kim, K.W., Park, S.H., Juhng, S.K. & Yoon, K.H. 2007, 'Colloidal gold nanoparticles as a blood-pool contrast agent for X-ray computed tomography in mice', *Investigative Radiology*, vol. 42, no. 12, pp. 797-806.

Cao, Y. 2010, 'Adipose tissue angiogenesis as a therapeutic target for obesity and metabolic diseases', *Nature Reviews Drug Discovery*, vol. 9, no. 2, pp. 107-15.

Carmeliet, P. 2003, 'Angiogenesis in health and disease', *Nature Medicine*, vol. 9, no. 6, pp. 653-60.

Cawthorn, W.P. & Sethi, J.K. 2008, 'TNF-α and adipocyte biology', *FEBS letters*, vol. 582, no. 1, pp. 117-31.

Chakravarty, K., Leahy, P., Becard, D., Hakimi, P., Foretz, M., Ferre, P., Foufelle, F. & Hanson, R.W. 2001, 'Sterol regulatory element-binding protein-1c mimics the negative effect of insulin on phosphoenolpyruvate carboxykinase (GTP) gene transcription', *Journal of Biological Chemistry*, vol. 276, no. 37, pp. 34816-23.

Chandra, P., Das, D. & Abdelwahab, A.A. 2010, 'Gold nanoparticles in molecular diagnostics and therapeutics', *Digest Journal of Nanomaterials and Biostructures*, vol. 5, no. 5, pp. 363–7.

Chen, H., Dorrigan, A., Saad, S., Hare, D.J., Cortie, M.B. & Valenzuela, S.M. 2013, 'In Vivo Study of Spherical Gold Nanoparticles: Inflammatory Effects and Distribution in Mice', *PLoS ONE*, vol. 8, no. 2, p. e58208.

Chen, H., Iglesias, M.A., Caruso, V. & Morris, M.J. 2011, 'Maternal cigarette smoke exposure contributes to glucose intolerance and decreased brain insulin action in mice offspring independent of maternal diet', *PloS One*, vol. 6, no. 11, p. e27260.

Chen, H., Simar, D., Pegg, K., Saad, S., Palmer, C. & Morris, M. 2014, 'Exendin-4 is effective against metabolic disorders induced by intrauterine and postnatal overnutrition in rodents', *Diabetologia*, vol. 57, no. 3, pp. 614-22.

Chen, Y.-S., Hung, Y.-C., Liau, I. & Huang, G. 2009, 'Assessment of the in vivo toxicity of gold nanoparticles', *Nanoscale Research Letters*, vol. 4, no. 8, pp. 858-64.

Chithrani, B.D., Ghazani, A.A. & Chan, W.C. 2006a, 'Determining the size and shape dependence of gold nanoparticle uptake into mammalian cells', *Nano letters*, vol. 6, no. 4, pp. 662-8.

Chithrani, B.D., Ghazani, A.A. & Chan, W.C.W. 2006b, 'Determining the size and shape dependence of gold nanoparticle uptake into mammalian cells', *Nano Letters*, vol. 6, no. 4, pp. 662-8.

Chithrani, B.D., Stewart, J., Allen, C. & Jaffray, D.A. 2009, 'Intracellular uptake, transport, and processing of nanostructures in cancer cells', *Nanomedicine: Nanotechnology, Biology and Medicine*, vol. 5, no. 2, pp. 118-27.

Cho, E.C., Xie, J., Wurm, P.A. & Xia, Y. 2009, 'Understanding the role of surface charges in cellular adsorption versus internalization by selectively removing gold

nanoparticles on the cell surface with a I2/KI etchant', *Nano letters*, vol. 9, no. 3, pp. 1080-4.

Cho, E.C., Zhang, Q. & Xia, Y. 2011, 'The effect of sedimentation and diffusion on cellular uptake of gold nanoparticles', *Nature Nanotechnology*, vol. 6, no. 6, pp. 385-91.

Cho, W.-S., Cho, M., Jeong, J., Choi, M., Han, B.S., Shin, H.-S., Hong, J., Chung, B.H., Jeong, J. & Cho, M.-H. 2010, 'Size-dependent tissue kinetics of PEG-coated gold nanoparticles', *Toxicology and Applied Pharmacology*, vol. 245, no. 1, pp. 116-23.

Chomczynski, P. 1993, 'A reagent for the single-step simultaneous isolation of RNA, DNA and proteins from cell and tissue samples', *Biotechniques*, vol. 15, no. 3, pp. 532-6.

Christiaens, V. & Lijnen, H.R. 2010, 'Angiogenesis and development of adipose tissue', *Mol Cell Endocrinol*, vol. 318, no. 1-2, pp. 2-9.

Cinti, S., Mitchell, G., Barbatelli, G., Murano, I., Ceresi, E., Faloia, E., Wang, S., Fortier, M., Greenberg, A.S. & Obin, M.S. 2005, 'Adipocyte death defines macrophage localization and function in adipose tissue of obese mice and humans', *Journal of Lipid Research*, vol. 46, no. 11, pp. 2347-55.

Colagiuri, S., Lee, C.M., Colagiuri, R., Magliano, D., Shaw, J.E., Zimmet, P.Z. & Caterson, I.D. 2010, 'The cost of overweight and obesity in Australia', *The Medical Journal of Australia*, vol. 192, no. 5, pp. 260-4.

Colman, E., Golden, J., Roberts, M., Egan, A., Weaver, J. & Rosebraugh, C. 2012, 'The FDA's assessment of two drugs for chronic weight management', *New England Journal of Medicine*, vol. 367, no. 17, pp. 1577-9.

Connor, E.E., Mwamuka, J., Gole, A., Murphy, Catherine J. & Wyatt, Michael D. 2005, 'Gold nanoparticles are taken up by human cells but do not cause acute cytotoxicity', *Small*, vol. 1, no. 3, pp. 325-7.

Coppack, S.W. 2001, 'Pro-inflammatory cytokines and adipose tissue', *Proceedings of the Nutrition Society*, vol. 60, no. 03, pp. 349-56.

Cornelius, P., Enerback, S., Bjursell, G., Olivecrona, T. & Pekala, P.H. 1988a, 'Regulation of lipoprotein lipase mRNA content in 3T3-L1 cells by tumour necrosis factor', *Biochemical Journal*, vol. 249, pp. 765-9.

Cornelius, P., Enerback, S., Bjursell, G., Olivecrona, T. & Pekala, P.H. 1988b, 'Regulation of lipoprotein lipase mRNA content in 3T3-L1 cells by tumour necrosis factor.', *Biochem J*, vol. 249, no. 3, pp. 765-9.

Craig, G.A., Allen, P.J., Mason, M.D. & Grobmyer, S.R. 2010, 'Synthesis, characterization, and functionalization of gold nanoparticles for cancer imaging', *Methods in Molecular Biology*, vol. 624, pp. 177-93.

Daneschvar, H.L., Aronson, M.D. & Smetana, G.W. 2016, 'FDA-Approved Anti-Obesity Drugs in the United States', *The American Journal of Medicine*, vol. 129, no. 8, pp. 879.e1-.e6.

Das, K. & Kar, P. 2005, 'Non alcoholic steatohepatitis', *The Journal of the Association of Physicians of India*, vol. 53, pp. 195-9.

De Franceschi, S. & Kouwenhoven, L. 2002, 'Nanotechnology: Electronics and the single atom', *Nature*, vol. 417, no. 6890, pp. 701-2.

De Jong, W.H., Hagens, W.I., Krystek, P., Burger, M.C., Sips, A.J.A.M. & Geertsma, R.E. 2008, 'Particle size-dependent organ distribution of gold nanoparticles after intravenous administration', *Biomaterials*, vol. 29, no. 12, pp. 1912-9.

Diez, J.J. & Iglesias, P. 2003, 'The role of the novel adipocyte-derived hormone adiponectin in human disease', *European Journal of Endocrinology*, vol. 148, no. 3, pp. 293-300.

Dobbins, R.L., Szczepaniak, L.S., Bentley, B., Esser, V., Myhill, J. & McGarry, J.D. 2001, 'Prolonged inhibition of muscle carnitine palmitoyltransferase-1 promotes intramyocellular lipid accumulation and insulin resistance in rats', *Diabetes*, vol. 50, no. 1, pp. 123-30.

Donnelly, K.L., Smith, C.I., Schwarzenberg, S.J., Jessurun, J., Boldt, M.D. & Parks, E.J. 2005, 'Sources of fatty acids stored in liver and secreted via lipoproteins in patients with nonalcoholic fatty liver disease', *Journal of Clinical Investigation*, vol. 115, no. 5, pp. 1343-51.

Dreaden, E., Alkilany, A., Huang, X., Murphy, C. & El-Sayed, M. 2012, 'The golden age: gold nanoparticles for biomedicine', *Chemical Society Reviews*, vol. 41, no. 7, pp. 2740-79.

Dreaden, E., Austin, L., Mackey, M. & El-Sayed, M. 2012, 'Size matters: gold nanoparticles in targeted cancer drug delivery', *Therapeutic Delivery*, vol. 3, no. 4, pp. 457-78.

Eck, W., Craig, G., Sigdel, A., Ritter, G., Old, L.J., Tang, L., Brennan, M.F., Allen, P.J. & Mason, M.D. 2008a, 'PEGylated gold nanoparticles conjugated to monoclonal F19 antibodies as targeted labeling agents for human pancreatic carcinoma tissue', *ACS Nano*, vol. 2, no. 11, pp. 2263-72.

Eck, W., Craig, G., Sigdel, A., Ritter, G., Old, L.J., Tang, L., Brennan, M.F., Allen, P.J. & Mason, M.D. 2008b, 'PEGylated gold nanoparticles conjugated to monoclonal F19 antibodies as targeted labeling agents for human pancreatic carcinoma tissue', *American Chemical Society Nano*, vol. 2, no. 11, pp. 2263-72.

Edvardsson, U., Bergström, M., Alexandersson, M., Bamberg, K., Ljung, B. & Dahllöf, B. 1999, 'Rosiglitazone (BRL49653), a PPARγ-selective agonist, causes peroxisome proliferator-like liver effects in obese mice', *Journal of Lipid Research*, vol. 40, no. 7, pp. 1177-84.

El-Sayed, I.H., Huang, X. & El-Sayed, M.A. 2005, 'Surface plasmon resonance scattering and absorption of anti-EGFR antibody conjugated gold nanoparticles in cancer diagnostics: applications in oral cancer', *Nano Letters*, vol. 5, no. 5, pp. 829-34.

El-Sayed, M.A. 2001, 'Some interesting properties of metals confined in time and nanometer space of different shapes', *Accounts of Chemical Research*, vol. 34, no. 4, pp. 257-64.

Eustis, S. & El-Sayed, M.A. 2006, 'Why gold nanoparticles are more precious than pretty gold: noble metal surface plasmon resonance and its enhancement of the radiative and nonradiative properties of nanocrystals of different shapes', *Chemical Society Reviews*, vol. 35, no. 3, pp. 209-17.

Faraday, M. 1857, 'The Bakerian lecture: experimental relations of gold (and other metals) to light', *Philosophical Transactions of the Royal Society of London*, vol. 147, pp. 145-81.

Faulk, W.P. & Taylor, G.M. 1971, 'An immunocolloid method for the electron microscope', *Immunochemistry*, vol. 8, no. 11, pp. 1081-3.

Ferreira, G.K., Cardoso, E., Vuolo, F.S., Galant, L.S., Michels, M., Gonçalves, C.L., Rezin, G.T., Dal-Pizzol, F., Benavides, R. & Alonso-Núñez, G. 2017, 'Effect of acute and long-term administration of gold nanoparticles on biochemical parameters in rat brain', *Materials Science and Engineering: C*, vol. 79, pp. 748-55.

Fischer, H.C. & Chan, W.C.W. 2007, 'Nanotoxicity: the growing need for *in vivo* study', *Current Opinion in Biotechnology*, vol. 18, no. 6, pp. 565-71.

Folch, J., Lees, M. & Sloane-Stanley, G.H. 1957, 'A simple method for the isolation and purification of total lipids from animal tissues', *Journal of Biological Chemistry*, vol. 226, no. 1, pp. 497-509.

Folkman, J. 1995, 'Angiogenesis in cancer, vascular, rheumatoid and other disease', *Nature Medicine*, vol. 1, no. 1, pp. 27-30.

Folkman, J. & Shing, Y. 1992, 'Angiogenesis', *Journal of Biological Chemistry*, vol. 267, no. 16, pp. 10931-4.

Fontaine, K.R., Redden, D.T., Wang, C., Westfall, A.O. & Allison, D.B. 2003, 'Years of life lost due to obesity', *Journal of American Medical Association*, vol. 289, no. 2, pp. 187-93.

Frandsen, J., Pedersen, S.B. & Richelsen, B. 1998, 'Long term follow up of patients who underwent jejunoileal bypass for morbid obesity', *The European Journal of Surgery*, vol. 164, no. 4, pp. 281-6.

Fredrick, A. 2006, *Textbook of Food and Nutrition*, Lotus Press, New Delhi.

Frens, G. 1973, 'Controlled nucleation for the regulation of the particle size in monodisperse gold suspensions', *Nature*, vol. 241, no. 105, pp. 20-2.

Gaggini, M., Morelli, M., Buzzigoli, E., DeFronzo, R.A., Bugianesi, E. & Gastaldelli, A. 2013, 'Non-alcoholic fatty liver disease (NAFLD) and its connection with insulin resistance, dyslipidemia, atherosclerosis and coronary heart disease', *Nutrients*, vol. 5, no. 5, pp. 1544-60.

Gaidhu, M.P., Anthony, N.M., Patel, P., Hawke, T.J. & Ceddia, R.B. 2010, 'Dysregulation of lipolysis and lipid metabolism in visceral and subcutaneous adipocytes by high-fat diet: role of ATGL, HSL, and AMPK', *American Journal of Physiology - Cell Physiology*, vol. 298, no. 4, pp. C961-C71.

Gardner, G., Halweil, B. & Peterson, J.A. 2000, *Underfed and overfed: the global epidemic of malnutrition*, vol. 150, Worldwatch Institute Washington, DC.

Ghosh, S. & Karin, M. 2002, 'Missing Pieces in the NF-κB Puzzle', *Cell*, vol. 109, no. 2, Supplement 1, pp. S81-S96.

Goossens, G.H. 2008, 'The role of adipose tissue dysfunction in the pathogenesis of obesity-related insulin resistance', *Physiology & Behavior*, vol. 94, no. 2, pp. 206-18.

Green, H. & Kehinde, O. 1975, 'An established preadipose cell line and its differentiation in culture II. Factors affecting the adipose conversion', *Cell*, vol. 5, no. 1, pp. 19-27.

Green, H. & Meuth, M. 1974, 'An established pre-adipose cell line and its differentiation in culture', *Cell*, vol. 3, no. 2, pp. 127-33.

Greenway, F.L., Fujioka, K., Plodkowski, R.A., Mudaliar, S., Guttadauria, M., Erickson, J., Kim, D.D., Dunayevich, E. & Group, C.-I.S. 2010, 'Effect of naltrexone plus bupropion on weight loss in overweight and obese adults (COR-I): a multicentre, randomised, double-blind, placebo-controlled, phase 3 trial', *The Lancet*, vol. 376, no. 9741, pp. 595-605.

Gregoire, F.M., Smas, C.M. & Sul, H.S. 1998, *Understanding adipocyte differentiation*, Journal Article, vol. 78.

Griffith, L.G. & Swartz, M.A. 2006, 'Capturing complex 3D tissue physiology in vitro', *Nature Reviews Molecular Cell Biology*, vol. 7, no. 3, pp. 211-24.

Grundy, S.M., Brewer, H.B., Cleeman, J.I., Smith, S.C. & Lenfant, C. 2004, 'Definition of metabolic syndrome report of the National Heart, Lung, and Blood Institute/American Heart Association Conference on scientific issues related to definition', *Circulation*, vol. 109, no. 3, pp. 433-8.

Guerciolini, R. 1997, 'Mode of action of orlistat', *International journal of obesity and related metabolic disorders: journal of the International Association for the Study of Obesity*, vol. 21, pp. S12-23.

Guha, M. & Mackman, N. 2001, 'LPS induction of gene expression in human monocytes', *Cellular Signalling*, vol. 13, no. 2, pp. 85-94.

Han, T., Van Leer, E., Seidell, J. & Lean, M. 1995, 'Waist circumference action levels in the identification of cardiovascular risk factors: prevalence study in a random sample', *British Medical Journal*, vol. 311, no. 7017, pp. 1401-5.

Hauner, H., Petruschke, T., Russ, M., Rohrig, K. & Eckel, J. 1995, 'Effects of tumour necrosis factor alpha (TNF alpha) on glucose transport and lipid metabolism of newly-differentiated human fat cells in cell culture.', *Diabetologia*, vol. 38, no. 7, pp. 764-71.

Hauner, H., Petruschke, T.H., Russ, M., Röhrig, K. & Eckel, J. 1995, 'Effects of tumour necrosis factor alpha (TNFα) on glucose transport and lipid metabolism of newly-differentiated human fat cells in cell culture', *Diabetologia*, vol. 38, no. 7, pp. 764-71.

Hayat, M.A. 1989, *Colloidal Gold. Principles, Methods, and Applications*, Academic Press, San Diego, CA.

Heilbronn, L.K. & Campbell, L.V. 2008, 'Adipose tissue macrophages, low grade inflammation and insulin resistance in human obesity', *Current Pharmaceutical Design*, vol. 14, no. 12, pp. 1225-30.

Hermann, R., Walther, P. & Müller, M. 1996, 'Immunogold labeling in scanning electron microscopy', *Histochemistry and Cell Biology*, vol. 106, no. 1, pp. 31-9.

Herrwerth, S., Rosendahl, T., Feng, C., Fick, J., Eck, W., Himmelhaus, M., Dahint, R. & Grunze, M. 2003, 'Covalent coupling of antibodies to self-assembled monolayers of carboxy-functionalized poly (ethylene glycol): protein resistance and specific binding of biomolecules', *Langmuir*, vol. 19, no. 5, pp. 1880-7.

Hill, A.A., Reid Bolus, W. & Hasty, A.H. 2014, 'A decade of progress in adipose tissue macrophage biology', *Immunological reviews*, vol. 262, no. 1, pp. 134-52.

Hill, J., Dorton, J., Sykes, M. & Digirolamo, M. 1988, 'Reversal of dietary obesity is influenced by its duration and severity', *International Journal of Obesity*, vol. 13, no. 5, pp. 711-22.

Hill, J.O., Melanson, E.L. & Wyatt, H.T. 2000, 'Dietary fat intake and regulation of energy balance: implications for obesity', *Journal of Nutrition*, vol. 130, no. 2, pp. 284S-8S.

Hiller, W. & Erich, C. 1999, 'Chapter 3: Gold and its compounds', in D. Breitinger & W. Herrmann (eds), *Synthetic Methods of Organometallic and Inorganic Chemistry*, George Thieme Verlag, Stuttgart, pp. 56-108.

Hillyer, J.F. & Albrecht, R.M. 2001, 'Gastrointestinal persorption and tissue distribution of differently sized colloidal gold nanoparticles', *Journal of Pharmaceutical Sciences*, vol. 90, no. 12, pp. 1927-36.

Hirschi, K.K. & D'Amore, P.A. 1997, 'Control of angiogenesis by the pericyte: molecular mechanisms and significance', in I.D. Goldberg & E.M. Rosen (eds), *Regulation of Angiogenesis*, Birkhauser Verlag, Basel, Switzerland, pp. 419-28.

Hotamisligil, G., Shargill, N. & Spiegelman, B. 1993a, 'Adipose expression of tumor necrosis factor-alpha: direct role in obesity-linked insulin resistance', *Science*, vol. 259, no. 5091, pp. 87-91.

Hotamisligil, G.S. 2006a, 'Inflammation and metabolic disorders', *Nature*, vol. 444, no. 7121, pp. 860-7.

Hotamisligil, G.S. 2006b, 'Inflammation and metabolic disorders', *Nature*, vol. 444, no. 7121, pp. 860-7.

Hotamisligil, G.S., Shargill, N.S. & Spiegelman, B.M. 1993b, 'Adipose expression of tumor necrosis factor-alpha: direct role in obesity-linked insulin resistance', *Science*, vol. 259, no. 5091, pp. 87-91.

Hu, F.B., Meigs, J.B., Li, T.Y., Rifai, N. & Manson, J.E. 2004, 'Inflammatory markers and risk of developing type 2 diabetes in women', *Diabetes*, vol. 53, no. 3, pp. 693-700.

Hu, M., Chen, J., Li, Z.-Y., Au, L., Hartland, G.V., Li, X., Marquez, M. & Xia, Y. 2006, 'Gold nanostructures: engineering their plasmonic properties for biomedical applications', *Chemical Society Reviews*, vol. 35, no. 11, pp. 1084-94.

Hyatt, A.D. & Eaton, B. 1992, *Immuno-gold electron microscopy in virus diagnosis and research*, CRC Press.

IDF 2006, *The IDF consensus worldwide definition of the metabolic syndrome*, International Diabetes Federation (IDF), Belgium.

Ioannides-Demos, L.L., Piccenna, L. & McNeil, J.J. 2010, 'Pharmacotherapies for obesity: past, current, and future therapies', *Journal of Obesity*, vol. 2011.

Janeway, C.A., Travers, P., Walport, M. & Shlomchik, M.J. 2001, *Immunobiology: the immune system in health and disease*, 5th Edn edn, Garland Science Publishing, New York.

Karakoti, A.S., Das, S., Thevuthasan, S. & Seal, S. 2011, 'PEGylated inorganic nanoparticles', *Angewandte Chemie International Edition*, vol. 50, no. 9, pp. 1980-94.

Kawai, T. & Akira, S. 2007, 'Signaling to NF-κB by toll-like receptors', *Trends in Molecular Medicine*, vol. 13, no. 11, pp. 460-9.

Kawakami, M., Murase, T., Ogawa, H., Ishibashi, S., Mori, N., Takaku, F. & Shibata, S. 1987, 'Human recombinant TNF suppresses lipoprotein lipase activity and stimulates lipolysis in 3T3-L1 cells.', *J Biochem (Tokyo)*, vol. 101, no. 2, pp. 331-8.

Keene, A.M., Peters, D., Rouse, R., Stewart, S., Rosen, E.T. & Tyner, K.M. 2012, 'Tissue and cellular distribution of gold nanoparticles varies based on aggregation/agglomeration status', *Nanomedicine*, vol. 7, no. 2, pp. 199-209.

Kelly, K.L., Coronado, E., Zhao, L.L. & Schatz, G.C. 2003, 'The optical properties of metal nanoparticles: the influence of size, shape, and dielectric environment', *Journal of Physical Chemistry B*, vol. 107, no. 3, pp. 668-77.

Kershaw, E.E. & Flier, J.S. 2004, 'Adipose tissue as an endocrine organ', *The Journal of Clinical Endocrinology & Metabolism*, vol. 89, no. 6, pp. 2548-56.

Khan, J.A., Pillai, B., Das, T.K., Singh, Y. & Maiti, S. 2007, 'Molecular effects of uptake of gold nanoparticles in HeLa cells', *ChemBioChem*, vol. 8, no. 11, pp. 1237-40.

Khlebtsov, N. & Dykman, L. 2011, 'Biodistribution and toxicity of engineered gold nanoparticles: a review of in vitro and in vivo studies', *Chemical Society Reviews*, vol. 40, no. 3, pp. 1647-71.

Kim, J.H., Kim, J.H., Kim, K.-W., Kim, M.H. & Yu, Y.S. 2009, 'Intravenously administered gold nanoparticles pass through the blood–retinal barrier depending on the particle size, and induce no retinal toxicity', *Nanotechnology*, vol. 20, no. 50, p. 505101.

Kinoshita, M., Uchida, T., Sato, A., Nakashima, M., Nakashima, H., Shono, S., Habu, Y., Miyazaki, H., Hiroi, S. & Seki, S. 2010, 'Characterization of two F4/80-positive Kupffer cell subsets by their function and phenotype in mice', *Journal of Hepatology*, vol. 53, no. 5, pp. 903-10.

Kolotkin, R., Meter, K. & Williams, G. 2001, 'Quality of life and obesity', *Obesity Reviews*, vol. 2, no. 4, pp. 219-29.

Kosteli, A., Sugaru, E., Haemmerle, G., Martin, J.F., Lei, J., Zechner, R. & Ferrante, A.W. 2010a, 'Weight loss and lipolysis promote a dynamic immune response in murine adipose tissue', *Journal of Clinical Investigation*, vol. 120, no. 10, pp. 3466-79.

Kosteli, A., Sugaru, E., Haemmerle, G., Martin, J.F., Lei, J., Zechner, R. & Ferrante, A.W. 2010b, 'Weight loss and lipolysis promote a dynamic immune response in murine adipose tissue', *J Clin Invest*, vol. 120, no. 10, pp. 3466-79.

Kral, J.G. & Näslund, E. 2007, 'Surgical treatment of obesity', *Nature Clinical Practice Endocrinology & Metabolism*, vol. 3, no. 8, pp. 574-83.

Krawczyk, M., Bonfrate, L. & Portincasa, P. 2010, 'Nonalcoholic fatty liver disease', *Best Practice & Research Clinical Gastroenterology*, vol. 24, no. 5, pp. 695-708.

Kuri-Harcuch, W. & Green, H. 1978, 'Adipose conversion of 3T3 cells depends on a serum factor', *Proceedings of the National Academy of Sciences*, vol. 75, no. 12, pp. 6107-9.

Lafontan, M. & Girard, J. 2008, 'Impact of visceral adipose tissue on liver metabolism: Part I: Heterogeneity of adipose tissue and functional properties of visceral adipose tissue', *Diabetes & Metabolism*, vol. 34, no. 4, Part 1, pp. 317-27.

Lanthier, N., Molendi-Coste, O., Horsmans, Y., van Rooijen, N., Cani, P.D. & Leclercq, I.A. 2010, 'Kupffer cell activation is a causal factor for hepatic insulin resistance', *American Journal of Physiology - Gastrointestinal and Liver Physiology*, vol. 298, no. 1, pp. G107-G16.

Lasagna-Reeves, C., Gonzalez-Romero, D., Barria, M.A., Olmedo, I., Clos, A., Sadagopa Ramanujam, V.M., Urayama, A., Vergara, L., Kogan, M.J. & Soto, C. 2010, 'Bioaccumulation and toxicity of gold nanoparticles after repeated administration in mice', *Biochemical and Biophysical Research Communications*, vol. 393, no. 4, pp. 649-55.

Lawrence, T. 2009, 'The nuclear factor NF-κB pathway in inflammation', *Cold Spring Harbor Perspectives in Biology*, vol. 1, no. 6, p. a001651.

LeBlanc, E.S., O'Connor, E., Whitlock, E.P., Patnode, C.D. & Kapka, T. 2011, 'Effectiveness of primary care–relevant treatments for obesity in adults: a systematic evidence review for the US Preventive Services Task Force', *Annals of Internal Medicine*, vol. 155, no. 7, pp. 434-47.

Lee, P.C. & Dixon, J. 2017, 'Pharmacotherapy for obesity', *Australian Family Physician*, vol. 46, no. 7, p. 472.

Leinonen, E., Hurt-Camejo, E., Wiklund, O., Hultén, L.M., Hiukka, A. & Taskinen, M.-R. 2003, 'Insulin resistance and adiposity correlate with acute-phase reaction and soluble cell adhesion molecules in type 2 diabetes', *Atherosclerosis*, vol. 166, no. 2, pp. 387-94.

Lemoine, A.Y., Ledoux, S. & Larger, E. 2013, 'Adipose tissue angiogenesis in obesity', *Thrombosis and Haemostasis*, vol. 110, no. 4, pp. 661-8.

Li, J.J., Hartono, D., Ong, C.-N., Bay, B.-H. & Yung, L.-Y.L. 2010, 'Autophagy and oxidative stress associated with gold nanoparticles', *Biomaterials*, vol. 31, no. 23, pp. 5996-6003.

Link, S. & El-Sayed, M.A. 1999, 'Spectral properties and relaxation dynamics of surface plasmon electronic oscillations in gold and silver nanodots and nanorods', *Journal of Physical Chemistry B*, vol. 103, no. 40, pp. 8410-26.

Lönn, M., Mehlig, K., Bengtsson, C. & Lissner, L. 2010, 'Adipocyte size predicts incidence of type 2 diabetes in women', *The FASEB Journal*, vol. 24, no. 1, pp. 326-31.

Lumeng, C.N., DelProposto, J.B., Westcott, D.J. & Saltiel, A.R. 2008, 'Phenotypic switching of adipose tissue macrophages with obesity is generated by spatiotemporal differences in macrophage subtypes', *Diabetes*, vol. 57, no. 12, pp. 3239-46.

Lumeng, C.N., DeYoung, S.M., Bodzin, J.L. & Saltiel, A.R. 2007, 'Increased inflammatory properties of adipose tissue macrophages recruited during diet-induced obesity', *Diabetes*, vol. 56, no. 1, pp. 16-23.

Lynch, I. & Dawson, K.A. 2008, 'Protein-nanoparticle interactions', *Nano Today*, vol. 3, no. 1, pp. 40-7.

Matsuzawa, Y., Funahashi, T. & Nakamura, T. 1999, 'Molecular Mechanism of Metabolic Syndrome X: Contribution of Adipocytokines · Adipocyte-derived Bioactive Substances', *Annals of the New York Academy of Sciences*, vol. 892, no. 1, pp. 146-54.

Maus, L., Spatz, J.P. & Fiammengo, R. 2009, 'Quantification and reactivity of functional groups in the ligand shell of PEGylated gold nanoparticles via a fluorescence-based assay', *Langmuir*, vol. 25, no. 14, pp. 7910-7.

May, M.J. & Ghosh, S. 1999, 'IκB Kinases: Kinsmen with Different Crafts', *Science*, vol. 284, no. 5412, pp. 271-3.

McGarry, J.D. & Brown, N.F. 1997, 'The mitochondrial carnitine palmitoyltransferase system—from concept to molecular analysis', *European Journal of Biochemistry*, vol. 244, no. 1, pp. 1-14.

McGrath, K.C., Li, X.H., Whitworth, P.T., Kasz, R., Tan, J.T., McLennan, S.V., Celermajer, D.S., Barter, P.J., Rye, K.-A. & Heather, A.K. 2014, 'High density lipoproteins improve insulin sensitivity in high-fat diet-fed mice by suppressing hepatic inflammation', *Journal of Lipid Research*, vol. 55, no. 3, pp. 421-30.

Meek, R., Urieli-Shoval, S. & Benditt, E. 1994, 'Expression of apolipoprotein serum amyloid A mRNA in human atherosclerotic lesions and cultured vascular cells: implications for serum amyloid A function', *Proceedings of the National Academy of Sciences*, vol. 91, no. 8, pp. 3186-90.

Mie, G. 1908, 'Pioneering mathematical description of scattering by spheres', *Annals of Physics*, vol. 25, pp. 377-445.

Minta, J.O. & Pambrun, L. 1985, 'In vitro induction of cytologic and functional differentiation of the immature human monocytelike cell line U-937 with phorbol myristate acetate', *American Journal of Pathology*, vol. 119, no. 1, pp. 111-26.

Mironava, T., Hadjiargyrou, M., Simon, M., Jurukovski, V. & Rafailovich, M.H. 2010, 'Gold nanoparticles cellular toxicity and recovery: effect of size, concentration and exposure time', *Nanotoxicology*, vol. 4, no. 1, pp. 120-37.

Mironava, T., Hadjiargyrou, M., Simon, M. & Rafailovich, M.H. 2014, 'Gold nanoparticles cellular toxicity and recovery: adipose derived stromal cells', *Nanotoxicology*, vol. 8, no. 2, pp. 189-201.

Mnyusiwalla, A., Daar, A.S. & Singer, P.A. 2003, "Mind the gap': science and ethics in nanotechnology', *Nanotechnology*, vol. 14, no. 3, pp. R9-R13.

Moghimi, S.M., Hunter, A.C. & Murray, J.C. 2001, 'Long-circulating and target-specific nanoparticles: theory to practice', *Pharmacological Reviews*, vol. 53, no. 2, pp. 283-318.

Mosser, D.M. & Edwards, J.P. 2008, 'Exploring the full spectrum of macrophage activation', *Nature reviews immunology*, vol. 8, no. 12, pp. 958-69.

Murano, I., Barbatelli, G., Parisani, V., Latini, C., Muzzonigro, G., Castellucci, M. & Cinti, S. 2008, 'Dead adipocytes, detected as crown-like structures, are prevalent in visceral fat depots of genetically obese mice', *Journal of Lipid Research*, vol. 49, no. 7, pp. 1562-8.

Murphy, C.J., Gole, A.M., Stone, J.W., Sisco, P.N., Alkilany, A.M., Goldsmith, E.C. & Baxter, S.C. 2008, 'Gold nanoparticles in biology: beyond toxicity to cellular imaging', *Accounts of Chemical Research*, vol. 41, no. 12, pp. 1721-30.

Murphy, C.J., Sau, T.K., Gole, A.M., Orendorff, C.J., Gao, J., Gou, L., Hunyadi, S.E. & Li, T. 2005, 'Anisotropic metal nanoparticles: synthesis, assembly, and optical applications', *Journal of Physical Chemistry B*, vol. 109, no. 29, pp. 13857-70.

Musso, G., Gambino, R. & Cassader, M. 2010, 'Non-alcoholic fatty liver disease from pathogenesis to management: an update', *Obesity Reviews*, vol. 11, no. 6, pp. 430-45.

Nathan, C.F. 1987, 'Secretory products of macrophages', *Journal of Clinical Investigation*, vol. 79, no. 2, pp. 319-26.

Nguyen, M.T.A., Favelyukis, S., Nguyen, A.-K., Reichart, D., Scott, P.A., Jenn, A., Liu-Bryan, R., Glass, C.K., Neels, J.G. & Olefsky, J.M. 2007, 'A subpopulation of macrophages infiltrates hypertrophic adipose tissue and is activated by free fatty acids via Toll-like receptors 2 and 4 and JNK-dependent pathways', *Journal of Biological Chemistry*, vol. 282, no. 48, pp. 35279-92.

NHLBI 1998, 'Clinical guidelines on the identification, evaluation, and treatment of overweight and obesity in adults', *Obesity Research*, vol. 6, pp. 51S-209S.

Ojea-Jimenez, I. & Puntes, V. 2009, 'Instability of cationic gold nanoparticle bioconjugates: the role of citrate ions', *Journal of the American Chemical Society*, vol. 131, no. 37, pp. 13320-7.

Olefsky, J.M. & Glass, C.K. 2010, 'Macrophages, inflammation, and insulin resistance', *Annual Review of Physiology*, vol. 72, pp. 219-46.

Opal, S.M. & DePalo, V.A. 2000, 'Anti-inflammatory cytokines', *Chest Journal*, vol. 117, no. 4, pp. 1162-72.

Osborn, O. & Olefsky, J.M. 2012, 'The cellular and signaling networks linking the immune system and metabolism in disease', *Nature Medicine*, vol. 18, no. 3, pp. 363-74.

Paciotti, G.F., Kingston, D.G.I. & Tamarkin, L. 2006, 'Colloidal gold nanoparticles: a novel nanoparticle platform for developing multifunctional tumor-targeted drug delivery vectors', *Drug Development Research*, vol. 67, no. 1, pp. 47-54.

Pan, Y., Neuss, S., Leifert, A., Fischler, M., Wen, F., Simon, U., Schmid, G., Brandau, W. & Jahnen-Dechent, W. 2007, 'Size-dependent cytotoxicity of gold nanoparticles', *Small*, vol. 3, no. 11, pp. 1941-9.

Pang, C., Gao, Z., Yin, J., Zhang, J., Jia, W. & Ye, J. 2008, 'Macrophage infiltration into adipose tissue may promote angiogenesis for adipose tissue remodeling in obesity', *Am J Physiol Endocrinol Metab*, vol. 295, no. 2, pp. E313-22.

Papavassiliou, G.C. 1979, 'Optical properties of small inorganic and organic metal particles', *Progress in Solid State Chemistry*, vol. 12, no. 3, pp. 185-271.

Parihar, A., Eubank, T.D. & Doseff, A.I. 2010, 'Monocytes and macrophages regulate immunity through dynamic networks of survival and cell death', *Journal of Innate Immunity*, vol. 2, no. 3, pp. 204-15.

Passmore, J.S., Lukey, P.T. & Ress, S.R. 2001, 'The human macrophage cell line U937 as an in vitro model for selective evaluation of mycobacterial antigen-specific cytotoxic T-cell function', *Immunology*, vol. 102, no. 2, pp. 146-56.

Patan, S. 2004, 'Vasculogenesis and angiogenesis', in M. Kirsch & P.M. Black (eds), *Angiogenesis in Brain Tumors*, Kluwer Academic Publishers, Netherlands, pp. 3-32.

Perlemuter, G., Bigorgne, A., Cassard-Doulcier, A.-M. & Naveau, S. 2007, 'Nonalcoholic fatty liver disease: from pathogenesis to patient care', *Nature Clinical Practice Endocrinology & Metabolism*, vol. 3, no. 6, pp. 458-69.

Pernodet, N., Fang, X., Sun, Y., Bakhtina, A., Ramakrishnan, A., Sokolov, J., Ulman, A. & Rafailovich, M. 2006, 'Adverse effects of citrate/gold nanoparticles on human dermal fibroblasts', *Small*, vol. 2, no. 6, pp. 766-73.

Phillips, H.S., Hains, J., Leung, D.W. & Ferrara, N. 1990, 'Vascular endothelial growth factor is expressed in rat corpus luteum', *Endocrinology*, vol. 127, no. 2, pp. 965-7.

Picot, J., Jones, J., Colquitt, J., Gospodarevskaya, E., Loveman, E., Baxter, L. & Clegg, A. 2009, 'The clinical effectiveness and cost-effectiveness of bariatric (weight loss) surgery for obesity: a systematic review and economic evaluation', *Health Technology Assessment* vol. 13, no. 41, pp. 1-190.

Pillay, J., Ozoemena, K.I., Tshikhudo, R.T. & Moutloali, R.M. 2010, 'Monolayer-protected clusters of gold nanoparticles: impacts of stabilizing ligands on the heterogeneous electron transfer dynamics and voltammetric detection', *Langmuir*, vol. 26, no. 11, pp. 9061-8.

Pissuwan, D., Cortie, C.H., Valenzuela, S.M. & Cortie, M.B. 2007, 'Gold nanosphere-antibody conjugates for hyperthermal therapeutic applications', *Gold Bulletin*, vol. 40, no. 2, pp. 121-9.

Pissuwan, D., Niidome, T. & Cortie, M.B. 2009, 'The forth coming applications of gold nanoparticles in drug and gene delivery systems', *Journal of Controlled Release*, vol. In Press, Corrected Proof.

Popkin, B.M. 2004, 'The nutrition transition: an overview of world patterns of change', *Nutrition Reviews*, vol. 62, no. 2, pp. S140-S3.

Popkin, B.M., Adair, L.S. & Ng, S.W. 2012, 'Global nutrition transition and the pandemic of obesity in developing countries', *Nutrition Reviews*, vol. 70, no. 1, pp. 3-21.

Popkin, B.M. & Nielsen, S.J. 2003, 'The sweetening of the world's diet', *Obesity Research*, vol. 11, no. 11, pp. 1325-32.

Purushotham, A., Schug, T.T., Xu, Q., Surapureddi, S., Guo, X. & Li, X. 2009, 'Hepatocyte-specific deletion of SIRT1 alters fatty acid metabolism and results in hepatic steatosis and inflammation', *Cell Metabolism*, vol. 9, no. 4, pp. 327-38.

Ramanathan, V. & Helderman, J.H. 2001, 'Cyclosporine formulations', *Current and Future Immunosuppressive Therapies Following Transplantation*, Springer, pp. 111-21.

Ramirez-Zacarias, J.L., Castro-Munozledo, F. & Kuri-Harcuch, W. 1992, 'Quantitation of adipose conversion and triglycerides by staining intracytoplasmic lipids with Oil red O', *Histochemistry*, vol. 97, no. 6, pp. 493-7.

Reddy, J.K. & Rao, M.S. 2006, 'Lipid metabolism and liver inflammation. II. Fatty liver disease and fatty acid oxidation', *American Journal of Physiology - Gastrointestinal and Liver Physiology*, vol. 290, no. 5, pp. G852-G8.

Roden, M. 2006, 'Mechanisms of disease: hepatic steatosis in type 2 diabetes—pathogenesis and clinical relevance', *Nature Clinical Practice Endocrinology & Metabolism*, vol. 2, no. 6, pp. 335-48.

Rodgers, R.J., Tschöp, M.H. & Wilding, J.P. 2012, 'Anti-obesity drugs: past, present and future', *Disease Models & Mechanisms*, vol. 5, no. 5, pp. 621-6.

Rosen, E.D., Sarraf, P., Troy, A.E., Bradwin, G., Moore, K., Milstone, D.S., Spiegelman, B.M. & Mortensen, R.M. 1999, 'PPAR gamma is required for the differentiation of adipose tissue in vivo and in vitro', *Molecular Cell*, vol. 4, no. 4, pp. 611-7.

Rosen, E.D. & Spiegelman, B.M. 2000, 'Molecular regulation of adipogenesis', *Annual Review of Cell and Developmental Biology*, vol. 16, no. 1, pp. 145-71.

Rosenbaum, D., Haber, R.S. & Dunaif, A. 1993, 'Insulin resistance in polycystic ovary syndrome: decreased expression of GLUT-4 glucose transporters in adipocytes', *American Journal of Physiology-Endocrinology And Metabolism*, vol. 264, no. 2, pp. E197-E202.

Rosenson, R.S., Tangney, C.C., Levine, D.M., Parker, T.S. & Gordon, B.R. 2004a, 'Elevated soluble tumor necrosis factor receptor levels in non-obese adults with the atherogenic dyslipoproteinemia', *Atherosclerosis*, vol. 177, no. 1, pp. 77-81.

Rosenson, R.S., Tangney, C.C., Levine, D.M., Parker, T.S. & Gordon, B.R. 2004b, 'Elevated soluble tumor necrosis factor receptor levels in non-obese adults with the atherogenic dyslipoproteinemia.', *Atherosclerosis*, vol. 177, no. 1, pp. 77-81.

Rosi, N.L. & Mirkin, C.A. 2005, 'Nanostructures in biodiagnostics', *Chemical Reviews*, vol. 105, no. 4, pp. 1547-62.

Roth, J., Qiang, X., Marbán, S.L., Redelt, H. & Lowell, B.C. 2004, 'The obesity pandemic: where have we been and where are we going?', *Obesity Research*, vol. 12, no. S11, pp. 88S-101S.

Rubino, F., Gagner, M., Gentileschi, P., Kini, S., Fukuyama, S., Feng, J. & Diamond, E. 2004, 'The early effect of the Roux-en-Y gastric bypass on hormones involved in body weight regulation and glucose metabolism', *Annals of Surgery*, vol. 240, no. 2, p. 236.

Rui, L. 2014, 'Energy Metabolism in the Liver', *Comprehensive Physiology*, vol. 4, no. 1, pp. 177-97.

Sadauskas, E., Danscher, G., Stoltenberg, M., Vogel, U., Larsen, A. & Wallin, H. 2009, 'Protracted elimination of gold nanoparticles from mouse liver', *Nanomedicine: Nanotechnology, Biology and Medicine*, vol. 5, no. 2, pp. 162-9.

Sadauskas, E., Wallin, H., Stoltenberg, M., Vogel, U., Doering, P., Larsen, A. & Danscher, G. 2007, 'Kupffer cells are central in the removal of nanoparticles from the organism', *Part Fibre Toxicol*, vol. 4, no. 10, p. 10.

Saltiel, A.R. & Kahn, C.R. 2001, 'Insulin signalling and the regulation of glucose and lipid metabolism', *Nature*, vol. 414, no. 6865, pp. 799-806.

Samuel, V.T., Liu, Z.-X., Qu, X., Elder, B.D., Bilz, S., Befroy, D., Romanelli, A.J. & Shulman, G.I. 2004, 'Mechanism of hepatic insulin resistance in non-alcoholic fatty liver disease', *Journal of Biological Chemistry*, vol. 279, no. 31, pp. 32345-53.

Sanyal, A.J., Campbell–Sargent, C., Mirshahi, F., Rizzo, W.B., Contos, M.J., Sterling, R.K., Luketic, V.A., Shiffman, M.L. & Clore, J.N. 2001, 'Nonalcoholic steatohepatitis: association of insulin resistance and mitochondrial abnormalities', *Gastroenterology*, vol. 120, no. 5, pp. 1183-92.

Sarin, H. 2010, 'Physiologic upper limits of pore size of different blood capillary types and another perspective on the dual pore theory of microvascular permeability', *Journal of angiogenesis research*, vol. 2, no. 1, p. 14.

Sárvári, A., Doan-Xuan, Q., Bacsó, Z., Csomós, I., Balajthy, Z. & Fésüs, L. 2015, 'Interaction of differentiated human adipocytes with macrophages leads to trogocytosis and selective IL-6 secretion', *Cell Death & Disease*, vol. 6, no. 1, p. e1613.

Sato, T., Hasko, D.G. & Ahmed, H. 1997, 'Nanoscale colloidal particles: monolayer organization and patterning', *Journal of Vacuum Science & Technology B: Microelectronics and Nanometer Structures*, vol. 15, pp. 45-8.

Sauer, H., Bekhite, M.M., Hescheler, J. & Wartenberg, M. 2005, 'Redox control of angiogenic factors and CD31-positive vessel-like structures in mouse embryonic stem cells after direct current electrical field stimulation', *Experimental cell research*, vol. 304, no. 2, pp. 380-90.

Schaeublin, N.M., Braydich-Stolle, L.K., Schrand, A.M., Miller, J.M., Hutchison, J., Schlager, J.J. & Hussain, S.M. 2011, 'Surface charge of gold nanoparticles mediates mechanism of toxicity', *Nanoscale*, vol. 3, no. 2, pp. 410-20.

Schaffer, J.E. 2003, 'Lipotoxicity: when tissues overeat', *Current Opinion in Lipidology*, vol. 14, no. 3, pp. 281-7.

Schenk, S., Saberi, M. & Olefsky, J.M. 2008a, 'Insulin sensitivity: modulation by nutrients and inflammation', *J Clin Invest*, vol. 118, no. 9, pp. 2992-3002.

Schenk, S., Saberi, M. & Olefsky, J.M. 2008b, 'Insulin sensitivity: modulation by nutrients and inflammation', *Journal of Clinical Investigation*, vol. 118, no. 9, pp. 2992-3002.

Schmid, G. 2008, 'The relevance of shape and size of Au55 clusters', *Chem Soc Rev*, vol. 37, no. 9, pp. 1909-30.

Schwartz, M.W., Woods, S.C., Seeley, R.J., Barsh, G.S., Baskin, D.G. & Leibel, R.L. 2003, 'Is the energy homeostasis system inherently biased toward weight gain?', *Diabetes*, vol. 52, no. 2, pp. 232-8.

Sclafani, A. 1989, 'Dietary-induced overeating', *Annals of the New York Academy of Sciences*, vol. 575, no. 1, pp. 281-91.

Semb, H., Peterson, J., Tavernier, J. & Olivecrona, T. 1987a, 'Multiple effects of tumor necrosis factor on lipoprotein lipase in vivo', *J Biol Chem*, vol. 262, no. 17, pp. 8390-4.

Semb, H., Peterson, J., Tavernier, J. & Olivecrona, T. 1987b, 'Multiple effects of tumor necrosis factor on lipoprotein lipase in vivo', *Journal of Biological Chemistry*, vol. 262, no. 17, pp. 8390-4.

Semmler-Behnke, M., Kreyling, W.G., Lipka, J., Fertsch, S., Wenk, A., Takenaka, S., Schmid, G. & Brandau, W. 2008, 'Biodistribution of 1.4-and 18-nm Gold Particles in Rats', *Small*, vol. 4, no. 12, pp. 2108-11.

Shewan, A., Marsh, B., Melvin, D., MARTIN, S., Gould, G. & James, D. 2000, 'The cytosolic C-terminus of the glucose transporter GLUT4 contains an acidic cluster endosomal targeting motif distal to the dileucine signal', *Biochemical Journal*, vol. 350, pp. 99-107.

Shi, Y. & Burn, P. 2004, 'Lipid metabolic enzymes: emerging drug targets for the treatment of obesity', *Nature Reviews. Drug Discovery*, vol. 3, no. 8, p. 695.

Shimomura, I., Hammer, R.E., Ikemoto, S., Brown, M.S. & Goldstein, J.L. 1999, 'Leptin reverses insulin resistance and diabetes mellitus in mice with congenital lipodystrophy', *Nature*, vol. 401, no. 6748, pp. 73-6.

Shoelson, S.E., Herrero, L. & Naaz, A. 2007, 'Obesity, inflammation, and insulin resistance', *Gastroenterology*, vol. 132, no. 6, pp. 2169-80.

Shukla, R., Bansal, V., Chaudhary, M., Basu, A., Bhonde, R.R. & Sastry, M. 2005, 'Biocompatibility of gold nanoparticles and their endocytotic fate inside the cellular compartment: a microscopic overview', *Langmuir*, vol. 21, no. 23, pp. 10644-54.

Simms, D., Cizdziel, P.E. & Chomczynski, P. 1993, 'TRIzol: A new reagent for optimal single-step isolation of RNA', *Focus*, vol. 15, no. 4, pp. 532-5.

Simpson, C.A., Agrawal, A.C., Balinski, A., Harkness, K.M. & Cliffel, D.E. 2011, 'Short-chain PEG mixed monolayer protected gold clusters increase clearance and red blood cell counts', *ACS Nano*, vol. 5, no. 5, pp. 3577-84.

Smirnova, E., Goldberg, E.B., Makarova, K.S., Lin, L., Brown, W.J. & Jackson, C.L. 2006, 'ATGL has a key role in lipid droplet/adiposome degradation in mammalian cells', *EMBO reports*, vol. 7, no. 1, pp. 106-13.

Smith, L.P., Ng, S.W. & Popkin, B.M. 2013, 'Trends in US home food preparation and consumption: analysis of national nutrition surveys and time use studies from 1965–1966 to 2007–2008', *Nutrition Journal*, vol. 12, no. 1, p. 45.

Sorisky, A., Molgat, A.S. & Gagnon, A. 2013, 'Macrophage-induced adipose tissue dysfunction and the preadipocyte: should I stay (and differentiate) or should I go?', *Advances in Nutrition: An International Review Journal*, vol. 4, no. 1, pp. 67-75.

Souza, S., Yamamoto, M., Franciosa, M., Lien, P. & Greenberg, A. 1998, 'BRL 49653 blocks the lipolytic actions of tumor necrosis factor-alpha: a potential new insulin-sensitizing mechanism for thiazolidinediones', *Diabetes*, vol. 47, no. 4, pp. 691-5.

Spiegelman, B. 1998, 'PPAR-gamma: adipogenic regulator and thiazolidinedione receptor', *Diabetes*, vol. 47, no. 4, pp. 507-14.

Spiegelman, B.M. & Flier, J.S. 2001, 'Obesity and the regulation of energy balance', *Cell*, vol. 104, no. 4, pp. 531-43.

Stavrou, D. 2008, 'Neovascularisation in wound healing', *Journal of Wound Care*, vol. 17, no. 7, pp. 298-302.

Steel, D.M. & Whitehead, A.S. 1994, 'The major acute phase reactants: C-reactive protein, serum amyloid P component and serum amyloid A protein', *Immunology Today*, vol. 15, no. 2, pp. 81-8.

Steinberg, G.R., Michell, B.J., van Denderen, B.J.W., Watt, M.J., Carey, A.L., Fam, B.C., Andrikopoulos, S., Proietto, J., Görgün, C.Z. & Carling, D. 2006, 'Tumor necrosis factor α-induced skeletal muscle insulin resistance involves suppression of AMP-kinase signaling', *Cell Metabolism*, vol. 4, no. 6, pp. 465-74.

Steirtman, R.M., Brodie, S.E. & Cohn, Z.A. 1976, 'Membrane flow during pinocytosis', *Journal of Cell Biology*, vol. 68, pp. 665-87.

Stephens, J.M., Lee, J. & Pilch, P.F. 1997, 'Tumor Necrosis Factor-α-induced Insulin Resistance in 3T3-L1 Adipocytes Is Accompanied by a Loss of Insulin Receptor Substrate-1 and GLUT4 Expression without a Loss of Insulin Receptor-mediated Signal Transduction', *Journal of Biological Chemistry*, vol. 272, no. 2, pp. 971-6.

Stephens, J.M. & Pekala, P.H. 1991a, 'Transcriptional repression of the GLUT4 and C/EBP genes in 3T3-L1 adipocytes by tumor necrosis factor-alpha', *J Biol Chem*, vol. 266, no. 32, pp. 21839-45.

Stephens, J.M. & Pekala, P.H. 1991b, 'Transcriptional repression of the GLUT4 and C/EBP genes in 3T3-L1 adipocytes by tumor necrosis factor-alpha', *Journal of Biological Chemistry*, vol. 266, no. 32, pp. 21839-45.

Suganami, T., Nishida, J. & Ogawa, Y. 2005, 'A paracrine loop between adipocytes and macrophages aggravates inflammatory changes role of free fatty acids and tumor necrosis factor α', *Arteriosclerosis, thrombosis, and vascular biology*, vol. 25, no. 10, pp. 2062-8.

Sumithran, P. & Proietto, J. 2013, 'The defence of body weight: a physiological basis for weight regain after weight loss', *Clinical Science*, vol. 124, no. 4, pp. 231-41.

Sun, K., Kusminski, C.M. & Scherer, P.E. 2011, 'Adipose tissue remodeling and obesity', *The Journal of Clinical Investigation*, vol. 121, no. 6, pp. 2094-101.

Surwit, R.S., Kuhn, C.M., Cochrane, C., McCubbin, J.A. & Feinglos, M.N. 1988, 'Diet-induced type II diabetes in C57BL/6J mice', *Diabetes*, vol. 37, no. 9, pp. 1163-7.

Sweeting, A.N. & Caterson, I.D. 2017, 'Approaches to obesity management', *Internal Medicine Journal*, vol. 47, no. 7, pp. 734-9.

Swinburn, B.A., Sacks, G., Hall, K.D., McPherson, K., Finegood, D.T., Moodie, M.L. & Gortmaker, S.L. 2011, 'The global obesity pandemic: shaped by global drivers and local environments', *The Lancet*, vol. 378, no. 9793, pp. 804-14.

Symonds, M.E. 2011, *Adipose tissue biology*, Springer Science & Business Media, New York.

Tahergorabi, Z. & Khazaei, M. 2013, 'The relationship between inflammatory markers, angiogenesis, and obesity', *ARYA Atherosclerosis*, vol. 9, no. 4, pp. 247-53.

Targher, G., Bertolini, L., Poli, F., Rodella, S., Scala, L., Tessari, R., Zenari, L. & Falezza, G. 2005, 'Nonalcoholic fatty liver disease and risk of future cardiovascular events among type 2 diabetic patients', *Diabetes*, vol. 54, no. 12, pp. 3541-6.

Templeton, A.C., Wuelfing, W.P. & Murray, R.W. 2000, 'Monolayer-protected cluster molecules', *Accounts of Chemical Research*, vol. 33, no. 1, pp. 27-36.

Tepper, O.M., Capla, J.M., Galiano, R.D., Ceradini, D.J., Callaghan, M.J., Kleinman, M.E. & Gurtner, G.C. 2005, 'Adult vasculogenesis occurs through in situ recruitment, proliferation, and tubulization of circulating bone marrow-derived cells', *Blood*, vol. 105, no. 3, pp. 1068-77.

TGA 2016, *AusPAR: Liraglutide*, Therapeutics and Goods Adminisration, viewed 24th July 2015, <https://www.tga.gov.au/auspar/auspar-liraglutide>.

Thompson, D. 2007, 'Michael Faraday's recognition of ruby gold: the birth of modern nanotechnology', *Gold Bulletin*, vol. 40, no. 4, pp. 267-9.

Thompson, D. & Wolf, A.M. 2001, 'The medical-care cost burden of obesity', *Obesity Reviews*, vol. 2, no. 3, pp. 189-97.

Tice, J.A., Karliner, L., Walsh, J., Petersen, A.J. & Feldman, M.D. 2008, 'Gastric banding or bypass? A systematic review comparing the two most popular bariatric procedures', *American Journal of Medicine*, vol. 121, no. 10, pp. 885-93.

Tilg, H. & Moschen, A.R. 2008, 'Inflammatory mechanisms in the regulation of insulin resistance', *Molecular Medicine*, vol. 14, no. 3-4, pp. 222-31.

Tomita, K., Tamiya, G., Ando, S., Ohsumi, K., Chiyo, T., Mizutani, A., Kitamura, N., Toda, K., Kaneko, T., Horie, Y., Han, J.-Y., Kato, S., Shimoda, M., Oike, Y., Tomizawa, M., Makino, S., Ohkura, T., Saito, H., Kumagai, N., Nagata, H., Ishii, H. & Hibi, T. 2006, 'Tumour necrosis factor α signalling through activation of Kupffer cells plays an essential role in liver fibrosis of non-alcoholic steatohepatitis in mice', *Gut*, vol. 55, no. 3, pp. 415-24.

Tsai, D.-H., DelRio, F.W., Keene, A.M., Tyner, K.M., MacCuspie, R.I., Cho, T.J., Zachariah, M.R. & Hackley, V.A. 2011, 'Adsorption and conformation of serum albumin protein on gold nanoparticles investigated using dimensional measurements and in situ spectroscopic methods', *Langmuir*, vol. 27, no. 6, pp. 2464-77.

Turkevich, J., Stevenson, P.C. & Hillier, J. 1951, 'A study of the nucleation and growth processes in the synthesis of colloidal gold', *Discusssions of the Faraday Society*, no. 11, pp. 55-75.

Unfried, K., Albrecht, C., Klotz, L.-O., Von Mikecz, A., Grether-Beck, S. & Schins, R.P. 2007, 'Cellular responses to nanoparticles: target structures and mechanisms', *Nanotoxicology*, vol. 1, no. 1, pp. 52-71.

Uysal, K.T., Wiesbrock, S.M., Marino, M.W. & Hotamisligil, G.S. 1997, 'Protection from obesity-induced insulin resistance in mice lacking TNF-[alpha] function', *Nature*, vol. 389, no. 6651, pp. 610-4.

van Herpen, N.A. & Schrauwen-Hinderling, V.B. 2008, 'Lipid accumulation in non-adipose tissue and lipotoxicity', *Physiology & Behavior*, vol. 94, no. 2, pp. 231-41.

van Hinsbergh, V.W.M., Koolwijk, P. & Hanemaaijer, R. 1997, 'Role of fibrin and plasminogen activators in repair-associated angiogenesis: in vitro studeis with human endothelial cells1', in I.D. Goldberg & E.M. Rosen (eds), *Regulation of Angiogenesis*, Birkhauser Verlag, Basel, Switzerland, pp. 391-411.

Vankoningsloo, S., Piens, M., Lecocq, C., Gilson, A., De Pauw, A., Renard, P., Demazy, C., Houbion, A., Raes, M. & Arnould, T. 2005, 'Mitochondrial dysfunction induces triglyceride accumulation in 3T3-L1 cells: role of fatty acid β-oxidation and glucose', *Journal of Lipid Research*, vol. 46, no. 6, pp. 1133-49.

Vemuri, V.K., Janero, D.R. & Makriyannis, A. 2008, 'Pharmacotherapeutic targeting of the endocannabinoid signaling system: drugs for obesity and the metabolic syndrome', *Physiology & Behavior*, vol. 93, no. 4, pp. 671-86.

Vesaratchanon, S., Nikolov, A. & Wasan, D.T. 2007, 'Sedimentation in nano-colloidal dispersions: Effects of collective interactions and particle charge', *Advances in Colloid and Interface Science*, vol. 134–135, no. 0, pp. 268-78.

Vilsbøll, T., Zdravkovic, M., Le-Thi, T., Krarup, T., Schmitz, O., Courrèges, J.-P., Verhoeven, R., Bugánová, I. & Madsbad, S. 2007, 'Liraglutide, a long-acting human glucagon-like peptide-1 analog, given as monotherapy significantly improves glycemic

control and lowers body weight without risk of hypoglycemia in patients with type 2 diabetes', *Diabetes Care*, vol. 30, no. 6, pp. 1608-10.

Wadden, T.A., Foreyt, J.P., Foster, G.D., Hill, J.O., Klein, S., O'Neil, P.M., Perri, M.G., Pi-Sunyer, F.X., Rock, C.L. & Erickson, J.S. 2011, 'Weight Loss With Naltrexone SR/Bupropion SR Combination Therapy as an Adjunct to Behavior Modification: The COR-BMOD Trial', *Obesity*, vol. 19, no. 1, pp. 110-20.

Wadden, T.A., Hollander, P., Klein, S., Niswender, K., Woo, V., Hale, P.M. & Aronne, L. 2013, 'Weight maintenance and additional weight loss with liraglutide after low-calorie-diet-induced weight loss: The SCALE maintenance randomized study', *International Journal of Obesity*, vol. 37, no. 11, pp. 1443-51.

Wakil, S.J., Stoops, J.K. & Joshi, V.C. 1983, 'Fatty acid synthesis and its regulation', *Annual Review of Biochemistry*, vol. 52, no. 1, pp. 537-79.

Wang, H. & Joseph, J.A. 1999, 'Quantifying cellular oxidative stress by dichlorofluorescein assay using microplate reader', *Free Radical Biology and Medicine*, vol. 27, no. 5, pp. 612-6.

Watkins, L.R., Maier, S.F. & Goehler, L.E. 1995, 'Immune activation: the role of pro-inflammatory cytokines in inflammation, illness responses and pathological pain states', *Pain*, vol. 63, no. 3, pp. 289-302.

Weisberg, S.P., Hunter, D., Huber, R., Lemieux, J., Slaymaker, S., Vaddi, K., Charo, I., Leibel, R.L. & Ferrante, A.W., Jr. 2006, 'CCR2 modulates inflammatory and metabolic effects of high-fat feeding', *J Clin Invest*, vol. 116, no. 1, pp. 115-24.

Weisberg, S.P., Hunter, D., Huber, R., Lemieux, J., Slaymaker, S., Vaddi, K., Charo, I., Leibel, R.L. & Ferrante Jr, A.W. 2006, 'CCR2 modulates inflammatory and metabolic effects of high-fat feeding', *Journal of Clinical Investigation*, vol. 116, no. 1, pp. 115-24.

Weisberg, S.P., McCann, D., Desai, M., Rosenbaum, M., Leibel, R.L. & Ferrante, A.W. 2003, 'Obesity is associated with macrophage accumulation in adipose tissue', *Journal of Clinical Investigation*, vol. 112, no. 12, pp. 1796-808.

Wellen, K.E. & Hotamisligil, G.S. 2003, 'Obesity-induced inflammatory changes in adipose tissue', *Journal of Clinical Investigation*, vol. 112, no. 12, pp. 1785-8.

West, D.B., Boozer, C.N., Moody, D.L. & Atkinson, R.L. 1992, 'Dietary obesity in nine inbred mouse strains', *American Journal of Physiology - Regulatory, Integrative and Comparative Physiology*, vol. 262, no. 6, pp. R1025-R32.

West, D.B. & York, B. 1998, 'Dietary fat, genetic predisposition, and obesity: lessons from animal models', *American Journal of Clinical Nutrition*, vol. 67, no. 3, pp. 505S-12S.

Weyer, C., Foley, J.E., Bogardus, C., Tataranni, P.A. & Pratley, R.E. 2000, 'Enlarged subcutaneous abdominal adipocyte size, but not obesity itself, predicts type II diabetes independent of insulin resistance', *Diabetologia*, vol. 43, no. 12, pp. 1498-506.

Whitson, B.A., Leslie, D.B., Kellogg, T.A., Maddaus, M.A., Buchwald, H., Billington, C.J. & Ikramuddin, S. 2007, 'Adipokine response in diabetics and nondiabetics following the Roux-en-Y gastric bypass: a preliminary study', *Journal of Surgical Research*, vol. 142, no. 2, pp. 295-300.

WHO 1995, *Physical status: The use of and interpretation of anthropometry, report of a WHO expert committee*, World Health Organization (WHO), Geneva.

WHO 2008, *Waist circumference and waist-hip ratio*, World Health Organization (WHO), Geneva.

WHO 2014a, *Global status report on noncommunicable diseases 2014*, World Health Organization (WHO), Geneva.

WHO 2014b, *Noncommunicable diseases country profiles 2014*, World Health Organization (WHO), Geneva.

WHO 2015a, *BMI classification*, World Health Organization, Geneva, viewed 7th May 2015, <http://apps.who.int/bmi/index.jsp?introPage=intro_3.html>.

WHO 2015b, *Fact sheet no. 311 - Obesity and overweight*, World Health Organization, Geneva, viewed 7th May 2015, <http://www.who.int/mediacentre/factsheets/fs311/en/>.

Wuelfing, W.P., Gross, S.M., Miles, D.T. & Murray, R.W. 1998, 'Nanometer gold clusters protected by surface-bound monolayers of thiolated poly (ethylene glycol) polymer electrolyte', *Journal of the American Chemical Society*, vol. 120, no. 48, pp. 12696-7.

Wunderlich, F.T., Ströhle, P., Könner, A.C., Gruber, S., Tovar, S., Brönneke, H.S., Juntti-Berggren, L., Li, L.-S., van Rooijen, N. & Libert, C. 2010, 'Interleukin-6 signaling in liver-parenchymal cells suppresses hepatic inflammation and improves systemic insulin action', *Cell Metabolism*, vol. 12, no. 3, pp. 237-49.

Xu, X., Stevens, M. & Cortie, M.B. 2004, 'In situ precipitation of gold nanoparticles onto glass for potential architectural applications', *Chemistry of Materials*, vol. 16, no. 11, pp. 2259-66.

Yah, C.S. 2013, 'The toxicity of gold nanoparticles in relation to their physiochemical properties', *Biomedical Research*, vol. 24, no. 3, pp. 400-13.

Yamashita, A., Soga, Y., Iwamoto, Y., Yoshizawa, S., Iwata, H., Kokeguchi, S., Takashiba, S. & Nishimura, F. 2007, 'Macrophage-adipocyte interaction: marked interleukin-6 production by lipopolysaccharide', *Obesity*, vol. 15, no. 11, pp. 2549-52.

Yen, H.J., Hsu, S.h. & Tsai, C.L. 2009, 'Cytotoxicity and immunological response of gold and silver nanoparticles of different sizes', *Small*, vol. 5, no. 13, pp. 1553-61.

Yu, Y.-H. & Ginsberg, H.N. 2005, 'Adipocyte signaling and lipid homeostasis', *Circulation Research*, vol. 96, no. 10, pp. 1042-52.

Zebisch, K., Voigt, V., Wabitsch, M. & Brandsch, M. 2012, 'Protocol for effective differentiation of 3T3-L1 cells to adipocytes', *Analytical Biochemistry*, vol. 425, no. 1, pp. 88-90.

Zhang, J.-M. & An, J. 2007, 'Cytokines, Inflammation and Pain', *International Anesthesiology Clinics*, vol. 45, no. 2, pp. 27-37.

Zhang, Q., Hitchins, V.M., Schrand, A.M., Hussain, S.M. & Goering, P.L. 2011, 'Uptake of gold nanoparticles in murine macrophage cells without cytotoxicity or production of pro-inflammatory mediators', *Nanotoxicology*, vol. 5, no. 3, pp. 284-95.

Zhang, X.-D., Wu, H.-Y., Wu, D., Wang, Y.-Y., Chang, J.-H., Zhai, Z.-B., Meng, A.-M., Liu, P.-X., Zhang, L.-A. & Fan, F.-Y. 2010, 'Toxicologic effects of gold nanoparticles in vivo by different administration routes', *International Journal of Nanomedicine*, vol. 5, pp. 771-81.